AFIT/GSO/ENG/99M-01

A COMPARATIVE ANALYSIS OF THE IRIDIUM® AND GLOBALSTAR® SATELLITE TRANSMISSION PATHS

THESIS

Kenneth E. Crowe

Squadron Leader, Royal Australian Air Force

AFIT/GSO/ENG/99M-01

The views expressed in this document are those of the author and do not reflect the official policy or position of the Department of Defense or the U.S. Government, or the Government of the Commonwealth of Australia.

AFIT/GSO/ENG/99M-01

A Comparative Analysis of the Iridium® and Globalstar® Satellite Transmission Paths

THESIS

Presented to the faculty of the Graduate School of Engineering

Of the Air Force Institute of Technology

Air University

Air Education and Training Command

In Partial Fulfillment of the Requirements for the

Degree of Master of Science in Space Operations

Kenneth E. Crowe

Squadron Leader, Royal Australian Air Force

March, 1999

AFIT/GSO/ENG/99M-01

A Comparative Analysis of the Iridium® and Globalstar® Satellite Transmission Paths

Kenneth E. Crowe, Master of Science in Space Operations

Squadron Leader, Royal Australian Air Force

Approved:

Richard A. Raines, Ph.D., Major, USAF Committee Chairman	1 Mar 99 date
Derrill T. Goldizen, Ph.D., Major, USAF Committee Member	1 Mar 99 date
William E. Wiesel, Ph.D., Committee Member	1 Mar 99 date

ACKNOWLEDGEMENTS

I would like to express my sincere appreciation to my thesis advisor, Major Richard Raines for his support and encouragement during the course of this thesis effort. His balanced judgement, patience and insight were invaluable to me. I would also like to thank my committee members, Major Derrill Goldizen and Dr. William Wiesel, for their guidance and advice. I have relied heavily upon their support, and the support of all of my USAF colleagues who assisted me during my research.

Of all those who have helped me, I owe my wife, Natalie, the greatest debt of gratitude. She bore the weight and extra responsibility of raising our two small children, and running a busy household while I studied. Due to the workload and stresses associated with the course, and living in a different country without the support of family and friends, this course has represented a considerable challenge to us both. If it was not for her uncomplaining support, I could not have completed my studies.

TABLE OF CONTENTS

LIST OF FIGURES

LIST OF TABLES

ABSTRACT

Low earth orbit Satellite-based Personal Communication Systems (S-PCS) such as Globalstar[1] and Iridium[2] will provide a valuable global communications asset for business, humanitarian aid and military operations. However, the level of coverage and the quality of the transmission path of these systems are strongly dependent on the latitude of the user and, due to their orbital characteristics, both systems provide reduced levels of coverage at low latitudes. Additionally, the L- and S-Band frequencies utilized by these systems are prone to ionospheric interference at low latitudes. In order to quantify these effects and allow a comparison to be conducted, both constellations are simulated and analyzed in terms of their transmission path elevation and azimuth angles, satellite visibility and levels of path attenuation.

The results indicate that the Globalstar constellation architecture provides a considerably better transmission path than Iridium's in several important areas, including path elevation angles, satellite visibility and susceptibility to ionospheric effects. For example, at low latitudes, Globalstar provides a 25% higher elevation angle and a 60% greater probability of multiple satellite coverage. These factors impact the expected levels of signal multipath effects, shadowing and blockage from terrestrial obstacles such as trees or buildings. To assist future study in this area, a unique set of equations has been developed which describe the distribution of Iridium and Globalstar path elevation angles entirely as a function of the user's latitude. In addition to the differences in path elevation angles, modeling indicates that ionospheric scintillation is a potentially serious problem for both systems. However, Globalstar is expected to suffer lower fade levels than Iridium due to its higher downlink frequency and multiple path availability. The research concludes that, within the scope of the analysis, Globalstar provides a higher quality transmission path for users at low to mid-latitudes.

---

[1] Iridium is a registered trademark and service mark of Iridium LLC
[2] Globalstar is a trademark of Globalstar, L.P.

CHAPTER 1

INTRODUCTION

The use of satellite constellations such as Iridium and Globalstar to provide Satellite Personal Communications Services (S-PCS) will undoubtedly play a role in the future of global telecommunications. These systems provide communications services to a mobile user and the quality of service offered by these systems is inextricably linked to the quality of the transmission path and the number of satellites in view. For Iridium and Globalstar the nature of the path and the number of available satellites varies dramatically with a user's latitude. The quality of the coverage, the number of satellites available the minimum elevation angle and several other important parameters are all latitude dependent. Additionally, the L and S-Band frequencies utilized by Iridium and Globalstar, although nearly ideal from a viewpoint of immunity to rainfall and gaseous attenuation effects, are prone to interference from the ionosphere at certain latitudes. Establishing the degree to which these factors affect the performance of these systems is the prime research goal of this thesis.

1.1 Research Goals

The primary research goals of this thesis are as follows:

- Compare the relative performance of the Iridium and Globalstar systems by modeling the satellite transmission path for a user located at any point on the earth. The path elevation and azimuth angles, the link attenuation and the number of available satellites will be comprehensively described as a function of latitude.
- Approximate the probability distribution of path elevation angles for both systems in terms of a statistical model. This data may provide an opportunity to more accurately assess the degree of multipath effects and shadowing from foliage and obstacles.

- Estimate the worst case effects of ionospheric scintillation at levels of solar activity which could be realistically expected over the next five years.

The analysis is intended to provide data for the further development or refinement of path models for satellite based personal communications systems. An accurate understanding of link characteristics for any user may assist in the assessment of terrestrial shadowing and blocking, or facilitate the design of fixed and vehicle mounted antennas. Additionally, the analysis may assist in the assessment of the potential operational impact of ionospheric scintillation.

1.2 Research Motivation

The Iridium and Globalstar systems are often presented primarily as a business tool and, understandably, the intended customer base is located in the mid to high latitudes covering the United States and Europe. Nonetheless, there are other important applications for which these global mobile personal communications services are extremely well suited.

The latitudes of ±20° make up a large proportion (34.2%) of the earth's surface and includes the Asian nations (Malaysia, Indonesia, and The Philippines), South America, Africa, part of India, and the northern part of Australia. Many of the nations at these lower latitudes may look to these systems to provide basic communications infrastructure which their countries lack. These satellite systems offer a means of achieving voice and low speed data communications without the enormous investments in terrestrial cabling infrastructure, an investment which is enormously costly to install, maintain and update, and which suffers higher rates of degradation in the harsh equatorial environment.

From a military viewpoint, reliable communications is essential if the Australian Defense Force (ADF) is to operate in its region of direct strategic interest. Australia's principal strategic interests are concentrated on the Asia-Pacific region, comprising the countries of East Asia, Southeast Asia, the South Pacific, the United States, and, perhaps increasingly in the future, Southern Asia. Notwithstanding this wider focus, Australia's most direct strategic interests

continue to include the inner arc of islands from Indonesia in the west through to Papua New Guinea, the Solomon Islands and the Southwest Pacific (Figure 1).

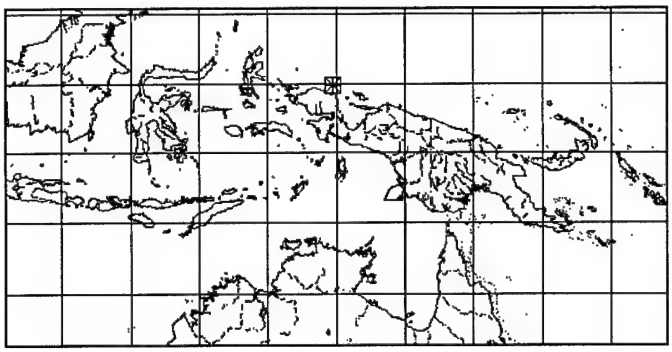

Figure 1 – Australia's Geographic Region of Interest

Any substantial military attack on Australia would most easily be mounted from or through these islands [McL97]. The ability to operate tactical military forces beyond its shoreline is an essential objective for Australia's national defense policy [Rob98]. Although the use of S-PCS systems is not currently part of the ADF's tactical communications inventory, the systems offer compelling advantages including portable, handsets offering voice fax, and low speed data services, relatively low cost of acquisition, and reliable global coverage.

Additionally, emergency and disaster relief services (of the type regularly conducted by the ADF) as well as foreign aid providers operating in the South East Asian region would benefit from the services offered by Iridium and Globalstar. The United Nations Department of Humanitarian Affairs examined the requirements for emergency telecommunications for humanitarian aid, concluding that reliable telecommunications under adverse conditions are an indispensable tool of disaster mitigation and disaster relief operations [Zim95]. Instantly available voice communications of the type offered by Iridium would allow relief operations to function much more effectively in an area devastated by floods, or hurricanes, earthquakes or other natural disaster [Swa95].

The advantages offered by such systems are compelling, however the promise of uninterrupted worldwide communications should not be taken for granted, especially at low

latitudes. These systems provide reduced low latitude and equatorial coverage when compared to the levels of coverage enjoyed by mid and high latitude users. This manifests itself primarily as a generally lower number of satellites in view at any one time. Additionally, those satellites that are in view may be at lower elevation angles, and therefore subject to greater propagation losses. Secondly, certain atmospheric effects, such as ionospheric scintillation are more likely at lower latitudes and can seriously impact signals at the frequencies used by Iridium, Globalstar, GPS and Intelsat. Due to the nature of these impairments, faster moving low earth orbiting satellite systems are affected more than geostationary systems operating in the same band (such as Intelsat). Finally, real-time voice systems such as Iridium and Globalstar cannot tolerate service interruptions, whereas spread spectrum data systems such as the Global Positioning System (GPS), which can tolerate multiple link outages simultaneously, are less effected.

An investigation and assessment of these factors will assist staff responsible for the planning, deployment and in-service support of these services. An additional benefit of this analysis is that by understanding the relationship between the user's latitude and the quality of the satellite coverage, an assessment of the impact of blocking and shadowing from terrestrial obstacles can be made.

1.3 Summary

This chapter has described the motivation for conducting this research and defined a set of goals. Chapter 2 provides the background necessary to support the research and presents a review of the current literature in the area of LEO path analysis and atmospheric effects. A wide selection of atmospheric and ionospheric impairments are discussed, with particular attention to those effects which are assessed as having the most impact. Chapter 3 explains the methodology used to simulate the two systems, and discusses the assumptions and limitations inherent in the modeling process. Chapter 4 presents and analyses the results of the simulation process and provides a comprehensive comparison between Iridium and Globalstar systems in terms of their

path geometry, satellite visibility and susceptibility to the effects of ionospheric scintillation. Chapter 5 contains conclusions from the research and recommendations for additional research.

CHAPTER 2

BACKGROUND AND LITERATURE REVIEW

2.1 Introduction

The aim of this chapter is three-fold. First, the Iridium and Globalstar system parameters which are essential to an understanding of the later analysis, are introduced. Second, the importance of elevation angle and satellite visibility to link performance is outlined. Third, the relevant atmospheric propagation impairments and the models which predict their impact on a transmission path are described.

The various orbital elements and constellation characteristics of the Iridium and Globalstar systems are described, however, since many features of these systems are not relevant to this thesis, such as the operation of Iridium's inter-satellite links or Globalstar's spread spectrum link characteristics, they are addressed only in a cursory manner. Several sources of information are available which describe the various technical aspects the Iridium and/or Globalstar systems [Com93, Dol93, Gaf95, Hut95, Mai95, Bru96, Cio96, Ste96, FoR98, FoR98-2].

All of the major propagation mechanisms are introduced and a brief review conducted to determine whether a particular propagation factor is relevant. Although many of the mechanisms and their attendant effects are outside the scope of this thesis, it is believed that a brief introduction of the effect both expands and consolidates a more thorough understanding of the factors which affect satellite link quality.

Several models are utilized in the course of the data analysis. They range from simple mathematical models describing the free space satellite path attenuation, to complex computer-based models predicting the impact of the ionosphere on link quality. The input parameters of these models require introduction and a discussion of their origin and predicted values. As the

scope of this thesis extends into the next solar cycle, predictions of several parameters, notably the expected sunspot numbers (SSNs) and geomagnetic indices are also required.

2.2 Iridium Overview

Iridium provides Satellite-based, Personal Communications Services (S-PCS) to permit worldwide voice, data, fax, paging communications. To achieve this global coverage, Iridium utilizes a constellation of 66 Low Earth Orbit (LEO) satellites in high inclination orbits to augment the coverage of the terrestrial cellular telephone network. A dual mode Iridium phone has been designed to place calls using the local cellular facilities, if available, or switch to an Iridium satellite when the user is outside the normal coverage area, or roams into an incompatible carrier's domain.

The Iridium satellite communicates to the ground users through three antennas which form a honeycomb pattern of 48 beams below each satellite. The circle of beams covers approximately 15.3 million km^2 and each beam (or cell as they are often called) is independent in terms of the frequencies it uses. As the satellite beam footprint moves over the ground, the subscriber signal is switched from one beam to the next in a hand-off process. A particular satellite maintains communications with users by handing over the call from cell to cell. As the satellites approach the poles, their footprints converge and the beams overlap. Outer beams are then turned off to eliminate this overlap and conserve spacecraft power.

During operation, the satellites relay data either directly to another Iridium handset, pager or other facility or to one of approximately 15 tracking ground stations (Gateways) which are located in strategic high traffic density locations. The role of these high capacity Gateway stations are to form the interface between the satellite network and the Public Switched Telephone Network (PSTN) [Cio96].

Many of the advantages of the Iridium system are made possible through the linking of the satellites into a contiguous network. Through the provision of inter-satellite links connecting

adjacent satellites, the constellation forms a network, able to relay data between adjacent satellites before linking directly to the user's handset or a Gateway. This reduces the dependence of the Iridium system on the other telecommunications carriers and improves the revenue potential of the system.

2.3 Globalstar Overview

At the time of writing, the Globalstar constellation was incomplete, having suffered a major launch failure [Glo98-2]. This system is designed to provide near-global voice, fax, data and messaging services using a combination of satellites and terrestrial telecommunications infrastructure. Users of Globalstar make or receive calls using hand-held or vehicle mounted terminals; calls are relayed through Globalstar's satellite constellation, to a ground-station and then through local terrestrial wireline and wireless systems to their end destinations. Like Iridium, the handsets are multi-mode, able to utilize a local cellular carrier's service if it is available, switching to satellites links if the terrestrial coverage is inadequate or incompatible with the handset's capabilities. Unlike Iridium, Globalstar's satellites do not utilize intersatellite links and the system is more reliant on the terrestrial telecommunications network if a user wishes to communicate outside a satellite's footprint. Each satellite carries two transponders, one to communicate with the gateway, the other to communicate with the user. If a signal is received from a handset, it is translated in frequency and relayed to the gateway for processing. If the gateway sends data to the satellite, it is relayed directly down to a user within the 16 beam footprint, which covers an area of approximately 61.5 million km^2 [Ste96].

2.4 Telecommunications Frequencies & Data Rates

Iridium. The primary links between the Iridium satellite and the terrestrial user operate in the L-Band (1616-1626.5 MHz) and utilize a combination of Frequency Division Multiple Access and Time Division Multiple Access (FDMA/TDMA) signal multiplexing to divide the

available spectrum into 3,840 carrier channels. Voice signals from the handset are modulated onto the carrier using a Quadrature Phase Shift Key (QPSK) modulation scheme and transmitted at 2400 bps using right hand circular polarization. The Ka-Band (19.4-19.6 GHz for downlinks; 29.1-29.3 GHz for uplinks) serves as the link between the satellite and the Gateways and earth terminals. Inter-satellite crosslink transponders operating in the Ka frequency band between 23.18 and 23.38 GHz. Both uplink and downlink occupy 100 MHz bandwidths and use right-hand circular polarization. The intersatellite links use 200 MHz bandwidth with vertical polarization [Mai95].

Globalstar. The Globalstar system's approach to communications is fundamentally different in several important aspects. While both systems employ a network architecture, Globalstar uses the satellites as bent-pipe transponders providing local area relay services; either to another handset or to a terrestrial gateway. In contrast with Iridium, which bypasses much of the terrestrial infrastructure, Globalstar integrates the PSTN and satellites to provide seamless communications. Whereas Iridium uses a contiguous band of L-Band frequencies for satellite to ground communications, Globalstar utilizes L Band (1610 – 1626.5 MHz) for the uplink and S-Band (2483.5 – 2500 MHz) for the downlink. These links employ left hand circular polarization and provide 2800 user channels. The high speed data communications link between the satellite and gateway utilizes C-Band for both uplink (5091-5250 MHz) and downlink (6875-7055 MHz). User segments are frequency-agile and use a variable rate encoding technique to provide data rates of 1.2 to 9.6 kbps. Variable rate encoding transmits 4.8 kbps when a voice signal is present but reduces the rate to 1.2 kbps during pauses. Toll-quality service is supported at 9.6 kbps [Cio96]. A significant difference between Iridium and Globalstar is its use of Code Division Multiple Access (CDMA) rather than TDMA for the subscriber channels. CDMA is a modulation and multiple access scheme based on direct sequence spread spectrum communications. Amongst its many advantages, this system offers greater spectrum efficiency and readily allows encryption of the channel. Additionally, Globalstar reportedly uses specialized

rake receivers to combine up to three available satellite paths to improve the quality of the received signal [Glo98]. This may serve to reduce the impact of multipath fading and obstacle blockage. Note that no assumptions are made concerning the signal processing capabilities of either system to add effective gain or improve the quality of the link.

2.5 Satellite Constellation Description

Iridium. The Iridium satellite constellation is formed from an Adams Rider constellation of 66 satellites arranged into six 11-satellite orbital planes inclined at approximately 86.4°. As the constellation was not in place until recently, previous papers [FoR98-2, Bru96, Kel97] addressing system performance have taken orbital parameters from open literature [Mai95]. However, at the time of preparation for this thesis (Oct 98), 77 satellites had been launched into orbit and the Iridium system was approaching operational status, despite some early in-orbit failures. In an effort to model the actual constellation parameters as closely as possible, ephemeris data was collected from NORAD's satellite database and actual constellation orbital elements were extracted. An analysis of the data provides the basic constellation parameters detailed in Table 1.

Globalstar. The Globalstar Constellation is planned to consist of 48 lightweight (450 kg) satellites orbiting in 8 orbital circular planes at 52° inclination. The satellites will be located at 1414 kms altitude, nearly twice that of Iridium satellites. Without the requirement for satellite inter connectivity, the satellites can be placed in a higher, more inclined orbit than Iridium. The increased altitude and number of orbital planes is expected to provide improved coverage at mid to low latitudes at the expense of link attenuation and signal delay. The inclination of the orbital planes limits the coverage to approximately 74°. Globalstar's orbital characteristics are also provided in Table 1.

Table 1 – Summary of Iridium and Globalstar Constellation Parameters

PARAMETER	IRIDIUM			GLOBALSTAR
	Public Literature e.g. [Mai95]	**NORAD Value (Aug 98)**	**Value Used in Modelling**	
No of Satellites	66	77 (incl. additional non-operational satellites)	66	48
Satellite Alt (kms)	780	773.8797	775	1414
Orbit eccentricity	0°	0.001446°	0° (Circular)	0°
No of Orbital Planes	6	6	6	8
Satellites per Plane	11	12 (incl. spares)	11	6
Average inclination	86.4°	Average 86.40886°	86.41°	52°
Plane Spacing				45°
1-2	31.6°	31.59°	31.6°	
2-3	31.6°	31.59°	31.6°	
3-4	31.6°	31.6°	31.6°	
4-5	31.6°	31.6°	31.6°	
5-6	31.6°	31.625°	31.6°	
6-1*	22°	21.995°	22°	
* Planes 1 and 6 are counter rotating.				
Phase Offset Between Adjacent Planes	18°	Average of 17.6°	18°	7.5°

Note that the values used are in close agreement with the values available in public literature. The constellation structure used in this thesis differs from previous studies by a 5 km reduction in altitude and an 0.01° inclination increase. These are not considered significant.

2.6 Transmission Path Characteristics

The quality of service provided by an S-PCS such as Iridium or Globalstar is strongly dependent on the quality of the path between the user and the satellite in use. The quality of the path is determined primarily by the absence or presence of propagation impairments along the transmission path. These impairments consist mainly of atmospheric effects and terrestrial

obstructions which interfere with the signal. The physical environment (trees, buildings, solid reflective surfaces etc) interact with the signal, through blocking or shadowing, or by providing multiple reflections to the receiver causing multipath problems. The antenna of the S-PCS handset is necessarily omni-directional and this design is especially prone to multipath scattering problems [Gol92]. Atmospheric effects are discussed in Section 2.9.

2.6.1 Elevation Angle

The elevation angle is that angle between the earth station's local horizon and the straight-line path between a user and a particular satellite. The severity of multipath and fading effects tend to be related to the elevation angle of the transmission path as most of the obstructions are fixed to the ground (e.g., trees and buildings). Free space attenuation is greatest at low path elevation angles, as the linear distance (ignoring ionospheric and tropospheric refractive effects) is greatest. Additionally, rainfall and atmospheric clear air effects are also dependent to varying degrees on the elevation angle of the path.

Several models exist to predict the effects of shadowing and fading for mobile (primarily vehicle mounted) applications. The Empirical Roadside Shadowing (ERS) Model, the Modified ERS and the Empirical Fading Model detailed in [But95] all operate at L-Band and utilize elevation angle directly in the equations. These models predict substantial fades (20 dB at 1% exceedence levels and 13 dB at 10%) in mobile applications at L-Band. It should be noted that these models, originally intended for vehicular applications, are not directly applicable to the S-PCS mobile communications path. Nonetheless, other studies [Akt95, Akt97] which have focussed on the S-PCS path in urban areas also indicate the dominance of the path elevation angle as one of the primary determinants of link quality.

Unlike geostationary satellite communications, the paths to satellites in a LEO constellation change in azimuth, elevation and range continuously. An understanding of the most

likely distribution of elevation angles can be combined with these models to more completely predict the level of expected impairment.

2.6.2 Satellite Diversity

A user that can access more than one satellite at any one time has a higher probability of obtaining an unobstructed communications path. The improvement in performance provided by multiple satellites/paths is particularly noticeable in an environment where roadside clutter or building blockage can present obstacles unpredictably in what may otherwise be an ideal path. To illustrate the benefits of having multiple satellites in view, propagation measurements performed with several aircraft simulating satellites indicate that the required link margin can be reduced by up to 70% when two or three simultaneous paths are available. The same research also indicated that the majority of the available improvement is achieved with just two visible satellites [Kar95]. Akturan and Vogel [Akt97] modeled the propagation path to the Globalstar constellation using photogrammetry techniques. This technique analyses a series of fisheye photographs which showed building blockage and shadowing from foliage to determine the levels of fade for different paths. He defined the baseline fade as that level of fading experienced when only the highest available satellite was selected, and further defined *diversity gain* as the reduction in fade (over baseline) when multiple satellites are available. The availability of alternative paths increases the probability of achieving a lower level of path fade (from multipath/shadowing and blocking) and can be treated as a gain.

The importance of the satellite visibility is illustrated by the results of Vogel's modeling which indicated that at 10% probability, the level of baseline fade in an urban environment in Tokyo, was estimated at 21.3 dB for the highest available satellite (no alternate satellite paths available). The availability of up to four satellites reduced the fade by up to 11.6 dB, hence providing a diversity gain of 11.6 dB. However, the benefits of satellite diversity were reduced

by approximately 50% when modeling a receiver located at Singapore (approximately equatorial), due to the generally reduced satellite visibility.

In summarizing the results of his modeling, Akturan stated that "path diversity significantly improves system availability in the low probability range and that the diversity gain achieved levels out after using two or three satellites." He also noted: "The Globalstar constellation appears to be optimized for mid-to-northern latitudes, offering the least diversity gain near the equator." Clearly, elevation angle and satellite visibility are important factors in the performance of the Iridium and Globalstar systems. An understanding of how these parameters change as a user moves around the planet provides important insights into the system's strengths and vulnerabilities.

The Iridium constellation, by virtue of the inclination of its orbital planes has the least number of satellites visible at the equator. Additionally, those satellites that are visible are at a generally lower elevation angle [Siw95]. Globalstar, with it's higher orbital altitude and lower inclination may provide superior link performance at low latitudes, however, high latitude coverage will suffer. Determining the degree to which the potential performance of satellite constellations such as Iridium and Globalstar are affected by the user's latitude is a primary objective of this study.

2.7 Satellite Link Calculations

Disregarding other losses, for an antenna of diameter d, with gain G_t, transmitting with a power P_t, the power flux density in W/m^2 at the receiver will be given by:

$$P_{fd} = \frac{P_t G_t}{4\pi d^2} \; watts/m^2 \tag{1}$$

The power received will be the product of the power flux density P_{fd} and the equivalent area of the receive antenna A.

$$P_r = P_{fd} A \quad watts \tag{2}$$

Turning now to the gain of the transmit antenna G_t, which can also be expressed as a function of the antenna area and signal wavelength λ:

$$G_t = \frac{\eta 4\pi A}{\lambda^2} \, watts/m^2 \tag{3}$$

where η is the antenna efficiency. This relation can be rearranged in terms of ηA, which is defined as the Effective Aperture Area, or A_e. The effective aperture of the antenna is related to the wavelength as follows:

$$A_e = \frac{G_r \lambda^2}{4\pi} \, m^2 \tag{4}$$

Substituting into equation 5 to find an alternative expression for P_r:

$$P_r = \left(\frac{P_t G_t}{4\pi d^2}\right) x \left(\frac{G_r \lambda^2}{4\pi}\right) \, watts \tag{5}$$

Rearranging to isolate terms:

$$P_r = P_t G_t G_r \left(\frac{\lambda}{4\pi d}\right)^2 \, watts \tag{6}$$

The last term in equation 6 is defined as the *free space path loss* L_{fs} and represents the natural reduction in strength as a signal propagates away from a transmitter. The free space path loss is proportional to the inverse square of the distance d from the transmitting antenna. Rewriting the equation in the more usual decibel representation:

$$P_r = \left(P_t + G_t + G_r - L_{fs}\right) dB \tag{7}$$

Equation 7 is an idealized representation of the total satellite link power budget. The effects of atmospheric propagation losses and noise associated with the environment and electronic systems must be taken into account before a reasonable estimation of the received signal quality can be made.

A fundamental requirement for acceptable satellite communications is the maintenance of a sufficiently high signal-to-noise ratio (S/N) on the link between the satellite and the ground

station. This ratio is often expressed as the Carrier power (C) to Noise power (N) ratio or C/N. The noise power in the received signal is the combination of the receiver noise power and the noise received from the sky (for the uplink) or the earth (for the downlink). Given the noise temperature of a source, such as the receiver and the sky, the noise power is given by:

$$N = k(T_r + T_{sky})B \tag{8}$$

where

k = Boltzmann's Constant

T_r and T_{sky} are the Receiver and sky temperatures respectively in Kelvin.

B = the Bandwidth of the receiver.

In decibel form, the downlink power budget equation is:

$$C/N = P_t + G_t + G_r - L_{fs} - L_{atmosphere} - 10\log_{10}[kB(T_r + T_{sky})] \quad dB \tag{9}$$

where:

P_t = Satellite Transmitter power in dBW

G_t = satellite antenna gain

G_r = Ground receiving antenna gain

L_{fs} = Free space path loss

$L_{atmosphere}$ = losses associated with the propagation of the electromagnetic signal through the atmosphere.

The uplink budget equation is identical to Equation 9 except that the T_{sky} is replaced with T_{earth}, the satellite receive antenna noise temperature due to the earth. In most digital communications systems, there will be a predicted Bit Error Rate *(BER)* for a given Carrier-to-noise (C/N). Usually C/N is converted to a ratio of Energy per bit (E_b,) to the Noise power per unit bandwidth or Noise Power Density (N_o,) in order to provide a standardized comparison. C/N

is related to E_b/N_o by the following relationship [LAR92]:

$$C/N = E_b/N_o + 10 \log R \tag{10}$$

where *R* is the data rate in bits per second (bps).

To receive a digital bit reliably, the amount of energy in the bit must exceed the noise spectral density by a specified amount. The E_b/N_o ratio provides a useful and universally accepted method of characterizing the probability of receiving an errored bit, an extremely important consideration in satellite communications. A typical curve of E_b/N_o, versus BER is shown in Figure 2.

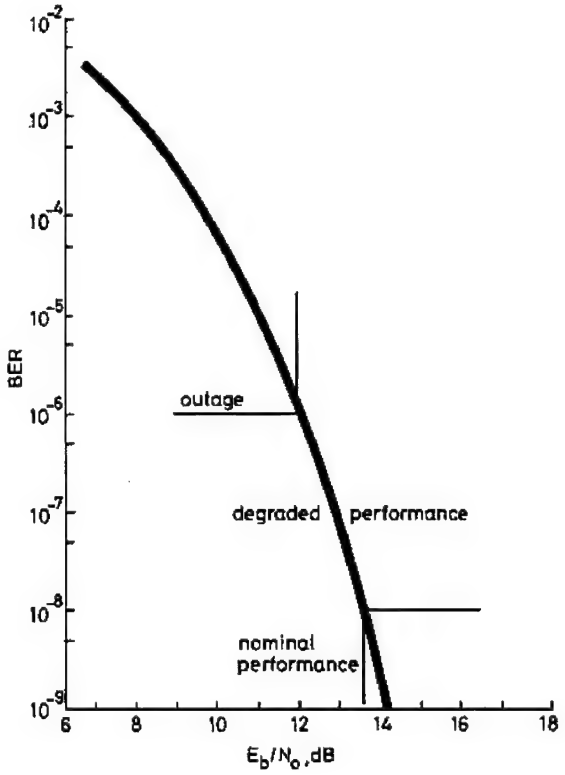

Figure 2 - BER vs. E_b/N_o [All89]

Equation 9 places into perspective the major factors which affect link quality. Most of the parameters are related to the system design or are otherwise outside of the immediate control of the user. The atmospheric effects which contribute to $L_{atmosphere}$ components are, however,

highly variable and depend on many factors. The analysis and prediction of these effects on the Iridium system is one of the primary focuses of this thesis.

2.8 Free Space Path Loss

As an electromagnetic wave travels away from an antenna, it experiences a natural reduction in its strength according to the square of the distance. The so called Free Space Loss is the major attenuation factor affecting satellite communications and is given by:

$$L_{fs} = \left(\frac{\lambda}{4\pi d}\right)^2 \tag{11}$$

An alternative expression which allows for the direct substitution of frequency (GHz) and range in km is:

$$L_{fs} = 92.4 + 20\log(Range) + 20\log(Freq) \tag{12}$$

where *Range* is in kms and *Freq* is in GHz.

This expression is often used for 'back of the envelope' calculations by radio engineers. The greatest range will be experienced when the satellite is low on the horizon (i.e., when the elevation angle is smallest). The practical limit for satellite communications, assuming an unobstructed path, is approximately 5°, although the simulations conducted in this study assume a lower limit of visibility of 8.2° for Iridium and 10° for Globalstar. The distance d from the satellite to a user at a certain elevation angle θ can be found by using Equation 13 [Lar92] below:

$$d = (R_e + h)\sqrt{1 + \left(\frac{R_e}{R_e + h}\right)^2 - 2\frac{R_e}{R_e + h}\cos(\theta)} \tag{13}$$

where R_e is the radius of the Earth (6378 kms), and h is the altitude of the satellite. The relationship between free space path loss, elevation angle and frequency is illustrated in Figure 3 and Figure 4.

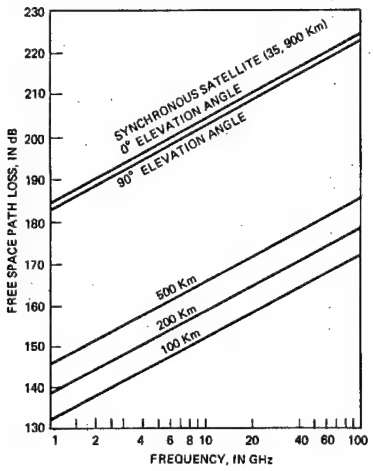

Figure 3 - Free Space Path Loss [Ipp86]

Note the degree to which higher frequency links suffer greater losses. This is important with Globalstar which utilizes different uplink and downlink frequencies. An idealized plot of free space path loss against varying elevation angles for both systems is illustrated in Figure 4.

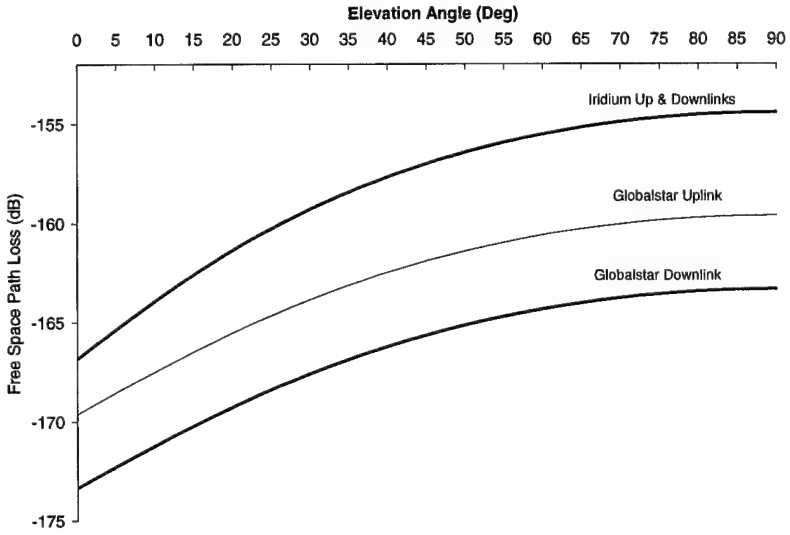

Figure 4 - Free Space Path Loss vs. Elevation Angle

As can be seen from Figure 4, the attenuation varies between its minimum when the satellite is directly overhead, to a maximum at the lower elevation angle constraint (Iridium - 8.2°, Globalstar - 10°). This calculation assumes a spherical earth. The deviation from these

results if a more accurate oblate earth model were used are negligible, although this is incorporated into the final constellation modeling. Note from Figure 4 that the effect of free space path loss is non-linear and most affects the lower elevation angles. Although the plots of elevation angle and path attenuation will follow the same basic shapes, the non-linear effects of free space path loss will tend to exaggerate differences at the low elevation angles, which becomes important at the lower latitudes. Accordingly, a plot or distribution of elevation angles cannot easily be re-scaled to provide link attenuation.

2.9 The Effect of the Atmosphere on Satellite Radiowave Propagation

A detailed discussion of the composition and structure of the earth's atmosphere is beyond the scope of this thesis, however, the characteristics which are relevant to a particular effect are introduced and described as required. Figure 5 illustrates the altitudes of the different layers showing the atmosphere's temperature and pressure profiles.

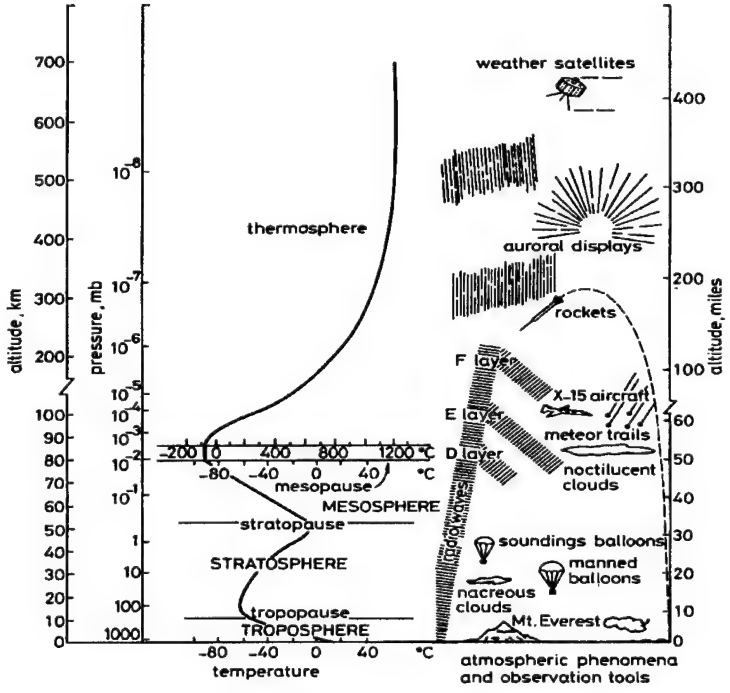

Figure 5 - Structure of the Atmosphere [All89]

For the purposes of developing an understanding of the atmospheric effects, it should be kept in mind that the atmosphere absorbs, reflects and refracts radio-waves at all frequencies to varying degrees. The clear air effects are mostly confined to the troposphere (where the earth's weather occurs) and stratosphere. The characteristic of the thermosphere which is most important to satellite communications is the ionization which occurs there, primarily as a result of the action of solar UV and x-rays. The ionized plasma which results forms a shell around the earth, called the ionosphere, affects electromagnetic waves below 10 GHz.

2.9.1 Propagation Mechanisms and Signal Effects

Before beginning a more detailed discussion of radiowave propagation in space communications, it is useful to introduce the general terms used to describe the propagation phenomena, or mechanisms, which can affect the characteristics of a radiowave. The mechanisms are usually described in terms of variations in the signal characteristics of the wave, as compared to the natural or free space values found in the absence of the mechanism. The definitions presented in Table 2 are intended to be general and introductory, nonetheless, the terms are often used incorrectly and a solid understanding is desirable. These propagation mechanisms impact one or more of the parameters or signal characteristics that can be observed or measured on a satellite link. The characteristics which are affected are its amplitude, phase, polarization, frequency bandwidth and angle of arrival [Ipp86].

Each of the propagation mechanisms affect one or more of the signal characteristics and it is usually not possible to determine the propagation mechanism responsible for a particular effect purely by observation or measurement of the change in the signal. Table 3 illustrates how each propagation mechanism can impact several signal parameters. For example, the reduction in signal level associated with rain in the link path is due to both absorption and scattering and it is important to differentiate amongst the mechanism, the effect and the cause.

Table 2 – Definition of Terms [IEE77]

Absorption.	A reduction in the amplitude (field strength) of a radiowave caused by an irreversible conversion of energy from the radiowave to matter in the propagation path.
Scattering.	A process in which the energy of a radiowave is dispersed in direction due to interaction with inhomogeneities in the propagation medium.
Refraction.	A change in the direction of propagation of a radiowave resulting from the spatial variation of refractive index of the medium.
Diffraction.	A change in the direction of propagation of a radiowave resulting from the presence of an obstacle, a restricted aperture, or other object in the medium.
Multipath.	The propagation condition that results in a transmitted radiowave reaching the receiving antenna by two or more propagation paths. Multipath can result from refractive index irregularities in the troposphere or ionosphere, or from structural and terrain scattering on the Earth's surface. The context of these effects in this thesis are addressed in Section 2.6.1. As it is not strictly an atmospheric effect, terrain induced multipath will not be addressed further in this thesis.
Scintillation.	Rapid fluctuations of the amplitude and the phase of a radiowave caused by small-scale irregularities in the transmission path (or paths) with time. Note that tropospheric and ionospheric scintillation have similar effects and share a common refractive mechanism, but the irregularities originate from different elements of the earth's atmosphere.
Fading.	The variation of the amplitude (field strength) of a radiowave caused by changes in the transmission path (or paths) with time. The terms fading and scintillation are often used interchangeably; however, fading is usually used to describe slower time variations, on the order of seconds or minutes, while scintillation refers to more rapid variations, on the order of fractions of a second in duration.
Frequency Dispersion.	A change in the frequency and phase components across the bandwidth of a radiowave, caused by a dispersive medium. A dispersive medium is one whose constitutive components (permittivity, permeability, and conductivity) depend on frequency (temporal dispersion) or wave direction (spatial dispersion).

Table 3 – Propagation Mechanisms to Signal Characteristics Cross Reference [Ipp86]

		MEASURABLE SIGNAL CHARACTERISTICS					
		Amplitude	Phase	Polarisation	Freq.	Bandwidth	Angle of Arrival
Propagation Mechanisms	Absorption.	X		X			
	Scattering	X	X	X		X	X
	Refraction	X	X	X		X	X
	Diffraction	X	X	X		X	X
	Multipath	X	X	X		X	X
	Scintillation	X	X				
	Fading	X					
	Frequency Dispersion				X	X	

2.9.2 Relevant Signal Propagation Impairments

Many of the propagation effects listed above are associated with a particular atmospheric condition or other propagation impairments. Many of the effects are dominant at either low or high frequencies. Ippolito [Ipp86] considers 3 GHz to be a point in the spectrum where a different set of factors begin to dominate, and 3 GHz is often considered a "turning point" in satellite communications where different propagation mechanisms become dominant. As Iridium and Globalstar user links operate below 2.5 GHz, there exists a temptation to incorporate only those effects which dominate below 3 GHz and dismiss those effects, such as rain attenuation, which generally have little effect for lower frequency links. However, the generally higher rainfall levels experienced in the region of interest, combined with the high probability of a low elevation angle path undermine this assumption. Accordingly, at this early stage all relevant communications impairments which fit within the scope of the study will be introduced and discussed. Those effects which may have an impact on link quality will be carried through to analysis in Chapter 4. Those propagation effects which will be discussed and modeled are briefly described below.

2.9.2.1 **Ionospheric Scintillation.** *Rapid fluctuations of the amplitude and phase of a radiowave, caused by electron density irregularities in the ionosphere.* Scintillation effects have been observed on links from 30 MHz to 7 GHz, with the bulk of observations of amplitude scintillation in the VHF (30-300 MHz) band [All89]. The scintillations can be very severe and can determine the practical limitation for reliable communications under certain atmospheric conditions. Ionospheric scintillations are most severe for transmission through equatorial, auroral, and polar regions; and during sunrise and sunset periods of the day. The modeling of this effect is a major part of this study.

2.9.2.2 **Gaseous Attenuation**. *A reduction in signal amplitude caused by the gaseous constituents of the Earth's atmosphere which are present in the transmission path.* Gaseous

attenuation is an absorption process, and the primary constituents of importance at space communications frequencies are oxygen and water vapor. Gaseous attenuation increases with increasing frequency, and is dependent on temperature, pressure, and humidity. [All89]. This effect will be incorporated in path modeling.

2.9.2.3 **Hydrometeor Attenuation**. *A reduction in signal amplitude caused by hydrometeors (rain, clouds, fog, snow, ice) in the transmission path.* Hydrometeors are the products formed by the condensation of atmospheric water vapor. Hydrometeor attenuation experienced by a radiowave involves both absorption and scattering processes. Rain attenuation can produce major impairments in space communications, particularly in the frequency bands above 10 GHz. Cloud and fog attenuation is much less severe than rain attenuation, however, it must be considered in link calculations, particularly for frequencies above 15 GHz. Dry snow and ice particle attenuation is usually so low that it is unobservable on space communications links operating below 30 GHz.

2.9.2.4 **Tropospheric Scintillation.** *Changes in the angle of arrival or the amplitude of a radiowave, caused by tropospheric refractive index variations.* The index of refraction of the troposphere at radio frequencies is a function of temperature, pressure, and water vapor content. Tropospheric refractive bending and amplitude fading can occur at frequencies above and below 3 GHz, but the problem is most pronounced at low elevation angles, i.e., 5° - 10°.

2.9.3 Effects Not Considered Further

The following effects, although relevant to satellite communications, are either out of the scope of this study, or are unlikely to affect the link quality.

2.9.3.1 **Polarization Rotation.** *A rotation of the polarization sense of a radiowave, caused by its interaction with electrons in the ionosphere, in the presence of the Earth's magnetic field.* This condition, referred to as the Faraday Effect, can seriously affect VHF space communications systems which use linear polarization. A rotation of the plane of polarization

occurs because the two rotating components of the wave progress through the ionosphere with different velocities of propagation. Faraday rotations of between .005 and 5 radians (0.3° to 285°) can occur at 1.6 GHz depending on the level of ionization within the ionosphere, with the effect decreasing with increasing frequency by the reciprocal of the frequency squared. As the antennas of the S-PCS mobile handset are most likely polarization independent, this effect will not be discussed further.

2.9.3.2 **Group Delay (or Propagation Delay).** *A reduction in the propagation velocity of a radiowave, caused by the presence of free electrons in the propagation path.* The group velocity of a radiowave is retarded (slowed down), thereby increasing the travel time over that expected for a free space path. This effect can be extremely critical for radio-navigation or satellite ranging links which require an accurate knowledge of range and propagation time for successful performance. Group delay will be about 0.5 μs at 1.6 GHz for an earth-space path at a 30° elevation angle, and is approximately proportional to $(1/f)^2$. The expected level of delay associated with this mechanism would be compensated for within the system handset or satellite and will not be included in detailed analysis.

2.9.3.3 **Multipath Fading and Scintillation**. *Variations in the amplitude and phase of a radiowave, caused by terrain and surface roughness conditions.* For a given terrain model, multipath and shadowing effects can be estimated given a distribution of path elevation angles. Nonetheless, the inclusion of terrain or structure induced multipath effects is complex and heavily dependent on the terrain model chosen. This thesis describes the distribution of elevation angles as a function of the user's latitude and further research may be able to employ this data to form more accurate multipath fading models.

2.9.3.4 **Radio Noise.** *The presence of undesired signals or power in the frequency band of a communications link, caused by natural or man-made sources.* The degradation of a signal's C/N is a natural consequence of atmospheric signal attenuation. However the impact of certain

ionospheric effects on the total noise budget may not be related to the level of fade in a straightforward manner and is beyond the scope of this thesis. However, the additional noise imposed on a link by atmospheric impairments would be included in a more complete study.

2.9.3.5 **Depolarization**. *A change in the polarization characteristics of a radiowave caused by (a) hydrometeors, primarily rain or ice particles; and (b) multipath propagation.* A depolarized radiowave will have its polarization state altered such that power is transferred from the desired polarization state to an undesired orthogonally polarized state, resulting in interference or crosstalk between the two orthogonally polarized channels. This study assumes that neither systems are sensitive to polarization changes, nor do they employ dual independent orthogonal polarized channels in the same frequency band to increase channel capacity. Under this assumption, the effect is not included in later analysis.

2.9.3.6 **Angle of Arrival Variations.** *A change in the direction of propagation of a radiowave caused by refractive index changes in the transmission path.* Angle of arrival variations are a refraction process, and generally are only observable with large aperture antennas (10 meters or more), and at frequencies well above 10 GHz [Flo87]. For obvious reasons, this impairment is not considered further.

2.9.3.7 **Bandwidth Coherence**. *An upper limit on the information bandwidth or channel capacity that can be supported by a radiowave, caused by the dispersive properties of the atmosphere, or by multipath propagation.* The coherence bandwidth for typical space communication frequencies is one or more GHz, and is not expected to be a severe problem, except for low elevation angle broadband links which must propagate through a plasma. Even then, the effects will probably be limited to fractions of a decibel [Ipp86].

2.9.3.8 **Antenna Gain Degradation.** *An apparent reduction in the gain of a receiving antenna caused by amplitude and phase de-correlation across the aperture.* This effect can be produced by intense rain; however, it is only observable with very large aperture antennas at

frequencies above about 30 GHz and for very long path lengths through the rain (i.e., low elevation angles) [Ipp86].

2.9.4 Magnitude of Non-Ionospheric Effects

Appendix A provides a collection of models which further describe the effects of hydrometeor attenuation, gaseous absorption and tropospheric scintillation. Models are also provided which allow the effects on a satellite link to be calculated. In order to assess their relative importance, an estimate of the effects of tropospheric scintillation, rainfall attenuation and gaseous absorption is provided in Figure 6.

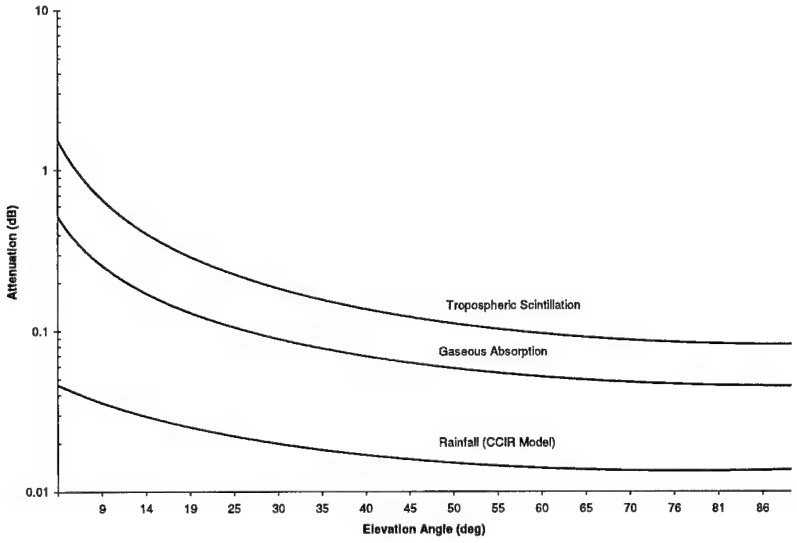

Figure 6 – Relative Effects of Non-Ionospheric Impairments

The JPL Database of Atmospheric Models [Ani98] was used to generate the plots in Figure 6. The models used to calculate the effects of tropospheric scintillation, gaseous absorption and rainfall are described in Appendix A. The effects are calculated for the Iridium downlink only (1.6 GHz) at the equator using standard models, for an exceedence ratio of 0.01%. That is, the levels of attenuation shown above are exceeded 0.01% of the time. The parameters used to calculate the levels of rainfall attenuation and gaseous absorption are typical for

equatorial latitudes. As can be seen, all three effects are minor in comparison with the levels of free space path loss predicted in Figure 4. Of the three effects modeled, tropospheric scintillation is substantially greater than rainfall or gaseous absorption. To illustrate the sensitivity of this effect to environmental parameters, the plot above is based on an antenna diameter of 5 cms at 55% efficiency, with humidity set to 70% and temperature to 20° Centigrade. At a higher temperature (35° C) and humidity levels (85%) commonly experienced at equatorial latitudes, the level of fade exceeds 4.5 dB at 5° elevation angle. Unfortunately, the difficulties associated with obtaining the required climatological input data precluded the incorporation of this effect in the study. Additionally, without accurate data regarding the handset's antenna diameter and efficiency, the fade figures are considered to be speculative at best.

In summary, although the effects of tropospheric scintillation are not included, they clearly have the potential to affect the link, especially at low elevation angles. Accordingly, this area represents an opportunity for further meaningful research. The effects of gaseous attenuation and rainfall, though minor, they are included in the modeling to provide additional accuracy. Ionospheric scintillation constitutes the most serious impairment and is discussed in the following section.

2.10 Ionospheric Effects

All satellite signals pass through at least a part of the earth's ionosphere. This region of the earth's atmosphere can affect signals to such an extent that communications (at certain frequencies) becomes impossible. Certain aspects of the ionosphere and their associated effects are reasonably well understood while others, such as ionospheric scintillation, are difficult to predict and potentially serious at L-Band frequencies. The dominant effects of the ionosphere are scintillation, rotation of the polarization (Faraday rotation), time delay of the signal, and frequency dispersion [CCI78, ITU531, All89]. As ionospheric scintillation is the dominant effect at L-Band frequencies, it will be discussed in more detail than the other effects. Ionospheric

scintillation is similar to the tropospheric scintillation effect described in Appendix A on page 139, but is due to scattering and refractive effects within the ionosphere. The ionosphere is a dispersive medium (i.e. it's index of refraction is frequency dependent) and radiowaves will diffract/refract at the edges of any irregularities in the medium. The resultant changes in the path of the radiowaves cause a complex process of reinforcement and cancellation of the signal waveform, which is observed as a rapid variation, or scintillation, in the intensity and phase of the received signal.

Factors which influence its severity include the time of the year, the local time, the level of solar activity (indicated by the sunspot number) and the level of geomagnetic activity (measured by planetary and local geomagnetic Indices). The prediction of the impact of ionospheric scintillation on a trans-ionospheric satellite signal requires the use of complex models which assess all these factors against a set of empirical data. In order to understand the morphology of the ionospheric scintillation phenomenon, and the principles underlying the operation of the models, a brief introduction to the nature and origin of these parameters is required. Additionally, as one of the objectives of this thesis is to provide an indication of the effect of ionospheric scintillation during the upcoming solar maximum, an introduction to the Solar Cycle is also provided. The following sub-sections provide the necessary background prior to a discussion of the chosen ionospheric scintillation model.

2.10.1 The Ionosphere

The ionosphere is one of the outermost layers of the earth's atmosphere. The radiation from the sun contains sufficient energy at short wavelengths to cause appreciable photo-ionization of the earth's tenuous atmosphere at high altitudes, resulting in a partially ionized region known as the ionosphere. As shown in Figure 7, the ionosphere is further divided into a number of layers denoted the D, E, F1 and F2, differentiated primarily by their photochemistry. Within the ionosphere, the recombination of the ions and electrons proceeds slowly, due to the

low gas densities, so that fairly high concentrations of free electrons persist even throughout the night [Tas94]. Figure 8 is a graph showing the electron density at various altitudes under typical conditions.

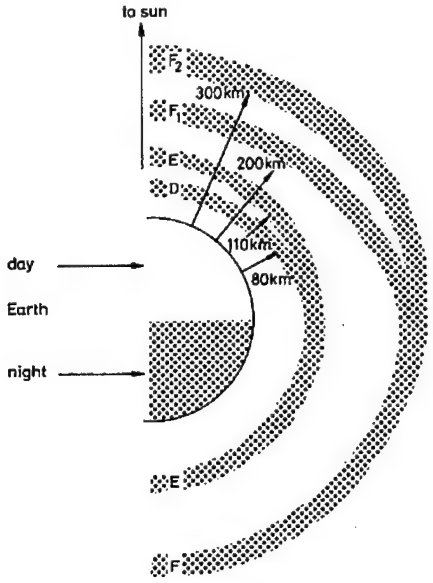

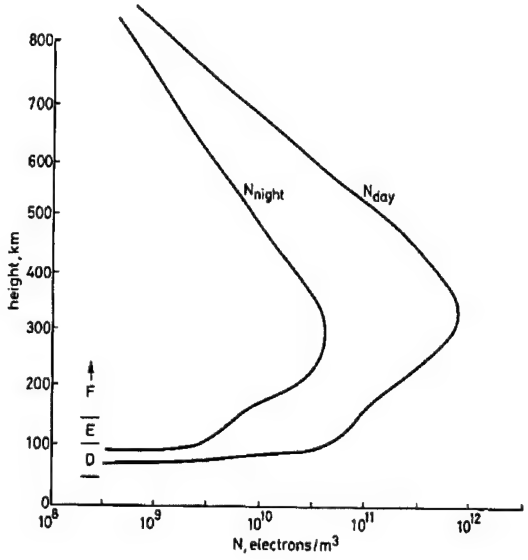

Figure 7 - Layers of the Ionosphere [All89]

Figure 8 - TEC Variation with Altitude [Tas94]

Note the higher concentration of electrons during the day due to photo-ionization, and the associated reduction due to recombination during the night. Note also the region of maximum ionization (the F2 region) at approximately 350 kms. In practice, the ionosphere has a lower limit of 50 to 70 kms, while the upper limit is not clearly defined. For the purposes of space communications, 2000 kms is often used, this being the limit for significant Faraday Rotation [Flo97]. Generally speaking, the background ionization has relatively regular diurnal, seasonal and 11-year solar cycle variations, and is strongly dependent on geographical locations and geomagnetic activity.

2.10.1.1 Calculation of Total Electron Content (TEC)

A number of effects, such as refraction, dispersion and group delay, are in magnitude directly proportional to the TEC. Consequently, knowledge of the TEC enables many important ionospheric effects to be estimated quantitatively. Denoted as N_T, the TEC can be evaluated by:

$$N_T = \int_s n_e(s)ds \tag{14}$$

where:

s = propagation path (m)

n_e = electron concentration (electrons/m^3).

Even when the precise propagation path is known, the evaluation of N_T is difficult because n_e has diurnal, seasonal and solar cycle variations. For modeling purposes, the TEC value is usually quoted for a zenith path having a cross-section of 1 m^2. The TEC of this vertical column can vary between 10^{16} and 10^{18} electrons/m^2, with the peak occurring during the sunlit portion of the day. The refractive and scattering effects which are believed to be the cause of ionospheric scintillation are related to the TEC gradients at irregularity boundaries.

2.10.1.2 Equatorial Ionosphere

Horizontal movements or winds occur in the ionosphere due to atmospheric solar and lunar tidal forces. The movement of charged particles in a magnetic field is analogous to a dynamo effect, resulting in an Eastward electric field during the day. This electric field exists in the Earth's magnetic field, which is almost horizontal at the geomagnetic equator. The electric fields in turn drive a current system, known as the electrojet, along the geomagnetic equator (see Figure 14) at an altitude of about 100kms and is concentrated in a strip only a few degrees wide in latitude. The current flows toward the east by day and the west by night, although the westward currents are almost unmeasurable due to the small electron densities at night.

The electric fields associated with the ionospheric currents generally drive a plasma convection in the F region at low geomagnetic latitudes that is upward and westward in the daytime and downward and eastward at night. The upward motion in the daytime raises freshly ionized plasma near the equator to great heights, where recombination is slow. Subsequent diffusion flow down the magnetic field lines under the action of gravity adds this extra plasma to that produced locally at higher latitudes. This phenomenon is referred to as the "Fountain Effect". The result of this plasma transport is that ionization peaks are formed in the sub tropics, one on each side of the magnetic equator, in a region termed the "Appleton Equatorial Anomaly". Figure 9 shows the location of the anomaly on either side of the geomagnetic equator.

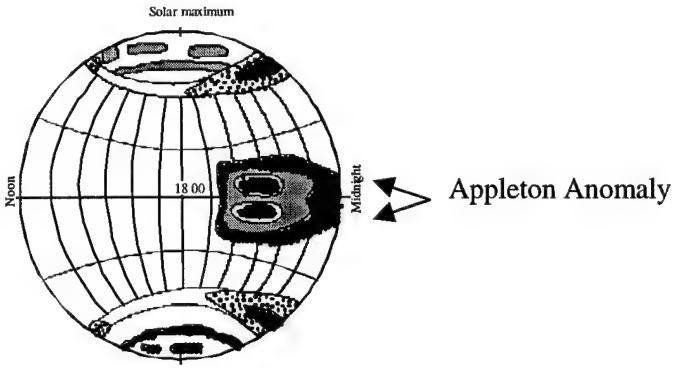

Figure 9 - Appleton Anomaly

The latitudes of the peak formation are often not symmetrical about the geomagnetic equator because the plasma transport along the magnetic field lines can interact with the neutral winds. The neutral winds usually cause plasma to be pushed from the summer to winter hemispheres near mid-day, so that the winter hemisphere anomaly is larger. Turbulence in the ionosphere is accompanied by rapid changes of electron density in both time and space that may last from several minutes to hours. At F region altitudes (225 – 400 kms), this instability is thought to be responsible for a spreading in depth of the ionosphere, a phenomenon termed "Spread-F". Equatorial Spread-F is almost exclusively a night-time phenomenon that is more

prevalent near the equinoxes. Under-dense plumes or bubbles of lower electron density (irregularities) propagate within the Spread-F region, and are influenced by geomagnetic field lines and electric field and drift rapidly, at velocities of up to 500 m/sec [Flo87] [Jur85]. The total electron concentrations, and hence the indices of refraction, are irregular at the boundaries of these bubbles, with changes in concentration as large as a factor of 10^2 to 10^3 in only a few kms. Scale sizes as small as 60 m have been observed from Atmosphere Explorer satellites, while the 50 MHz ionospheric research radar at Jicamarca in Peru extends this limit down to 3 m. Not only are the radar returns enhanced by up to 60 or 70 dB during spread F, but also these abnormal signals can appear in a time of less than 8 msec over regions of tens of kms.

2.10.1.3 The Solar Cycle

Ionospheric radiowave scintillation is associated with several factors, including the occurrence of sunspots. Sunspots are extended regions on the Sun with a stronger magnetic field but a lower temperature (3500° - 4500° K) than the surrounding photosphere (5800° K). The sunspots radiate less energy than the undisturbed photosphere of the Sun and are therefore visible as dark spots on the surface of the Sun. Sunspots were first observed by Galileo in 1610 shortly after he started observing the sun with his new telescope. Daily observations were started at the Zurich Observatory in 1749 and with the addition of other observatories continuous observations were obtained starting in 1849. The relative sunspot number R (or Wolf or Zurich number) remains as the single most important index for the general level of solar activity and is calculated according to

$$R = k(n + 10g) \tag{15}$$

Where;

n = Number of individual spots visible on the solar disk

g = number of sunspot groups

k = station constant

Although sunspots themselves produce only minor effects on solar emissions, the solar events and resultant magnetic activity that accompanies the sunspots can produce dramatic changes in the ultraviolet and soft x-ray emission levels. These events, such as solar flares and coronal mass ejections, influence the earth's magnetic field and the ionosphere. The Sunspot Number is a coarse proxy measure for the frequency and severity of these events. Changes in the level of overall solar activity have important consequences for the Earth's geomagnetic field and upper atmosphere.

One of the major characteristics of the Sun is the cyclic nature of its levels of solar activity. The sunspot record (extract in Figure 10) indicates the cycle has a mean period of 11.04 +/- 2.02 years; the period has ranged from 8.0 to 17.1 yr. since the first observed maximum in 1615 [All73].

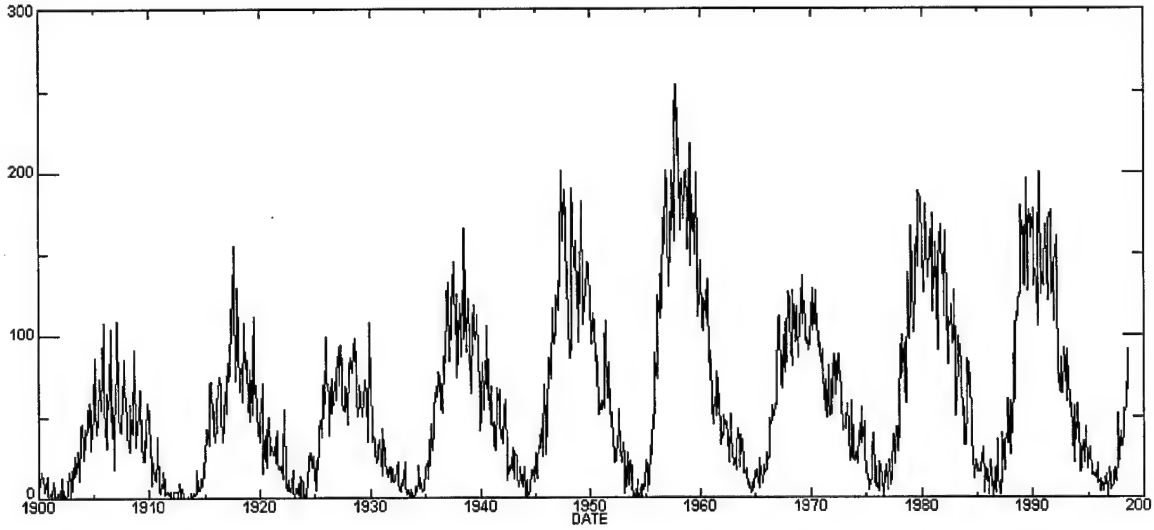

Figure 10 - Record of Sunspot Activity

The 22nd recorded sunspot cycle (termed: Solar Cycle 22) ended in 1996 and sufficient data has been collected on Solar Cycle 23 to predict its characteristics. Predictions from September 1998 [Jos97, Jos97-2, Tho98] indicate a maximum smoothed monthly sunspot number near 160 (between the values of 130 and 190) near March, 2000 (between June 1999 and January

2001). Figure 11 provides the most recent forecasts available. This data is provided in tabular form in Table 13 in Appendix B.

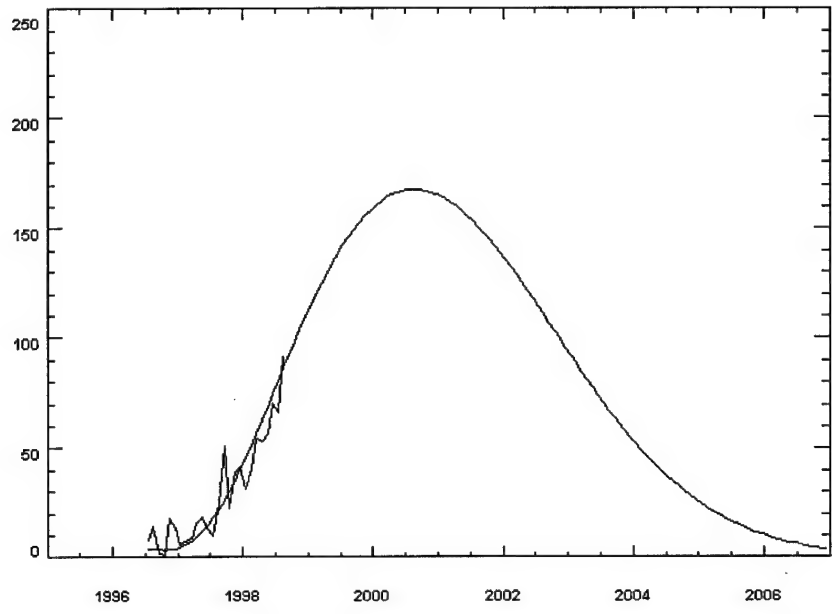

Figure 11 – Prediction Of Sun Spot Number for Solar Cycle 23 [Tho98]

2.10.1.4 Geomagnetic Activity

The temporal characteristics and intensity of ionospheric scintillation are also affected by the level of geomagnetic activity. The essential effect of geomagnetic activity is to delay the onset and dampen the severity of scintillation [Sec95]. Geomagnetic disturbances can be monitored by ground-based magnetic observatories recording the three magnetic field components (effectively x, y and z). The K-index is a quasi-logarithmic local index of the 3-hourly range in magnetic activity relative to an assumed quiet-day curve for a single geomagnetic observatory site. First introduced by J. Bartels, [Bar39] it consists of a single integer (0 to 9) for each 3-hour interval of the Universal Time day (UT). The planetary 3-hour-range index K_p is the mean standardized K-index from 13 geomagnetic observatories between 44° and 60° northern or southern geomagnetic latitude. (The name K_p originates from the German "*p*lanetarische *K*ennziffer" or "planetary index"). The scale for K_p is 0 to 9 expressed in thirds of a unit, e.g. 5-

is $4\ ^{2}/_{3}$, 5 is 5 and 5+ is $5\ ^{1}/_{3}$. This planetary index is designed to measure solar particle radiation by its geomagnetic effects. Since the K and K_p indices are quasi logarithmic, they are not suitable for simple averaging to obtain a daily index. The 3-hourly a_p index is the conversion of the Kp index to a linear scale. In order to obtain a linear scale from K_p, J. Bartels provides the following table to derive a three-hour *equivalent range* a_p index:

Table 4 – Geomagnetic Index Conversion Table [Bar39, Tas94]

K_p	0o	0+	1-	1o	1+	2-	2o	2+	3-	3o	3+	4-	4o	4+
a_p	0	2	3	4	5	6	7	9	12	15	18	22	27	32
K_p	5-	5o	5+	6-	6o	6+	7-	7o	7+	8-	8o	8+	9-	9o
a_p	39	48	56	67	80	94	111	132	154	179	207	236	300	400

This table is made in such a way that at a station at about dipole latitude 50°, a_p may be regarded as the range of the most disturbed of the two horizontal field components, expressed in the unit of 2 nT (nano Teslas). The A_p index (note upper-case A) is found by averaging eight, 3-hourly a_p readings to determine an average daily (24 hr) planetary index [Tas94].

In a similar manner to the predictions of Sunspot Numbers, geomagnetic average daily planetary indices (A_p) have been predicted for solar cycle 23. Joselyn [Jos97-2] predicts a maximum smoothed monthly A_p of 24.9 (95th percentile) in August of 2004 [Jos97, Jos97-2]. The WBMOD ionospheric Scintillation model requires the input of two K_p (3 hour) index values; the average value to be used over the run and the value at local sunset. Since the A_p values provided above are the average of eight 3 hour a_p observations, the value of K_p at sunset cannot be accurately determined. However, as solar cycle 23 is predicted to be similar in nature and behavior to the previous two cycles [Jos97, Jos97-2] historical values of K_p and a_p taken over the period of Solar Cycle 22 are able to provide an indication of the expected values. This data was provided by the Australian Ionospheric Prediction Service and is further discussed in Chapter 3.

2.10.2 Ionospheric Scintillation

One of the most severe potential disruptions along a trans-ionospheric propagation path for signals below 3 GHz is caused by ionospheric scintillation [Jur85, Ipp86, All89]. The scintillation effect is mainly the result of forward scattering and diffraction, where small-scale irregular structures in the ionization density cause scintillation phenomena in which the steady signal at the receiver is replaced by one which is fluctuating in amplitude, phase, polarization and apparent direction of arrival. In effect, the scattering and diffraction mechanisms cause a signal to bend in on itself, causing an unpredictable process of (sometimes intense) reinforcement and cancellation. As illustrated in Figure 12, it is the TEC gradient at the boundary of the irregularity which causes the bending of the signal.

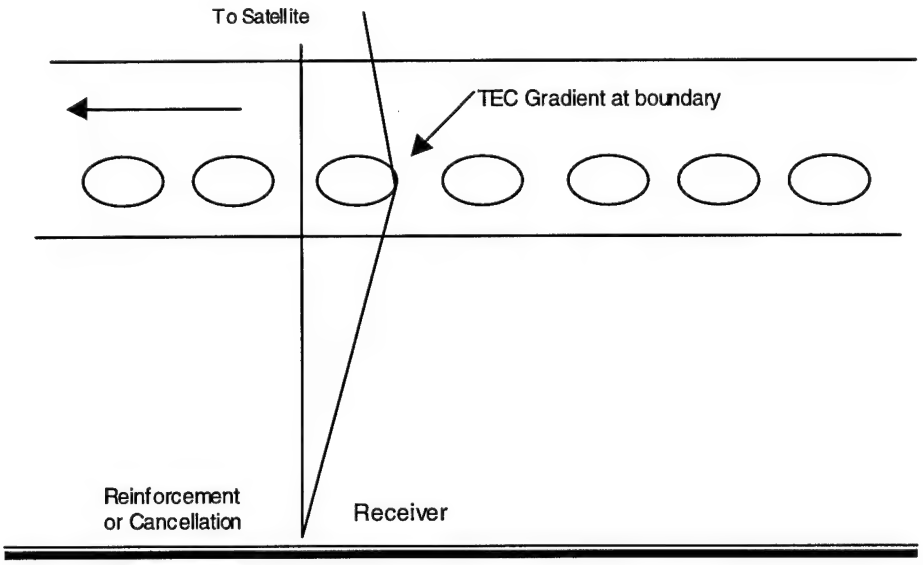

Figure 12 - Mechanism of Ionospheric Scintillation

It is the relative movement of these irregularities through the communications path which result in the rapid fluctuations of signal intensity. Note that faster moving low earth orbiting satellites, such as Iridium, would be more susceptible to ionospheric scintillation effects than geostationary satellites, due to the higher relative velocities [Tas94]. As noted in the figure, the scintillation process consists of reinforcement as well as fades. Of the total peak-to-peak

fluctuation resulting from scintillation, the ratio of reinforcement to cancellation would be approximately 1/3:2/3.

To illustrate the scintillation effect, Figure 13 shows a signal amplitude trace of ionospheric scintillation at GPS frequencies (1.5 GHz). Note the degree of variation in amplitude at the L1 and L2 frequencies of around 20 dB. This rapid fading is sufficient to cause most GPS receivers to lose lock completely. Additionally, the normal in-built ionospheric delay correction algorithms function less effectively in the presence of severe fading. Frequencies between 100 MHz (VHF) and 3 GHz (S-Band) are especially susceptible, although frequencies up to 11.5 GHz have been affected during intense solar activity [Oga80]. These ionospheric effects can ultimately determine a links effectiveness and availability, especially in equatorial regions where scintillation is generally more severe.

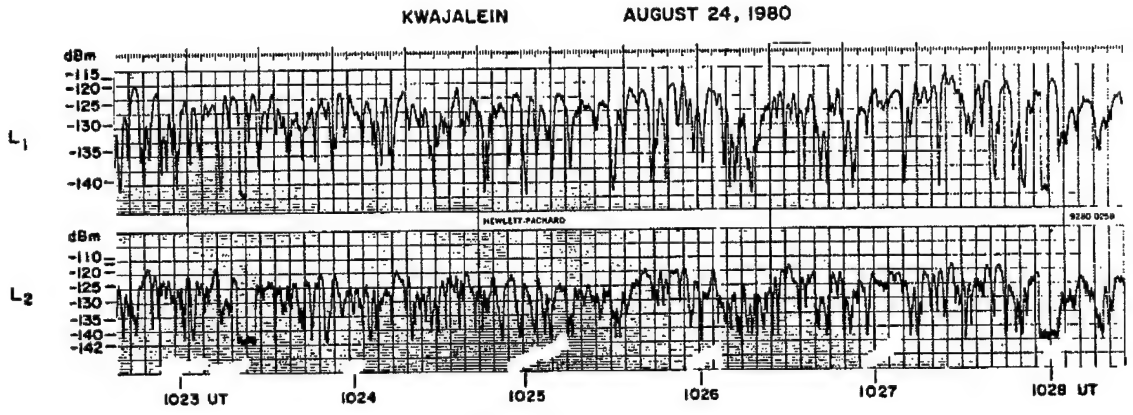

Figure 13 - Example of Ionospheric Scintillation [Jur85]

The most commonly-used parameter characterizing the intensity fluctuations is the Scintillation Index S_4, [All89] defined by:

$$S_4 = \sqrt{\frac{\langle I^2 \rangle - \langle I \rangle^2}{\langle I \rangle^2}} \tag{16}$$

where I is the intensity of the signal and $\langle I \rangle$ denotes averaging. In less formal terms, S_4 can be

described as the ratio of the standard deviation of the received power σ_x to the mean m_x, or:

$$S_4 = \frac{\sigma_x}{m_x} \tag{17}$$

Effectively, the index measures the time averaged fractional change in the amplitude of the wave detected by the receiver equipment. The index is used to grade the severity of scintillation, and an S_4 index of 0.5 has been defined as the demarcation between weak and strong scintillations, with receiver saturation generally occurring at a level of 1.0 [Jur85]. The parameter S_4 is associated with the variation of the amplitude of the received signal. Empirically, Table 5 provides a convenient conversion between S_4 and the approximate peak-to-peak signal fluctuations P_{fluc} (dB) to be expected.

Table 5 - Scintillation Index vs dB Fluctuation

S_4	P_{fluc} (dB)
0.1	1.5
0.2	3.5
0.3	6
0.4	8.5
0.5	11
0.6	14
0.7	17
0.8	20
0.9	24
1.0	27.5

2.10.2.1 Geographic, and Solar Cycle Dependence

Geographically, there are three intense zones of scintillation, two at high latitudes (North and South Polar regions) and the other centered within ± 20° of the geomagnetic equator. The geomagnetic equator differs markedly from the normal 0° latitude geographic equator, as shown in Figure 14. A pictorial representation of the locations of increased disturbance and the predicted scintillation fades is shown in Figure 15. Note from Figure 14 and Figure 15 that the

location of peak Ionospheric scintillation in the Appleton Anomaly places the area of maximum impact within the region of operations of the Australian Defense Force.

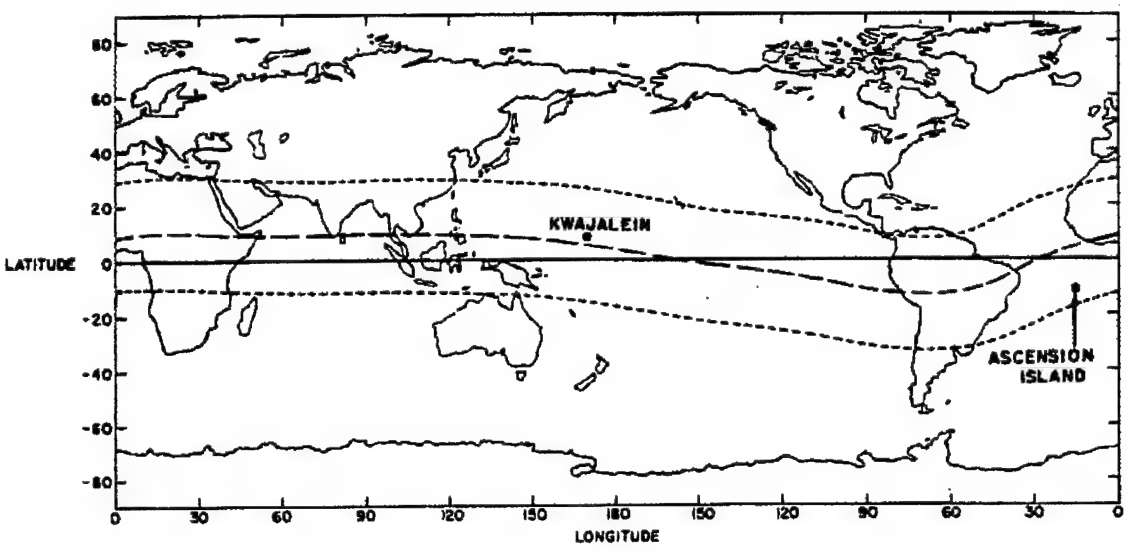

Figure 14 - Geomagnetic Equator [Tas94]

Severe scintillation has been observed up to several (≈ 4) GHz in the Appleton Anomaly, while in the middle latitudes scintillation mainly affects VHF signals. From empirical data taken at the peak of Solar Cycle 21, fading levels of 5-7 dB average and >20 dB peak were experienced

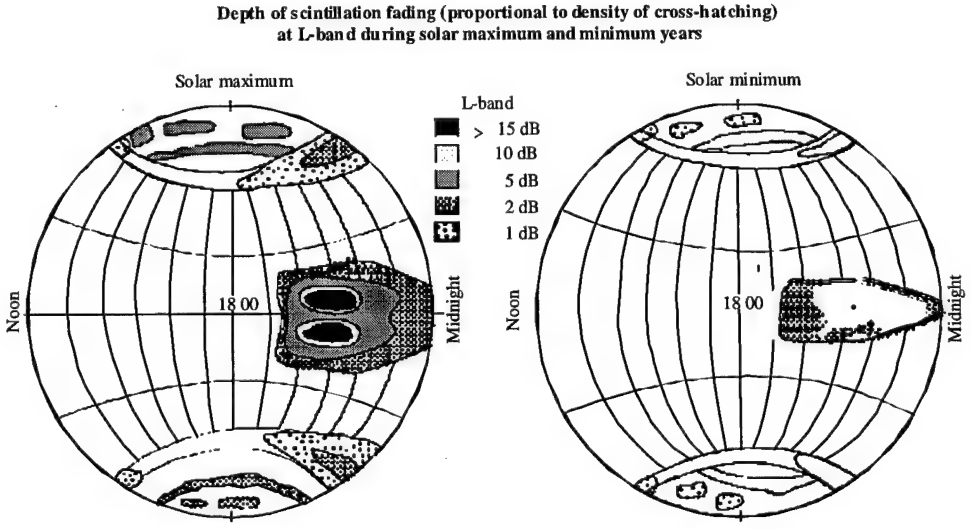

Figure 15 - Regions of Elevated Ionospheric Scintillation [Flo87, Jur85, ITU97]

on an L-Band (1.542 GHz) maritime satellite link for 10% of the time. Additionally, isolated peaks of greater than 25 dB fade sustained for several seconds [All89]. In all observed instances, there is a pronounced night-time maximum of activity as indicated in Figure 15. A summary of scintillation characteristics is provided in Table 6 below.

Table 6 - Summary of Solar and Temporal Dependence [All89]

SUN SPOT NUMBER DEPENDENCE	TEMPORAL DEPENDENCE
Strong correlation between annual scintillation occurrence and the annual sun-spot number	Annual scintillation activity varies in an 11-year cycle in concert with solar sun-spot cycle
Strong correlation between the amplitude of the scintillations and the monthly sun-spot number	Peak annual scintillation activity occurs at or just after the equinox periods
No strong correlation between individual scintillation event occurrences and daily sun-spot number	Peak daily scintillation activity occurs approximately one hour after sunset at the ionospheric height

Ionospheric sunset occurs later than terrestrial sunset due to the altitude of the ionosphere. A typical scintillation event has its onset after local ionospheric sunset and an event can last from 30 min to hours. For equatorial stations in years of solar maximum, ionospheric scintillation occurs almost every evening after sunset, with the peak-to-peak fluctuations of signal level at 4 GHz exceeding 10 dB in magnitude [Ram97].

2.10.2.2 The WBMOD Scintillation Prediction Model

The WBMOD program provides estimates of the level of scintillation, both intensity and phase, which may be experienced on a transionospheric propagation path defined by the user. The estimates are based on climatological models of the global distribution and behavior of the ionospheric F-region plasma-density irregularities that cause the scintillation, and on a single-regime power-law propagation theory to calculate the scintillation levels [Sec96]. The model used in this analysis has been updated to incorporate measurements taken at five additional equatorial stations over periods ranging from 1976 to 1989. The nature of the improvements and a comparison of the model predictions with actual measured results is provided in [Sec95].

The propagation model implemented in WBMOD is that described in [Rin79]. This model assumes that all propagation is line-of-sight, and that the scintillation effects can be calculated as though the effect of the ionospheric irregularities can be ascribed to an infinitely thin, phase-changing screen set at some altitude within the irregularity layer. A propagating ray passing through the screen will have its phase changed according to the refractive characteristics of the irregularities, and the resulting intensity and phase scintillation will develop as the ray propagates beyond the screen to the receiver. Two scintillation indices are calculated using Rino's theory: the standard deviation of phase, σ_{ϕ}, and the standard deviation of the signal power normalized to the average received power, S_4. The S4 index can be used to calculate the intensity fade which is the parameter described in this thesis.

2.10.2.3 Model Limitations

The model cannot predict the short term effects of Ionospheric Scintillation as it does not model the distribution of individual plume structures. It derives a set of conditions from the input parameters and applies it equally across the sky for a particular moment in time. The model cannot be used in the same manner as a rain or gaseous absorption model, where levels of fade are directly and instantaneously related to the prevailing physical conditions. The results must be interpreted as long term worst case levels. Accordingly, by taking the relevant parameters from the orbital model and applying initial conditions (SSN, K_p, local time etc), the output describes the worst case levels of fade which could be experienced under those conditions. The actual levels of fade will depend upon whether the transmission path passes through an irregularity. The short term variations in the levels of fade which are evident in the output plots are due to the changes in the relative position and velocity of the satellite and the user. Nonetheless, the model still provides valuable data regarding the maximum level of fade and the likely variations which may be experienced as a result of the changes in the satellite's relative position and velocity.

All of the data used in developing the environment models was taken from satellites at altitudes in excess of 800 km. Since the scintillation effects are imposed at the phase screen (nominal altitude of 350 km), the results for scenarios in which the satellite end of the system is at altitudes below 800 km will tend to over-estimate the scintillation levels. This effect will increase as the altitude of the satellite decreases. As the height of the Iridium satellites are 780 kms, the effect of this limitation should be minimal. Finally, only F-region irregularities are included in the model.

2.11 Review of Relevant Literature

A major part of this study consists of characterizing the link between a user and the Iridium and Globalstar constellations. Although a review of the available literature indicates no equivalent studies have been conducted, several papers are available which focus on the comparative performance of the two constellations. Notable amongst these are two theses by Naval Postgraduate School students Stelianos and Ciocco. Ciocco [Cio96] focuses on the channel capacity of the systems based on an analysis of the modulation and multiple access schemes, and Stelianos [Ste96] addresses the suitability for military use of several systems, including Iridium and Globalstar. Both of these studies describe many of the system characteristics, mainly taken from their FCC filings. Although general references to the impact of a user's latitude are contained within the papers, neither provides meaningful data that would allow the objective assessment of link characteristics.

In describing the characteristics of the Iridium constellation, Siwiak [Siw97] provides an expression for the PDF and CDF of elevation angles, and plots the median and minimum elevation angles as a function of latitude. On initial inspection, this information appears to preempt the research presented in this thesis. However, the expression for the PDF is based on a single satellite and does not represent a valid expression for the PDF and CDF of the Iridium constellation as a whole. The expression for the distributions cannot easily be adapted to

different latitudes or integrated to form a single latitude-dependent expression for all elevation angles. Siwiak also provides a plot which describes the median and minimum elevation angles of the Iridium system. However, the author does not indicate if the analysis is based on all available satellites, or the highest path. If the plot is intended to represent all available elevation angles, then the data is in error as it shows the minimum path angle increasing as latitude rises. Clearly, satellites will always be available at the minimum elevation angle, regardless of the user's latitude. If the author intended to describe the median and minimum elevation angles after the paths were processed to obtain the best angle, then the graphs provide a reasonable approximation to the findings in this study. Notwithstanding this, the author does not provide any details of the analysis, nor is the performance contrasted against any other system.

Keller [Kel97] performs a comparative analysis of the elevation angle probability of four S-PCS systems; Globalstar, Iridium, Odyssey and ICO. The paper does not address the distribution of elevation angles per se, rather, it provides a lower limit of elevation angle, given a certain probability and number of satellites the user wishes to acquire. The data is limited in that it appears to be valid only at +/-60° and provides no simple method of extracting absolute satellite visibility probabilities. Nonetheless, one of the plots contained within Keller's work does provide data which agrees with the results obtained in this study to within approximately 15%. However, Keller does not provide data on different latitudes, nor does it address path attenuation, and azimuth distributions.

CHAPTER 3

ANALYSIS AND MODELING METHODOLOGIES

3.1 Introduction

The purpose of this chapter is to describe and support the methods used to achieve the objectives of the research, and to properly define the scope and limitations of the chosen methods. In Section 3.2, the required outputs are defined to provide a baseline, followed by a description of the method and process used to meet the objectives. In Sections 3.5 and 3.6, the orbital and atmospheric models are described and all assumptions, settings and parameter selections stated. In Section 3.7, the processing methods used to obtain the required results are described, followed by a discussion of the verification process.

3.2 Required Outputs

The intention of this research is to characterize the transmission path to the Iridium and Globalstar S-PCS systems in terms of a user's latitude. To achieve this, the following data is required for each latitude increment:

- Tables and plots showing the number of satellites in view as a proportion of the total observation time.
- Probability density and time-plots of elevation and azimuth angles to all satellites which meet the visibility constraints.
- Elevation angle, azimuth and attenuation distribution and time-plots of the path to the highest satellites.
- Details of the distribution which most closely fits the available elevation angle data.
- Data showing the degree of fading due to Ionospheric Scintillation.

It is important to state that this study is not intended to portray one system's performance as superior to the other. The study focuses on the geometry of the path and the conclusions and analysis cannot be used solely to determine the final quality of communications or the reliability of the link. There are many differences in the design and operation of the two systems and the determination of communications quality is based on many factors, path characteristics being only one aspect.

3.3 Method of Analysis

There are at least three methods of generating the data required to satisfy the requirements as stated; direct measurement, analytical modeling and simulation. The requirement to gather data at a number of latitudes precludes the direct measurement of link parameters. The employment of analytical methods would require the generation and integration of a complex set of equations describing the relative movements of two large LEO satellite constellations. Simulation is relatively straightforward as software packages exist [STK40, Sat20] which account for all of the potential physical effects including solar and lunar gravity and the non-spherical shape of the earth. Additionally, these packages have in-built functions which perform the complex calculations required to determine relative position and velocity vectors. This specialized data is required as input for the model used to predict the effects of ionospheric scintillation.

Given that simulation is the most appropriate method of producing the data, the selection of the most appropriate software package was based on three major factors. The availability of standard and tailorable reports, the ability to express relative positional and velocity data in a variety of coordinate frames, and the availability of a variety of standard gaseous and rain attenuation models all determined the most suitable package.

3.4 Overview of Process

An orbital simulation package was used to model each of the constellations and simulate the path to a user. Simulated users were located at 5° increments in the northern hemisphere along the 135° longitude line. The establishment of the meridian line at 135° reflects the area of interest for the Australian Defense Force. Due to the natural symmetry of the constellations around the equator, most aspects of the path are identical for a user located at the same latitude in either the either Northern or Southern hemispheres. Additionally, most aspects of the analysis are insensitive to a user's longitude. The ionospheric effects, being related to location of the geomagnetic equator and other factors is the exception. Figure 16 describes the higher level process employed to achieve the objectives of the report.

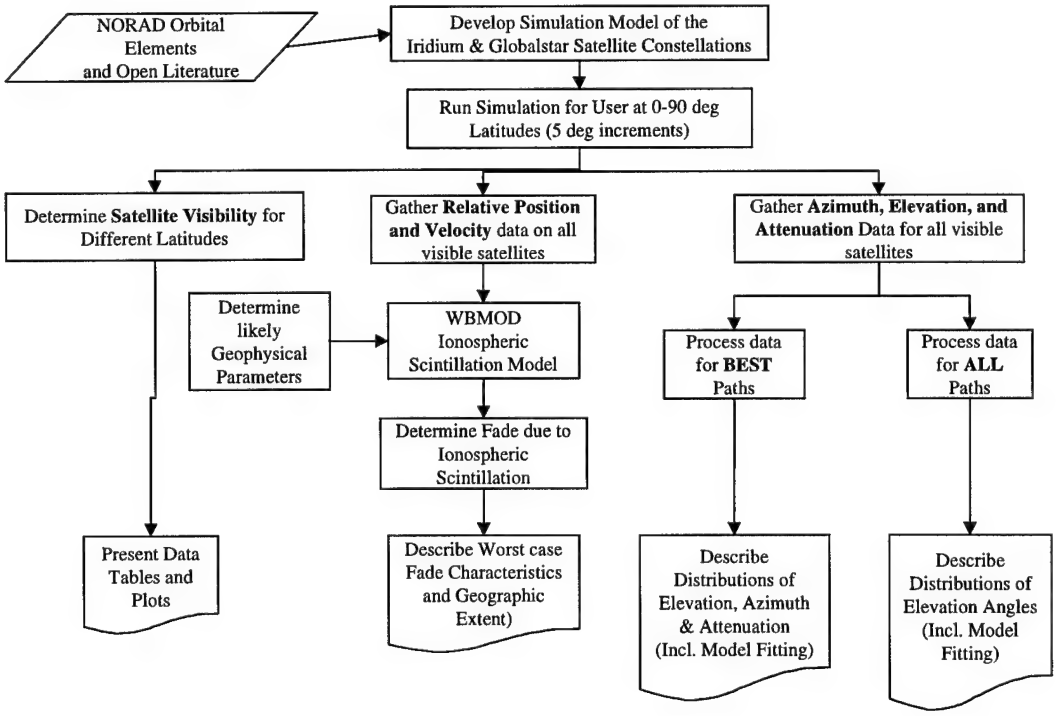

Figure 16 – Analysis Process Flowchart

Following the process shown in Figure 16, a commercial orbital software simulation package was used to create the two constellations using the orbital parameters described in Chapter 2. The simulation package was then configured to generate Iridium and Globalstar path

geometry, link losses and satellite data, which was then processed for presentation, or for input to WBMOD. To achieve this, a custom report was designed which provided 14 individual parameters for each observation. These consisted of Time (seconds), X, Y, Z position and Velocity vectors (meters) relative to the user, Azimuth (deg), Elevation (deg), Range (km), Free Space Path Loss (dB), Rain Attenuation based on the users position calculated using the CCIR method (dB), gaseous attenuation (dB) and total link attenuation (dB). The file was exported as a comma delimited text file for later processing by MATLAB [MAT98]. MATLAB code was written which scanned the STK output data files and identified each satellite observation, and recorded the transitions. From this data set, records of satellite visibility, number and average duration of satellite observations per day were extracted.

The data was processed to remove erroneous observations and output to a file of elevation and azimuth angles. This data was later processed using Expert Fit for distribution model fitting. The file was reprocessed to create a second data set detailing the path to the highest satellite. This data was used to model elevation angles and link attenuation distributions. Additionally, the position and velocity data was processed to generate an input file for WBMOD. WBMOD in turn generated scintillation fade predictions for three sets of environmental conditions. At all major points in the analysis, MATLAB produced plots to illustrate the results of the analysis. Some manual manipulation and merging of data was required, this was done using Microsoft Excel Version 7.

IBM compatible Personal Computers (233 MHz Pentium Processor with 64MB RAM) were used to run the orbital simulations and process data. The generation of the reports from STK required approximately 20 minutes per facility and had to be manually configured for each satellite in the constellation. Seven separate MATLAB programs were run to process the data from each latitude and each of these took on average 20 minutes. The total machine processing time is estimated at 90 hours. This excludes the time required to reformat data for different programs and conduct the distribution fitting process using Expert Fit and SAS-JMP [JMP97].

3.5 Simulation Model

SatLab [Sat20] and Satellite Tool Kit [STK40] were compared against the processing requirements defined above. STK was assessed as providing the required level of functionality without requiring the user to utilize and establish links to a separate modeling package (BONeS Designer in the case of SatLab). Nonetheless, SatLab was used to create certain specialized figures (e.g. Figure 27) and a review of the most recent release indicates at least equivalent functionality to STK. Iridium and Globalstar simulation models were created in STK as two independent constellations using the orbital parameters described in paragraph 2.2. The orbits were propagated using the J2 propagator with animation and reporting intervals of 30-seconds. The J2 propagator accounted for the oblate shape of the earth and more accurately models the path of the satellite over a lengthy period.

Each of the 19 facilities was equipped with a receiver with QPSK modulation and right hand circular polarization characteristics to allow STK to calculate link budget data. STK requires a receiver and transmitter be placed at each end of the link in order to generate the link attenuation data. Although several different receiver parameters were specified, they are not irrelevant to this study as the parameters are used to calculate other specifications such as G/T, C/N or EIRP. Similarly, although a transmitter was simulated on each satellite, apart from the frequency, the parameters were not relevant to the analysis.

The frequencies used in the simulation affect the levels of ionospheric scintillation, as well as free space, rain and gaseous absorption losses. Downlink transmission frequency for Iridium was specified at 1620 MHz and Globalstar at 2500 MHz. These frequencies were also used in other models and calculations requiring the specification of frequency. None of the models exhibited a substantial level of sensitivity to frequency, and output attenuation levels varied typically by less than 0.01dB across the range of allowable frequencies.

3.5.1 Specification of Atmospheric Impairments

The CCIR rainfall model was utilized rather than the Crane Global Model for the calculation of attenuation due to rainfall. An exceedence rate of 0.01% was selected, being a commonly used level specified in open literature. As the levels of attenuation calculated did not typically exceed 0.4 dB for the link, the value of repeating the analysis at varying exceedence levels was deemed to be limited. Likewise, the levels of attenuation due to gaseous absorption rarely exceeded 0.2 dB at a water vapor level of 7.5 g/m^3 @ 20° Centigrade. Variations within the limits normally experienced caused negligible variation from this low value. All other parameters were set at default values which did not affect the calculation of link losses.

3.5.2 Period of Simulation

With the constellation model in place, a period of simulation must be selected which correctly represents and includes all characteristics and relevant events. The ideal situation is to determine the period for the constellation to repeat itself (i.e., the period of time taken for the same satellites to be in the same points in the sky at the same time of the day). In more concise terms, the constellation will repeat when the time for an integer number of satellite orbits coincides with an integer number of sidereal days. Therefore, for a constellation with satellites that orbit the earth 2 times per day, the constellation will repeat every 24 hours (disregarding precession). In the case of Iridium, each satellite (as modeled) orbits the earth approximately 14.35 times per day, indicating a period of 6020.91 seconds. Analysis of these parameters indicates that the number of Iridium orbits required to get the satellites within 500 seconds of their original starting point on the earth's surface would require 2467 orbits or 171 days 23 hours 40 minutes of simulation time. To get within 100 seconds would require 12,331 orbits or 2 years 129 days and 7½ hours. Finer levels of agreements required commensurately longer simulation times. The situation is similar for Globalstar with over two years required to get within 100 seconds of the original starting point. Simulations for durations such as these are beyond the

capabilities of the software packages and would require an inordinate amount of processing time and disk space. Given that the entire data population base was prohibitively large, a shorter simulation time which provided a representative sample was required. In order to determine the optimum simulation time, the cycles contained within the satellites' movements were inspected, and a statistical analysis conducted on several sample runs.

In order to determine the optimum time, the characteristics of the movements of the satellites from the point of view of a stationary observer were examined. To allow a stationary user to pass under each of the orbital planes, a simulation period which captures at least one complete revolution of the earth under the entire constellation is required. This would capture the contribution provided by all regularly spaced planes, as well as the 22° separation between Iridium's first and sixth planes. Accordingly, the simulation must be at least 24 hours long.

With an understanding of the cyclic nature of the Iridium constellation, a statistical comparison was conducted on several different simulation times. To determine the simulation run time which provided a representative distribution of elevation angles while balancing the overhead associated with processing all observations, several orbital simulations were performed for a user located at the equator. Table 7 provides a moment comparison of four different simulation periods.

Note that the 100,000-second simulation time period at 30-second sample time agreed with the longer 1,000,000 second run to within 1% in average, median, variance and all major percentiles. Although longer simulations at shorter sample periods were run, negligible changes in the distribution characteristics occurred when lengthening the period of observation beyond 100,000 seconds. Accordingly, a simulation period of 100,000 seconds was selected based on a balance of processing time and accuracy.

Table 7 – Iridium Elevation Angle Moment Comparison

Observation type	4 Hours - 30 Second Sample Period	12 Hours - 10 Second Sample Period	28 hrs - 30 Second Sample Period (100,000 Secs)	277 hrs - 30 Second Sample Period (1,000,000 Secs)
Minimum observation	8.199	8.199	8.199	8.199
Maximum observation	87.609	87.609	87.609	87.609
Average	21.41904	22.79638	21.698	21.48
Median	17.698	17.99	16.692	16.698
Variance	206.0679	214.3445	204.59	206.38
Coefficient of variation	0.6702	0.64223	0.65	0.6688
Skewness	1.65078	1.52563	1.6129	1.6313
Kurtosis	5.73849	5.18497	5.5754	5.632
1st percentile	8.199	8.199	8.199	8.199
5th percentile	8.79925	8.5616	8.1999	8.1992
10th percentile	9.19995	9.286	9.0809	9.0999
90th percentile	40.6914	43.7238	42.011	42.003
95th percentile	53.677	54.3764	52.29	52.913
99th percentile	71.18094	72.78064	71.647	71.676

A similar analysis was conducted for Globalstar constellation. Simulations were run for 12 hours, and 1, 3, 5 and 14 days to establish the optimum simulation time. The statistical analysis indicated 24 hours to be acceptable. Negligible changes in the distributions of elevation angles were observed beyond this point.

3.6 Ionosphere Scintillation Effects

The WBMOD ionospheric scintillation model predicts the level of fade given certain environmental, temporal and geographic parameters. The selection of these factors dramatically affects the levels of predicted fade and it is important to select a plausible and realistic combination that a user would reasonably experience. The following input parameters to WBMOD are discussed: day of year, sunspot number, geomagnetic activity level, and exceedence level. Due to the number of variables and the requirement to frame the worst case effects, only two levels of solar activity and one level of geomagnetic activity are selected. One parameter is varied between the first and the second, then a second parameter is varied between the second and

the third. This approach maximizes the diversity of environmental factors, while ensuring that effects are compared because only one parameter is being changed between scenarios.

3.6.1.1 Exceedence Levels

Exceedence levels were set at 99%, providing reasonable certainty that the effects predicted would not be exceeded for most (99%) of the time. The use of this figure is believed to be both intuitively useful, and in line with normal telecommunications practices.

3.6.1.2 Sunspot Number

For the solar activity level, Figure 11 and Table 13 in Appendix B show the predicted levels of sunspot numbers for the current (#23) solar cycle. The two levels chosen are 160 and 80, the first representing the worst case peak, the second representing a more frequently occurring level with a broader likelihood. Lower levels of solar activity are not modeled. Sunspot levels of above 80 are likely between July 1988 and April 2003, while the peak of 160 is likely to be experienced between June 1999 and January 2001. Both of these periods are within the period of commercial operation of Globalstar and Iridium.

3.6.1.3 Day of the Year

As detailed in Chapter 2, scintillation effects are worst at the equinox (shortest day) and least at the solstice (longest day). These two dates correspond approximately to days 80 (March 20) and 180 (June 28) respectively for the Northern Hemisphere. Note that there are two equinoxes and solstices per year and their occurrences are different for the Northern and Southern hemispheres. For the Northern hemisphere, a second equinox and solstice occur on 21 December and 22 September respectively.

3.6.1.4 Geomagnetic Indices

Ionospheric scintillation is moderated by high geomagnetic activity levels and WBMOD requires the user to specify the value of K_p valid for the duration of the simulation, and the value at the time of the previous local sunset. Given that the objective of the study is to define a

realistic upper level of fade intensity that a user could reasonably expect when deployed to affected regions, a frequently occurring value of K_p should be chosen which is known to be associated with high levels of ionospheric scintillation. To enable reasonable estimates to be made, the advice of the Ionospheric Prediction Service of Sydney Australia was sought. The data received [Tho98-2] was processed to provide provides forecasts of Kp index values for the remainder of Solar Cycle #23. The processed data is reproduced in Figure 17.

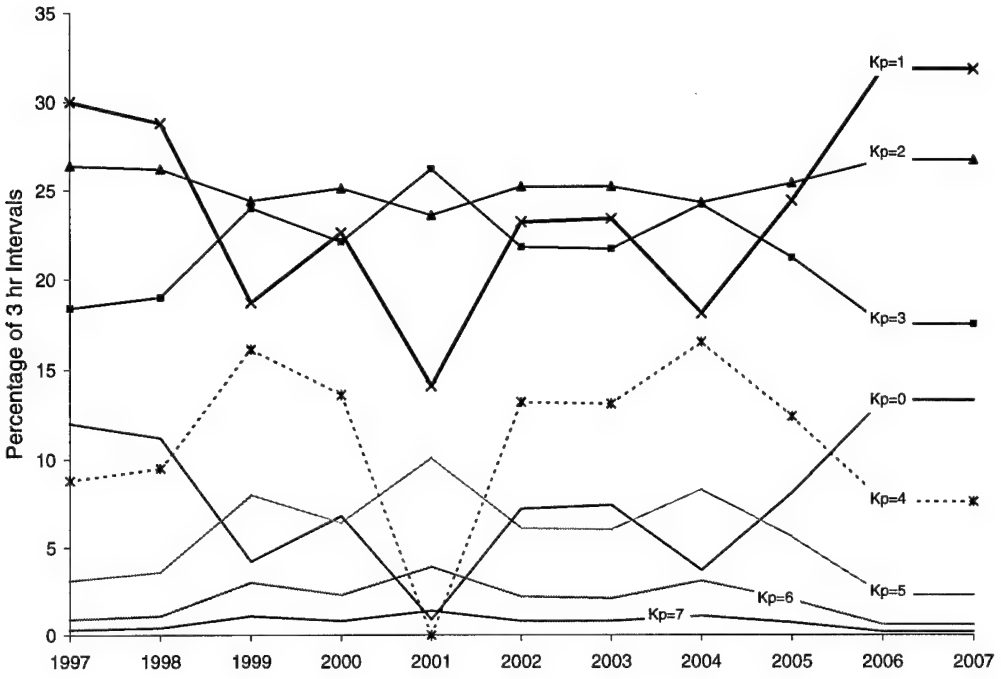

Figure 17 – Kp (3 Hr Index) Prediction for Cycle 23

The plot shows eight lines representing the percent occurrence of different levels of 3 hourly geomagnetic activity. The three most frequently occurring levels are K_p = 1, 2 or 3, and K_p = 1 (bold line) was chosen as a balance between the most frequently occurring and the level that would produce the highest fading. A K_p value of one was also used for the sunset value. Based on these assumptions, three sets of environmental parameters were assembled into representative scenarios for modeling.

3.6.1.5 Environmental Scenario #1

Worst case with high sunspot number of 160 at equinox (day 80) with K_p level of one. These conditions could reasonably be expected around March 2000 and represent the combination of environmental factors which would produce the highest levels of ionospheric scintillation.

3.6.1.6 Environmental Scenario #2

Moderate case with high sunspot number of 160 at solstice (day 180) with K_p level of one. These conditions could reasonably be expected around June 2000. The later day of the year would be expected to reduce the level of fading.

3.6.1.7 Environmental Scenario #3

Moderate case with medium sunspot number of 80 at Equinox (day 80) with K_p level of one. These conditions could reasonably be expected to occur between July 1998 and May 2003, especially around the March and December equinoxes. Note the broad range of times that the conditions could be met or exceeded. This is the prime reason for the inclusion of the lower sunspot number, which could be expected to reduce the magnitude of the effects.

The modeling is intended to provide an understanding of the range of possible effects by defining three sets of conditions most likely to be associated with scintillation. The solar and geomagnetic conditions specified under these different scenarios are not limited to specific times of the year. The levels of ionospheric scintillation are dependent on a variety of solar, temporal and geographic parameters and an unfavorable combination of conditions may occur any time throughout the year. For example Figure 18 represents the monthly variation in sunspot numbers around the smoothed 12 month moving average for Cycle 22.

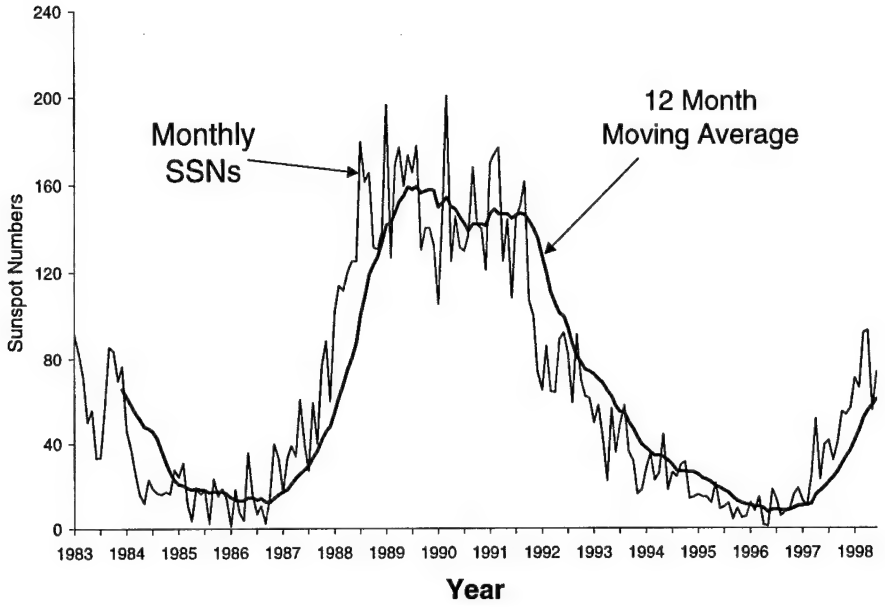

Figure 18 – Monthly and Smoothed Sunspot Numbers [NOA99]

As can be seen, the values vary significantly around the average, indicating that the levels of solar activity defined in the three scenarios may occur outside the limited range of times indicated. Based on a wider analysis of all recorded monthly sunspot numbers (since 1749), levels greater than 80 have been observed 21.45% of the time.

3.6.1.8 Best Path Analysis

Modeling was conducted on the best path available for both constellations under the three different sets of environmental conditions and the processed results are presented as separate Iridium and Globalstar graphs. The raw fade levels are presented as a plot covering a 24 hour period. The fading levels are then combined with the free space and the gaseous absorption losses associated with that latitude to provide a total fade profile, again over a 24 hour period. This latter profile represents the total possible path attenuation when all relevant effects are taken into account.

Note that the selection of the best path did not include consideration of scintillation levels in the analysis. The highest satellites were chosen, and scintillation fades were overlaid onto the

existing path losses. Consideration was given to combining scintillation fading with free space and gaseous attenuation for all available links in any 30 second interval, then choosing the lowest level of attenuation as the best path. The processing would then choose the path which minimized all attenuating effects, including scintillation. This method was rejected as the results would be of limited relevance due to the unpredictable nature of scintillation. In contrast with the relatively stable and predictable atmospheric losses, a relatively small change in any of the environmental parameters would change the scintillation profile and render the path selection invalid.

3.6.2 Other WBMOD Model Parameters

Several other parameters and settings are required for WBMOD. For simplicity and ease of interpretation of the results, one-way, satellite-to-ground communications is specified. If two-way communications is specified, a level of correlation between the scintillation experienced on the uplink and downlink is required. The behavior of this aspect of Iridium and Globalstar receivers is unknown, and the degree of correlation would have required separate study to ascertain. The systems are specified as phase insensitive for similar reasons to those above. Finally, the internal models for the outer scale of the irregularity spectrum and drift velocity are used, rather than specifying separate custom parameters.

3.6.3 Alternative Ionospheric Scintillation Models.

A second model provided by the International Telecommunication Union (ITU) under Recommendation ITU-R P.531-4 "Ionospheric Propagation Data and Prediction Methods Required for the Design of Satellite Services and Systems" (May 1997) is also available. The model uses empirical data taken from two stations as a basis for the prediction of scintillation effects. To employ this model, the user must estimate effects graphically, based on a limited selection of empirical data. Additionally, a frequency scaling approximation allows the user to

adapt the data to different frequencies. In contrast to this method, the WBMOD scintillation model incorporates readings from several stations and has been refined to incorporate equatorial effects. It estimates the effects of satellite relative position and velocity and provides the capacity to read from a file of orbital data. The WBMOD model is available from North West Research Associates [Sec97] at no charge to USAF personnel. For these reasons, the ITU model is not used in this analysis.

3.6.4 Caution on Interpretation of Results

The models used in WBMOD are based on empirical data collected at a number of sites over several years each. The levels and duration of the fades predicted from these models are the most severe a user could reasonably expect within 99% of the time, if a link was operated under the defined conditions. Scintillation is actually related to the unpredictable movements of ionospheric irregularities across the signal's path, and the prediction of individual fades is not currently possible. The WBMOD model assumes that an irregularity was distributed evenly across the sky and interfered with all signals passing through it (i.e. that scintillation conditions are continuously active). Accordingly, the actual fading effects are extremely unlikely to be continuous, as shown in the model outputs.

3.7 Data Processing Methods

The data produced from the orbital simulation must be processed to obtain the required outputs. MATLAB [MAT98] and Expert Fit [Exp98] were used to perform the bulk of the data processing while many of the plots and minor processing tasks conducted using Excel Version 7.0. Full listings of the MATLAB code are included at Appendix F. and the methodology behind several of the main modules is discussed below.

3.7.1 Number of Satellites in View

The number of satellites in view is important in determining the benefits of satellite diversity and link redundancy. STK provides accurate start and stop times for each individual satellite's visibility, and this data must be processed to determine cumulative visibility statistics. Two methods of processing this data were assessed.

Time Step Method: Consists of reading satellite access statistics into a matrix and stepping through in small steps to determine how many satellites were visible over the duration of the time step. In order that the processing times are not prohibitive, a time step in the order of 5-10 seconds is used. Figure 19 shows two problems associated with this method.

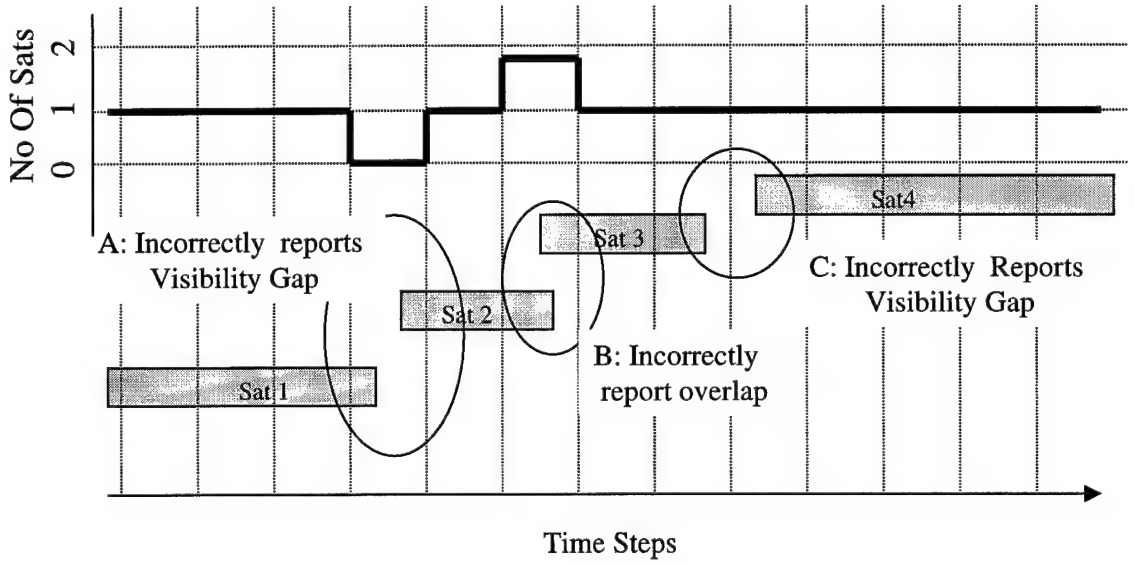

Figure 19 – Time Step Method Problems

The dotted vertical lines represent time steps, and the solid bars indicate satellite accesses (i.e., when a satellite moves into or drops out of visibility). Under this processing method, each transition must be moved to its closest time step. The solid trace on the upper axis shows the processed output. Under this method, satellites which appear or disappear close to each other (i.e., less than the time step seperation) may be incorrectly lumped together. This is illustrated in the three circled areas (A, B and C in Figure 19) and the resulting incorrect upper trace. Although

for short periods the effects on the visibility statistics will be limited, the problem does tend to distort the data. Regardless what the time step and number of processing steps, some form of truncation or approximation is required when a continuous data set is converted to discrete observations, and some level of error will result.

Transition Method: The transition of every satellite into and out of view is tracked with no rounding or approxinmation of the actual transition time. A transition into view is assigned a value of '1', and a transition out of view is assigned a value of '-1'. The series of transitions is then integrated to determine the number of satellites in view at any time. Figure 20 illustrates the additional accuracy obtained when using this method.

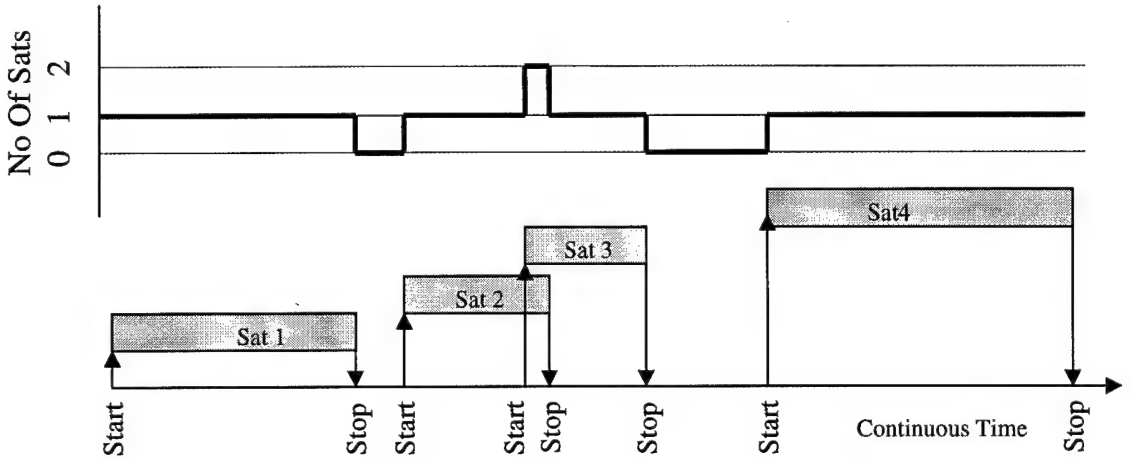

Figure 20 – Transition Method

The use of the transition method requires the development of additional code, however it avoids the problems associated with ambiguous readings, which may cause the actual satellite visibility to be misrepresented. This factor is considered especially important in the equatorial regions where periods with no satellites above the minimum elevation constraint is considered possible.

3.7.2 Distribution of all Elevation Angles

STK was configured to take observations at 30 second intervals for latitudes between the equator and 90° at 5° increments. Data is collected for Azimuth and elevation angles, as well as the range to all visible satellites. When tracking a satellite, STK starts recording path data when a satellite rises above the lower elevation angle limit. The satellite is tracked and report lines written to file at 30 second intervals, with a final observation when the satellite drops below the lower elevation constraint. The final observation can come before the end of the 30 second interval and may not represent a valid reading. Figure 21 illustrates the process of acquiring a satellite at the minimum elevation angle, taking readings every 30 seconds as the satelite passes overhead, and the insertion of the closing reading as the satellite drops out of view.

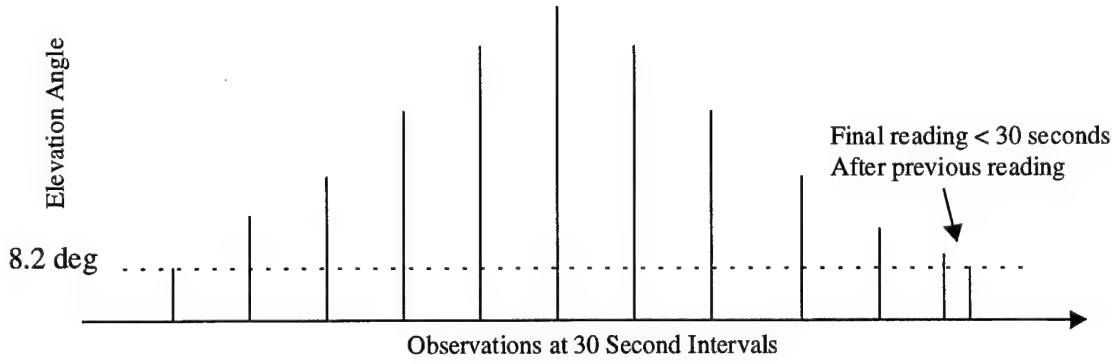

Figure 21 – Final Reading Problem

These closing readings must be removed by post-processing the data. A MATLAB program was written which identified the final reading, and applied a user specified time filter to determine whether the observation was discarded or retained. If the closing observation occurs within the filter time, it is rejected as invalid. In order to determine the sensitivity of the data to different filter values, an analysis was conducted to determine the effect of the filter and the optimum filter setting. Four filter values (15, 20, 25 and 29 seconds) were applied to a full data set of Iridium elevation angles taken from the equatorial facility. As the filter value was increased the number of "invalid" samples removed increased also. The analysis revealed that

approximately 3% of samples were removed when the maximum 29 second filter was used. These samples were all at the minimum elevation value (8.2°). Shorter filter times resulted in a lower rate of rejection. The analysis demonstrates that the effect of applying a filter is minimal and a filter value of 20 seconds was selected as a reasonable mid-range value. The application of this filter value rejects readings which are not sustained for at least $^2/_3$ of the 30 second observation period.

3.7.3 Best Elevation Angles

The STK simulation package provides details on all available paths, with a corresponding timestamp for each observation. A scatterplot of all elevation angles to an equatorial station accessing the Globalstar constellation is provided in Figure 22.

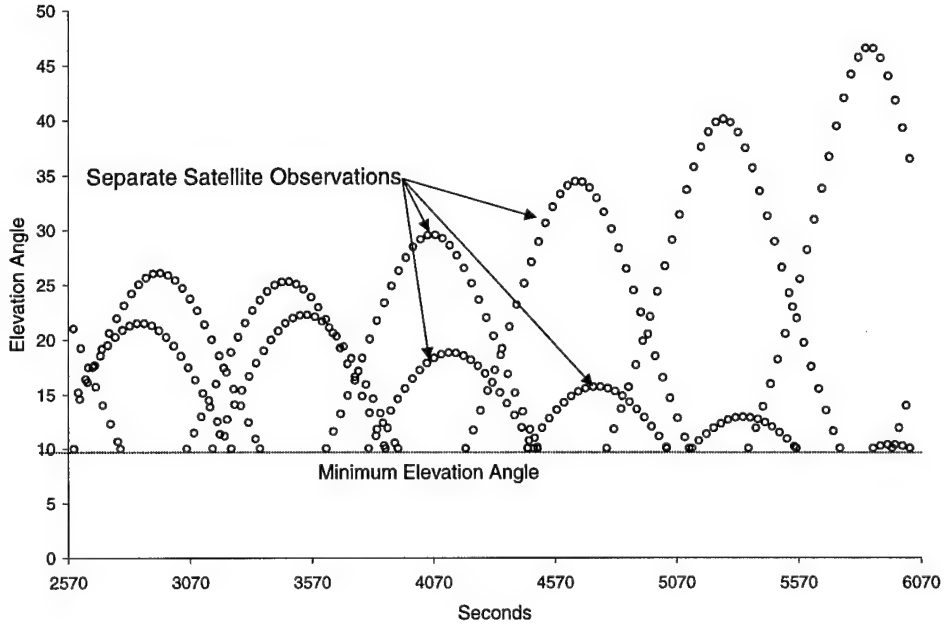

Figure 22 – Scatter-plot of All Elevation Angles

Each circle in the figure above illustrates a satellite observation, and each of the curves represents a separate satellite moving into and out of view. Note the periods of multiple satellite observations where several curves overlap. To determine the best path, a moving 30 second

'window' was used to capture all observations within a 30 second period. The highest path within the 30-second period is recorded, which is effectively represented by the drawing a curve on the top of the points in Figure 22.

To provide a cross check, two parameters are checked in determining the best path; the link attenuation level, and the elvation angle. The observation with the highest elevation angle was compared with the path of least attenuation; if the paths are to different satellites, a caution flag is set to alert that there is a conflict between the two paths. In all cases, the path with the highest elevation angle coincided with the path with the least attenuation. Once identified, this observation is written to a separate matrix for analysis.

3.7.4 Coordinate Transformations for WBMOD

WBMOD normally relies on the input of data directly from the keyboard. The user inputs the characteristics of a single transmission path, or provides the start and stop points of a circular orbit. In order to determine the full range of scintillation effects relevant to each constellation's geometry, and to allow comparison of the scintillation levels with the path characteristics, a more comprehensive input method is devised. The WBMOD reads correctly formatted file data directly and calculates scintillation fade levels and other parameters such as S_4 index levels and phase variance. The data must be provided in a file with the following characteristics [Sec96]:

TIME:	Number of seconds since Midnight (GMT).
SLAT and SLON:	Satellite LATitude and LONgitude in spherical-earth coordinates (degrees positive (+) North and +East).
SALT:	Satellite ALTitude above a spherical earth of radius 6371.2 kms.
V_X, V_Y and V_Z:	Components of the satellite velocity in the local (+North, +East, and +Down) coordinate system in m/s.

The data derived from the STK simulation provides the position of the satellite in Cartesian (X, Y, Z) coordinates relative to the center of the earth (Earth-Centered-Earth-Fixed (ECEF)) with X pointing to Greenwich, England, and Z pointing towards the North Pole. The velocity components are provided in the same reference frame. Coordinate transformations are required before the data can be input to WBMOD. The following transformations describe the process used in this study and are adapted from [Bat71]:

Step 1: Convert User's Lat/Lon/Alt (LLA) spherical coordinates to geocentric Cartesian coordinates:

$$\begin{aligned} x_{ecef} &= r_{\oplus}\cos(\lambda)\cos(\delta) \\ y_{ecef} &= r_{\oplus}\cos(\lambda)\sin(\delta) \\ z_{ecef} &= r_{\oplus}\sin(\lambda) \end{aligned} \tag{18}$$

where λ = Latitude, δ = Longitude and $r_{\oplus}$ = radius of the earth.

Step 2: Translate the origin of the $[XYZ]_{sat}$ coordinates to the user's position:

$$\begin{bmatrix} x \\ y \\ z \end{bmatrix}_{satellite}^{ecef} = \begin{bmatrix} x \\ y \\ z \end{bmatrix}_{satellite}^{user} + \begin{bmatrix} x \\ y \\ z \end{bmatrix}_{user}^{ecef} \tag{19}$$

Step 3: Calculate the LLA of the satellite for input to WBMOD:

$$\begin{aligned} Altitude &= \sqrt{x^2 + y^2 + z^2} - r_{\oplus} \\ \lambda &= \tan^{-1}\left(\frac{z}{\sqrt{x^2 + y^2}}\right) \\ \delta &= \tan^{-1}\left(\frac{y}{x}\right) \end{aligned} \tag{20}$$

Step 4: Rotate the ECEF relative velocity components first around the z-axis by the longitude of the user (135°), then around the y-axis by the latitude (0° - 90°):

$$\begin{bmatrix} x_{vel} \\ y_{vel} \\ z_{rel} \end{bmatrix}_{ecef} = \begin{bmatrix} \cos(\lambda_{user}) & 0 & \sin(\lambda_{user}) \\ 0 & 1 & 0 \\ -\sin(\lambda_{user}) & 0 & \cos(\lambda_{user}) \end{bmatrix} \times \begin{bmatrix} \cos(\delta_{user}) & \sin(\delta_{user}) & 0 \\ -\sin(\delta_{user}) & \cos(\delta_{user}) & 0 \\ 0 & 0 & 1 \end{bmatrix} \times \begin{bmatrix} x_{vel} \\ y_{vel} \\ z_{rel} \end{bmatrix}_{user} \quad (21)$$

The positive down direction of the relative velocity required by WBMOD is opposite to that provided by the transformation and the sign of the z component must be reversed prior to employing it to generate the input files to WBMOD. The WBMOD model is not sensitive to small positional or velocity differences, so that the earth's oblateness was neglected for the conversion. All of the above transformation matrices were implemented in MATLAB to operate on the STK generated simulation outputs. The process was verified against a test data set provided in the WBMOD user guide.

3.8 Distribution Fitting

Expert Fit Version 1.5 is used to determine which probability distribution provides the most accurate representation of certain data sets. Data was prepared using custom MATLAB code and written to a text file which was read directly into Expert Fit and analyzed. Data files ranged from 2500 samples to Expert Fit's upper limit of 8000 samples. Each data type is analyzed using three separate bounding techniques using the guided fitting facility. The data statistical moments of mean median, variance skewness and kurtosis are then compared to determine the model which provided the most consistent best fit across the data sets. Lower bounds were set at the minimum sample observation, 0° or the lower elevation limit (8.2° or 10°). The upper limit was set at infinity for the first two and 90° for the last. A single distribution did not necessarily provide an ideal fit across the data sets. At several points, the chosen distribution represents a compromise against the convenience of using a single distribution.

3.8.1 Error Definition Method

The use of a distribution to approximate empirical data is not prudent unless the user is aware of the level of error associated with the fitting process. The method chosen to describe the level of error is to define each distribution with two scores: the mean and maximum error. The mean score represents the average distance between the model line and the data as a proportion of the total sample size. The maximum score is simply the maximum excursion between the data and best model fit.

As an example of the nature of the mean and maximum error values, Figure 23 below shows the distribution of all elevation angles Globalstar for a user located at 35° latitude (Florida) with two instances of the Johnson S_B model fitted against the sample.

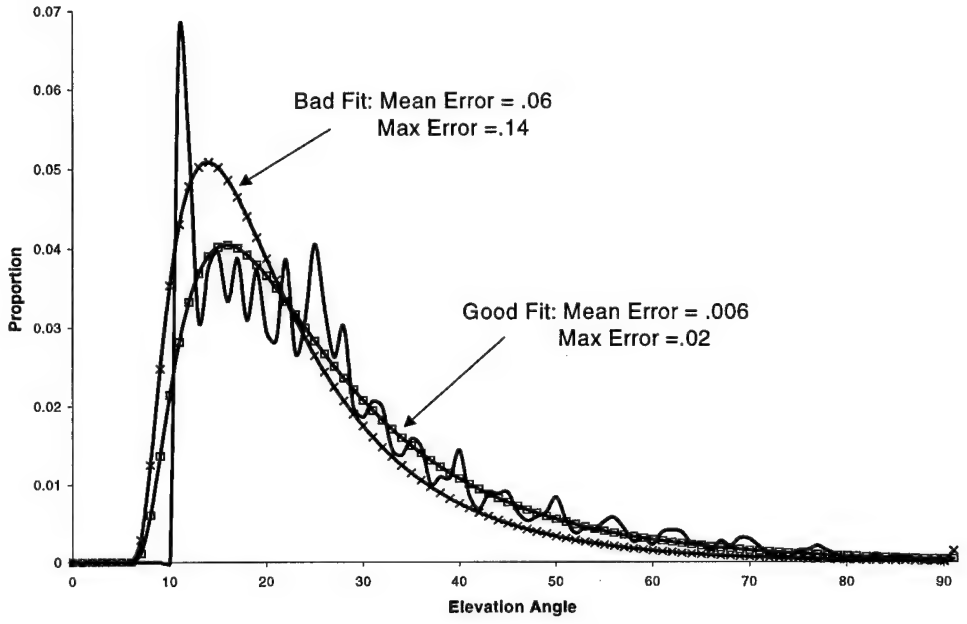

Figure 23 – Illustration of Model Fit Error Scores

The data set is represented by the uneven line and the two curves represent the two attempts at fitting the data set with the same model. The mean and maximum error scores are shown on the graph and graphically represent the goodness of the fit. Note the degree of error between the sample and the "bad Fit" curve. In this case, the maximum error is confined to the

lower latitudes. The sample data in Figure 23 is based on a histogram bin size of 1° elevation angle. The large number of values between 10° and 11° tend to exaggerate the magnitude of the lower two bins. For this reason, the excursions between the model fit and the sample data appear large at low elevation angles. This is mainly a byproduct of the histogram bin size selection rather than an indication that the model does not match at these values. Note that this method of defining the error is independent of the bin size chosen to represent the data histogram. When representing a distribution as discrete bin histogram, a larger bin size naturally increases the proportion scale on the vertical axis. A very narrow bin size will have smaller numbers on the proportion scale because more bins contain a smaller proportion of the sample size. Therefore, the error reported should not be compared against the vertical scale of any of the histograms presented in this analysis.

Another interpretation of the error score is through the use of the distribution comparison plot provided in Expert Fit. This plot shows the differences between a sample and the model as a proportion of the total sample size in a continuous graphical form. As an example, Figure 24 below shows three fits to the distribution of Iridium best elevation angles for 15° latitude

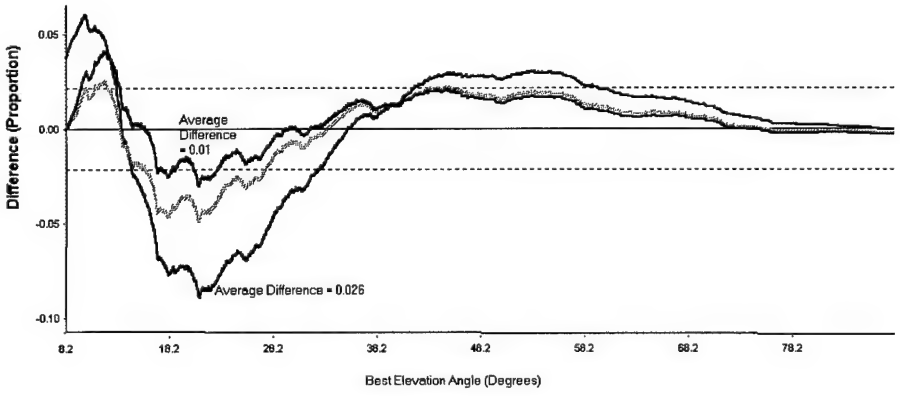

Figure 24 – Differences Plot

The scores on the vertical axis are the errors between the sample data and the model approximations. The makers of Expert Fit urge the user to exercise caution if the distribution lies outside the horizontal dotted lines on the plot.

3.9 Verification and Validation

Verification processes were conducted at several steps to ensure the models, methods and algorithms were functioning as intended and that there were no coding problems or errors of logic. The primary methods of verification were through the application of test data, comparison with known good data, manual recalculation using separate models, and inspection of outputs for consistency with orbital principles. Additionally, as detailed in Chapter 2 (background section), Iridium and Globalstar constellations were compared against NORAD observations wherever possible.

Due to the possibility of ambiguity in the selection of STK's in-built model parameters, the levels of free space path loss, rain attenuation and gaseous absorption predicted were compared against the levels calculated by the methods outlined in Chapter 2. In all cases the results were identical (for Free Space Path Loss) or within 0.1 dB for other losses. The discrepancies with the calculation of rainfall losses and gaseous absorption were traced to minor differences in the specification of parameters and interpretations in the boundaries of the rain graphs. Personal correspondence with Analytical Graphics [Joh98] verified that the same sets of equations were being used by STK's internal models and those detailed in Chapter 2.

The WBMOD model was configured to operate from an input file produced by custom written MATLAB code. Several aspects of the WBMOD ionospheric scintillation model operation and the correct interpretation of the required coordinate frames were confirmed with the author [Sec98]. Additionally, the WBMOD user guide [Sec96] provides a test data set to verify the program had been correctly compiled. This data set consists of a block of satellite position and velocity elements and the corresponding expected WBMOD outputs when this data was processed. By configuring STK to emulate the satellite scenario, the operation of the orbital simulation package, STK custom report format and MATLAB coordinate transformation code

was also verified. The operation of existing commercial packages such as Expert Fit, MATLAB and Excel was not subject to verification.

Validation of the methods employed in this study would generally require the deployment of a test station to different latitudes to record path data. The results would then be compared with this report to confirm that the analysis and models correctly represent the operation of a user accessing a constellation of LEO satellites. As detailed in Section 3.3, resource constraints prevented this approach and none of the methods in this report was subjected to a validation process.

3.10 Summary

This Chapter has described the objectives, methodology, process and assumptions underlying this research. Several specialized methods have been developed to process and present the data. The requirement for these methods, and a description of the processes involved has also been provided. Finally, the compromises and assumptions which are necessary to limit the scope of the research were also described. With the process and methodology described, the results of the research can now be provided.

CHAPTER 4

ANALYSIS AND PRESENTATION OF RESULTS

The purpose of this chapter is to present the results of analysis which characterize the changes in the quality of the Iridium and Globalstar satellite constellation coverage with varying latitude. Additionally, it describes the worst case effects of ionospheric scintillation in the lower latitudes to the north of Australia. Given that the focus of the thesis is to examine the changes in the nature of the link with user latitude, the emphasis of the analysis is on describing the relevant aspect or characteristic which impacts link quality, and determining the nature and extent of its latitudinal dependence.

The analysis is presented in a number of stages, with a specific aspect of the link (e.g. elevation, azimuth etc.) addressed in each stage. The communications links of the two constellations are addressed separately, followed by a comparative analysis. The analysis is largely conducted in accordance with the flowchart at Figure 16 and wherever possible, quantitative measures are provided to illustrate the differences between the two systems.

4.1 Introduction

The quality of coverage offered by a constellation can be considered as a function of the number of satellites in view simultaneously, the geometry of the available transmission paths, and the losses associated with these paths. Within well-defined limits, these parameters display a strong dependency on latitude and a regular cyclic variation with time. An understanding of these factors can be used to either gain an appreciation of potential link performance, or to provide data for the operational management of the system.

This study focuses on the link characteristics of two satellite constellations: Iridium and Globalstar. The constellation configurations of these systems differ in several key areas and it is primarily the inclination, altitude and number of satellites per plane which determine many of the

path characteristics. Figure 25 shows an orbital trace of one satellite from each constellation projected onto an equidistant cylindrical projection of the earth's surface for a 24-hr period.

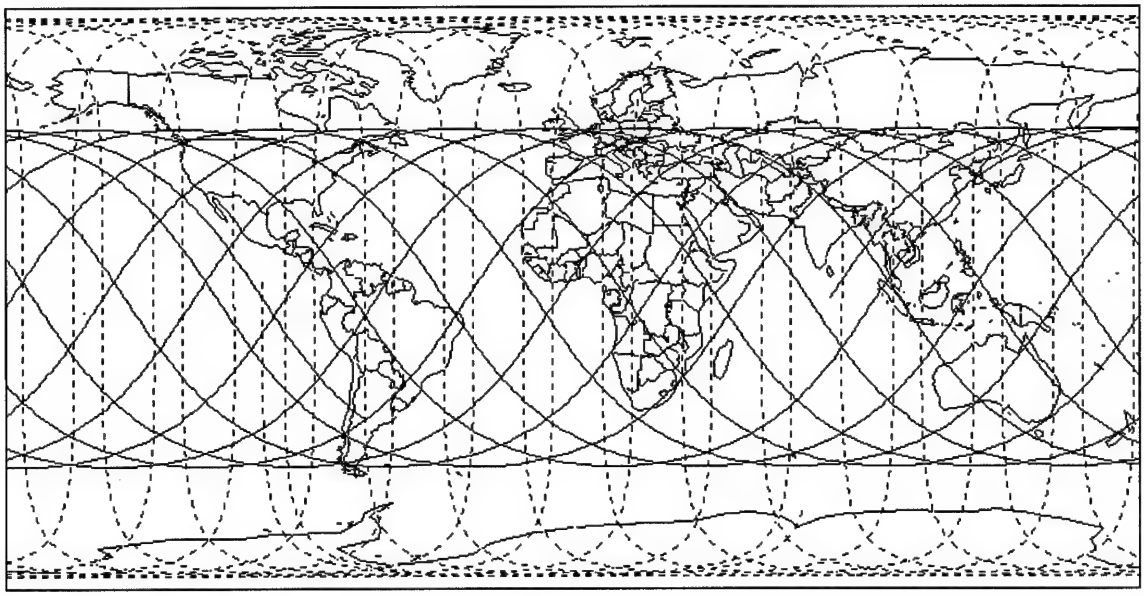

Figure 25 - Orbital Trace of an Iridium (dotted) and a Globalstar Satellite

Globalstar's satellites spend their entire orbit within the most densely populated regions of the world, while Iridium satellites spend 1/3 of their time in transit over the high latitude and polar regions above 60°. Accordingly, Globalstar provides more efficient use of the available satellites at the expense of continuous coverage above 70°. Iridium's lower satellite altitude provides lower levels of free space path loss than Globalstar at the expense of the additional coverage provided by Globalstar's higher orbit. Although Iridium offers a potentially lower level of direct path attenuation, Globalstar provides more in-view satellites, and offers higher elevation angle paths. Iridium's six orbital planes cross the equator at almost 90°, while Globalstar's eight orbital planes cross at only 52°. These factors would tend to provide Globalstar an advantage in equatorial and mid latitude coverage, at the expense of the higher latitudes, even though Iridium has a 37% higher satellite count. All of these competing factors are analyzed and compared to determine the relative performance of the two systems for a user at any latitude.

4.2 Satellite Visibility

The number of in-view satellites is an important parameter in the assessment of the quality of a constellation's coverage and both constellation's coverage vary markedly with latitude. The analysis is summarized in two graphs, with individual lines used to describe the probability that a particular number of satellites is visible to a user at a certain latitude. Only satellites above the minimum elevation angle constraint are included in the analysis. Apart from the application of this visibility limit and the removal of erroneous readings (see Section 3.4), no filtering is performed on the simulation results. Note that the statistics are drawn from all available satellites and that statements regarding latitudes generally apply to both northern and southern hemispheres (i.e., a general principal of reciprocity applies, except when addressing the azimuthal variations and ionospheric scintillation effects). Individual traces are smoothed to improve readability and discrete data is provided in tabular form in Appendix C. Iridium's visibility characteristics, its strengths and weaknesses will be discussed initially, followed by Globalstar. A comparative analysis is then provided.

4.2.1 Iridium

Due to the constellation architecture (most notably its near-polar orbit inclination) the Iridium constellation provides the densest coverage at mid-to-high latitudes. Figure 26 summarizes the results of the analysis described in Section 3.7.1 and illustrates the latitudinal variations of satellite visibility. Each of the nine satellite traces in Figure 26 describes the probability that a certain number of satellites is visible at any time. For example, at 50° latitude, one satellite is in view for 17.9% of the time, two satellites for nearly 60% of the time and three satellites for 20.3% of the time. Four satellites are visible for only a small fraction of the time (1.9%). For any particular latitude, all the probabilities sum to one. Appendix C and Figure 26

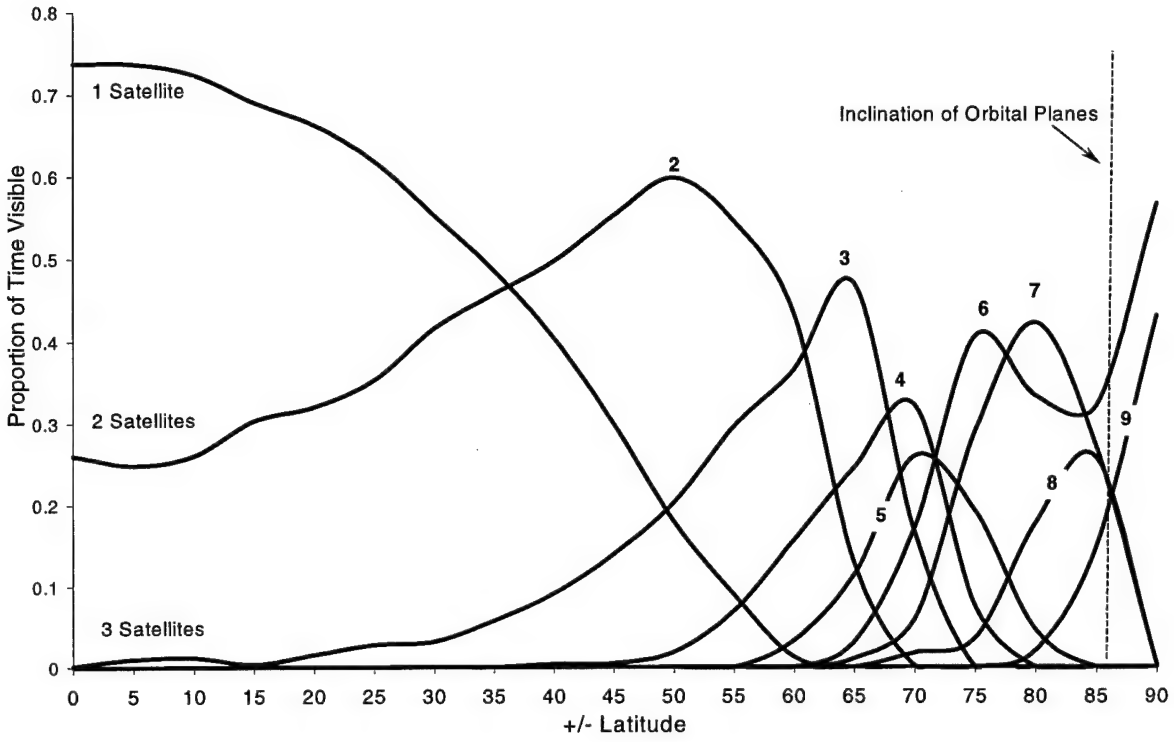

Figure 26 – Iridium Satellite Visibility vs. Latitude

illustrate that the availability of multiple satellites is generally confined to the latitudes above 30°. A user must be located above 30° or below -30° latitude before it becomes more likely that multiple satellites are available. A user located inside 30° will most likely (probability < 0.5) not experience multiple satellite visibility. The quality of the coverage and the rate of its improvement increase as the latitude rises. Above 50° latitude there is a rapid rise in the availability of satellites. Nonetheless, the equatorial and low latitudes (< 25°) are not well served in terms of the number of satellites visible to a user. This limited number of available paths may increase the severity and duration of multipath related fading, although the system capacity would not be expected to be taxed due to the limited number of users at these latitudes.

It is, perhaps, surprising that the single satellite coverage extends in latitude up to 60° latitude. With the convergence of the orbital planes, one would expect that multiple satellite

visibility would be available at all times at such a high latitude. Figure 27 illustrates the orientation of satellites which provides high (5) and low (1) satellite observations.

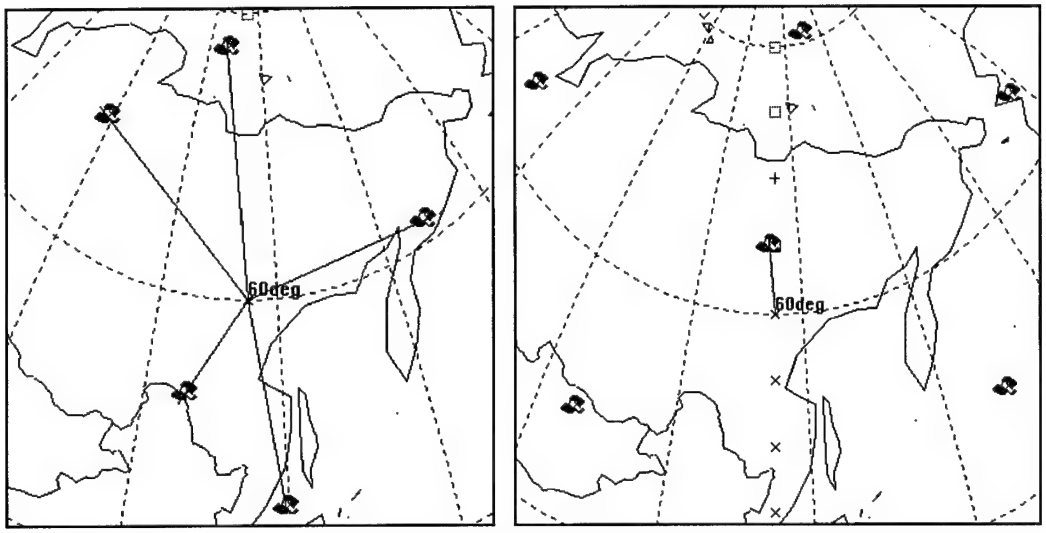

Figure 27 – Five Satellite (Left) and One Satellite (Right) Coverage at 60° Latitude

The left half of Figure 27 shows a station located at 60° latitude, 135° longitude, with five separate lines radiating out to satellites, indicating that five satellites are above the 8.2° elevation constraint and visible to the user. The right side of the figure shows a particular orientation of satellites to the user which results in the infrequent single satellite observation. In the case modeled above, the period of single satellite visibility is limited to only 25 seconds. After this time the user reverted to an extended period of multiple satellite observation.

The period of least satellite visibility occurs when a satellite is passing almost directly overhead, indicating that although there is only one satellite available to the user, that satellite is located in an ideal position with minimum range and highest elevation angle. In general, the Iridium constellation provides the greatest number of satellites when the available path elevation angles are least. Further details of the distribution of elevation angles for situations where only one satellite is available is provided in Section 4.3.2.

4.2.2 Globalstar

The visibility characteristics of the Globalstar constellation are readily apparent from the plot of satellite visibility in Figure 28.

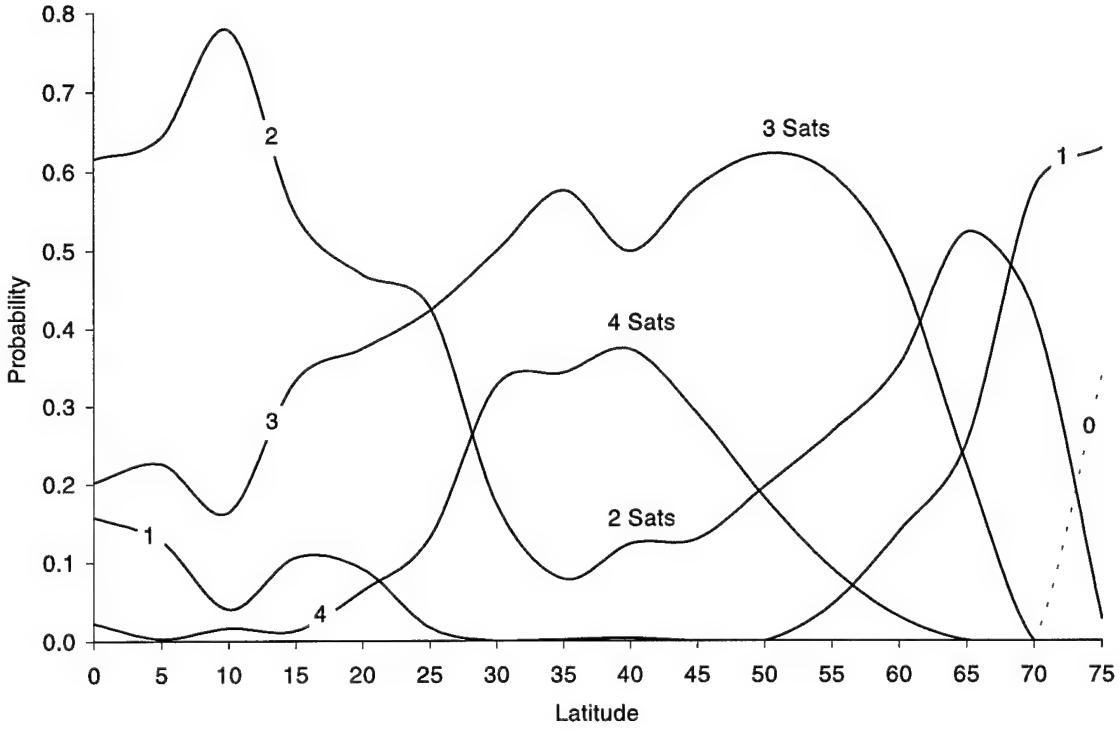

Figure 28 – Satellite Visibility -Globalstar

The Globalstar constellation provides a generally larger number of satellites at the low to mid latitudes. Under 25° latitude, a user would experience single satellite coverage less than 10% of the time, with two and three satellite visibility being the norm. The availability of four satellite coverage does not begin to become significant (> 10%) until above 25° latitude. Prime latitudes for Globalstar's coverage extend from 25° to 60° where three satellite coverage is most likely, and the optimum latitudes which provide the most occurrences of three and four satellite visibility range from approximately 30° to 55°, encompassing CONUS and the densely populated areas of Europe. From approximately +/- 55° latitude the coverage declines so that the limit of continuous

global coverage is between +/- 70°-74°. Approximately 66% coverage exists at 75° with gaps of between 30 seconds and 11 minutes, with an average gap length of 5.75 minutes. Globalstar provides little or no coverage at or above 80° latitude.

4.2.3 Comparative Analysis

The ideal situation in any comparison is to provide the reader with statements regarding the relative quality of the two systems e.g., "Constellation A provides 20% better coverage than Constellation B". However, providing simple and easily understood measures which quantify the relative performance of these constellations is difficult. Satellite visibility is an enabling factor in several different measurable qualities of a S-PCS network, such as satellite redundancy, link reliability, immunity to multipath, path delay, diversity gain etc. The use of a weighting function which assigns a utility score to each measure could be used, however, the value system for such a comparison is arbitrary, and can be selected to favor any particular quality factor. A more equitable method is to simply compare the probabilities of one, two or three satellite observations. This requires a simple addition of probabilities. That is, the probability of greater than two satellite visibility is simply the sum of the probabilities of three, four, five etc satellite visibilitities. Graphs illustrating three different levels of multi-satellite coverage are presented below. The plots shown in Figure 29 below indicate the probability of a user accessing more than one (i.e., 2, 3, 4, 5 etc) satellites simultaneously. As can be seen from Figure 29 the Globalstar constellation provides substantially better multi-satellite (>1) coverage for the low to mid latitudes. On average, Globalstar provides a 60% greater likelihood of multi-satellite coverage from the equator to 30°. This figure drops to 28.4% for the latitudes between 35° and 60°, and above 60° the Iridium constellation provides on average, a 70.38% improvement over Globalstar

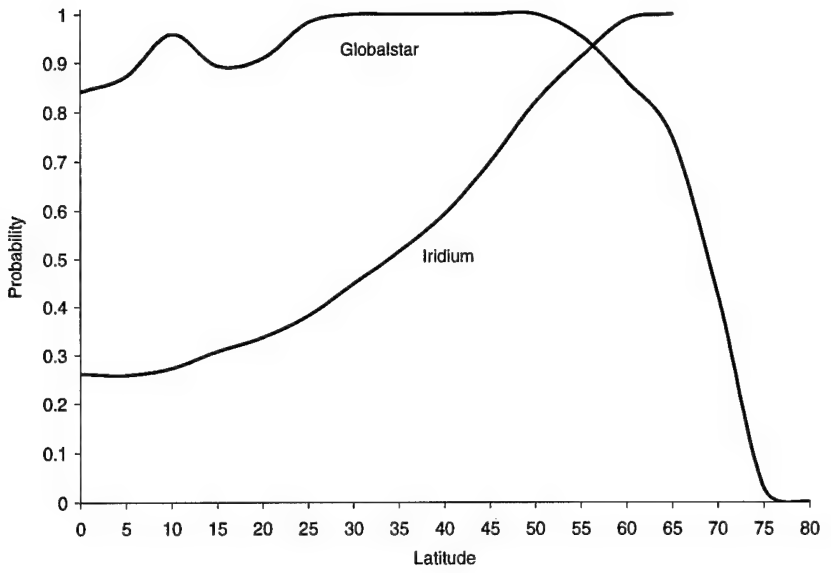

Figure 29 – Probability of more than One Satellite Visible

for multi-satellite coverage. Most notably though, for a low latitude user below 20°, Globalstar is almost three times more likely to provide multi-satellite coverage than Iridium. Figure 30 shows the probability of accessing more than two (i.e. 3, 4, 5, 6, 7 etc) satellites simultaneously.

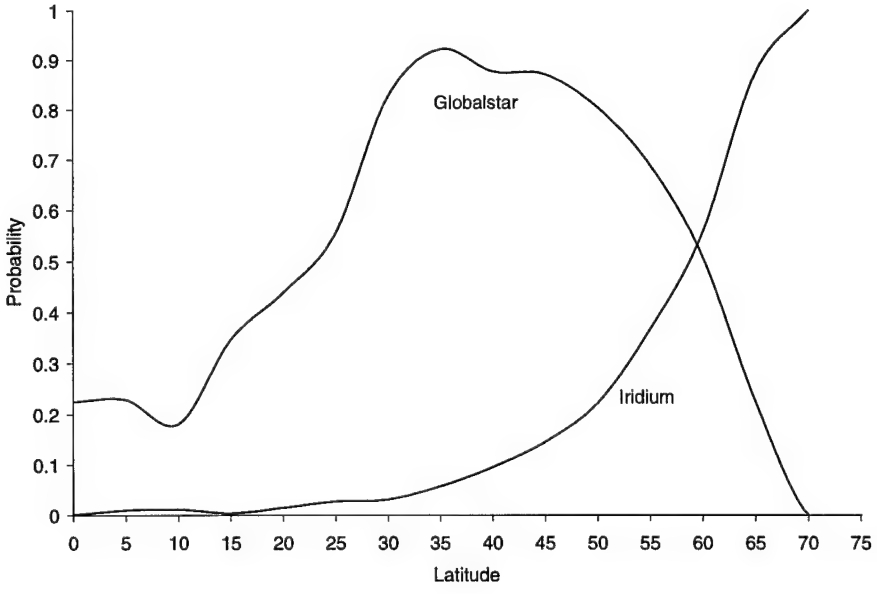

Figure 30 – Probability of More than Two Satellites Visible

If more than two satellites are required, the Globalstar constellation provides coverage with three or more satellites for most of the time between the latitudes of ± 25° to ±60°. Above 60°, Iridium provides a much greater level of coverage (of >2 satellites), extending to up to nine-satellite coverage. Figure 31 illustrates the probability of accessing more than three satellites simultaneously.

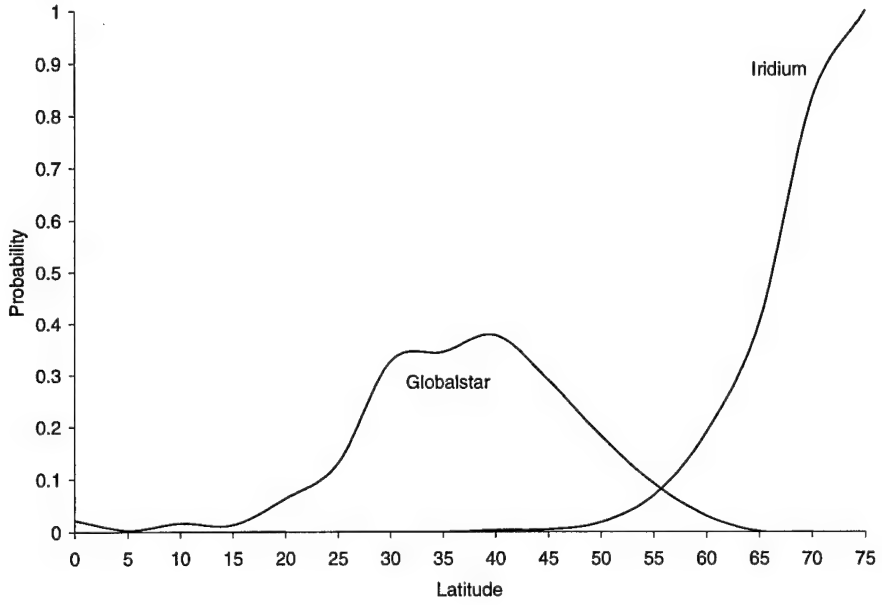

Figure 31 - Probability of More than Three Satellites Visible

The availability of four or more satellites provides the majority of the usable diversity gain [Akt97] and Globalstar provides almost continuous three satellite coverage at the mid latitudes, with four satellite coverage a substantial (approximately 35%) proportion of the time. Iridium provides negligible coverage by more than three satellites at these latitudes and would be expected to suffer from multipath fading more often than Globalstar, or require a higher link margin to provide the same signal strength. Above 55° Iridium's near polar orbit provides an increasing level of multi satellite coverage. Note the dramatic acceleration in coverage for Iridium above 60°.

4.2.4 Number and Duration of Satellite Observations

It should be noted that, to obtain the results above as a single measure, all probabilities are normalized against the total number of satellite observations, which varies with latitude. For the purposes of this study, a satellite observation is defined as the continuous tracking of a new satellite from the point it appears above the horizon to the time it disappears from view. The number of satellites available for communication, combined with the duration of the observation impact the call setup and handover process. Disregarding other factors such as satellite loading levels and path blockage limitations, a user with more satellites available would be expected to achieve a higher call success rate. Additionally, if the available satellites, on average remain in view longer, the calls do not need to be handed over to another satellite, a process which increases the risk of call dropout. A constellation which provides a higher number of satellite observations may also provide a greater level of redundancy and a higher tolerance to unserviceable satellites. Figure 32 describes the variation with latitude of the total number of

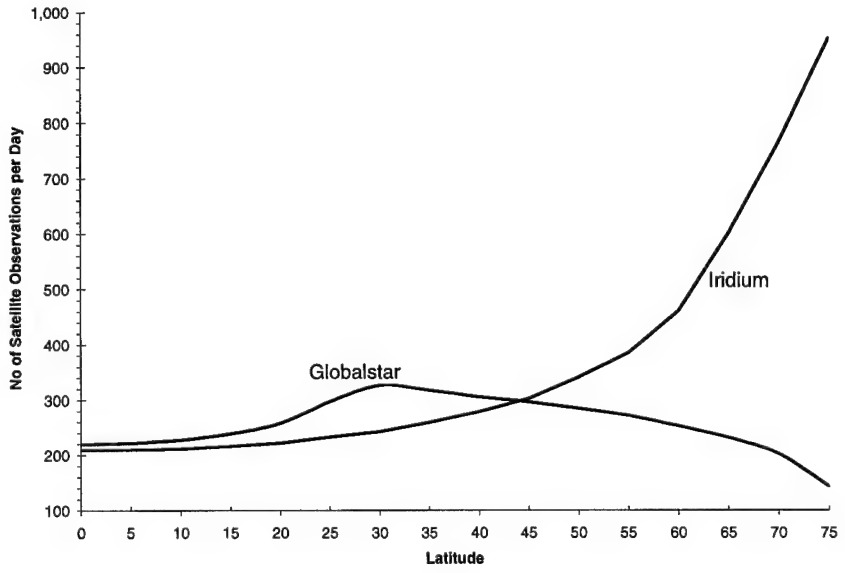

Figure 32 – Total Daily Number of Separate Satellite Observations

satellite observations in a 24-hour period. As expected for Iridium, as the latitude of the user rises, the near-polar orbit provides an increasing number of satellite observations per day. At 70°, Iridium provides nearly four times as many satellites observations than Globalstar in any 24 hour period. However, at latitudes below 45°, Globalstar provides more satellite observations, and, as shown in Figure 33, those observations are generally between 60-80% longer in duration.

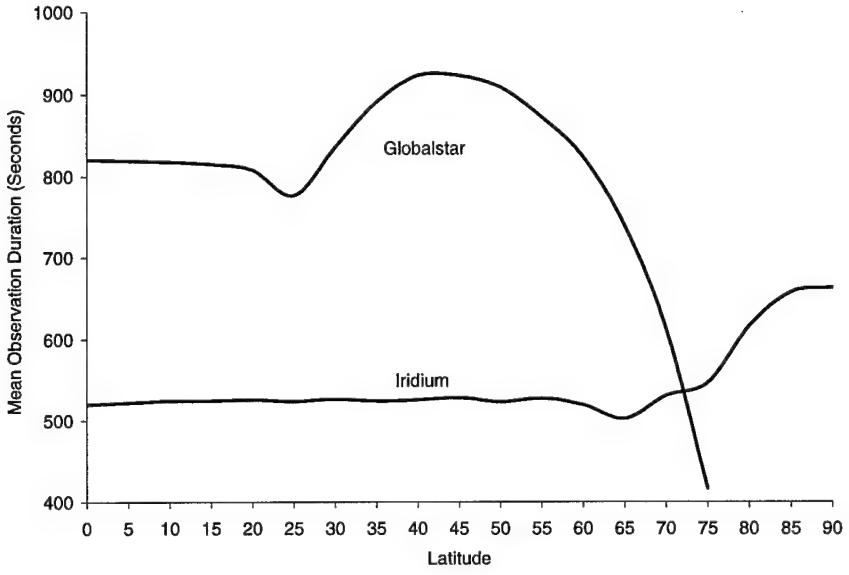

Figure 33 – Average Observation Duration

While the longest mean duration satellite observation for Iridium at low to mid latitudes is more or less fixed at approximately 520 seconds (8 mins 40 secs), Globalstar provides a higher duration observation at all latitudes until approximately 72°. The duration peaks at approximately 45° latitude at 922 seconds (15 mins 22 secs). The peak in Globalstar's mean duration reflects the higher number of satellites available at the mid latitudes and the generally higher elevation angles of these satellites. These two factors combined with the generally higher number of satellites to skew the mean observation duration higher. In contrast to Globalstar, Iridium's near-polar orbit provides consistent transition times until the planes begin to come

together at higher latitudes. From this point the higher number of visible satellites, with higher median elevation angles begins to positively influence Iridium's observation times.

Note that the peak average observation duration for Globalstar is approximately 45° latitude, which is 7° less than the constellation's orbit inclination. Although theory predicts that the greatest duration observation of a single satellite at 52° inclination will be at 52° latitude, the effect of averaging all observations, and combining a large number of satellites is to slightly reduce the latitude where the maximum occurs.

4.2.5 Nil Equatorial Coverage - Iridium

Note that from Appendix C, the simulation indicates that for small amounts of time (17 seconds in 24 hours at the equator and 4 seconds at ± 5°) no satellites were visible within the minimum elevation constraints. These observations are not shown in Figure 26 due to the small values. This is not considered important as the violation times were limited to only several seconds, were distributed evenly throughout the sample, and only occurred within 5° of the equator. Additionally, relaxing the 8.2° elevation angle to approximately 8° provided continuous observation. Nonetheless, Iridium's claim of continuous global coverage appears to be "strained" at the equator.

4.3 Path Characteristics

The characteristics of a S-PCS transmission path are heavily influenced by its elevation angle. The elevation angle is of prime importance in determining the degree of free space path loss, atmospheric attenuation and fading/shadowing caused by terrestrial obstructions such as trees or buildings. The distribution of these parameters and the nature of their sensitivity to a user's latitude help to characterize link quality as a function of latitude.

A single numerical descriptor (e.g. mean, median, etc) cannot accurately convey the nature of the shape of a distribution. Simple average scores do not capture the skewing of the

distribution with rising latitude, and they may be inordinately affected by the relatively infrequently occurring higher elevation angles. This is especially true at the lower latitudes where the distributions have relatively long tails. The median score may more accurately describe the nature of the distribution as it will not be as heavily influenced by the presence of a few high readings. Accordingly, the median is used where a simple description of a skewed distribution is required.

4.3.1 Distribution of All Elevation Angles

The distribution of all available elevation angles to all visible satellites provides an indication of the quality of the full range of available paths. This analysis characterizes the distribution of all paths and attempts to define a model that approximates its distribution as a function of latitude.

Simulations are conducted to take samples of all visible satellites at 30-second intervals, also recording the exact time the satellite came into, and dropped out of view. The data is processed to remove invalid observations (see Section 3.7.2) and the distribution of the elevation angles computed. Probability Density Functions (PDFs) are presented in the individual system sections below, and Cumulative Distribution Functions (CDFs) are presented in the comparative analysis. A full set of CDF plots for both systems is provided at Appendix D.

4.3.1.1 Iridium

Figure 34 shows the probability distribution function of all elevation angles between the equator and 60° latitude. The 3D graph consists of 13 individual PDFs combined to form a surface, and is used to illustrate the similarity in the distributions of the elevation angle samples.

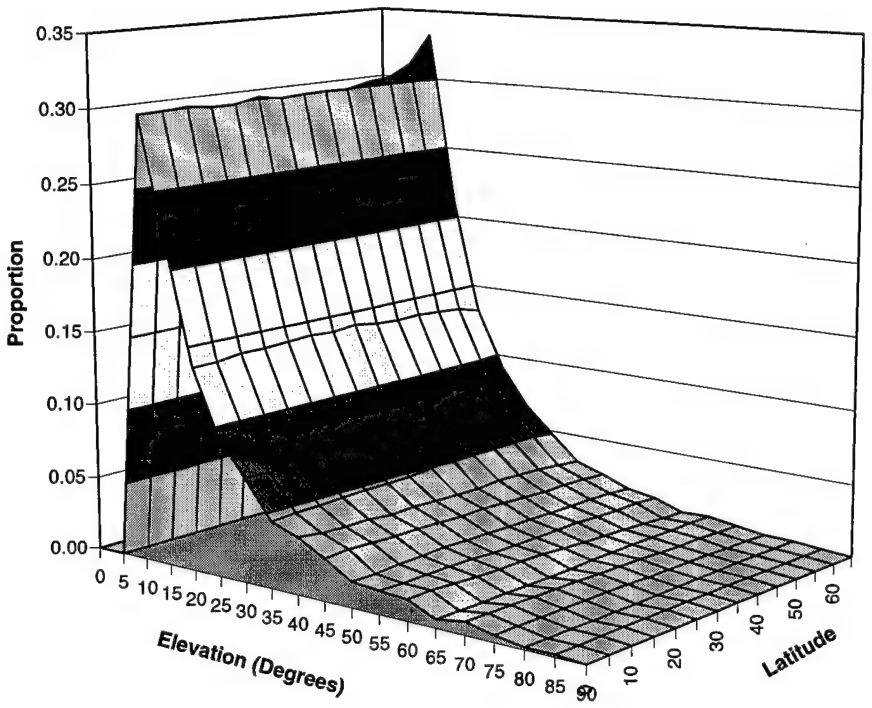

Figure 34 - PDFs of Iridium Elevation Angles (Equator to 60 deg Latitude)

The major feature evident in the PDF is its consistent shape; the distribution remains fairly independent of latitude until approximately 60° latitude. The implication of this is that system designers can rely on a fairly unchanging distribution of path elevation angles over a wide range of latitudes. Additionally, a single CDF can be used to estimate the probability that satellites below a certain elevation angle are visible.

The level of homogeneity of the individual distributions from 0°-50° latitude was tested using the Kruskal-Wallis test [Law91] at level of significance of 0.01 (4 degrees of freedom). The test statistic of 0.028 was less than the critical value of 13.277 and the distributions were found to be homogeneous. The level of homogeneity was reduced for the higher latitudes from 50°-60° but still satisfied the Kruskal-Wallis criteria (test statistic of 0.948 against a critical value of 9.210 for 0.01 level of significance). Accordingly, the hypothesis of homogeneity of the

distributions of all elevation angles was supported for latitudes between 0° and 60° and a single equation was used to describe it's shape.

The relative stability of this PDF with rising latitude appears to contradict common sense. With the convergence of the planes one would expect that, with more satellites available, the elevation angles would tend to rise sooner. However, an examination of the number of satellites available versus latitude (Figure 32) shows that the effects do not begin to become dramatic until after 60°. Although there are, on average, more satellites in the sky at mid latitudes, they are still distributed in the same manner. This is addressed in more detail when Iridium's elevation angles are compared with Globalstar's.

Above 60° the increasing satellite visibility begins to influence the distribution of elevation angles. Figure 35 shows the distribution for the remainder of the higher latitudes by plotting the PDF from 40° - 90° latitude.

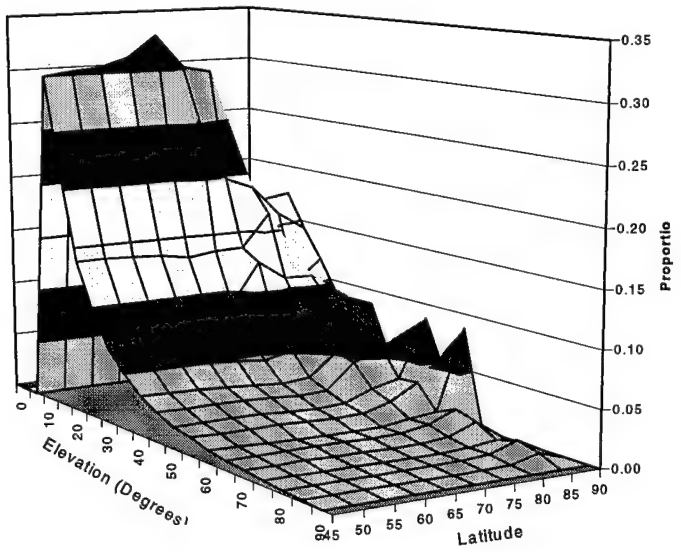

Figure 35 – PDF of All Elevation Angles - 40° to 60° Latitude

The distribution of elevation angles changes markedly above 60°, providing higher elevation angles at the expense of the low angles. The raised ridge in the 3D distribution and the sharp drop in the number of low angles illustrates this effect. This change is due to the convergence of the orbital planes, providing a higher number of visible satellites at progressively higher elevation angles. The increase in the number of visible satellites is also illustrated in the plots of observation numbers (Figure 26) and duration (Figure 32).

The intersection of all satellite planes is located at 86.4° latitude. At approximately 86.4° latitude, the highest density of satellites with the highest elevation angles is found. The intersection is largely stationary in the Earth Centered Inertial coordinate system but rotates in an Earth Centered Fixed frame, to which the user is fixed. The prominent spike(s) in the shape of the PDF at the latitudes between 80° and 90° are due to the rotation of the user under the intersection of orbital planes. Effectively, the user located at the 85° latitude location moves to a position under the intersection every 24 hours. The bulge in the middle elevation angles is due to the frequent high elevation angle observations during this period.

4.3.1.2 Globalstar

The PDF for the elevation angles to all available paths for Globalstar is provided in Figure 36. In a similar manner to Iridium, the PDF of all path elevation angles for Globalstar is relatively unchanged between the equator and ± 20° latitude.

An analysis of the data sets between 0° and 20° using the standard Kruskal Wallis test available in Expert Fit is conducted at test level 0.01. As the test statistic, 2.077, is less than the critical value of 9.210, the hypothesis that the data sets are homogeneous cannot be rejected. A plot of the differences indicates that the worst case average difference between any two of the four data sets is 0.00346 (as a proportion of the total sample) with a maximum of 0.01072. Between 25° and 55° the elevation angles are generally higher, as shown by the elevated ridgeline in the center of Figure 36.

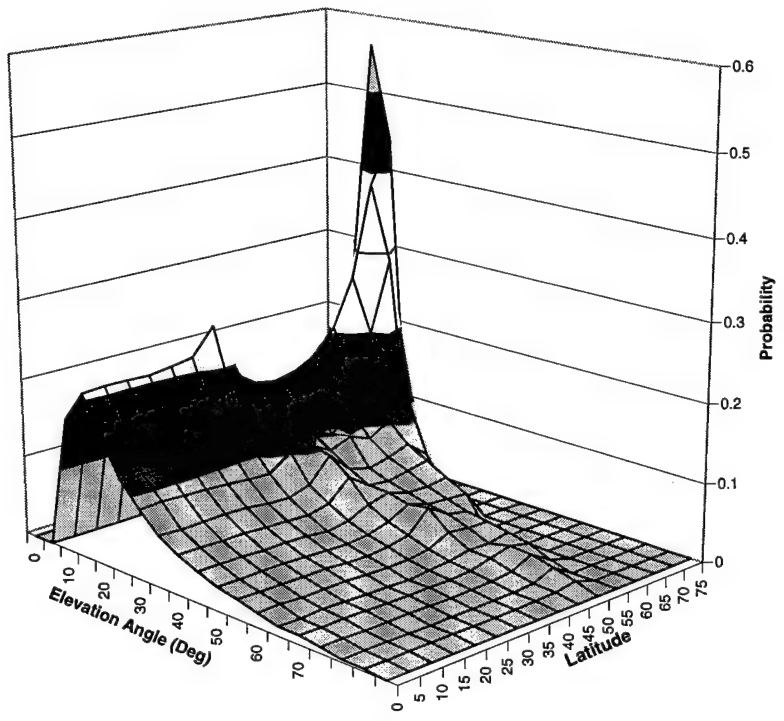

Figure 36 – PDF of Globalstar Path Elevation Angles

This ridgeline in the PDF aligns with the optimum latitudes for satellite visibility (30° to 55°) referred to in paragraph 4.2.2. The large spike at the end of the PDF plot indicates that at latitudes above 65°, the user can only access a satellite at low elevation angles. Satellite visibility drops off as the user rises above the constellation's orbital plane inclination (52°), and the satellites are seen lower in the sky.

4.3.1.3 Comparison and Discussion

A comparative analysis of the elevation angle of all paths focuses on the performance of the two constellations in terms of their elevation angle CDFs, and the probabilities of obtaining a link below either 20° or 30°. Both indices will be provided at representative latitudes. The greater than 20° and greater than 30° probability curves are provided to allow one of the most critical aspects of link performance to be quickly established. That is, how often the user experiences low elevation angles.

The cumulative distribution of all elevation angles is used to compare and contrast the quality of the link in terms of its elevation angle. The CDF in this case provides a probability that the elevation angle will less than or equal to a certain value. A CDF curve that is shifted to the higher elevation angles (to the right when plotted on the x-axis) indicates a generally higher elevation angle experienced by the user (desirable). For two CDFs plotted on the same axes, the horizontal distance between the two curves represents an improvement in path elevation angle; the rightmost curve providing the higher elevation angle for a given probability. As the graph is a cumulative plot, the vertical distance between the graphs represents the increased likelihood of experiencing elevation angles up to a certain value. A higher plot means a higher chance of obtaining a low elevation angle (undesirable). Figure 37 compares the distribution of all elevation angles of the two constellations at the equator.

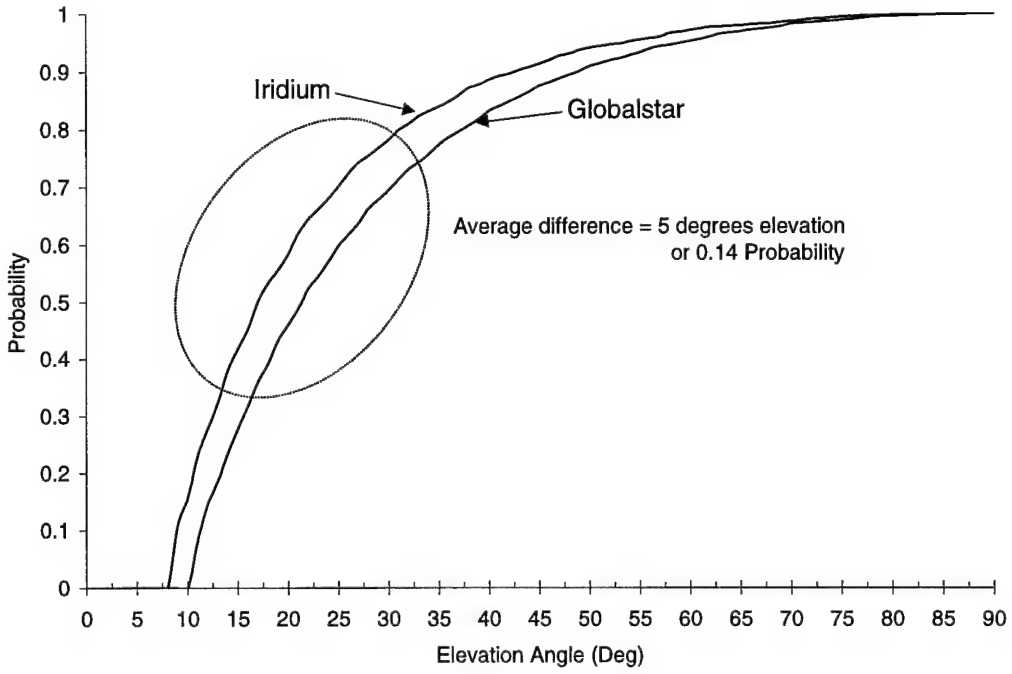

Figure 37 – Equatorial CDFs of Iridium and Globalstar

At the equator, Globalstar offers elevation angles up to 5° higher than Iridium at the same level of probability. In effect, at any random point in time the Globalstar user will be operating

into a satellite approximately 5° higher than the user of the Iridium system. Figure 38 provides the same plots for a user located at 40° latitude.

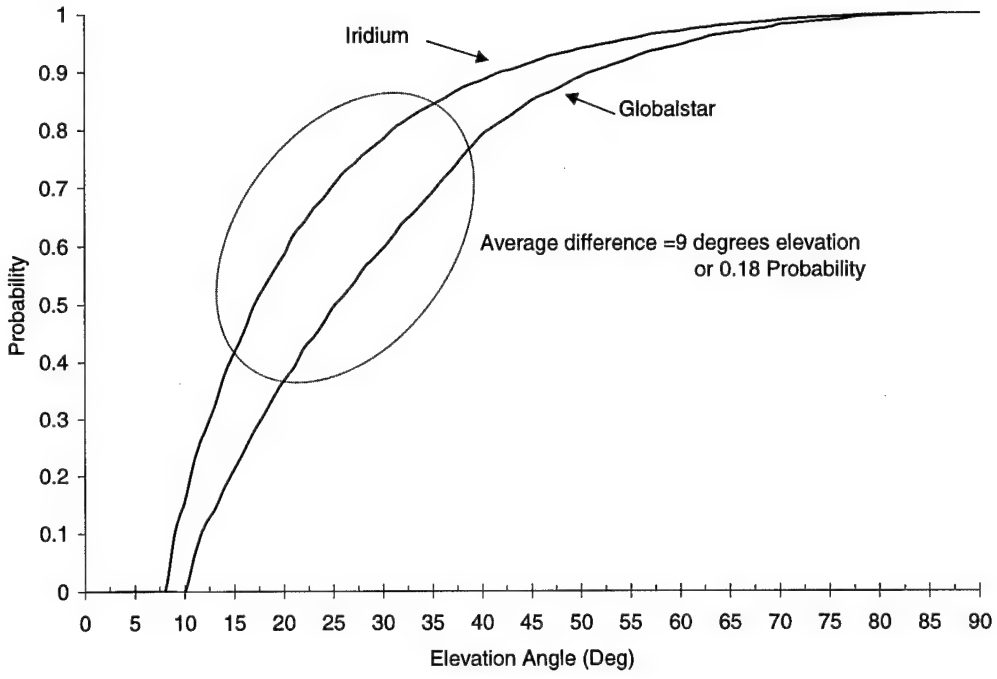

Figure 38 – Iridium and Globalstar 40° Latitude CDF's

Note that the improvement offered by Globalstar is more pronounced at this latitude, with up to 11° improvement in elevation angle for a given probability. Globalstar's greatest level of improvement is provided for elevation angles between 20° and 35°. Note that the two Iridium CDF's are almost identical, illustrating the homogeneity that the Kruskal-Wallis test confirms. Additional plots for 30°, 50° and 60° are provided at Appendix D.

Given that the effects of multipath, absorption and scattering from physical obstacles in an urban, suburban or rural environment increase with decreasing path elevation, the probability of obtaining a path under a threshold value was investigated. Elevation angles of 20° and 30° were set as the thresholds as most of the severe effects could be expected below these values. Figure 39 illustrates the differences between the two constellations in terms of path elevation angles.

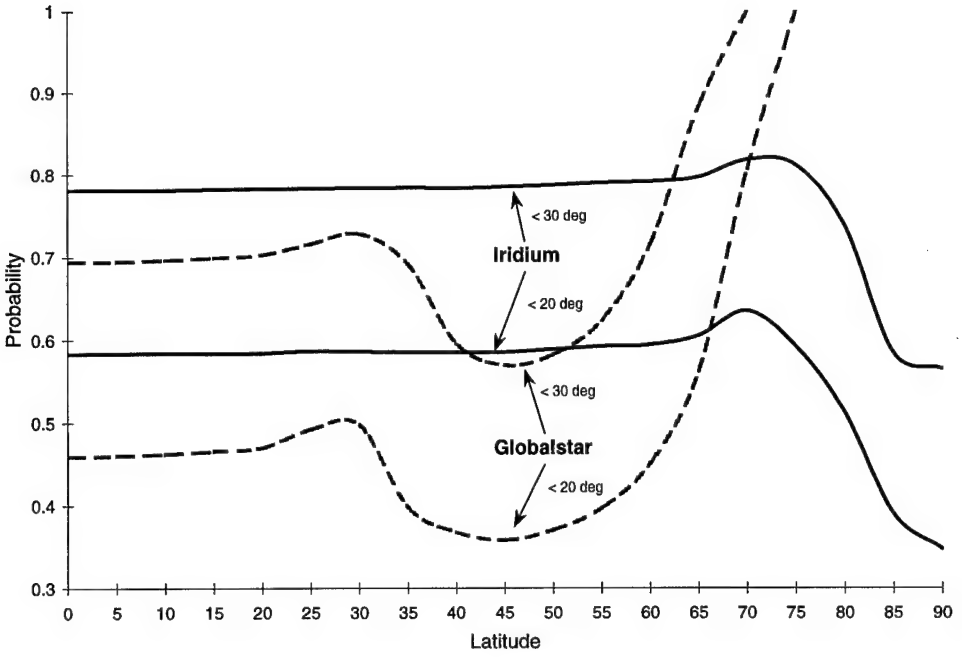

Figure 39 – 20° and 30° Exceedence Curves

Two pairs of curves are provided in Figure 39, each showing the probability of obtaining an elevation angle of less than 20° or 30°. Lower curve positions are more desirable to a user, indicating a lower probability of obtaining these low elevation angles. Addressing only the <30° curves, below 60° latitude, Globalstar provides a 6% - 22% reduction in the likelihood of a path under 30° elevation angle. The mid latitudes, between 35° and 55°, provide the greatest average improvement of approximately 16%. The situation is similar for the lower (greater than 20°) threshold, with similar values of improvement. The absolute values for the greater than 20° curve support the statement that, at low to mid latitudes, Globalstar is unlikely ($\rho < 0.5$) to provide a path with an elevation angle of less than 20°, while Iridium is more likely ($\rho > 0.5$) to provide such a path.

As the user's latitude increases beyond 60°, the Iridium constellation becomes more likely to provide a higher elevation angle path, and Globalstar's performance degrades rapidly. This behavior is expected as the user moves above Globalstar's orbit inclination. A plot of the

median path elevation angles provided in Figure 40 supports these general observations and conclusions.

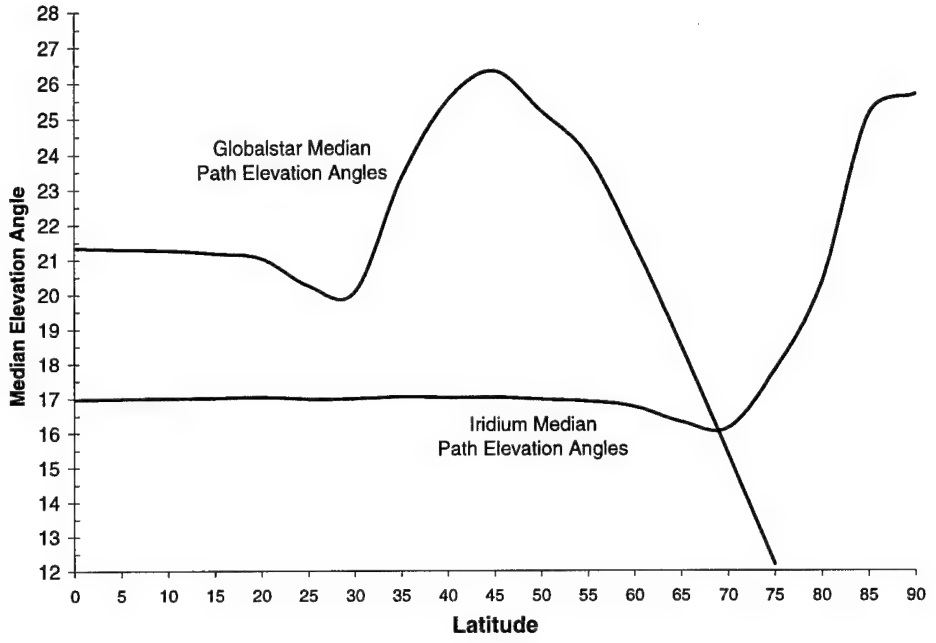

Figure 40 – Median Path Elevation Angle – All Satellites

Note from Figure 40 that the features of the median curves correspond closely with similar features in the exceedence curves at Figure 39 (i.e. higher median elevation angles correspond with a dip in the greater than 20° and greater than 30° probability curves).

If mean elevation angles are required rather than the median, they follow the median up until approximately 60° latitude, but are in general higher by approximately 5°. The mean and median scores coincide at the higher latitudes where the distribution of elevation angles is almost symmetrical.

4.3.2 Single Satellite Coverage - Iridium

As shown in Figure 26, at low latitudes, Iridium is more likely to provide single rather than multi-satellite coverage. With only one satellite available for communications, the available elevation angles becomes more critical. As can be seen from Figure 40, the median elevation

angle for all available satellites remains at 17° from the equator to 60°. Analysis of the times when only one satellite is visible indicates that the median elevation angle begins at 25.6° at the equator, and increases to 50.1° by 50° latitude in a roughly square law relationship. To generalize, if the user is unfortunate enough to operate in a period when only one satellite is visible, that satellite is most likely at a high elevation angle. A regression analysis is conducted on the 12 data sets of single satellite observations and an equation derived which provides the single satellite median elevation angle. The equation is valid between 0° and 60° latitude and describes with a coefficient of determination (R^2) of 0.9872.

$$\theta_{Median} = 0.4241(\lambda)^2 - 2.0951(\lambda) + 28.214 \tag{22}$$

where λ = Latitude

For a user located at the equator, the periods of single satellite coverage are evenly distributed throughout the observation period. In general, the user experiences single satellite coverage for 6 to 7 ½ minute periods, followed by periods of multiple coverage lasting between one and three minutes. This cycle generally remains constant until the two counter-rotating planes pass over head and the user enjoys continuous multiple coverage for approximately 60 minutes before restarting the cycle.

A complete analysis of the behavior of the Iridium system when only one satellite is available can be made utilizing the figures and data produced by the MATLAB code titled "elevsort.m". This program provides a complete set of plots, histograms and files describing the path elevation angles when only one satellite is visible to the user. A complete listing is provided at Appendix F.

4.3.3 Model Fitting - All Elevation Angles

The determination of a single distribution function which reliably and accurately describes the elevation angle as a function of latitude is more useful than the empirical data alone.

Such a mathematical model may prove useful in the development of constellation-specific roadside fading or multipath shadowing models. Existing radiowave propagation models such as the Empirical Roadside Shadowing (ERS) or Modified ERS models allow the specification of only a single elevation angle to predict the level of fade due to scattering and other multipath effects. Additionally, these models are valid only for angles between 20° and 60°, a range which is of limited value for S-PCS applications such as Iridium.

Expert Fit software is used to determine the most appropriate distribution which consistently described the distribution of all observed elevation angles. As stated previously, Iridium's distribution of all elevation angles is stable until 60° latitude and the distribution is approximated by a single distribution from -60° latitude to +60° latitude. For Globalstar, however, the path elevation angles are stable only between ±20° latitude. Outside of these latitudes, the distribution varies significantly up to its upper limit of 70°. Nonetheless, a single distribution is used to approximate the full range of latitudes for Globalstar, with the errors mainly associated with the mid-latitudes.

The selection of the most appropriate distribution is based on a structured model fitting process using Expert Fit. Three bounding scenarios (see Section 3.8) are used to fit the 31 bounded and unbounded continuous probability distribution models available in Expert Fit. The models are automatically applied to each latitude's sample set, then ranked by Expert Fit according to its internal proprietary fitting algorithms. The statistical moments and the error distributions of the top five models are extracted from Expert Fit and manually analyzed. The moments are compared to determine the models that provide the most accurate fit at the low to mid elevation angles across all latitudes. The unbounded model selected to represent the population of elevation angles consistently ranked first against all available continuous distributions in Expert Fit. Where a bounded distribution is required the model selected consistently (10 out of 12 times) provided the most accurate representation of the sample data.

The times when it did not provide the most accurate fit, the selected model was ranked either second or third.

For Iridium, two distributions are provided which adequately describe the elevation angles between the equator and ± 60° latitude. The choice of which to use depends on the application. If a non-negative continuous distribution having a lower limit of 8.2° is required, an Exponential distribution provides the closest level of fit. If the application can tolerate a distribution which is defined to lower elevation angles than are physically valid, the Johnson S_B distribution provides substantially better accuracy.

The exponential distribution of elevation angles (θ) is described by:

$$f(\theta) = \frac{1}{13.77} \times e^{\left[\frac{-(\theta - 8.2)}{13.77}\right]} \tag{23}$$

The equation above represents the distribution of elevation angles a user could expect to obtain from the Iridium system at any point on the earth's surface between the latitudes of ±60°. The distribution is defined for elevation angles above 8.2° and is valid to 90°. The cumulative distribution function for all elevation angles is provided by the expression:

$$F(\theta) = 1 - e^{\left[\frac{-(\theta - 8.2)}{13.77}\right]} \tag{24}$$

A closer fit to the simulation data is available using the Johnson S_B bounded continuous distribution. The Johnson S_B distribution is defined by Equation 25.

$$f(\theta) = \frac{\alpha_2 (b-a)}{(\theta - a)(b - \theta)\sqrt{2\pi}} e^{\left\{-\frac{1}{2}\left[\alpha_1 + \alpha_2 \ln\left(\frac{\theta - a}{b - \theta}\right)\right]^2\right\}} \tag{25}$$

where a = *Lower endpoint of distribution*

b = *Upper endpoint of distribution*

$\alpha 1$ = *Shape Parameter #1*

$\alpha 2$ = *Shape Parameter #2*

The Cumulative Distribution is provided by Equation 26.

$$F(\theta) = \Phi\left[\alpha_1 + \alpha_2 \ln\left(\frac{\theta - a}{b - \theta}\right)\right] \tag{26}$$

Where Φ indicates the Normal Cumulative Distribution Function defined for the value in the bracketed expression. The parameters derived from Expert Fit model fitting for substitution into the distribution are as follows:

Lower endpoint (a):	6.35
Upper endpoint (b):	108.33
Shape #1 (α_1):	1.8
Shape #2 (α_2):	0.845

The upper endpoint parameter "b" is used to be consistent with other bounded continuous distributions. The Johnson S_B distribution is generally characterized in terms of a scale parameter defined: β = (b-a). Note that the distribution is defined from the upper to the lower endpoints but is valid only between 8.2° and 90°. Figure 41 below shows the distribution with both models fitted. The errors associated with the fit are also shown. The interpretation of the error scores is provided in Chapter 3.

The irregular curve representing the sample data is based on a histogram bin size of 1° elevation angle. The large number of values between 8.2 and 10° tend to exaggerate the magnitude of the lower two bins. For this reason, the excursions between the model fit and the sample data appear large at low elevation angles. This is mainly a byproduct of the histogram bin size selection rather than an indication that the model does no match at these values. Nonetheless, 95% of the errors noted in the plot are located at the low end of the distribution below 10°.

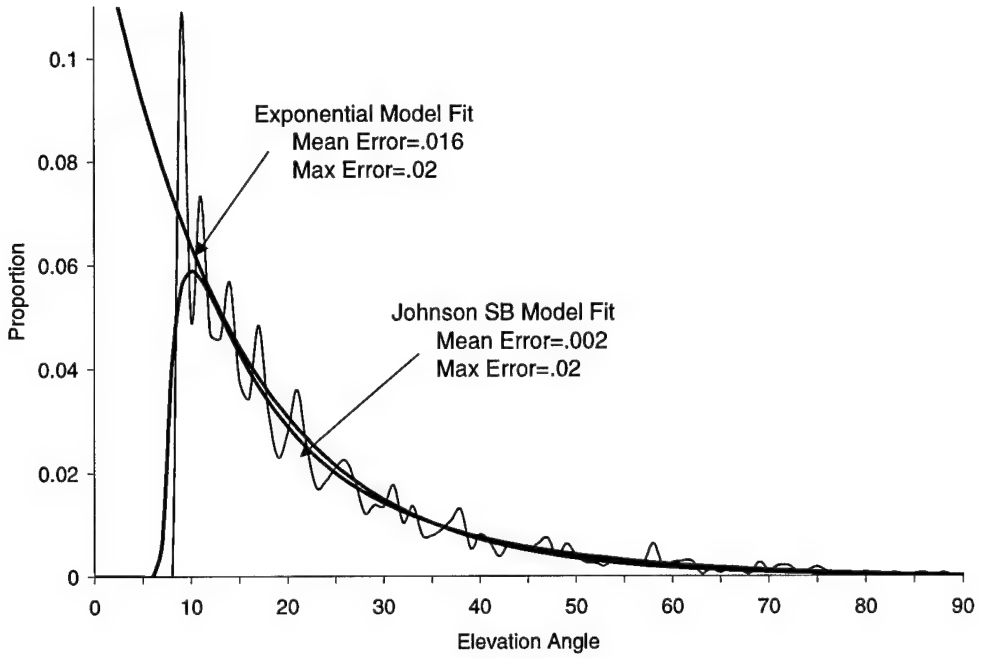

Figure 41 – Fit of Exponential and Johnson Distributions

Although the distribution provides substantially better accuracy than the exponential, the Johnson S_B distribution may cause problems in applications requiring a naturally bounded minimum elevation angle. If this is not critical, the Johnson S_B is preferred over the exponential.

4.3.3.1 Globalstar

Model fitting using Expert Fit is performed at latitudes from the equator to 70° with the Johnson S_B distribution consistently ranked above all other models. Table 8 provides the parameters for the Johnson S_B model derived from an analysis by Expert Fit, including error scores for each latitude step. Note that the errors are primarily restricted to the latitudes between 35° and 50° with the greatest deviation at 45°. In particular, caution should be exercised in the use of this distribution for latitudes of 40° and 45°. An indication of the quality of the fit at these latitudes is provided in Figure 23 where two Johnson S_B distributions are fit against a data set. Note that the worst case mean and maximum errors listed in Table 8 are close to the "Good" fit to the data. All other distribution errors are very close to or better than the "Good" fit.

Table 8 – Johnson SB Model Parameters

Latitude	Lower Endpoint	Upper Endpoint	Shape #1	Shape #2	Average Error	Maximum Error
0	8.1173	95.8621	1.4020	0.8105	0.0020	0.0085
5	8.1240	98.0476	1.4355	0.8167	0.0020	0.0085
10	8.1625	96.2616	1.4055	0.8054	0.0020	0.0085
15	8.2123	96.3978	1.4204	0.8068	0.0020	0.0085
20	8.2323	94.4420	1.3931	0.7972	0.0020	0.0085
25	8.5553	90.8116	1.3557	0.7489	0.0020	0.0085
30	7.2371	226.4368	2.9398	1.0722	0.0069	0.0214
35	5.3426	255.1679	3.3060	1.2690	0.0056	0.0233
40	6.0000	90.0000	1.1154	0.9395	0.0079	0.0306
45	7.2000	100.0000	1.1758	0.8668	0.0182	0.0410
50	8.2343	96.0223	0.9831	0.7059	0.0045	0.0146
55	8.4836	82.2313	0.9613	0.7127	0.0033	0.0124
60	8.3260	58.0880	0.7697	0.7501	0.0034	0.0136
65	8.5297	38.0679	0.4899	0.7362	0.0032	0.0155
70	8.8972	24.5607	0.2459	0.7045	0.0038	0.0164

A regression analysis is conducted using SAS-JMP [JMP97] to derive a set of equations which could be used to describe the shape and location parameters in terms of a user's latitude. A single set of equations which covered the full range of latitudes from 0° to 60° could not be derived without an unacceptable (greater than 20% of the sample size at some points) level of error. A piecewise method is employed which breaks the range into two bands of latitude: from 0° to 20°, and 25° to 60°. The distributions between 0° and 20° latitude are relatively stable and the use of a simple mean of each score may be sufficient. However, the small changes in the lower endpoint and shape parameter data is described better using a set of equations. The section from 25° to 60° changes markedly, requiring curves with third power coefficients to provide the required degree of accuracy. The equations which describe the Johnson SB distribution

parameters between 0° and 20° are as follows:

$$\left.\begin{array}{ll} \text{Lower endpoint (a)} & 8.10602+.00637(\lambda) \\ \text{Upper endpoint (b)} & 96.2 \\ \text{Shape \#1 } (\alpha 1) & 1.40474+.00679(\lambda)-0.00065(\lambda)^2+.00001(\lambda)^3 \\ \text{Shape \#2 } (\alpha 2) & 0.8146-0.00073(\lambda) \end{array}\right\} \quad (27)$$

where λ = *Latitude.*

The latitudes between 25 and 60° show substantial changes in their distribution shape parameters but can be described by the following equations.

$$\left.\begin{array}{ll} \text{Lower endpoint (a)} & 13.2351-0.30488(\lambda)+0.00379(\lambda)^2 \\ \text{Upper endpoint (b)} & -293.97+30.307(\lambda)-0.71494\ (\lambda)^2+0.00525(\lambda)^3 \\ \text{Shape \#1 } (\alpha_1) & -12.695+1.16742(\lambda)-0.02988(\lambda)^2+.00024(\lambda)^3 \\ \text{Shape \#2 } (\alpha_2) & -3.998574+0.38387(\lambda)-0.009436(\lambda)^2+0.0000734(\lambda)^3 \end{array}\right\} \quad (28)$$

The errors associated with using the equations derived from the regression analysis are detailed in Table 9 below.

Table 9 – Regression Errors - Johnson S_B Distribution Fit

Latitude	Errors Associated with Equations 27 & 28	
	Average	Max
0	0.0022	0.0133
5	0.0016	0.0118
10	0.0016	0.0098
15	0.0016	0.0127
20	0.0020	0.0121
25	0.0072	0.0317
30	0.0103	0.0373
35	0.0057	0.0276
40	0.0085	0.0330
45	0.0121	0.0332
50	0.0140	0.0366
55	0.0083	0.0262
60	0.0230	0.0418

These errors represent the difference between the distributions derived from the use of the Equations 27 and 28 above and the sample data. The reader is cautioned against approximating the latitude (λ) coefficients in any of the equations described above. Any approximation will cause substantial errors in the parameters, causing large errors in the distribution approximations.

4.3.4 Best Elevation Angles

Disregarding the unpredictable effects of shadowing and multipath, the path of least attenuation is that with the highest elevation angle. The characterization of the system performance in terms of its best elevation provides a best-case picture of the system's potential link performance. By characterizing the path in terms of its best elevation angle, the upper limit of its performance is effectively bounded.

The analysis focuses on the median value of the best elevation angle, and the greater than 20° and greater than 30° exceedence curves. The median values for each latitude are plotted with upper and lower percentile values to illustrate the spread of the distribution. The two exceedence curves describe the worst case path performance of the two systems.

4.3.4.1 Iridium

A plot of the best elevation angle for the Iridium constellation for a user located at the equator is provided at Figure 42. The lower sub plot under the main graph shows the variation over a 24 hour period, while the main plot shows an expanded view of a 2 ½ hr portion of the day. The enlarged view shows the lower elevation constraint of 8.2° as a dotted line. The plot is dominated by two frequency components; the first is the gradual movement of the earth below the orbital planes, the second is the more rapid movement of individual satellites across the view of the observer. With six orbital planes, the user experiences the major peaks in elevation angle 12

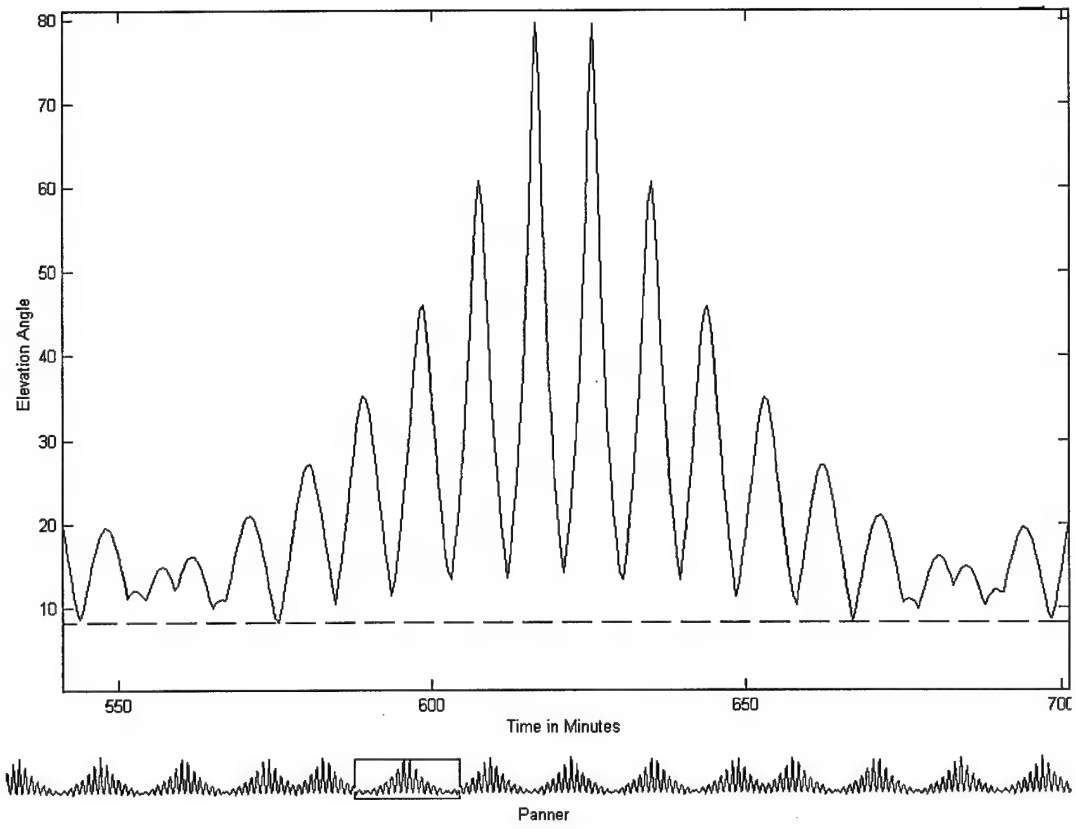

Figure 42 – Plot of Best Elevation Angle (equator) - Iridium

times during a 24 hour period. As satellites transit overhead, the path to the highest satellite changes abruptly. The sharp lower points in the plot indicate a change of satellite. The slight upward curve of the base of the upper plot indicates satellites are handed off at higher elevation angles as the orbital plane moves overhead. As the latitude rises above 50°, satellites become denser, and transitions become more frequent and occur at higher elevation angles. Additional curves appear between the existing peaks and the satellite handoff occurs more frequently and at higher elevation angles.

If a single satellite was tracked continuously from the North, directly overhead to the South, the period of observation would be 11.1 minutes. In general though, a satellite is tracked for only 9 minutes before a better satellite becomes available. The exception to this occurs when the user is located between orbital planes and all visible satellites are low on the horizon. This is shown in Figure 42 as the small ripples on either side of the larger peaks. At these times, the

elevation angles vary over a smaller range (typically 3° at the equator, 5° at 40° latitude and 15° at 60° latitude), and the satellites hand-over more often. Note that the best elevation angle very rarely drops below the minimum cutoff; the points where it crosses this line represent periods of no satellite visibility (see Section 4.2).

4.3.4.2 Globalstar

Figure 43 shows the best path elevation angle for a user accessing the Globalstar system at the equator. Referring to the lower plot, Globalstar's best elevation angle displays a cyclic

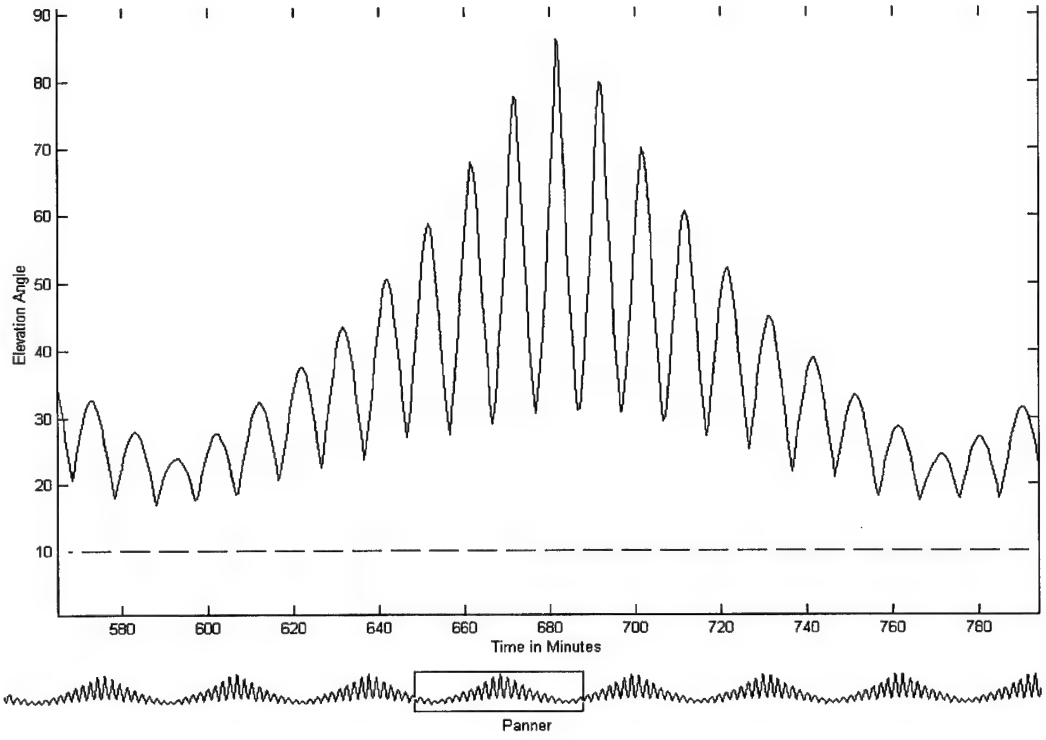

Figure 43 – Trace of Best Elevation Angle (equator) - Globalstar

pattern with eight cycles in a 24 hour period. With eight orbital planes it would initially seem that there should be 16 cycles per day as the user passes under 16 orbital planes in a single rotation of the earth. The reason for the lower than expected number of cycles relates to the inclination of the orbital planes. Whereas Iridium's best satellites were drawn from a maximum of two planes, a Globalstar user utilizes up to four planes simultaneously. For an equatorial user,

the two ascending planes combined with the two descending planes form a 'box' around the user. This box is seen as the diamond shape bound by Globalstar's planes at the equator in Figure 25. This box migrates eastward, providing a slowly rising and falling set of path elevation angles at eight cycles per day.

The 10-minute cycles in Figure 43 actually consist of between one and four satellites handing over control of the path. The smooth curve of Globalstar's 10 minute cycle of best elevation angles is actually comprised of up to four separate sections, each to a different satellite, and each section lasting between one and 10 minutes.

4.3.4.3 Statistical Comparison

The distribution of best elevation angles is best described graphically with the use of PDF histograms. An analysis of the raw histograms indicates that the distributions for both constellations vary markedly with latitude. Iridium favors the mid-to-high latitudes, while Globalstar shows a tendency to favor the lower to mid latitudes with little or no coverage at the high latitudes. To gain an initial appreciation of the nature of the differences in the best elevation angle, Figure 44 shows the median values for both systems as a function of latitude. The tenth and ninetieth percentiles are also provided as dotted lines to illustrate the range of values in the distribution.

In the low to mid latitudes from the equator to 55°, the Globalstar constellation provides median elevation angles between 13° and 23° higher than Iridium. Additionally, while Globalstar's tenth percentile rarely drops under 20°, Iridium's lower percentile curve does not rise above 20° until a user is higher in latitude than the tip of the United Kingdom, at approximately 60° latitude. Nonetheless, beyond this point Iridium quickly overtakes Globalstar and its peak reading of 53° (at 85° latitude) exceeds Globalstar's peak (at 45° - 50° latitude) by several degrees.

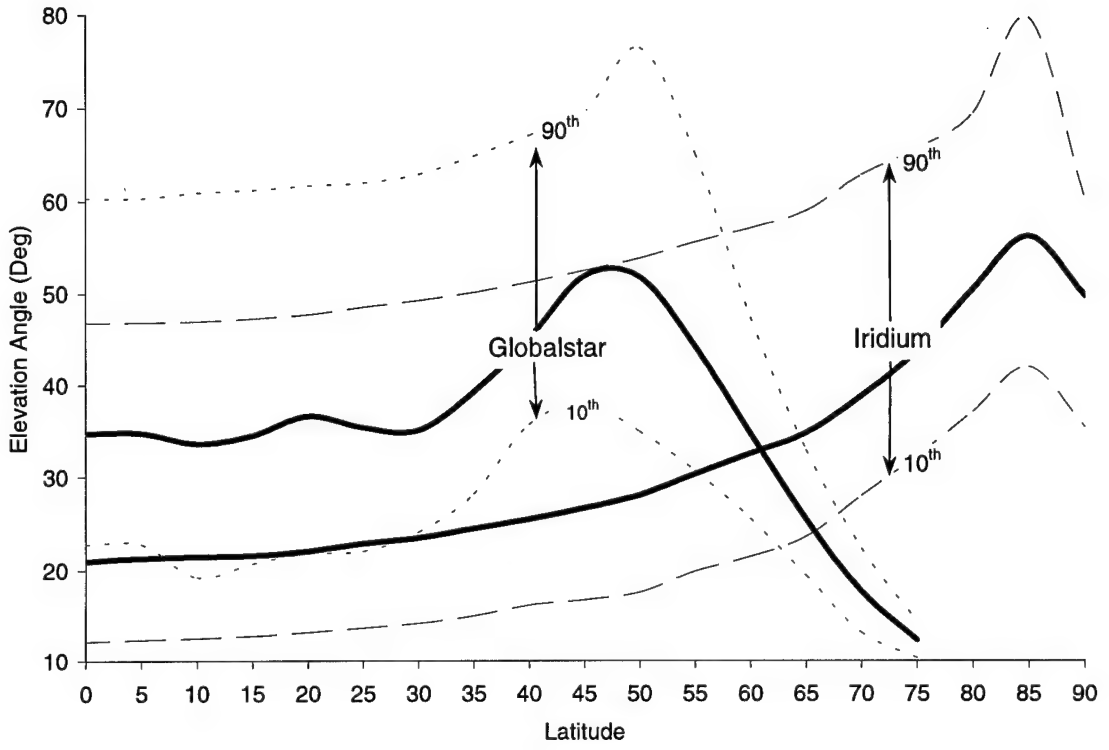

Figure 44 - Median Best Elevation Angles (10^{th} and 90^{th} Percentile Curves)

To illustrate the lower boundaries of each system's performance, Figure 45 shows the probability of the elevation angle of a randomly chosen path being less than 20° or 30°. A plot lower in the scale indicates a lower probability (desirable) of obtaining a poor link. Conversely, a plot located higher in the scale indicates a user is more likely to access a satellite at these low elevation angles.

Note that Iridium's best paths are likely to be under 30° elevation below (say) the US-Canada border (approximately 50° latitude), while Globalstar users have a much lower likelihood of obtaining an elevation angle under 20°. The implication of these figures is that, even when considering the best possible path offered by the two systems, Iridium is likely to suffer substantially greater levels of shadowing and multipath effects than Globalstar.

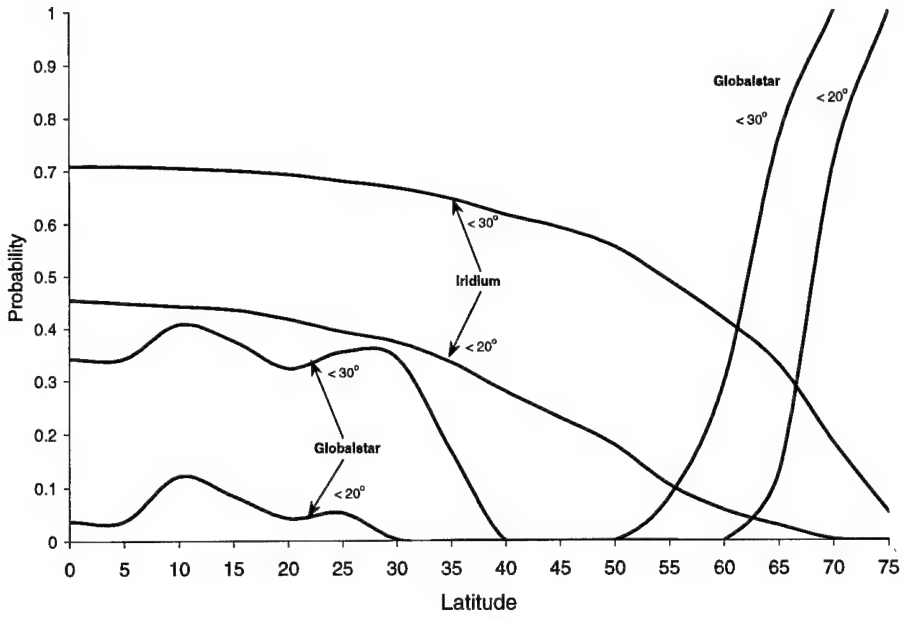

Figure 45 – Exceedence Curves for Best Elevation Angles of <20° and <30°

4.3.5 Model Fitting - Best Elevation Angles

The Gamma function provides the most consistently accurate fit to the distribution of best elevation angles for the Iridium constellation. The density function of the Gamma distribution is described by :

$$f(\theta) = \frac{(\theta - \gamma)^{\alpha-1}}{\beta^{\alpha}\Gamma(\alpha)} e^{\left[\frac{-(\theta-\gamma)}{\beta}\right]} \tag{29}$$

where γ = *Location*

α = *Scale*

β = *Shape*

The parameters of the closest approximation Gamma distribution are provided in Table 10 for latitudes between 0° and 60°. The mean and maximum errors are provided as separate columns beside the parameters. As the shape parameter is not an integer the cumulative distribution has no closed form and an integral method must be used.

Table 10 – GAMMA Distribution Parameters – Iridium

		Parameters				
		Location: γ	**Scale: β**	**Shape: α**	**Average Error**	**Maximum Error**
Latitude	0	8.1989	11.4975	1.53115	0.01087	0.03908
	5	8.1999	11.2046	1.58243	1.15E-02	0.03904
	10	8.1999	10.8128	1.65825	1.28E-02	0.04556
	15	8.208	11.3619	1.56683	0.01367	0.04957
	20	8.8709	11.13	1.62	0.01308	0.04578
	25	10.233	12.0186	1.42794	9.59E-03	0.03236
	30	10.327	11.3502	1.55588	0.01188	0.04096
	35	10.6529	10.7629	1.69176	0.01304	0.04487
	40	12.0249	11.3011	1.59159	9.81E-03	0.03203
	45	13.1669	12.4534	1.43567	7.33E-03	0.02124
	50	11.5999	9.81216	2.10454	0.01168	0.0382
	55	13.5179	10.1557	2.04283	8.30E-03	0.02576
	60	13.9509	9.02248	2.47147	9.87E-03	0.03478

A regression analysis was conducted against the parameters in Table 10 to determine a set of equations which could be used to more conveniently approximate the data. The three equations derived from this process are provided below:

$$\left.\begin{array}{ll} \gamma \text{ (Location):} & 1/\gamma = 0.13043 - 0.00107\ (\lambda) \\ \beta \text{ (Scale):} & \beta = 12.0567 - 0.04632\ (\lambda) \\ \alpha \text{ (Shape):} & 1/\alpha = 0.70108 - 0.00419\ (\lambda) \end{array}\right\} \quad (30)$$

The errors between the data set and the distributions derived using these equations is provided in Table 11 below. As expected, the errors associated with the equation-derived distributions are generally greater than the original distributions. An indication of the magnitude of the error is provided by comparing the initial Expert Fit Model with the equation-derived model at 45° latitude. The regression fit at this latitude is illustrated as it has the second largest error and is located in a populous region of the earth. Figure 46 shows the 45° latitude sample data as a histogram, with the Expert Fit approximation (from Table 10) and the equation derived approximation (from Table 11) provided as comparisons.

Table 11 – Gamma Model Parameters and Errors

Latitude	Errors Associated with Equation 30	
	Average	Max
0	0.01326	0.05837
5	9.99E-03	0.04505
10	9.84E-03	0.03639
15	0.01083	0.04111
20	0.0122	0.04528
25	0.01464	0.06184
30	0.01681	0.0731
35	0.0163	0.0692
40	0.01538	0.06042
45	0.01652	0.06631
50	0.01351	0.03182
55	0.01093	0.02593
60	0.02446	0.0612

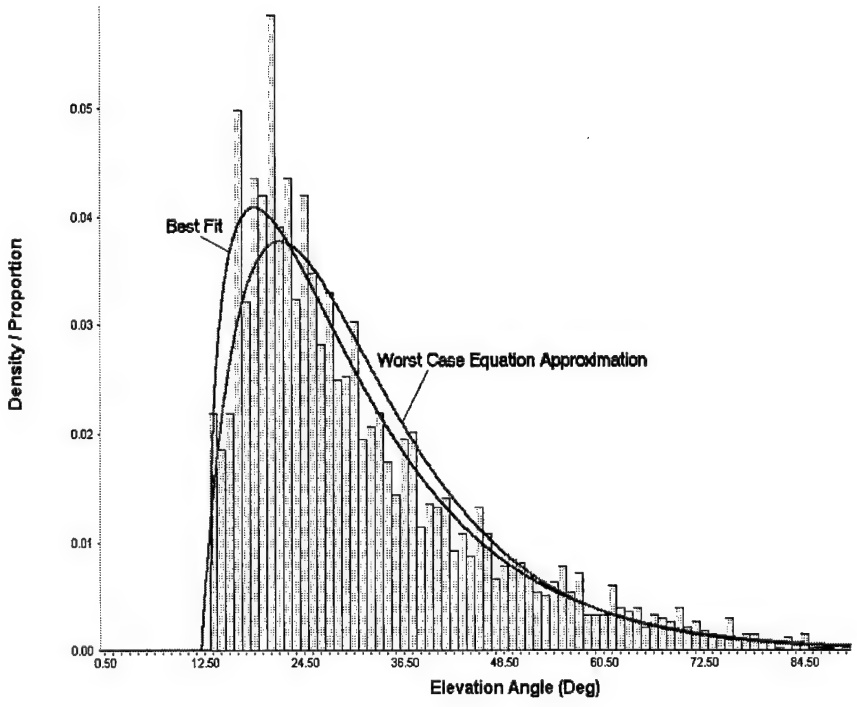

Figure 46 – Illustration of Worst Case Error

The suitability of the equation-derived model as a substitute for the empirical data depends on the application. Once again, the magnitude of the excursions between the histogram

and the models are primarily due to the selection of bin sizes. Additionally, the error values should not be compared against the y-axis as its scale is dependent on the bin size chosen.

Globalstar. The distributions of the best elevation angles to the Globalstar constellation did not display sufficient consistency to enable a single model to approximate the sample.

4.3.6 Path Attenuation

For all L- or S-Band satellite systems, the losses associated with a transmission path are dominated by the free space path loss, which is a function of both frequency and elevation angle. Rain and gaseous absorption make up only a small component of the total attenuation, adding only 0.5 dB to free space path attenuation values (see Figure 6).

Path attenuation data is produced using the in-built models within STK. The attenuation data is extracted after the output is processed to determine the best path. The resulting data is analyzed using Perfect Fit software to determine the relevant characteristics. A full set of attenuation data for each latitude is incorporated with the ionospheric scintillation plots at Appendix E.

The analysis of transmission path attenuation concentrates on the link to the highest satellite (best path). Defining attenuation using the best path provides an upper boundary on path performance, and the analysis presented here defines the best case path characteristics. The actual path used by the system is equal to or worse than the statistics described here.

4.3.6.1 Iridium

The total path attenuation for a user operating into the highest available satellite in the Iridium constellation is described in Figure 47. Rather than simply plotting a single point estimator, such as the median, the series of five curves describes the changing shape of the distribution with latitude. The plots indicate that the levels of attenuation reduce smoothly with rising latitude, but are reasonably stable when viewed over a 20° latitude range. For the low latitude user, the median path attenuation is reasonably

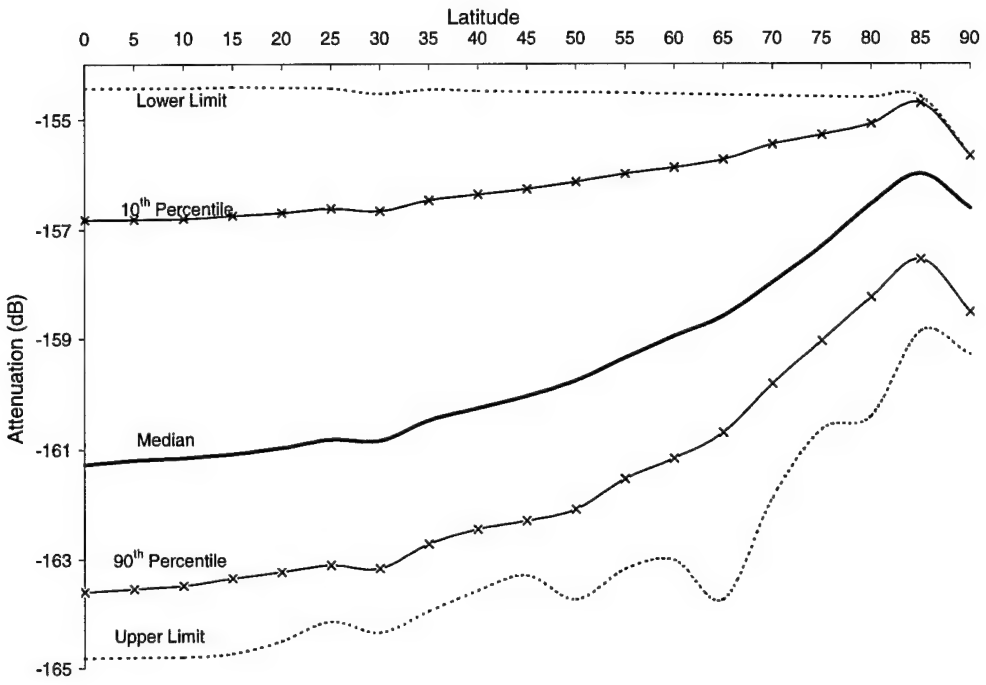

Figure 47 – Iridium Best Path Attenuation Statistics

stable at approximately 161 dB, reducing by only 3 dB up to 70° latitude. While the lower limit of path losses is set by the spacecraft altitude, the upper limit varies across its total range by less than 6 dB, and by less than 2 dB in the low to mid latitudes. The skewness of the distribution is evident by the off-centered placement of the median curve between the upper and lower percentiles.

4.3.6.2 Globalstar Downlink

The distribution of path losses (dB) for the downlink to a Globalstar user is described in Figure 48. Globalstar's median path attenuation is relatively stable at approximately 167 dB until the 30° latitude point. Between 30° and 60° latitude the path attenuation is up to 2 dB lower, before increasing rapidly at the higher latitudes.

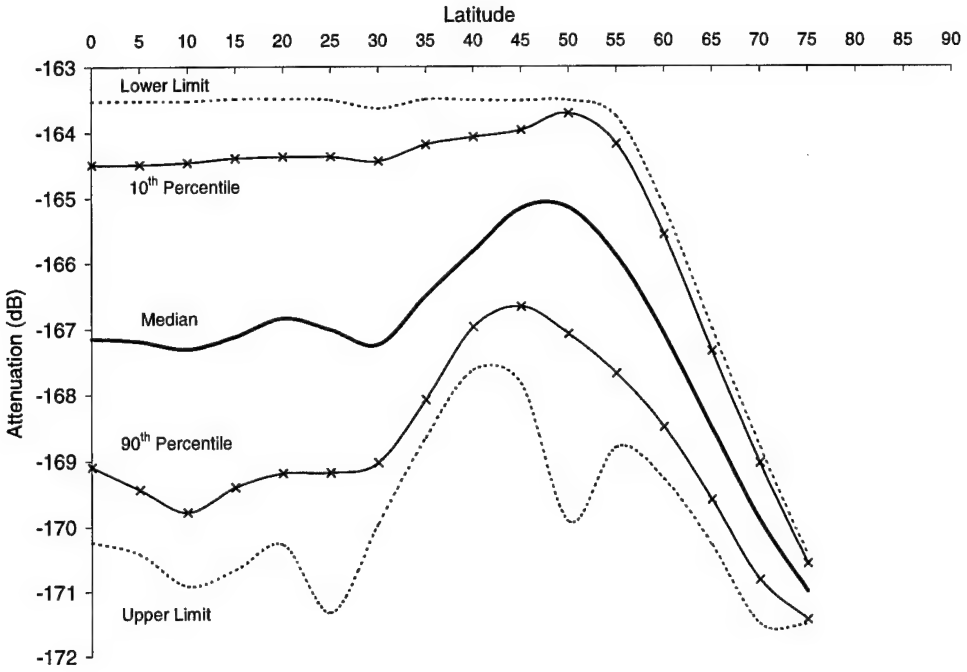

Figure 48 – Globalstar Best Path Attenuation Statistics

An important aspect of this analysis is that only the downlink is considered in the analysis of path losses. In the case of Iridium, uplink and downlink channels share a common frequency band, and the statistics presented in Figure 47 above applies to both links. However, Globalstar uses L-Band (1610 - 1626.5 MHz) for the uplink and S-Band (2483.5 - 2500 MHz) for the downlink. Assuming the same path is used for the uplink and downlink, the Free Space Path Losses will be 3.73 dB *more* for the downlink, due to the frequency dependence of these losses (See Figure 4). Additionally, it is assumed that the difference in gaseous attenuation and rain losses between the up and downlinks is negligible. If these assumptions are accepted, the Globalstar curves presented above should be shifted up by 3.73 dB to reflect the uplink losses. This has the effect of reducing the differences between the two systems. Note that with the use of handheld transceivers, the uplink is most likely to have the least link margin available and the use of the lower frequency makes best use of the limited power available.

4.3.6.3 Comparative Analysis

The differences between the Iridium and Globalstar median path losses are illustrated in Figure 49. The vertical distance between the Iridium plot and either of the two Globalstar plots represents the difference in the link losses. Figure 49 illustrates that Globalstar's utilization of the lower uplink frequency reduces the difference between the two systems significantly.

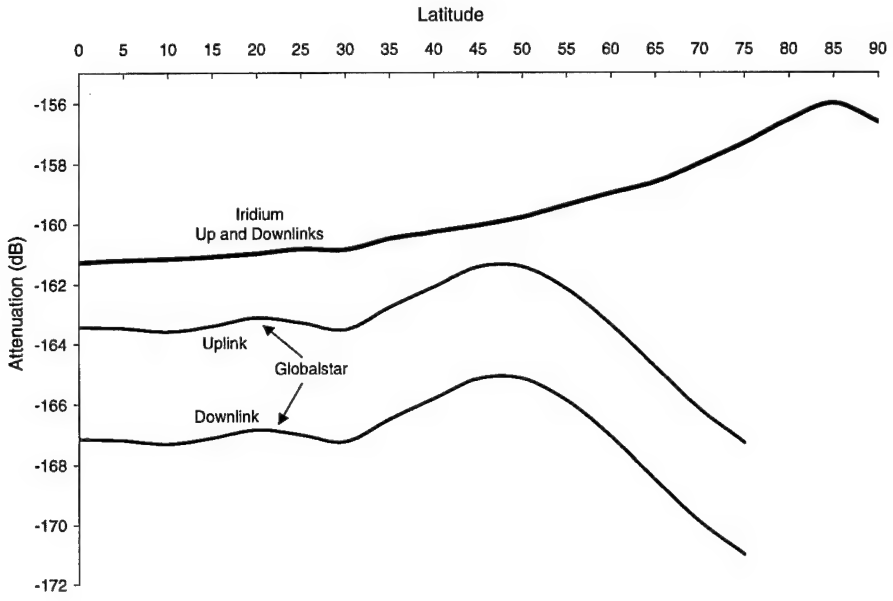

Figure 49 – Median Path Losses

For the uplink, the difference between the two systems does not vary by more than 1.5 dB until the user's latitude rises above 55°. Above this latitude Globalstar's link elevation angles decrease while Iridium's improve, thus increasing the difference in path losses. Note that the handheld devices utilized for S-PCS communications are generally battery operated and employ omni-directional antennas. These factors place severe constraints on the maximum power output and EIRP available for the uplink. In light of this, it is not surprising that the lower frequency is employed on the uplink.

Note that the losses on the best (highest available) path are modeled, so the difference between Globalstar and Iridium uplinks is not constant. The best path for a Globalstar satellite is

generally higher than an Iridium satellite and this works to diminish the disadvantage of the higher orbit. To illustrate this point, in the heavily populated mid latitudes, the difference in uplink path losses is only 2 dB, and sometimes less. This is perhaps surprising considering that Globalstar satellites orbit at almost twice the altitude of Iridium. Note also that the two systems utilize different communications techniques, and these may provide additional gains or losses. No attempt is made to imply that communications will be more effective or reliable with either system.

4.3.7 Azimuth Angles

The nature of the azimuth angles is of relevance when considering the issue of multipath and shadowing effects. In this section the time varying characteristics of the azimuth angle to the highest satellite are discussed, as well as the general case of the distribution of all azimuth angles. As will be seen, the latitude of the user influences the distribution of azimuth angles and, unlike elevation angles, the effects differ according to the hemisphere in which the user is located. The distribution of satellites for both constellations is presented in the familiar radar plot format used to describe antenna radiation patterns. The probability of a satellite being observed at a particular azimuth angle is proportional to the distance from the center of the plot. In order that an understanding of the latitudinal dependence of the parameter, only the trends and notable features are discussed.

4.3.7.1 Iridium

The azimuth angle to the satellite varies according to the same cycles as the elevation angles. Figure 50 shows the azimuth of the path to the highest satellite.

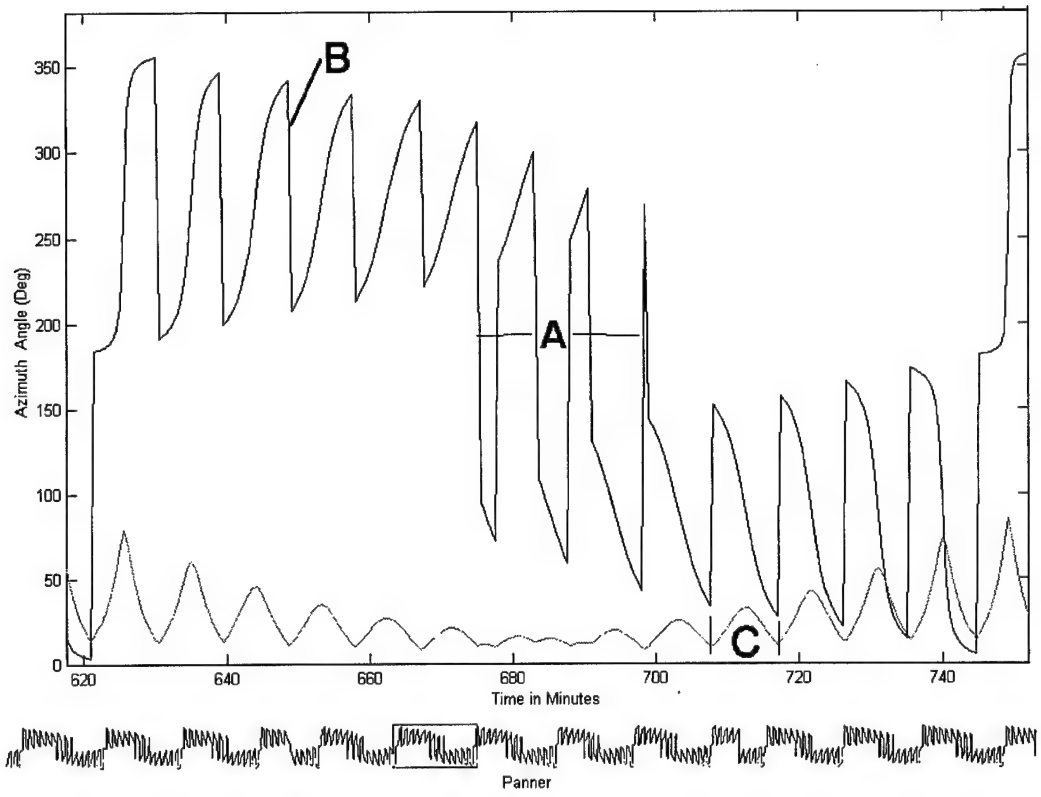

Figure 50 – Iridium Path Azimuth Angles (with Elevation Angle sub-plot)

The small plot at the lower part of the figure represents the changes in the path azimuth over a 24 hour period. The larger plot above it is an expanded view of the small boxed area, which represents approximately 2 hours. The path azimuth closely follows the best elevation angle cycles discussed in Section 4.3.4. To aid in visualizing the relationship, a faint line showing the best elevation angle has been added to the plot.

As seen from Figure 50, the path is generally to either the East or West of the user. As the user approaches the midpoint between planes, the path oscillates rapidly from side to side as satellites in adjacent planes compete for the best elevation angle. Note that the period of side-to-side oscillation is greatest when the user is midway between the counter-rotating planes (see "A" on the plot). The sharp vertical transitions in azimuth ("B) indicate a satellite changeover. The correlation between the satellite changeover, elevation and azimuth changes are shown at the lower right of the main plot ("C").

Analysis of the distribution of the full range of all path azimuth angles reveals a strong latitude influence. Figure 51 shows the distribution of azimuth angles for four users located at the equator, 40°, 50° and 60°.

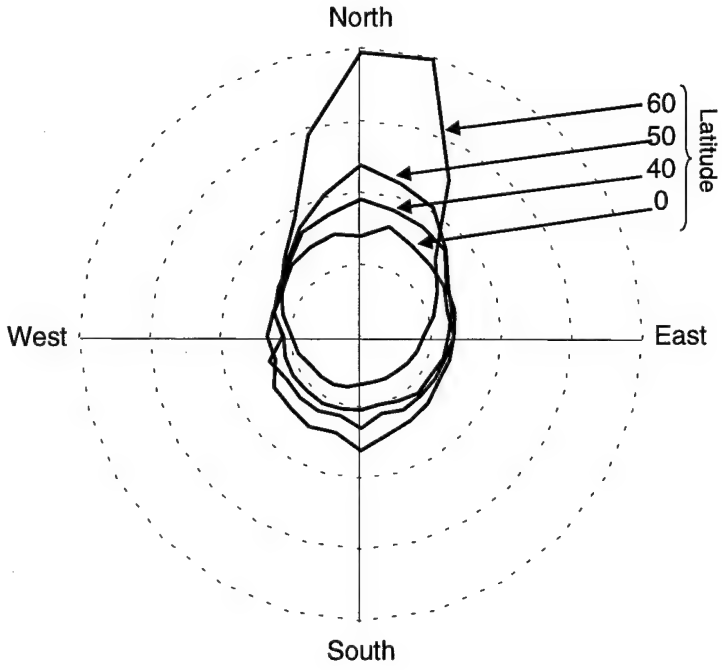

Figure 51 – Azimuth Distributions of All Paths

At latitudes below 30°, paths between a user and a satellite are equally distributed in azimuth; the probability distribution can be best described as 'omni-directional'. As the user moves above 40° latitude, the distribution of azimuth angles begins to gradually favor the north. Beyond 50° latitude, the effect increases markedly so that for users located at 60° latitude, a satellite is up to six times more likely to be seen to the north than to the south. At more reasonable latitudes of around 50° (Paris or Toronto), the distributions indicate the weighting is closer to 80% more likely. The effect is reversed for the southern hemisphere, with azimuth angles tending to favor the southern skies as a user moves south.

The reason for this dependence is related to the near-polar nature of the orbital planes. The orbital planes begin to converge towards the poles and more satellites are visible where the

planes are closer together. This is the essential reason for the increase in satellite visibility (see Figure 26) with increasing latitude. This principle is illustrated in the series of SatLab screenshots shown in Figure 52.

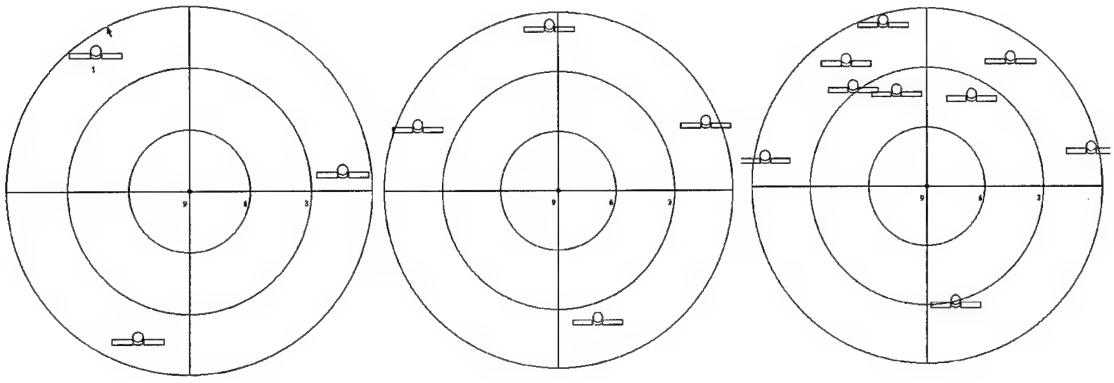

Figure 52 – Fisheye Observer Views at 0°, 50° & 75° Latitude - Iridium

The figure shows three fisheye observer views looking upwards from three different latitudes. The center of the plot represents straight upwards and the outer concentric circle is the horizon. North is at the top of each figure and satellites are arranged in the full 360° azimuthal coverage. Note the even azimuth distribution of satellites at the equator, and the manner in which the satellites tend to cluster in the northern sectors at higher latitudes. The plots are representative of the general distribution of satellites and do not imply this condition exists continuously.

4.3.7.2 Globalstar

In a similar manner, the distribution of azimuth angles for a Globalstar user at different latitudes is presented. From Figure 53, three statements can be made regarding the azimuth of Globalstar satellites. First, the low latitude plots (0° to 20°) are reasonably omni-directional. As the latitude of the user rises above 25° and approaches the 52° orbit inclination, satellites begin to favor an east-west line. As shown in Figure 25, at 52° Globalstar's satellites are at the peak of

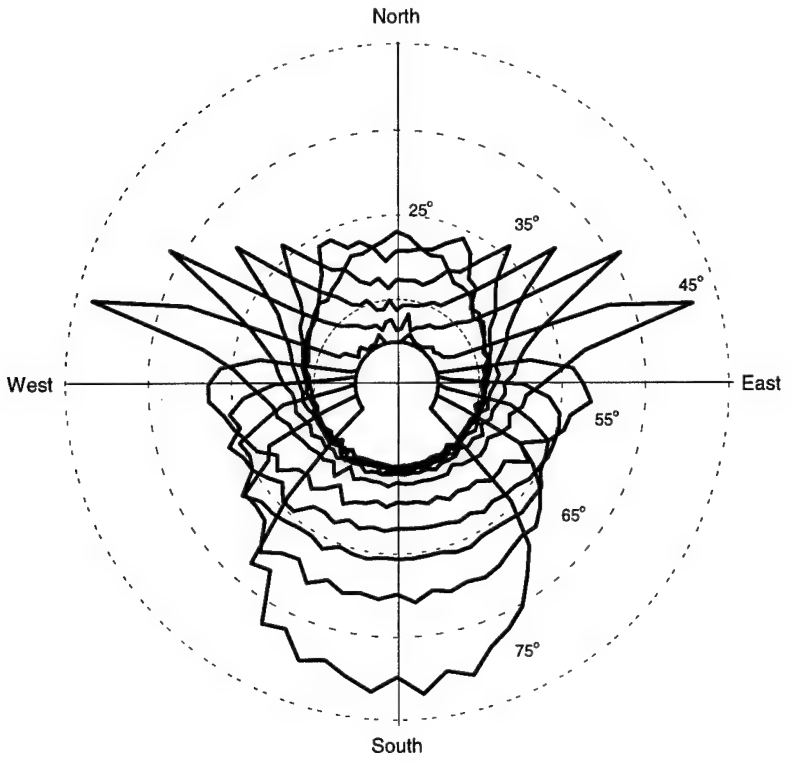

Figure 53 – Azimuth to All Satellites

their longitudinal ascension and the orbits 'flatten out' before continuing into a descending pass of the equator. Finally, as the user moves to higher latitudes, the satellites begin to appear more often in the southern sky. The reason for this is not the same as for Iridium, which related to a clustering of the satellites at the poles. Rather, Globalstar's orbits simply do not extend to these extreme latitudes and the quality of the link, in terms of its path geometry, degrades.

4.3.7.3 Comparative Analysis

For Iridium, there are few departures from an omni-directional pattern until the user travels above 40°. Additionally, the effects are not marked until above 60° latitude. Globalstar, however, displays a dramatic tendency to provide satellites to the user that are either to the east or west at latitudes around 52°. The implications of this are that blockage may be more of a problem at these latitudes if the user does not have a clear path to the east or west. However, the

availability of more Globalstar's satellites at a higher elevation angle than Iridium at these latitudes serves to mitigate the impact of this factor.

4.4 Ionospheric Effects

Modeling of the two system's paths indicates that ionospheric scintillation can affect L- and S-Band signals and cause short term fades in excess of 12 dB under certain conditions. An understanding of the extent and duration of the scintillation effects, if they do occur, is an important aspect of the operation of L-Band S-PCS systems at low latitudes. Ionospheric scintillation is influenced by several environmental factors including sunspot number, geomagnetic activity and the time of the year. A multivariate analysis which incorporates the full range of these effects is beyond the scope of this thesis.

The analysis of the scintillation is restricted to the hours of 1800 and 0400 hours. Outside these times scintillation is unlikely to be present. Therefore, the fade levels quoted are for these periods only. The scintillation activity is characterized by the use of average levels and moving averages. Average levels of fading are quoted as a means of identifying the latitudes with the highest and lowest levels of activity. A 30 minute moving average trace is used to illustrate the trend in activity over an operationally useful period. Shorter periods of averaging display a high level of variation, while averaging the raw data over longer periods disguises useful trends in the nature of the fading. Please note that the moving average plots do not imply that a user would experience continuous fades at the levels indicated, rather a user may experience fades at unpredictable times within the envelope defined by the graph. The graphs define the upper limit of activity and are not intended to indicate continuous and predictable fade levels.

It is important to note that, due to time constraints, the simulations and modeling were only conducted for the downlink. Globalstar utilizes a higher frequency for the downlink, which tends to be less affected by ionospheric scintillation. The L-Band uplink frequencies are the same

as Iridium's but are not modeled. Additionally, all modeling is conducted at 135° longitude. The scintillation effects follow the geomagnetic equator, which varies markedly according to the user's longitude. The effects are believed to be similar if the user is in the same location relative to the Appleton Anomaly.

4.4.1 Iridium Downlink

The average fading level is useful for determining the general trends of scintillation with latitude. It allows the peak latitude to be determined and the different scenarios to be ranked in terms of their effects. Figure 54 shows the fading due to ionospheric scintillation predicted by WBMOD, averaged over the 10-hour period from 1800 to 0400 hours.

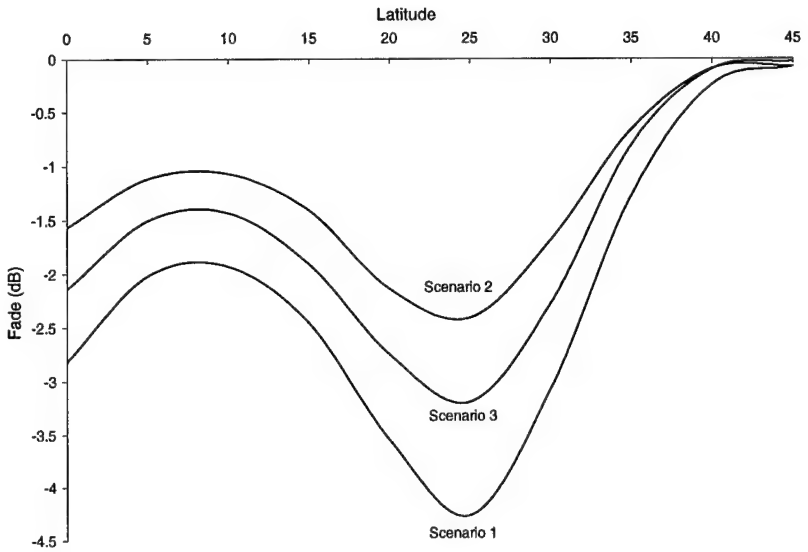

Figure 54 – 10 Hour Average Fade levels for Iridium (6 p.m. to 4 am)

The combination of environmental factors defined under Scenario 1 (see Section 3.6) causes the highest levels of average fade. At 135° longitude, the peak effects occur at 25°, which is approximately 1000 kms south of Tokyo. If the graph were to be extrapolated to the lower latitudes (left of the figure), a second peak would be apparent at approximately 8° latitude (between the island of Papua New Guinea/Irian Jaya and Darwin in the North of Australia). The

location of the minima at approximately 8° latitude aligns with the location of the geomagnetic equator (Figure 14) and the peaks align with the approximate locations of the Appleton Anomalies (Figure 9). Note that the simulations are conducted at 5° and 10° latitude and graphical smoothing places the minima at 8°. As modeling is only conducted at 10°, this is referred to as the "minimum".

The fade associated with ionospheric scintillation varies with the relative position and velocity of the user and highest available satellite. As shown in Appendix E and Figure 55 below, for Iridium, the fades typically oscillate between a low of 0-4 dB to a maximum of 12.9 dB, repeating this cycle every 9 minutes. Figure 55 shows an expanded 100 minute section of the trace of the worst case levels of fade at 25° latitude under Scenario #1 conditions.

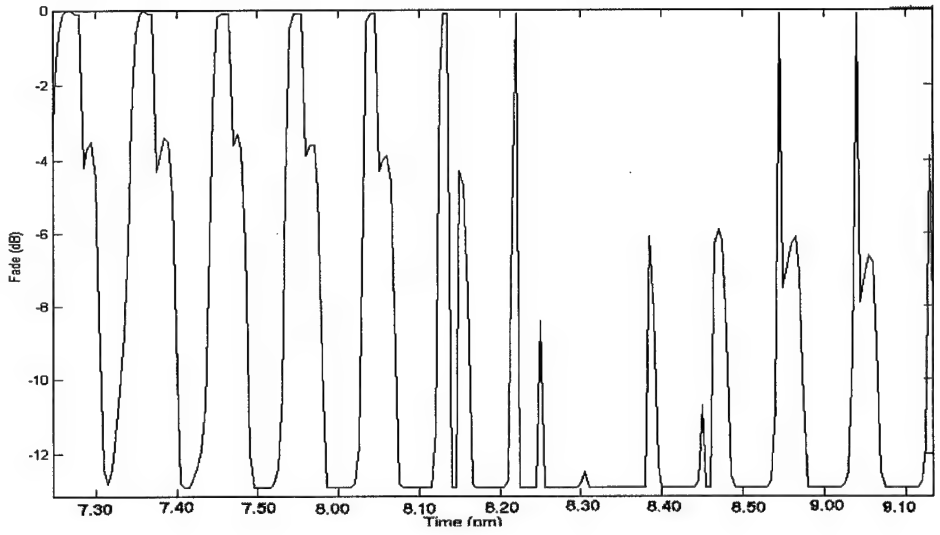

Figure 55 – Expanded View of Worst Case Scintillation Fades

Note that only the fade associated with scintillation is represented; other link losses are not shown. The time scale represents the local evening (p.m.) time. The rate of change is typically gradual, the fade rises from its minimum to maximum level in 3-5 minutes. Abrupt changes in the level across the full range of readings occur when the link changes from one satellite to another. This indicates that during periods of ionospheric scintillation a satellite

handoff may cause a call dropout if the receiver is sensitive to large changes in received signal level. Note also from Figure 55 that at the 670-715 minute period (2010 to 2055 hours local), the level of fading is most severe. This time represents the period of peak scintillation activity for this location. For other scenarios and latitudes, the short term profile of the scintillation activity follows a similar pattern, only the degree of attenuation differs.

4.4.1.1 **Scenario 1: Solar Maximum at Equinox (probable around March and December 2000).** Two moving average fade levels are provided in Figure 56 to illustrate the level of variation between the minimum at approximately 10° and maximum at 25° latitude.

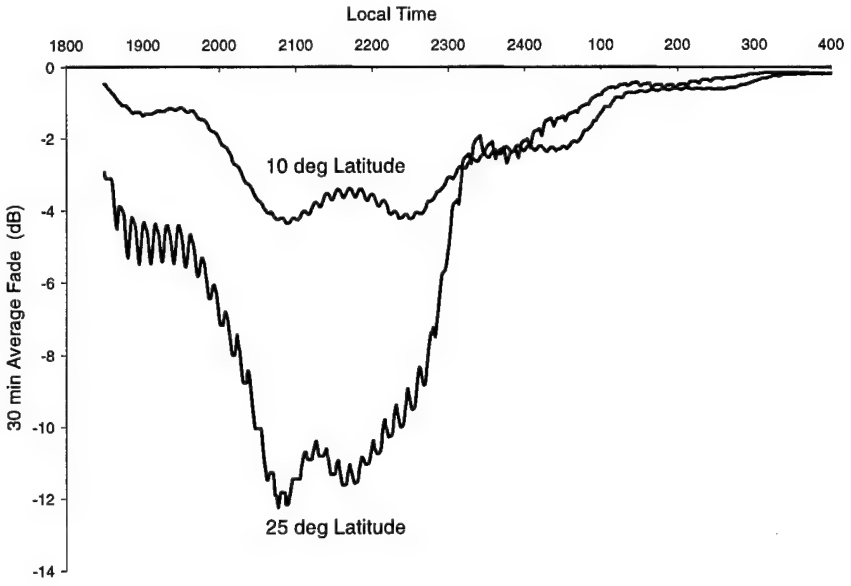

Figure 56 - Scenario 1, 30 Minute Moving Average Fade levels (10° & 25° Lat)

The upper plot (smaller losses) represents the fades at 10° latitude, the lower plot represents a user at 25° latitude. The curves for other latitudes between 0° and 45° can be estimated using the plots at Appendix E and Figure 54. Under Scenario 1 environmental conditions WBMOD predicts a maximum 30-minute average fade of 12.2 dB at 25° latitude with fades exceeding 3 dB between 1830 to 2300 hours local. The period of peak (>10 dB) fades

occurs generally between 2030 and 2230 hours local. It is interesting to note that even at 10° latitude, fades greater than 3 dB are possible between 2015 to 2300 hours.

The combination of free space path loss, gaseous absorption and scintillation comprises the total path loss in the presence of scintillation. If these three losses are taken into account the total path loss on an Iridium link at 25° latitude and 135° longitude under these environmental conditions can range between 154.4 and 176.7 dB, a dynamic range of 22.3 dB. The upper and lower limits for other latitudes can be established from an inspection of Appendix E.

4.4.1.2 **Scenario 2: Solar Maximum at Solstice (probable around June or September 2000).** Figure 57 provides the results of simulation for minimum latitude (10°) and maximum (25°).

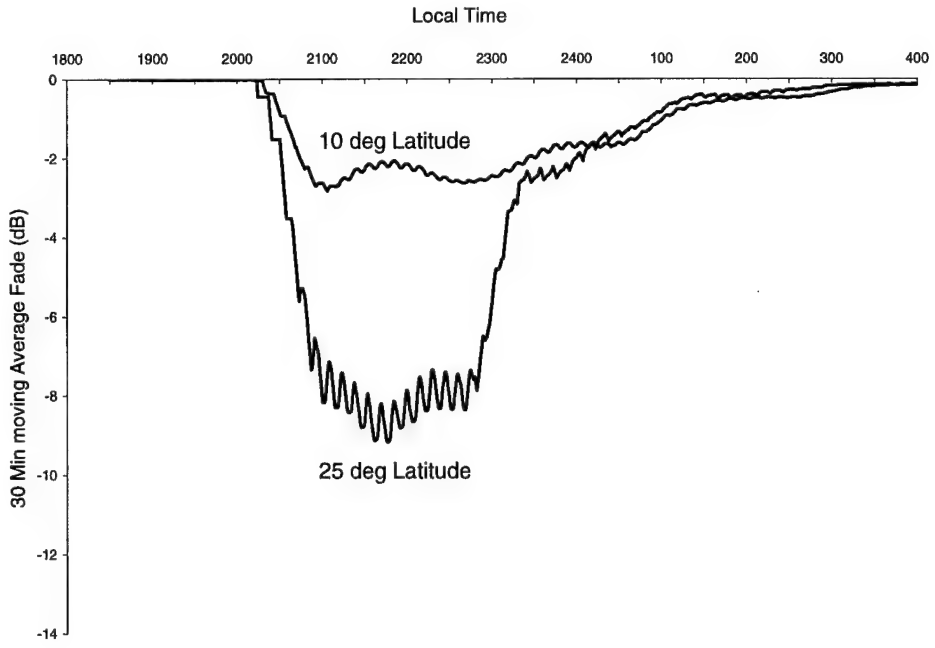

Figure 57 - Scenario 2, 30 Minute Moving Average Fade levels (10° & 25° Lat)

Fades in excess of 3 dB are likely between the hours of 2230 and 2300 hours local at 25° latitude. The level of fade at 10° does not quite reach 3 dB but could be expected to exceed this figure on latitudes above and below. Examining the moving average plot of Figure 57, the

maximum level of fade is approximately 4 dB less than Scenario1, and due to a 2 hour later start, the duration of the activity is less. Of the three scenarios simulated, Scenario #2 provided the lowest levels of scintillation for Iridium.

4.4.1.3 **Scenario 3: Moderate Solar Activity Levels (SSN=80) at Equinox** (probable during March and December between July 1998 and May 2003). As can be seen from Figure 58, scintillation levels arising under Scenario 3 conditions are midway between the least and the greatest. However, the commencement and duration is similar to that for Scenario #1.

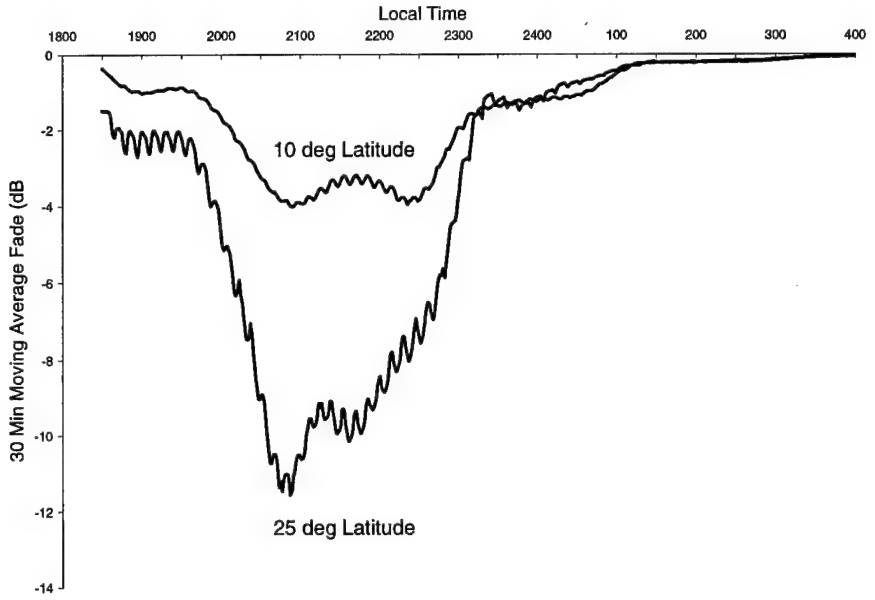

Figure 58 - Scenario 3, 30 Minute Moving Average Fade levels (10° and 25° Latitude)

Under these environmental conditions, WBMOD predicts a maximum 30-minute average fade of 11.6 dB at 25° latitude with fades exceeding 3 dB between 1945 to 2300 hours local. The period of peak (>10 dB) fades occurs for a 45 minute period between 2015 and 2100 hours local. At 10° latitude, greater than 3 dB fades are possible between 2030 and 2230 hours. Although the sun spot number was reduced, the scintillation levels remain similar with all other factors remaining unchanged from Scenario #1. Within the limited scope of this modeling, the day of the year has a greater effect than the sun spot number.

4.4.2 Globalstar Downlink

In most cases, Globalstar's higher downlink frequency reduces its susceptibility to Ionospheric scintillation. The 10 hour average and 30 minute moving average plots indicate a similar profile to Iridium, but at a reduced level. Figure 59 shows the fading levels as a function of latitude under all three scenarios.

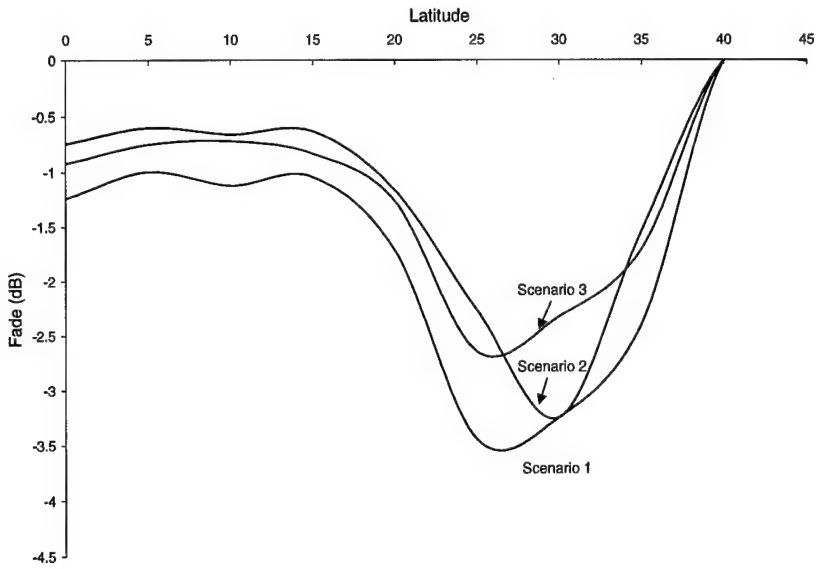

Figure 59– 10 Hour Average Fade levels for Globalstar (6 p.m. to 4 am)

Note from Figure 59 that Scenario 1 provides the greatest level of fading, with Scenarios 2 and 3 in respectively lower ranks. Figure 60 illustrates the worst case levels of scintillation (no other attenuation effects) for Globalstar at 25° latitude between the hours of 1900 and 2315 hours local. The fading generally varies between the minimum and maximum levels with a cycle of approximately 19 – 21 minutes duration. The fading shown in Figure 60 has additional cycles inserted between the fundamental 19 – 21 minute period and is the worst case for Globalstar (for 99% of the time). Again, the sharp transitions are related to a change in satellite, and the slower transitions are associated with the gradual change in the relative positions and velocities of the user and satellite. The dotted line is located at the 3 dB fade level.

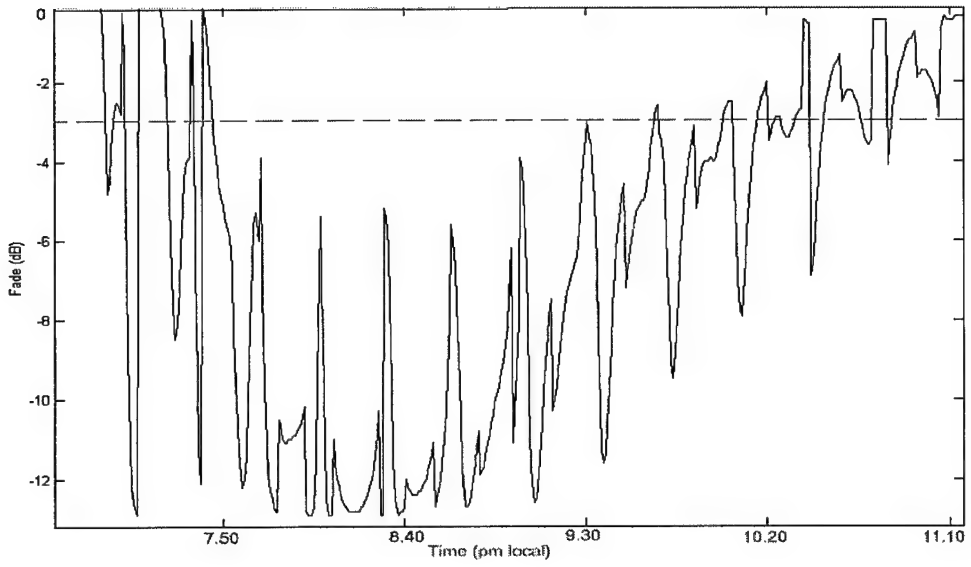

Figure 60 - Expanded View of Worst Case Scintillation Fades

4.4.2.1 **Scenario#1:** Maximum levels of scintillation occur at 25° latitude with a minimum at 10°. Figure 61 illustrates the minimum and maximum fading levels at 10° and 25° latitudes respectively.

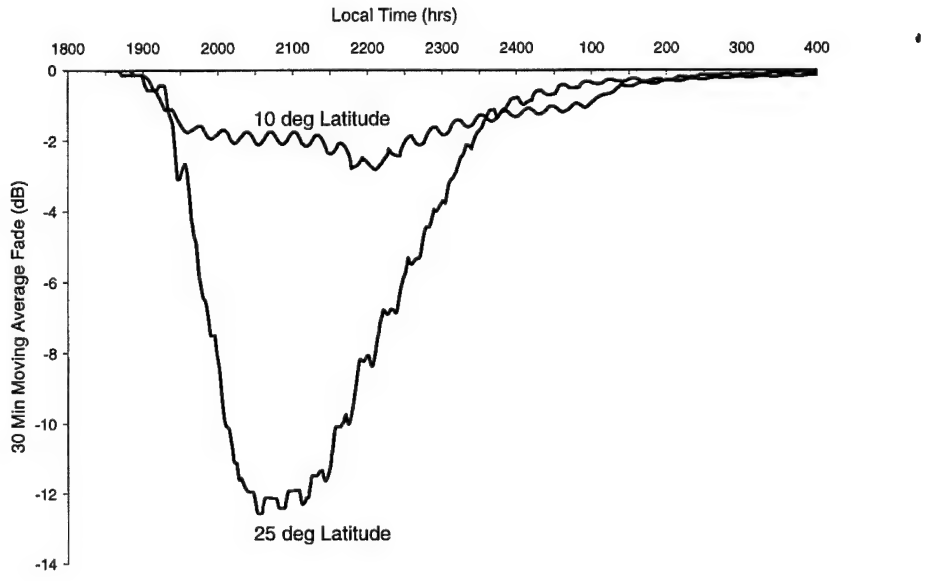

Figure 61 - Scenario 1, 30 Minute Moving Average Fade levels (10° & 25° Lat)

At 25° latitude, the fade levels greater than 3 dB occur between 1930 and 2330 hours. The maximum occurs at approximately 2030 hours and severe fading (>10 dB) occurs for a 90 minute period from 2000 to 2030 hours local. The peak of 12.8 dB occurs at approximately 2030 hours. Minimum levels of fade occur at 10° latitude and only occasionally exceed 2 dB. With the effects of free space path loss and gaseous attenuation combined, the signal varies between -163.4 and -184.0 dB, a dynamic range of 20.6 dB.

4.4.2.2 **Scenario 2:** Maximum levels of scintillation occur at 30° latitude and were generally 2 dB lower than for scenario #1. Figure 62 illustrates the minimum and maximum fading levels at 10° and 25° latitudes respectively.

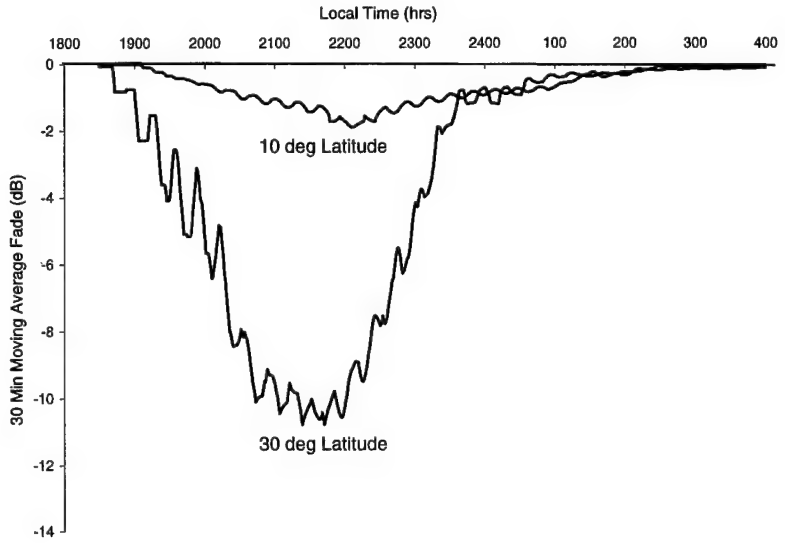

Figure 62 - Scenario 2, 30 Minute Moving Average Fade levels (10° & 30° Lat)

At 30°, the fade levels greater than 3 dB occurs between approximately 1930 and 2330 hours and reaches a peak of 10.6 dB at 2130 hours. Fade levels at 10° latitude did not exceed 2 dB. The spikes which are particularly prominent on the top of the 30 minute average waveform tend to follow the sharp transitions in the plot of azimuth angles. This shows that the sharp transitions in the scintillation plots coincide with the satellite handoffs.

4.4.2.3 **Scenario 3:** The 30 minute moving average plots for 10° and 25° are provided in Figure 63 below.

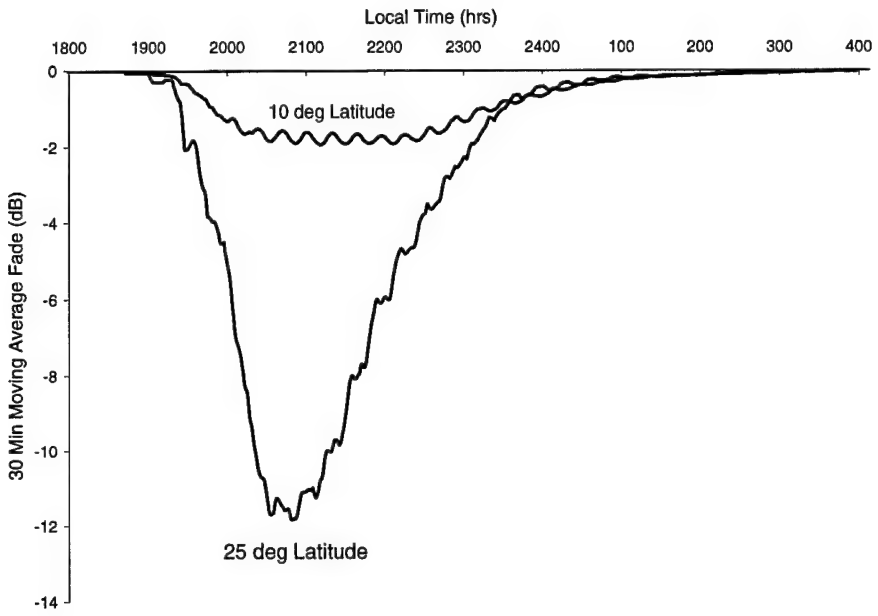

Figure 63 - Scenario 3, 30 Minute Moving Average Fade levels (10° & 25° Lat)

The plot is similar in structure to Scenario 1, with only a slight (½ to ¾ hour) reduction in the duration of the greater than 3 dB scintillation level. Under this scenario, the fades exceed 3 dB from 1945 - 2245 hours, a period of 3 hours. The peak (>10 dB) period lasts approximately one hour, commencing at about 2015 hours local. The highest level of fade is 12 dB occurring at 2100 hours.

4.4.3 Comparative Analysis

A comparison between the two systems is difficult due to the number of variables, the limited scope of the analysis, and the difficulties in characterizing an unpredictable event such as ionospheric scintillation. Nonetheless, within the scope of this study and the measures employed, Globalstar is generally less affected than Iridium by ionospheric scintillation.

An initial appreciation of the differences in the relative performance of the two systems can be provided by comparing the plots of the Scenario 1 curves of Figure 54 and Figure 59. Figure 64 shows the changes with latitude in the average fade levels for both systems.

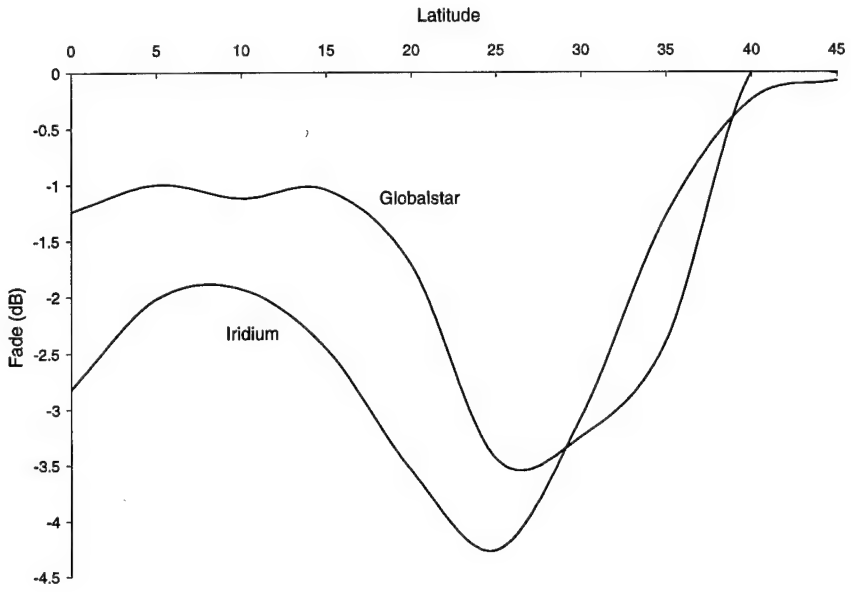

Figure 64 – Comparison of Worst Case Average Fade

As can be seen, Iridium generally suffered greater levels of fading than Globalstar until 30° latitude. However, between 30° and 40° latitude Iridium is less affected than Globalstar. A comparative examination of the data indicates this is due to both an approximation in WBMOD, and the azimuth distributions of the two systems. WBMOD predicts whether a signal is affected by scintillation by creating an infinitely thin scintillation sheet which has definite edges. If a signal intercepts the sheet, scintillation effects are calculated. If not, then the signal is assumed to be free of scintillation. At 25°-30°, Globalstar begins to start favoring an east-west path (see Figure 53), whereas Iridium starts to favor a northerly path (see Figure 51). The more northerly path tends to place Iridium's paths out of the scintillation, while the east-west tendency keeps Globalstar's path in the scintillation region. This is the underlying reason for the skewing of the plots of Figure 59.

Notwithstanding the azimuth distribution effects, the two systems performed differently under the three sets of environmental conditions. Figure 65 below illustrates the duration of the worst case scintillation effects for the three scenarios.

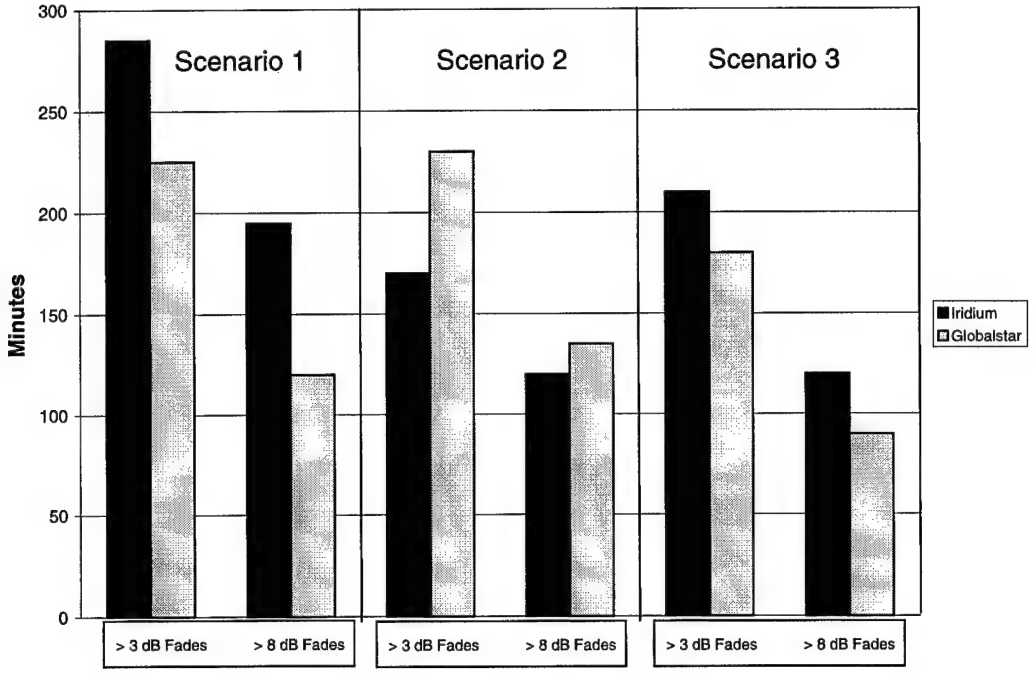

Figure 65 – Scintillation Fade Duration

Under the worst case scintillation conditions defined by Scenario 1 at 25° latitude, Globalstar performs better than Iridium. Although the peak fade levels are the same at 12.5 dB, Iridium maintains a high level (> 8 dB) for 1hr 15 minutes longer and a moderate (> 3 dB) fade for 1 hour longer. Under Scenario 3, the situation is similar, except that the duration of the scintillation is generally an hour less and reduced by approximately 2 dB throughout the range. In contrast to Scenarios 1 and 3, Iridium suffered lower levels of fading than Globalstar, under Scenario 2 conditions, for shorter durations. However, this effect is generally restricted to 25° latitude. An analysis of Globalstar's scintillation fades at other latitudes indicates that Globalstar is affected most at 25°, the latitudes on either side show lower effects than Iridium. When

considering the fades at other latitudes than the peaks, Iridium fades were generally between 1 to 3 dB higher (30 minute average).

In general terms, Globalstar is expected to provide approximately 2 dB lower fade under most conditions modeled, when averaged over a 30 minute period. A notable exception to this generalization occurs at 25° to 30° latitude with high sunspot activity in late June, where Iridium's response is similar or slightly better. Apart from this exception, ionospheric scintillation affects Globalstar's downlink later in the evening, for a shorter duration and at lower levels. Additionally, with ionospheric effects incorporated into the total link losses, Iridium's total range of losses is 22.3 dB, compared to 20.6 for Globalstar.

4.4.3.1 **Impact of Multiple Satellites**. Ionospheric scintillation can cause severe fading (5-7 dB average, > 20 dB peak for 10% of the time) to *geostationary* satellite transmission paths under worst case environmental conditions [Oga80]. The high relative velocity between user and LEO satellites would be expected to reduce the duration of any severe fading as the path passes through an irregularity rather than linger within it. However, it is believed that the greatest protection is provided by the availability of multiple diverse paths and a responsive link control mechanism which can sense severe impairments and quickly switch to an alternative path. Assuming that both LEO systems have the capability of monitoring alternative paths and dynamically allocating different satellites to the user, Globalstar's substantially better coverage at low and mid latitudes should provide a greater level of immunity than iridium.

4.4.3.2 **Operational Interpretation of Results**. The operational interpretation of the data is that if a user were to operate a link to the satellites under the geomagnetic, solar and temporal conditions defined, fades of similar intensity to the plots may be experienced. As the model does not deal with the spatial distribution of the irregularities, individual incidents of fade cannot be predicted. Fades due to ionospheric scintillation may occur unpredictably, but generally within the outer envelope of fade intensity defined by the plot. The distribution and movement of the irregularities which induce the rapid fades are complex and no models exist at

this time which can be used to predict the total effect. The ideal method of determining the actual impact would appear to be deploy to an affected area and monitor signal levels for evidence of scintillation. Secondly, the reader is cautioned against interpreting the results of this analysis for any other longitude than 135°. The effects follow the line of the geomagnetic equator, meaning that the peaks which occur at -5° and 25° latitude above Australia may occur at the equator and -20° when considering the Americas. Figure 14 and other references [Oga80] [Sec97] [Wha97] should be used as a guide in estimating the location of the Appleton Anomalies and the associated peaks and troughs.

CHAPTER 5

SUMMARY AND CONCLUSIONS

The motivation for this thesis has focussed on the performance of two fundamentally different S-PCS systems at equatorial and low latitudes. These latitudes cover much of the developing world and also encompass the areas of Australia's principal strategic interest. The analysis was extended to all latitudes to provide a more complete understanding of the two systems and to allow a comprehensive comparison. The geometry of the transmission path and the number of visible satellites are prime factors in assessing the relative performance of these S-PCS systems in a variety of applications.

5.1 Summary

5.1.1 Visibility and Elevation Angle. The analysis confirms that Iridium provides truly global coverage for all users, regardless of latitude. The constellation architecture provides minimum coverage at the equator and a gradual improvement with rising latitude. However, equatorial coverage is minimal and substantial improvements are not realized until the user reaches latitudes of 50° and above. Above this latitude the quality of coverage rises dramatically. In contrast with Iridium, Globalstar services only the latitudes between approximately ± 70°. At the low to mid latitudes, the higher satellite altitude and lower orbit inclination provides the Globalstar user with substantially higher satellite visibility than Iridium, generally by one or two satellites. A Globalstar user is more than twice as likely to experience multiple satellite coverage than an Iridium user until latitudes of approximately 35° (San Diego) are reached. Above these latitudes, Iridium gains on Globalstar until approximately 55° latitude (Glasgow, UK) when Iridium's coverage begins to dominate. The analysis has found that Globalstar's coverage is highest in the densely populated latitudes between 25° and 55°, providing up to four satellites to

the user at elevation angles between 5° and 11° higher than Iridium. Below 55° latitude, the median elevation angles to Globalstar's best satellites are between 13° and 23° higher than Iridium. Above 60° altitude, Iridium generally dominates in the areas of satellite visibility and elevation angle. These figures illustrate the potentially higher levels of path performance offered by Globalstar for users at the low to mid latitudes.

5.1.2 Azimuth. The azimuth characteristics of the systems differ according to their constellation characteristics. As the Iridium user moves towards either hemisphere's higher latitudes, the convergence of the orbital planes tends to form clusters of satellites in the poleward direction, either North or South. The implies that, for a user in the upper mid to high latitudes of the northern hemisphere, obstructions to the North would tend to have a greater impact on satellite visibility than those to the south. Globalstar users face a similar problem in that satellites tend to be located toward the poles at around 30° - 40°, and to the east or west around 52° latitude. For Globalstar, the skewing effect at latitudes below 25° is mild, but becomes pronounced as the user approaches 52° with the probability of accessing a satellite to the east or west approximately four times that of accessing on to the North or South. As the Globalstar user ventures above 52°, the satellites appear more and more in the southern sky, until system access is lost. Globalstar' higher azimuth variability may have implications in its susceptibility to signal multipath and shadowing effects.

5.1.3 Ionospheric Scintillation. Ionospheric Scintillation can affect both system downlinks, possibly causing fades in excess of 12 dB under certain environmental conditions. The fades vary according to the relative position and velocity of the user and satellite and are worst between the hours of 6 pm to 4 am with peak fades generally experienced around 9 pm. The low latitude effects are limited to the areas around the geomagnetic equator and are most likely around March 2000, the expected time of the solar maximum. Globalstar's higher downlink frequency reduces the effects by approximately 2 dB and the higher availability of

satellites may provide additional levels of link redundancy. The analysis did not address the uplink.

5.2 Conclusions

The results of extensive analysis of data from simulations of Globalstar and Iridium constellations indicate that the user's latitude is a major factor in satellite visibility, and the distribution of path elevation and azimuth angles. Additionally, modeling has shown that ionospheric scintillation is a potentially serious problem for both systems under certain conditions. The analysis indicates that, in the low to mid latitudes Globalstar will provide its users with a considerably greater number of satellites at higher elevation angles than Iridium. The distribution of path characteristics tends to indicate that blockage, shadowing, and multipath interference effects will be lower for Globalstar than for Iridium. Additionally, Globalstar's higher downlink frequency and the availability of multiple paths reduces the severity of fades due to equatorial ionospheric scintillation. For these reasons, the Globalstar system may be a more suitable choice for the low latitude user.

However, although the link between the user and the satellite is arguably one of the most important factors in a system's performance, it is not possible to compare the systems based on the performance of their transmission paths alone. The systems differ fundamentally in their approach to providing global S-PCS services and the user's requirements will determine which system provides the best performance.

5.3 Recommended Further Research

Two areas present themselves as prime areas for follow-on research. Firstly, the results of the simulation analysis may be verified by physically deploying a test station to an area known to be affected by ionospheric scintillation. This would have the effect of validating (or otherwise) the models and assumptions used in the analysis. The results of such research would be of

interest to communications specialists planning to deploy such systems on a large scale, or for critical applications such as search and rescue, humanitarian aid, or military operations. Secondly, multipath effects, shadowing and blocking represent potentially serious impairments to both systems, and Iridium in particular. The development of complete multipath fade models which utilize the equations presented in this research may assist in predicting the impact on LEO S-PCS systems.

5.4 Summary

The purpose of this thesis has been to provide a comparative analysis of the transmission path to the Iridium and Globalstar satellite constellations. The worst case impact of ionospheric scintillation has also been predicted through modeling for a particular region of interest to the Australian Defense Force.

The motivation for the thesis and the necessary background required to estimate the impact of the relevant atmospheric impairments were provided in Chapter 1 and Chapter 2 respectively. The methodology, process, assumptions and limitations of the research are detailed in Chapter 3, with the analysis and presentation of results provided in Chapter 4.

APPENDIX A - ATMOSPHERIC MODEL DISCUSSION AND CALCULATIONS

This Appendix provides background discussion relating to relevant atmospheric effects which could be expected to impair the propagation of Iridium and Globalstar signals. It is important that the models used to calculate the atmospheric effects are described to support the conclusions relating to the relative impact of the effects. Clear air effects are discussed first, with hydrometeors (rain, snow, fog etc) following. Several of the mathematical models have been implemented in Microsoft Excel 5.0 [Ani98] and these programs are used as required throughout this thesis. In particular, these programs were used to verify the rain and gaseous absorption calculations performed by STK.

A.1 "CLEAR AIR" EFFECTS

This section addresses the effects on a satellite signal of apparently clear air. These effects consist mainly of:

- absorption of the signal by water vapor and the gaseous components of the atmosphere;
- scintillation caused by refractive and scattering effects in the troposphere;
- cross-polarization effects;
- decrease in antenna gain due to wave-front incoherence, and
- beam spreading loss.

Models are described for gaseous absorption and tropospheric scintillation and procedures used for obtaining the estimated effects provided. For the reasons outlined in Chapter 2, the last three effects are not discussed.

A.1.1 Attenuation by Atmospheric Gases

There are many gaseous constituents to the dry atmosphere which interact with a radio link. These gases include the atmosphere's principle components which are oxygen 21%, nitrogen 78%, argon 0.9% and carbon dioxide 0.1% - all well mixed up to a height of 100 kms which is the region of the earth's atmosphere termed the Homosphere (see Figure 5). These proportions are fairly constant but the water vapor content is highly variable, up to a maximum of 100% humidity which equates to 1.7% by volume of the standard US atmosphere [Tas94] [Ipp86] [NDA76].

A radiowave travelling through the atmosphere is attenuated due to the gaseous components present in the transmission path. Signal degradation can be minor or severe, depending on the frequency, temperature, pressure, and water vapor concentration. The principal interaction mechanism involving gaseous constituents and a radio wave is molecular absorption, which results in a reduction in signal amplitude. The absorption of the radio wave results from a quantum level change in the rotational energy of the molecule, and occurs at a specific resonant frequency or narrow band of frequencies. The resonant frequency of interaction depends on the energy levels of the initial and final rotational energy states of the molecules. Only oxygen and water vapor have observable resonance frequencies in the bands of interest for space communications. Figure 66 shows the level of specific signal attenuation in dB/km as a function of frequency for both oxygen and water vapor. Note the oxygen attenuation band between 57 and 63 GHz. This band is sometimes used for inter-satellite communications as there will be negligible interference with terrestrial transceivers.

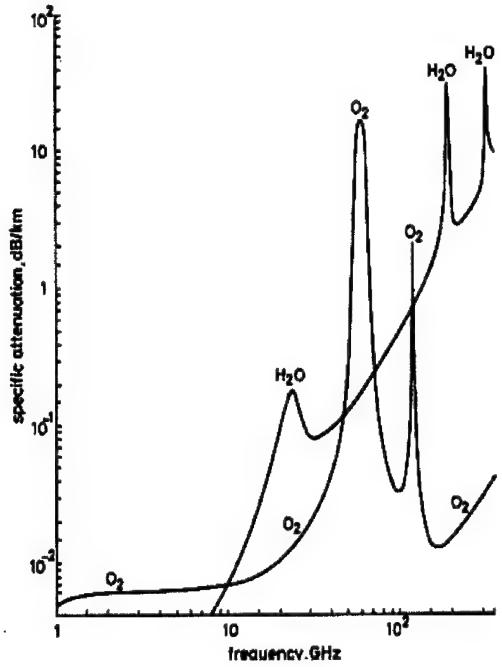

Figure 66 - Oxygen and Water Vapor Specific Attenuation [All89]

A useful and easily applied procedure for determining the total slant path attenuation for space communications links has been developed from direct measurements of 220 radiosonde profiles representing all seasons and geographic locations. This procedure provides the total attenuation at any location and elevation angle, based on local surface temperature and water vapor concentration.

The model described is used to calculate the median gaseous absorption loss expected for a given value of surface water vapor density, ρ_w, for frequencies up to 350 GHz (excluding the 57-63 GHz band for which information may be obtained from [ITU676]. The mathematical model used in this thesis to calculate gaseous attenuation effects is described in detail below.

A.1.2 Gaseous and Water Vapor Attenuation Model [ITU676]

Parameters required for the method include:

f: frequency (GHz)

θ: path elevation angle

h_S: height (km) above mean sea level of the Earth terminal; if unknown, a value of $h_S = 0$ will give somewhat conservative results

ρ_W : water vapour density (g/m^3) at the surface (i.e., at height h_S) for the location of interest.

In general, the mean or median value of ρ_w for a month or year is input to the model. Representative median values can be obtained from [ITU836], however Relative Humidity readings are available from most national weather services and a conversion process is provided below in Equation B-3. Since the model assumes an averaged height profile for water vapor density, application of the calculation procedure to periods of less than one month may introduce inaccuracies and is not recommended.

Step 1: Calculate the specific attenuations at the surface for dry air γ_o, and water vapor, γ_w, for the frequency, f, and the water vapor density, ρ_w. The determination of the specific attenuations can be performed in two ways; by either reading the values directly from Figure 66 above, or utilizing Equations B-1 and B-2. This calculations used in this study utilizes the equations described below, although for most purposes an estimation from the graph should be sufficient and is certainly more straightforward.

$$\gamma_0 = \left[3.79x10^{-3} f + \frac{0.265}{(f-63)^2 + 1.59} + \frac{0.028}{(f-118)^2 + 1.47} \right] x(f+198)^2 x10^{-3} \quad dB/km \quad for\, f > 63GHz \qquad \text{(A- 1)}$$

$$\gamma_w = \left[0.050 + 0.0021\varsigma + \frac{3.6}{(f-22.2)^2 + 8.5} + \frac{10.6}{(f-183.3)^2 + 9} + \frac{8.9}{(f-325.4)^2 + 26.3} \right] x f^2 x \varsigma x10^{-4} \quad dBs/km \qquad \text{(A- 2)}$$

Note that f is in GHz and ζ is the Water Vapor Density in g/m^3. The surface Water Vapor Density at a given surface temperature T_o may be found from the ideal gas law:

$$\rho_o = RH_s \frac{e_s}{R_w(T_o - 373)} \qquad \text{(A- 3)}$$

where:

RH = Relative Humidity (ie 50%=0.5)

R_w = 0.461 J/g K

e_s = saturated partial pressure of water vapor (psia)

The portion of the frequency band between 57 and 63 GHz is generally not used for terrestrial satellite communications but can be used for intersatellite links where minimal interference with terrestrial links is required. The equations for specific attenuation due to oxygen are valid for a pressure of 1013 mb (approximately 1 ATM) and a temperature of 15 Celsius. More complete values at alternative temperatures and pressures are available (generally using a FORTRAN program) and are available at specialist sites on the Internet.

Step 2: Compute the equivalent heights for dry air h_o, and water vapor, h_w. For frequencies below 57 GHz, the value of h_o is taken to be 6 kms, and for higher frequencies h_o is calculated from Equations B-4 and B-5.

$$h_o = 6 + \frac{40}{(f-118.7)^2+1} \; km \quad \text{for } 63<f<350 \text{ GHz} \tag{A- 4}$$

$$h_w = h_{w0}\left[1 + \frac{3.0}{(f-22.2)^2+5} + \frac{5.0}{(f-183.3)^2+6} + \frac{2.5}{(f-325.4)^2+4}\right] km \tag{A- 5}$$

where h_{w0} is the water equivalent height and takes the following values:

h_{w0} = 1.6 kms in clear weather, and

h_{w0} = 2.1 in rain

Step 3: Calculate the total slant path gaseous attenuation, A_g, through the atmosphere.

– For $\theta > 10°$:

$$A_g = \frac{\gamma_o h_o e^{(h_s/h_o)} + \gamma_w h_w}{\sin\theta} \quad \text{dB} \tag{A- 6}$$

For $\theta \leq 10°$:

$$A_g = \frac{\gamma_o h_o e^{(h_s/h_o)}}{g(h_o)} + \frac{\gamma_w h_w}{g(h_w)} \quad \text{dB} \tag{A- 7}$$

with:

$$g(h) = 0.661x + 0.339\sqrt{x^2 + 5.5(h/R_e)} \tag{A- 8}$$

$$x = \sqrt{\sin^2\theta + 2(h_s/R_e)} \tag{A- 9}$$

where h is to be replaced by h_o or h_w as appropriate.

In this prediction method, R_e is the effective Earth radius after accounting for refraction [ITU834]. Typically, a value of $R_e = 8\,500$ km is appropriate where the height of the earth station above sea level (h_s) is ≤ 1 km. For $h_s > 1$ km see [ITU676]. Note that Equations B-6 to B-9 are engineering formulae derived from equations (10) to (13b) of [ITU676], based on the following approximations:

$$\cos\theta \approx 1; \sin^3\theta << \sin\theta; h_s^2 R_e^2 << 4h_s R_e \tag{A- 10}$$

Note that $x = \sin\theta$ for $h_s = 0$.

A.1.3 Tropospheric Scintillation

Atmospheric turbulence can seriously affect satellite-earth links at frequencies above 10 GHz. The turbulence produces time-varying modifications of the refractive index and thus affects propagation of radiowaves on terrestrial and earth-space paths by generating random amplitude, phase and angle of arrival fluctuations, called tropospheric scintillation. In general, the impact of rain on communication signals is predominant. However, scintillation becomes important for low-margin systems operating at frequencies above 10 GHz and at low elevation angles (≤4° on inland paths, and ≤5° on maritime or coastal paths). It has been observed that, at

high frequencies and for low elevation angles, scintillation may contribute as much as rain, or even more, to the total fade measured. This is especially true for time percentages greater than 1% and therefore becomes important for low margin systems. The impact of tropospheric scintillation effects depend on the magnitude and structure of the refractive index variations, increasing with frequency and with the path length through the atmosphere, and decreasing as the antenna beam-width decreases because of aperture averaging. Knowledge of the dynamic characteristics of scintillation is also important for the design of up-link power control and antenna tracking systems. The effect of Tropospheric Scintillation on a signal is dramatically illustrated by a series of oscilloscope traces (Figure 67) taken from ground stations located in Columbus, Ohio.

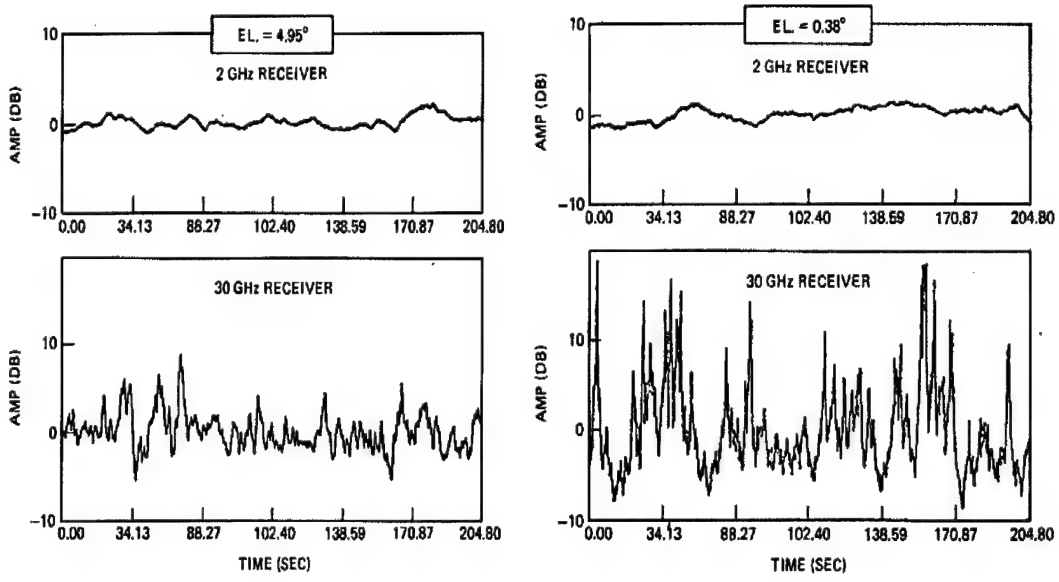

Figure 67 - Tropospheric Scintillation Effects at Low Elevation Angles [Ipp86]

A.1.4 Long Term Average Tropospheric Scintillation Model (CCIR/ITU Model)

A general technique for predicting the cumulative distribution of tropospheric scintillation at elevation angles greater than 4° is provided below. It is based on monthly or longer averages of temperature t (°C) and relative humidity H, and reflects the specific climatic conditions of the site. As the averages of t and H vary with season, distributions of scintillation

fade depth exhibit seasonal variations, which may also be predicted by using seasonal averages of t and H in the method. Values of t and H may be obtained from weather information for the site(s) in question.

The procedure has been tested at frequencies between 7 and 14 GHz, but is recommended for applications from 4 GHz up to at least 20 GHz [ALL89, ITU453]. Parameters required for the method include:

t: average surface ambient temperature (°C) at the site for a period of one month or longer

H: average surface relative humidity (%) at the site for a period of one month or longer

f: frequency (GHz), where 4 GHz $\leq f \leq$ 20 GHz

θ: path elevation angle, where $\theta \geq 4°$

D: physical diameter (m) of the earth-station antenna

η: antenna efficiency; if unknown, $\eta = 0.5$ is a conservative estimate.

Step 1: For the value of t, calculate the saturation water vapor pressure, e_s, (kPa),

$$e_s = \frac{5854\, x\, 10^{\left(20 - \frac{2950}{(273+t)}\right)}}{(273+t)^5} \quad millibars \qquad \text{(A- 11)}$$

Step 2: Compute the wet term of the radio refractivity, N_{wet}, corresponding to e_s, t and H as follows:

$$N_{wet} = \frac{3730.H.e_s}{(273+t)^2} \qquad \text{(A- 12)}$$

Step 3: Calculate the standard deviation of the signal amplitude, σ_{ref}, used as reference:

$$\sigma_{ref} = 3.6 \times 10^3 + 10^4 \times N_{wet} \quad \text{dB} \qquad \text{(A- 13)}$$

Step 4: Calculate the effective path length L according to:

$$L = \frac{2h_L}{\sqrt{\sin^2\theta + 2.35 \times 10^{-4}} + \sin\theta} \quad \text{m} \qquad \text{(A- 14)}$$

where $h_L = 1\,000$ m (h_L is the height of the turbulent layer);

Step 5: Estimate the effective antenna diameter, $D_{eff,}$ from the geometrical diameter D, and the antenna efficiency η:

$$D_{eff} = \sqrt{\eta} D \quad \text{m} \tag{A- 15}$$

Step 6: Calculate the antenna averaging factor from:

$$g(x) = \sqrt{3.86(x^2+1)^{11/12} \bullet \sin\left[\frac{11}{6}\arctan\frac{1}{x}\right] 7.08x^{5/6}} \tag{A- 16}$$

with:

$$x = 1.22 D_{eff}^2 (f / L) \tag{A- 17}$$

where f is the carrier frequency (GHz).

Step 7: Calculate the standard deviation of the signal for the considered period and propagation path:

$$\sigma = \sigma_{ref} f^{7/12} \frac{g(x)}{(\sin\theta)^{1.2}} \tag{A- 18}$$

Step 8: Calculate the time percentage factor $a(p)$ for the time percentage, p, of concern in the range $0.01\% < p \leq 50\%$:

$$a(p) = 0.061(\log_{10} p)^3 + 0.072(\log_{10} p)^2 1.71 \log_{10} p + 3.0 \tag{A- 19}$$

Step 9: Calculate the scintillation fade depth for the time percentage p by:

$$A_s(p) = a(p)\,\sigma \quad \text{dB} \tag{A- 20}$$

Additional models are available which allow the calculation of the deep and shallow fading parts of the scintillation/multipath fading distribution of elevation angles less than 5°. The interested reader should consult [ITU90, ITU618-5].

A.2 RAIN AND OTHER HYDROMETEORS

Rain effects are often the greatest source of variability in satellite communications links. Rain attenuation, like other effects such as tropospheric and ionospheric scintillation, are expressed in probabilistic rather than absolute terms. In order to gain an understanding of the typical attenuation effects, a rain attenuation model is often used. As is often the case with atmospheric effects, a number of different models exist in open literature, and not any one provides better attenuation predictions for all cases (year, rain zone area, elevation angel etc). Some of the more popular models include:

- Dutton Dougherty Attenuation Prediction Model
- Lin Rain Attenuation Model
- Crane Global Rain Attenuation Model
- CCIR Rain Attenuation Model
- Modified 1982 CCIR Model
- Simple Attenuation Model (SAM)
- Two Component Model
- Rice-Holmberg Rain Model (rain rate prediction model)

Comparative analyses of the various rain attenuation prediction models have been carried out [Ipp84, Mac84, Kar87] and it appears that, if weight is given to those attenuation measurements that have been conducted for periods in excess of two years when comparing measured results to predictions, the ITU model [ITU618] is generally to be preferred. This is due to its inherent simplicity and its reasonable accuracy - at least for frequencies of about 30 GHz or below. The procedure for the ITU model is set out in step-by-step form in Section 2.2.1.1 of [ITU618] and is duplicated below.

A.2.1 ITU/CCIR Rainfall Attenuation Prediction Model

The following procedure provides estimates of the long-term statistics of the slant-path rain attenuation at a given location for frequencies up to 30 GHz. The following parameters are required:

$R_{0.01}$: point rainfall rate for the location for 0.01% of an average year (mm/h)

h_S: height above mean sea level of the earth station (km)

θ : elevation angle

φ : latitude of the earth station (degrees)

f: frequency (GHz).

The geometry of the satellite transmission path relevant to the following calculations is illustrated in Figure 68.

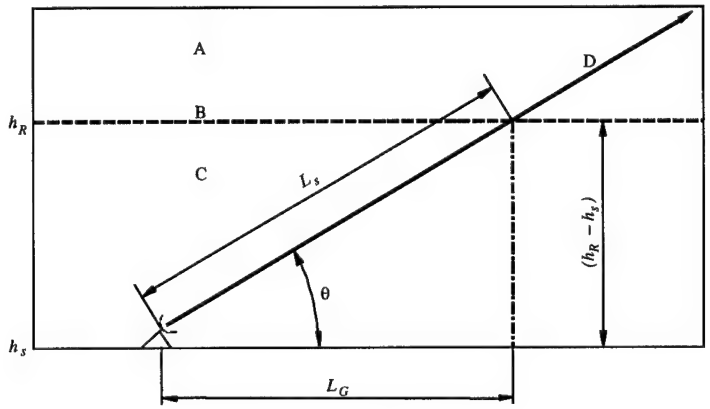

Figure 68 - Slant Path Geometry [ITU618]

Step 1: Calculate the effective rain height, h_R, for the latitude of the station φ:

$$h_R(\text{km}) = \begin{cases} 5 - 0.075(\varphi - 23) & \text{for } \varphi > 23^\circ & \text{Northern Hemisphere} \\ 5 & \text{for } 0^\circ \le \varphi \le 23^\circ & \text{Northern Hemisphere} \\ 5 & \text{for } 0^\circ \ge \varphi \ge -21^\circ & \text{Southern Hemisphere} \\ 5 + 0.1(\varphi + 21) & \text{for } -71^\circ \le \varphi < -21^\circ & \text{Southern Hemisphere} \\ 0 & \text{for } \varphi < -71^\circ & \text{Southern Hemisphere} \end{cases}$$

Step 2: *For* $\theta \geq 5°$ compute the slant-path length, L_s, below the rain height from:

$$L_s = \frac{(h_R h_s)}{\sin\theta} \quad \text{km} \tag{A- 21}$$

For $\theta < 5°$, the following formula is used:

$$L_s = \frac{2(h_R h_s)}{\left(\sin^2\theta + \frac{2(h_R h_s)}{R_e} \right)^{1/2} + \sin\theta} \quad \text{km} \tag{A- 22}$$

Step 3: Calculate the horizontal projection, L_G, of the slant-path length from:

$$L_G = L_s \cos\theta \qquad \text{km} \tag{A- 23}$$

Step 4: Obtain the rain intensity in mm/hr, $R_{0.01}$, exceeded for 0.01% of an average year (with an integration time of 1 min) from local sources such as the weather service or, for US DOD personnel, by requesting data from the Air Force Combat Climatology Center. If these more accurate sources are not available, a set of contour maps may be found by referring to [ITU837].

Step 5: Calculate the reduction factor, $r_{0.01}$, for 0.01% of the time for $R_{0.01} \leq 100$ mm/h:

$$r_{0.01} = \frac{1}{1 + L_G / L_0} \tag{A- 24}$$

where $L_0 = 35 \exp(-0.015\, R_{0.01})$.

For $R_{0.01} > 100$ mm/h, use the value 100 mm/h in place of $R_{0.01}$.

Step 6: Obtain the specific attenuation, γ_R, using the frequency-dependent coefficients given in Table 12 below, and the rainfall rate, $R_{0.01}$, determined from Step 4, by using:

$$\gamma_R = k(R_{0.01})^{\alpha} \qquad \text{dB/km} \tag{A- 25}$$

Table 12 - Specific Attenuation Coefficients

Frequency(GHz)	k_h	k_v	α_h	α_v
1	0.0000387	0.0000352	0.912	0.880
2	0.000154	0.000138	0.963	0.923
4	0.000650	0.000591	1.121	1.075
6	0.00175	0.00155	1.308	1.265
7	0.00301	0.00265	1.332	1.312
8	0.00454	0.00395	1.327	1.310
10	0.0101	0.00887	1.276	1.264
12	0.0188	0.0168	1.217	1.200
15	0.0367	0.0335	1.154	1.128
20	0.0751	0.0691	1.099	1.065
25	0.124	0.113	1.061	1.030
30	0.187	0.167	1.021	1.000
35	0.263	0.233	0.979	0.963
40	0.350	0.310	0.939	0.929
45	0.442	0.393	0.903	0.897
50	0.536	0.479	0.873	0.868
60	0.707	0.642	0.826	0.824
70	0.851	0.784	0.793	0.793
80	0.975	0.906	0.769	0.769
90	1.06	0.999	0.753	0.754
100	1.12	1.06	0.743	0.744
120	1.18	1.13	0.731	0.732
150	1.31	1.27	0.710	0.711
200	1.45	1.42	0.689	0.690
300	1.36	1.35	0.688	0.689
400	1.32	1.31	0.683	0.684

Note that both horizontal and vertical polarization cases are provided.

Step 7: The predicted attenuation exceeded for 0.01% of an average year is obtained from:

$$A_{0.01} = \gamma_R L_s r_{0.01} \qquad \text{dB} \qquad \text{(A- 26)}$$

Step 8: The estimated attenuation to be exceeded for other percentages of an average year, in the range 0.001% to 1%, is determined from the attenuation to be exceeded for 0.01% for an average year by using:

$$\frac{A_p}{A_{0.01}} = 0.12 p^{(0.546+0.043\log p)} \qquad \text{(A- 27)}$$

This interpolation formula gives factors of 0.12, 0.38, 1 and 2.14 for 1%, 0.1%, 0.01% and 0.001%, respectively.

Step 9: If desired, the value of p corresponding to a given value of A_p may be computed from the inverted form of Equation B-27:

$$p_R = 10^{11.628\left(0.546+\sqrt{0.298+0.172\log(0.12\bullet A_{0.01}/A_p)}\right)} \qquad \text{(A- 28)}$$

with the constraint that:

$$A_{0.01}/A_p \geq 0.15 \qquad \text{(A- 29)}$$

This method provides an estimate of the long-term statistics of attenuation due to rain. When comparing measured statistics with the prediction, allowance should be given for the rather large year-to-year variability in rainfall rate statistics [ITU678].

A.2.2 Other Hydrometeors

Cloud, fog, hail, ice and snow all affect radiowave propagation to varying degrees. However, the attenuation due to cloud and fog [Slo82] is less than 0.3 dB at Iridium's L-Band frequencies. Additionally, hail, ice and snow play a minor role in producing attenuation on a satellite link, especially in the region of interest where such effects are confined to the regions above 3000 m altitude.

A.3 Non-Geostationary Paths

The prediction method provided above was derived for applications where the elevation angle remains constant. For non geostationary, multi-visibility satellite constellations employing satellite path diversity (i.e. switching to the least impaired path), an approximate calculation can be made assuming that the spacecraft with the highest elevation angle is being used.[ITU1188].

This method should be used for constellations such as Teledesic, GPS, Iridium, and Globalstar. Note however that the L-Band frequencies (approx. 1.6 GHz) used in such systems as GPS or Iridium are not generally susceptible to the attenuation effects of rainfall. This is one of the primary reasons for the great value placed in the acquisition of these frequencies.

A.4 Combined Effect of Rain Attenuation and Tropospheric Scintillation

The effects of rainfall and Tropospheric Scintillation can be combined for equal exceedence probabilities. In this case, overall signal fading is estimated by:

$$A(p) = \sqrt{A_R^2(p) + A_S^2(p)} \quad \text{dB} \tag{A- 30}$$

where:

A: total attenuation excluding gaseous absorption (dB)

A_R: rain attenuation (dB)

A_S: signal fade due to scintillation (dB), as estimated with Equation B-20.

APPENDIX B - PREDICTED SUNSPOT NUMBERS FOR SOLAR CYCLE 23

Table 13 – Predicted Monthly Sunspot Numbers [Tho98]

Year	Jan	Feb	Mar	Apr	May	Jun	Jul	Aug	Sep	Oct	Nov	Dec
1995	24.2	23.0	22.1	20.6	19.2	18.2	17.0	15.4	13.4	12.1	11.3	10.8
1996	10.4	10.1	9.7	8.4	8.0	8.5	8.4	8.3	8.4	8.8	9.8	10.4
1997	10.5	11.0	13.5	16.5	18.3	20.3	22.6	25.1	28.4	31.9	35.1	39.1
1998	43.8	48.9	53.5	58.2	63.8	69.2	75.3	81.9	87.9	93.8	99.8	105.6
1999	111.4	116.7	121.1	125.9	130.3	135.3	140.5	144.3	147.5	151.4	154.8	156.8
2000	157.4	157.7	159.9	160.0	158.5	157.6	156.2	155.0	154.3	152.8	150.7	148.4
2001	148.0	148.8	148.3	147.7	148.5	148.7	147.4	146.2	145.0	142.5	140.2	138.7
2002	136.8	134.0	129.6	125.3	121.6	118.0	115.1	111.0	106.7	103.7	100.3	95.9
2003	90.7	86.0	83.1	80.6	77.3	74.0	71.0	68.8	65.7	61.6	58.6	57.1
2004	56.2	55.6	54.5	52.8	50.7	48.0	44.4	40.6	38.3	37.6	36.3	33.9
2005	31.4	29.0	26.9	25.2	24.0	23.2	22.5	21.9	20.9	19.6	18.5	17.9
2006	17.3	16.5	15.6	14.6	13.5	12.4	11.7	11.1	10.5	9.7	9.0	8.8

APPENDIX C - TABLES OF SATELLITE VISIBILITY

Table 14 - Probability of Satellite Visibility vs. Latitude (Iridium)

Latitude	Number of Satellites Visible - IRIDIUM									
	0	1	2	3	4	5	6	7	8	9
0	1.75x10-4	0.738	0.261	0.001	-	-	-	-	-	-
5	4.93 x 10-5	0.737	0.249	0.010	-	-	-	-	-	-
10	-	0.724	0.261	0.012	-	-	-	-	-	-
15	-	0.690	0.304	0.004	-	-	-	-	-	-
20	-	0.662	0.320	0.015	-	-	-	-	-	-
25	-	0.618	0.353	0.028	-	-	-	-	-	-
30	-	0.552	0.416	0.032	-	-	-	-	-	-
35	-	0.485	0.457	0.058	-	-	-	-	-	-
40	-	0.404	0.497	0.092	0.004	-	-	-	-	-
45	-	0.299	0.552	0.141	0.005	-	-	-	-	-
50	-	0.179	0.598	0.203	0.019	-	-	-	-	-
55	-	0.089	0.544	0.296	0.070	-	-	-	-	-
60	-	0.012	0.432	0.366	0.157	0.033	-	-	-	-
65	-	-	0.128	0.469	0.246	0.115	0.031	0.011	-	-
70	-	-	0.001	0.166	0.322	0.260	0.173	0.060	0.017	-
75	-	-	-	-	0.075	0.193	0.406	0.290	0.036	-
80	-	-	-	-	-	0.046	0.334	0.422	0.178	0.020
85	-	-	-	-	-	-	0.321	0.271	0.258	0.149
90	-	-	-	-	-	-	0.566	0.001	0.002	0.431

Table 15 - Probability of Satellite Visibility vs. Latitude (Globalstar)

Latitude	Number of Satellites Visible - GLOBALSTAR					
	0	1	2	3	4	5
0	-	0.157928	0.616359	0.202484	0.022612	-
5	-	0.127453	0.643711	0.225529	0.003307	-
10	-	0.040872	0.777985	0.164183	0.016961	-
15	-	0.106702	0.546589	0.333079	0.013629	-
20	-	0.091528	0.469373	0.37483	0.064269	-
25	-	0.017258	0.427893	0.423219	0.13163	-
30	-	-	0.173823	0.499263	0.326913	-
35	-	-	0.07885	0.575989	0.34309	0.002071
40	-	-	0.123662	0.499019	0.373449	0.00387
45	-	-	0.129611	0.580471	0.289918	-
50	-	-	0.196067	0.621791	0.182143	-
55	-	0.045804	0.265936	0.596193	0.092067	-
60	-	0.138849	0.352235	0.478407	0.030508	-
65	-	0.251874	0.522846	0.224408	0.000872	-
70	-	0.57759	0.422319	9.14E-05	-	-
75	0.336913	0.628766	0.028276	-	-	-

APPENDIX D - ELEVATION ANGLE CUMULATIVE DISTRIBUTION FUNCTIONS

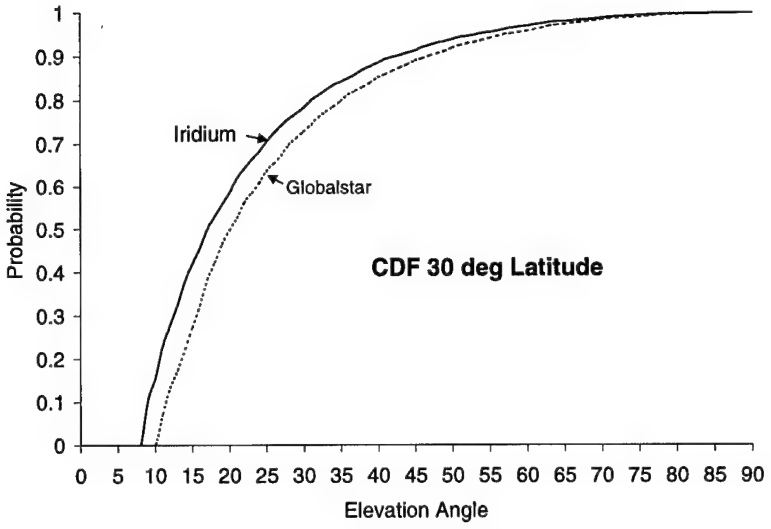

Figure 69 – CDF of Elevation Angles for 30° Latitude

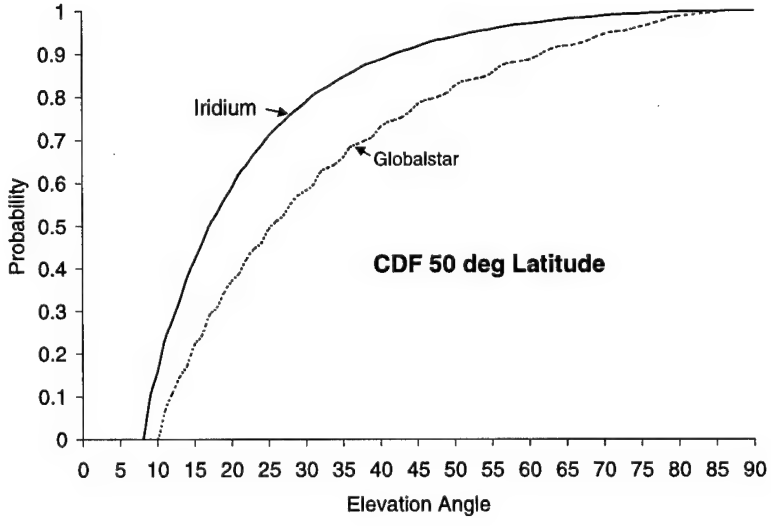

Figure 70 – CDF of Elevation Angles for530° Latitude

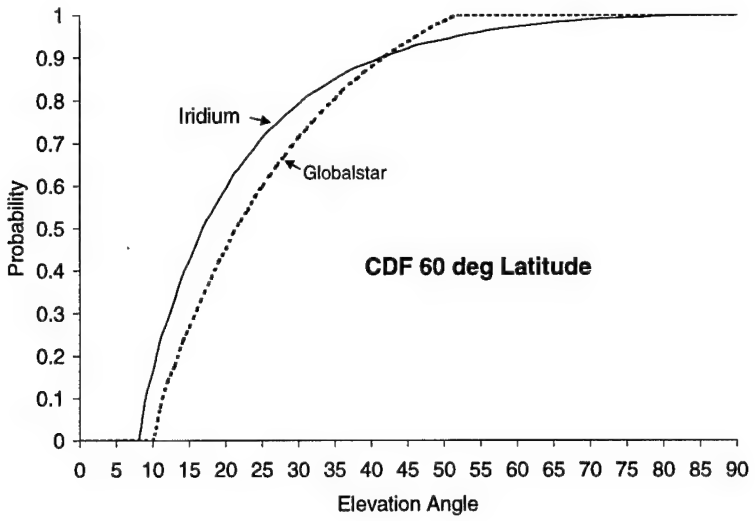

Figure 71 – CDF of Elevation Angles for 60° Latitude

APPENDIX E - PATH ATTENUATION PLOTS

The following pages show the levels of ionospheric scintillation predicted by the WBMOD model under three different scenarios of temporal, solar and geomagnetic conditions. The plots are presented in landscape format with Iridium and Globalstar presented side by side to facilitate comparison of the two systems. The constellation, latitude and the specific environmental conditions are printed individually on each plot.

SCENARIO 1

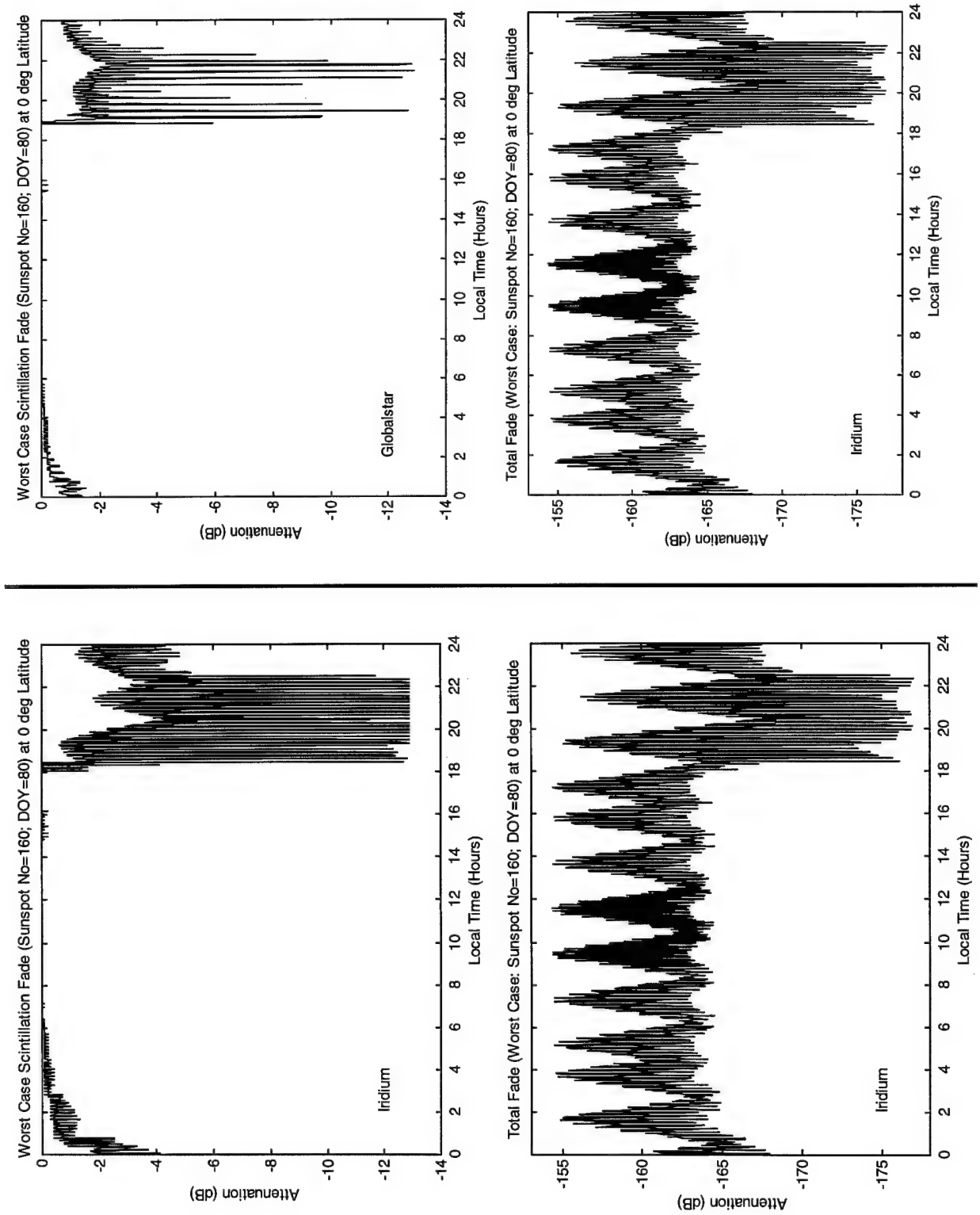
Worst Case Scintillation Fade (Sunspot No=160; DOY=80) at 0 deg Latitude
Attenuation (dB)
Local Time (Hours)
Globalstar
Total Fade (Worst Case: Sunspot No=160; DOY=80) at 0 deg Latitude
Iridium

SCENARIO 1

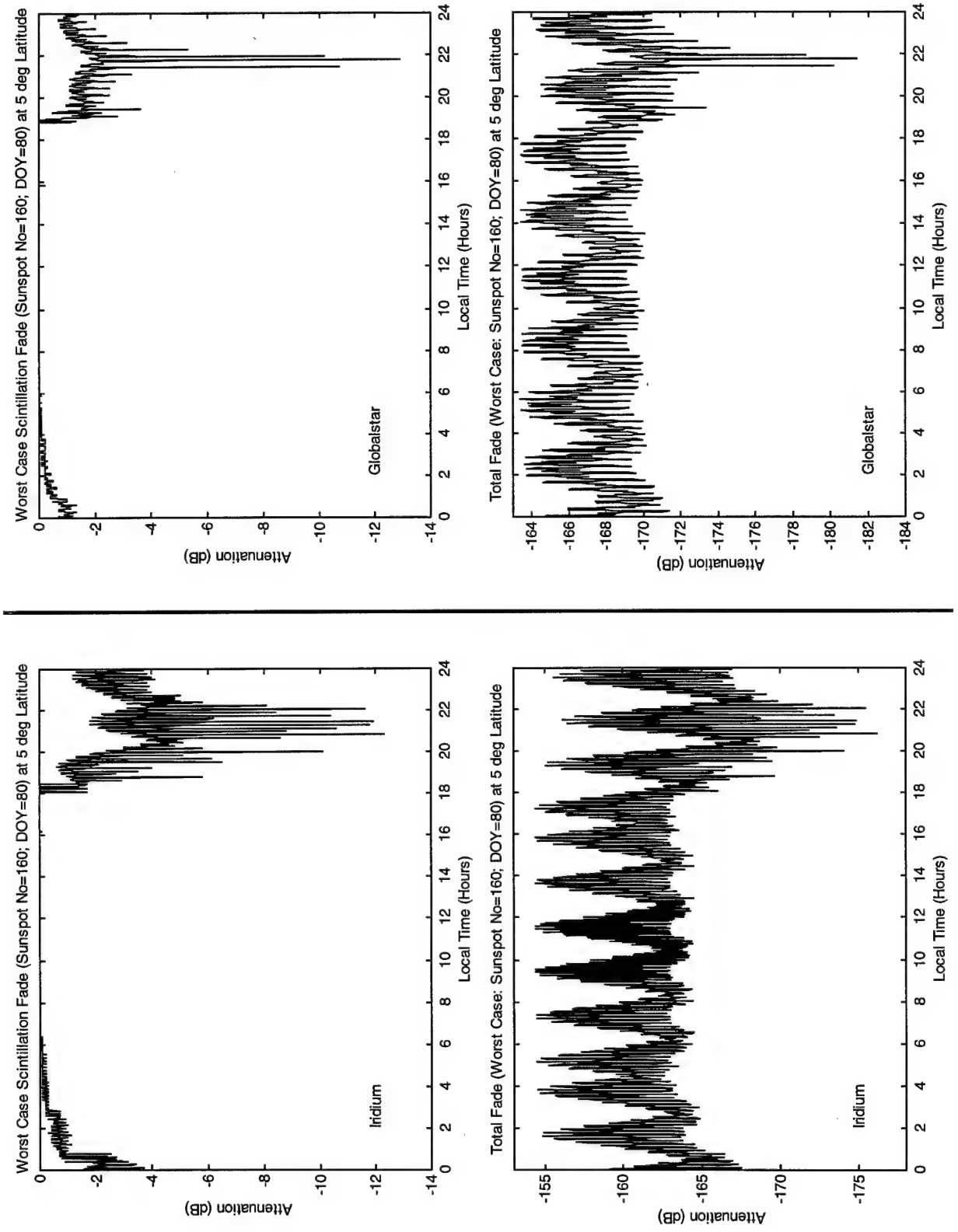
Worst Case Scintillation Fade (Sunspot No=160; DOY=80) at 5 deg Latitude
Attenuation (dB)
Local Time (Hours)
Globalstar
Total Fade (Worst Case: Sunspot No=160; DOY=80) at 5 deg Latitude
Attenuation (dB)
Local Time (Hours)
Globalstar
Worst Case Scintillation Fade (Sunspot No=160; DOY=80) at 5 deg Latitude
Attenuation (dB)
Local Time (Hours)
Iridium
Total Fade (Worst Case: Sunspot No=160; DOY=80) at 5 deg Latitude
Attenuation (dB)
Local Time (Hours)
Iridium

SCENARIO 1

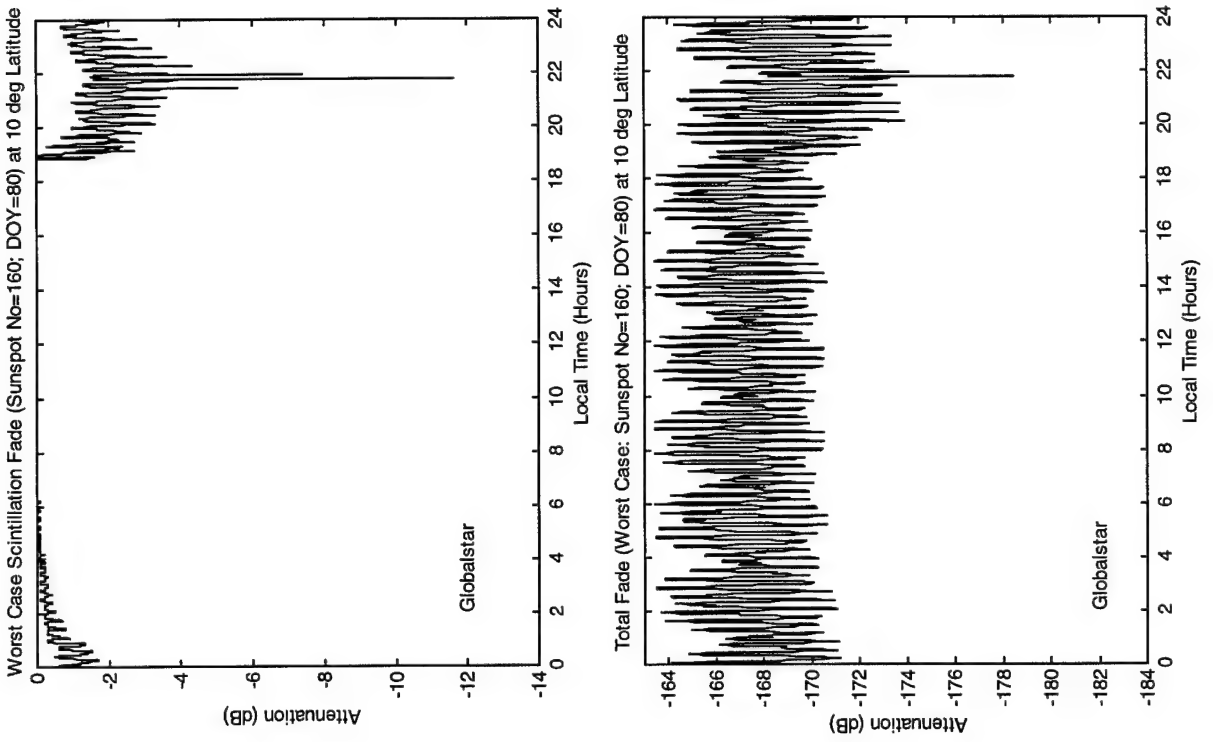
Worst Case Scintillation Fade (Sunspot No=160; DOY=80) at 10 deg Latitude
Attenuation (dB)
Local Time (Hours)
Globalstar
Total Fade (Worst Case: Sunspot No=160; DOY=80) at 10 deg Latitude
Attenuation (dB)
Local Time (Hours)
Globalstar

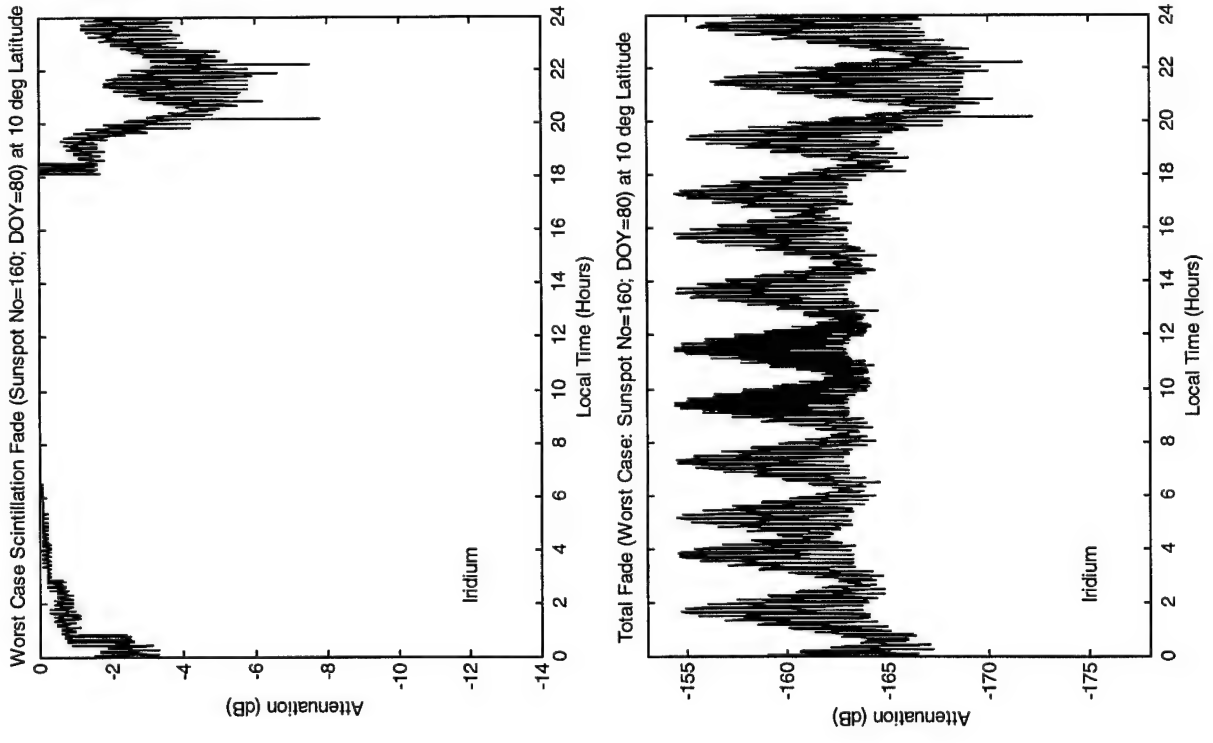
Worst Case Scintillation Fade (Sunspot No=160; DOY=80) at 10 deg Latitude
Attenuation (dB)
Local Time (Hours)
Iridium
Total Fade (Worst Case: Sunspot No=160; DOY=80) at 10 deg Latitude
Attenuation (dB)
Local Time (Hours)
Iridium

SCENARIO 1

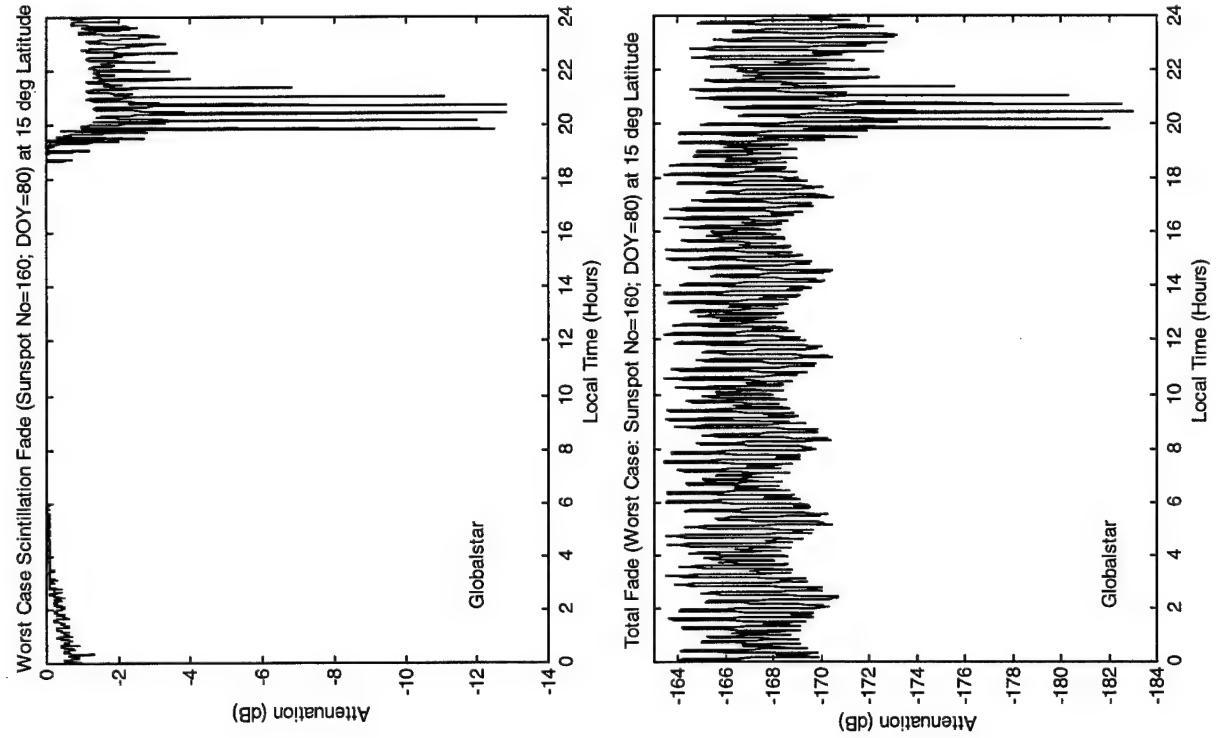
Worst Case Scintillation Fade (Sunspot No=160; DOY=80) at 15 deg Latitude
Attenuation (dB)
Local Time (Hours)
Globalstar
Total Fade (Worst Case: Sunspot No=160; DOY=80) at 15 deg Latitude
Attenuation (dB)
Local Time (Hours)
Globalstar

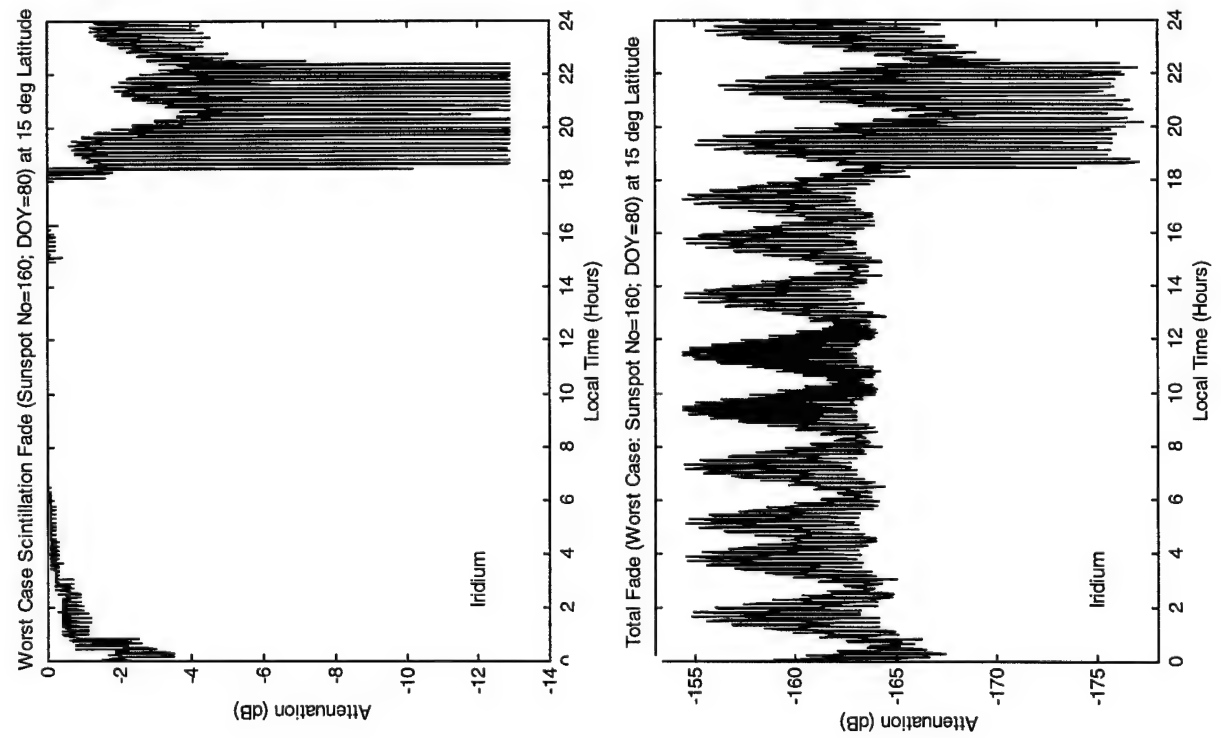
Worst Case Scintillation Fade (Sunspot No=160; DOY=80) at 15 deg Latitude
Attenuation (dB)
Local Time (Hours)
Iridium
Total Fade (Worst Case: Sunspot No=160; DOY=80) at 15 deg Latitude
Attenuation (dB)
Local Time (Hours)
Iridium

SCENARIO 1

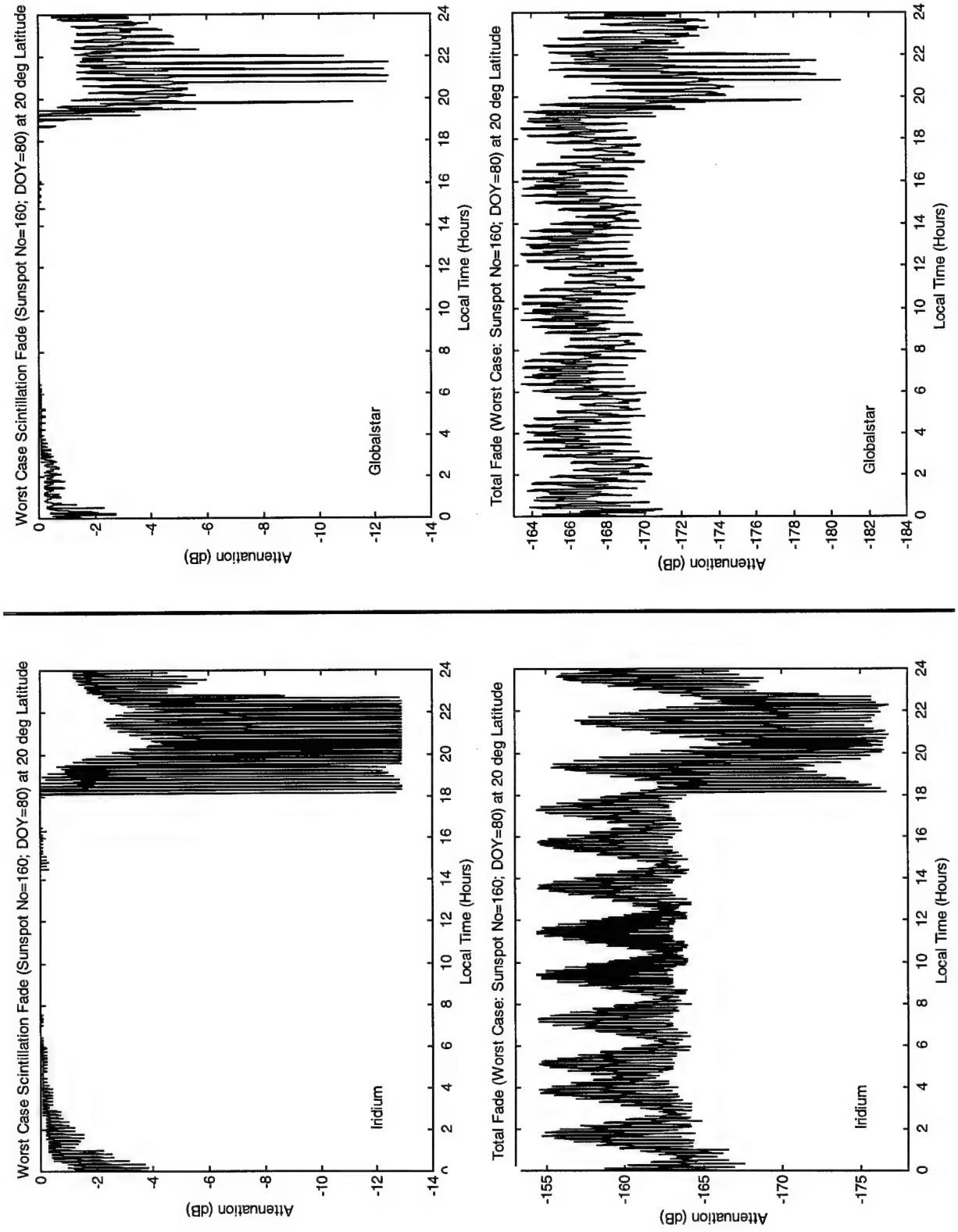
Worst Case Scintillation Fade (Sunspot No=160; DOY=80) at 20 deg Latitude
Attenuation (dB)
Local Time (Hours)
Globalstar
Total Fade (Worst Case: Sunspot No=160; DOY=80) at 20 deg Latitude
Attenuation (dB)
Local Time (Hours)
Globalstar
Worst Case Scintillation Fade (Sunspot No=160; DOY=80) at 20 deg Latitude
Attenuation (dB)
Local Time (Hours)
Iridium
Total Fade (Worst Case: Sunspot No=160; DOY=80) at 20 deg Latitude
Attenuation (dB)
Local Time (Hours)
Iridium

SCENARIO 1

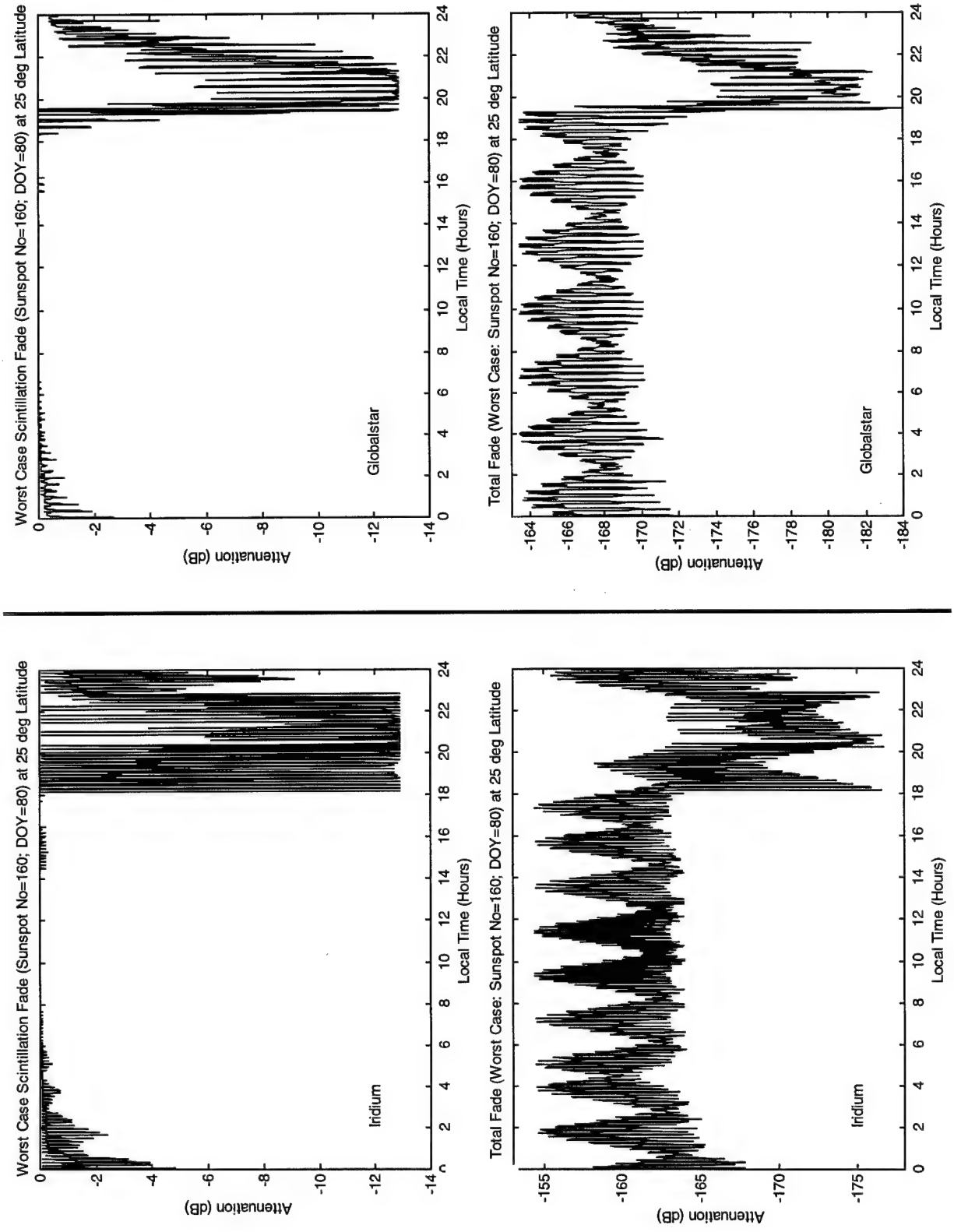
Worst Case Scintillation Fade (Sunspot No=160; DOY=80) at 25 deg Latitude
Attenuation (dB)
Local Time (Hours)
Globalstar
Total Fade (Worst Case: Sunspot No=160; DOY=80) at 25 deg Latitude
Attenuation (dB)
Local Time (Hours)
Globalstar
Worst Case Scintillation Fade (Sunspot No=160; DOY=80) at 25 deg Latitude
Attenuation (dB)
Local Time (Hours)
Iridium
Total Fade (Worst Case: Sunspot No=160; DOY=80) at 25 deg Latitude
Attenuation (dB)
Local Time (Hours)
Iridium

SCENARIO 1

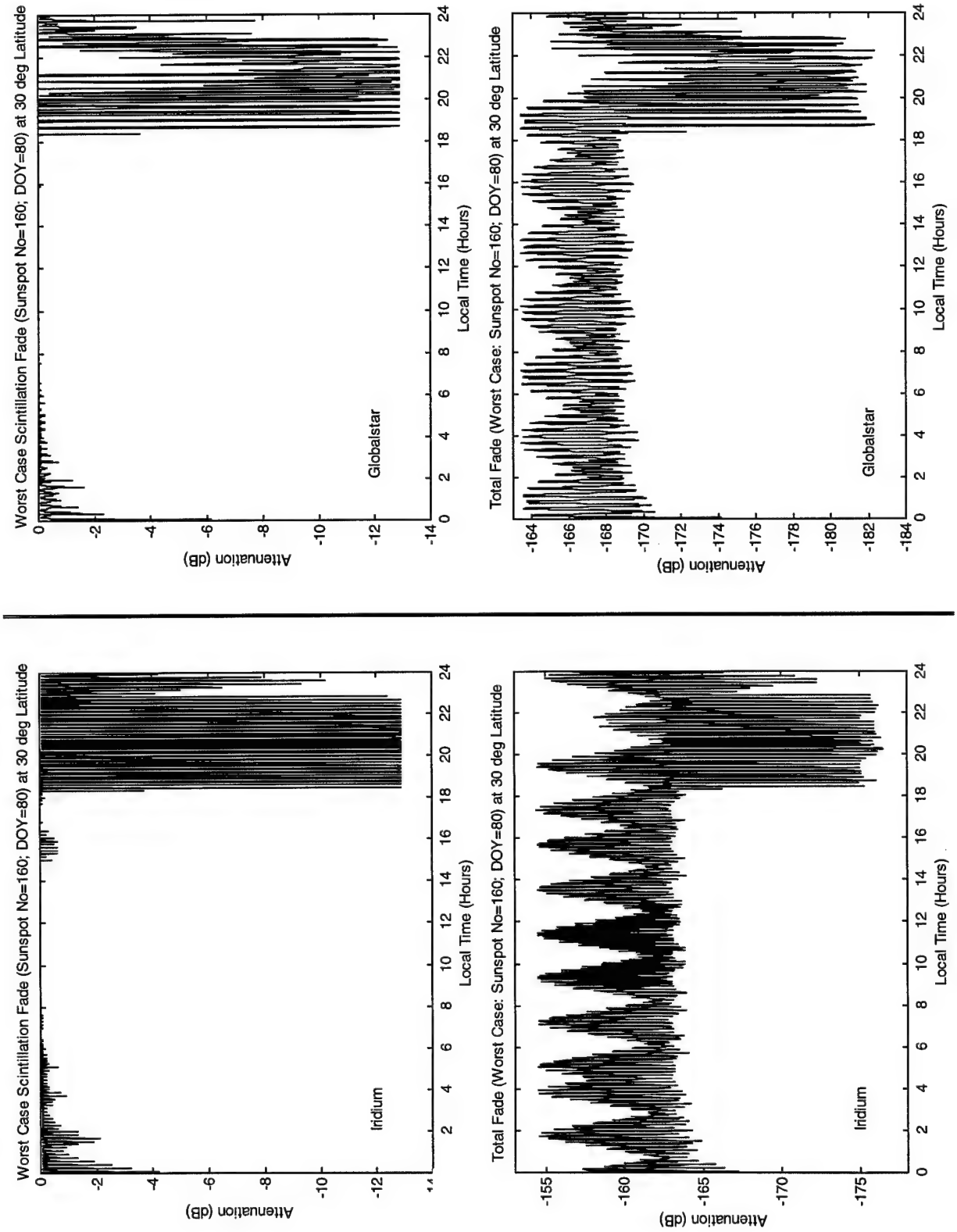
Worst Case Scintillation Fade (Sunspot No=160; DOY=80) at 30 deg Latitude
Attenuation (dB)
Local Time (Hours)
Globalstar
Total Fade (Worst Case: Sunspot No=160; DOY=80) at 30 deg Latitude
Attenuation (dB)
Local Time (Hours)
Globalstar
Worst Case Scintillation Fade (Sunspot No=160; DOY=80) at 30 deg Latitude
Attenuation (dB)
Local Time (Hours)
Iridium
Total Fade (Worst Case: Sunspot No=160; DOY=80) at 30 deg Latitude
Attenuation (dB)
Local Time (Hours)
Iridium

SCENARIO 1

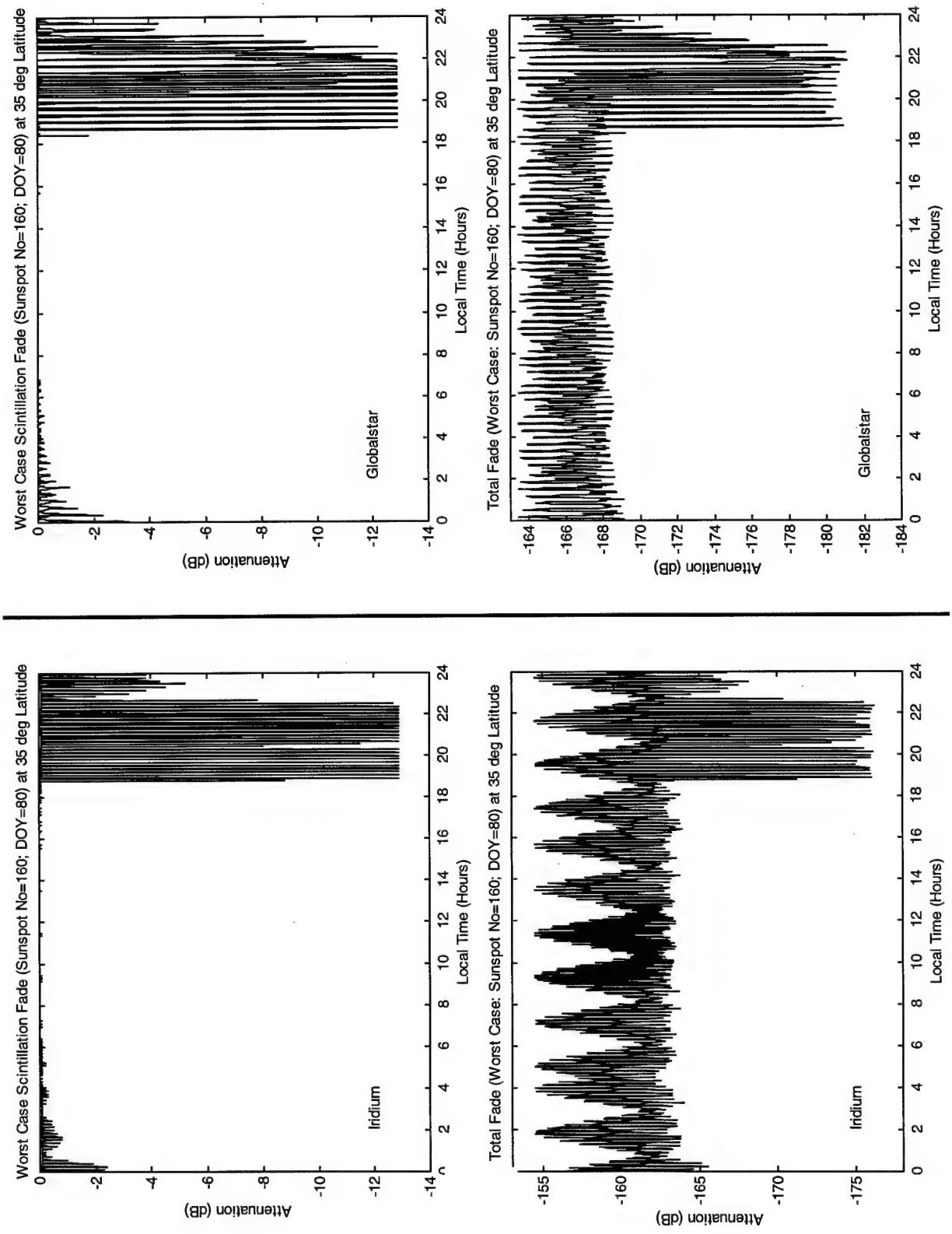
Worst Case Scintillation Fade (Sunspot No=160; DOY=80) at 35 deg Latitude
Attenuation (dB)
Local Time (Hours)
Globalstar
Total Fade (Worst Case: Sunspot No=160; DOY=80) at 35 deg Latitude
Attenuation (dB)
Local Time (Hours)
Globalstar
Worst Case Scintillation Fade (Sunspot No=160; DOY=80) at 35 deg Latitude
Attenuation (dB)
Local Time (Hours)
Iridium
Total Fade (Worst Case: Sunspot No=160; DOY=80) at 35 deg Latitude
Attenuation (dB)
Local Time (Hours)
Iridium

SCENARIO 1

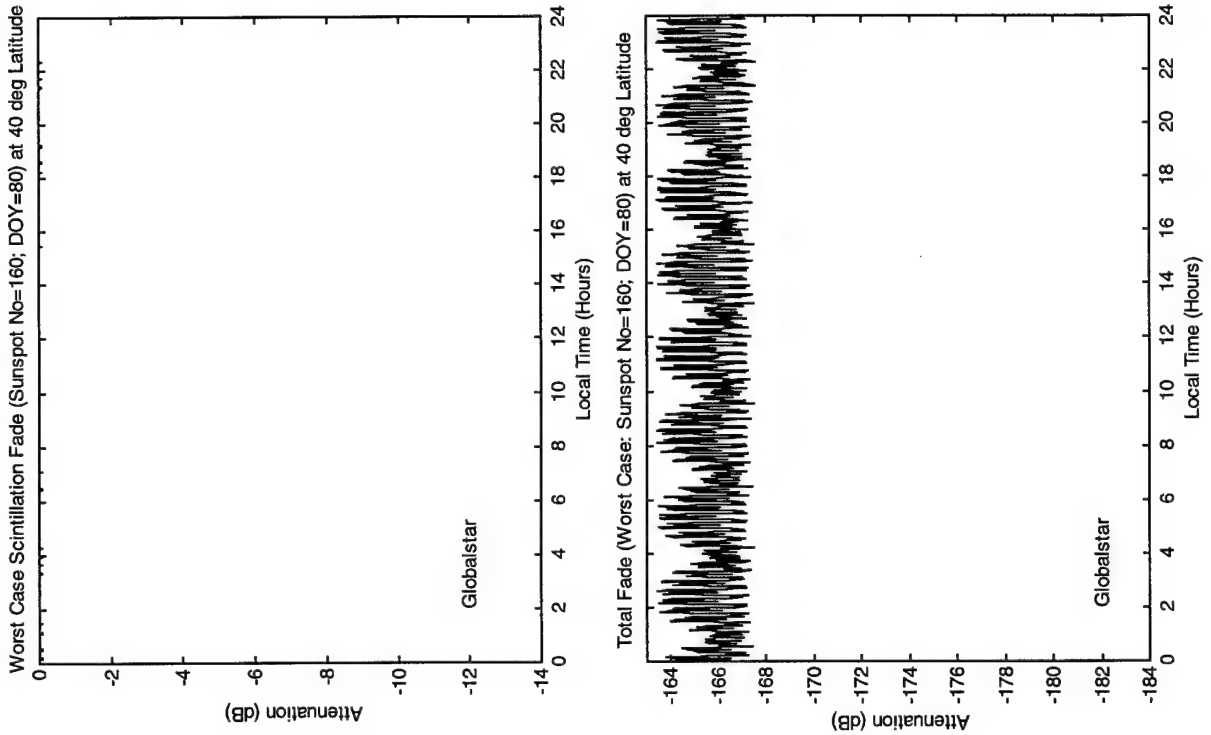
Worst Case Scintillation Fade (Sunspot No=160; DOY=80) at 40 deg Latitude
Attenuation (dB)
Local Time (Hours)
Globalstar
Total Fade (Worst Case: Sunspot No=160; DOY=80) at 40 deg Latitude
Attenuation (dB)
Local Time (Hours)
Globalstar

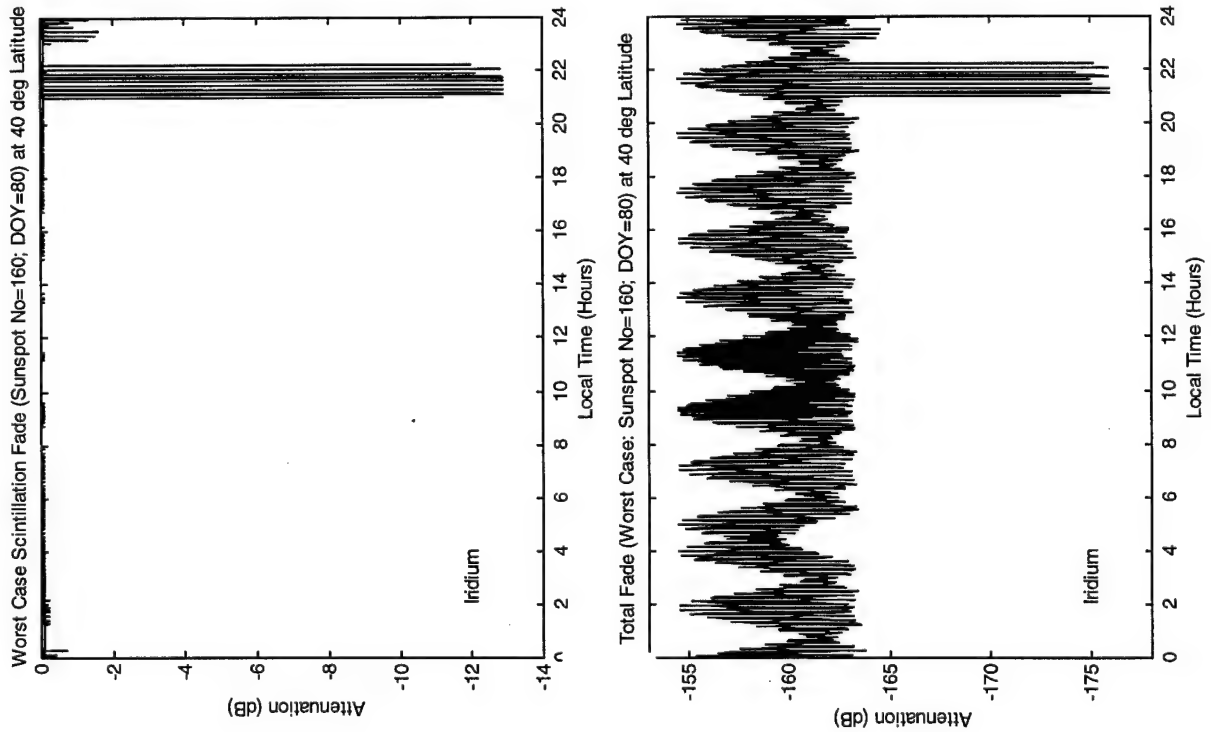
Worst Case Scintillation Fade (Sunspot No=160; DOY=80) at 40 deg Latitude
Attenuation (dB)
Local Time (Hours)
Iridium
Total Fade (Worst Case: Sunspot No=160; DOY=80) at 40 deg Latitude
Attenuation (dB)
Local Time (Hours)
Iridium

SCENARIO 1

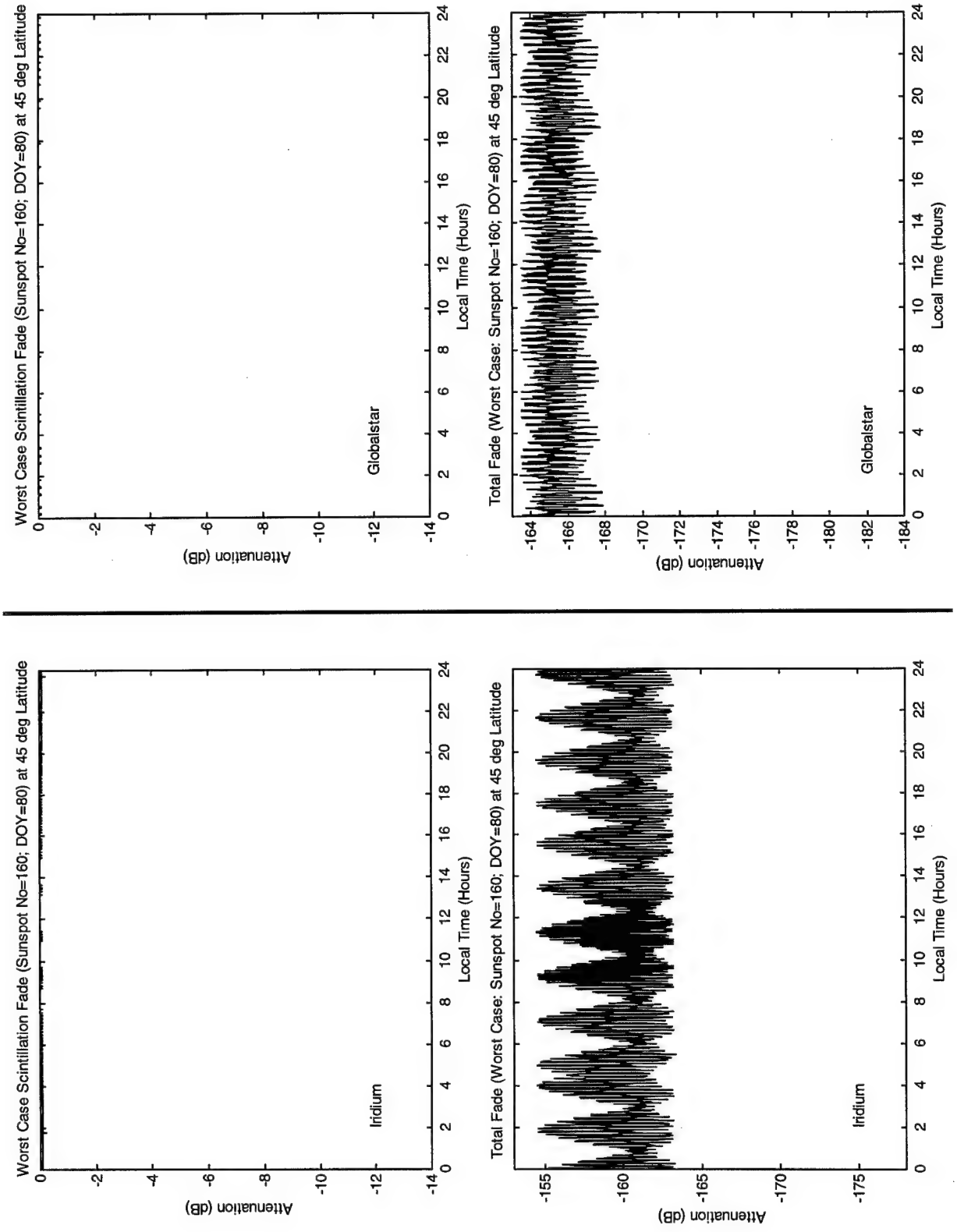
Worst Case Scintillation Fade (Sunspot No=160; DOY=80) at 45 deg Latitude
Attenuation (dB)
Local Time (Hours)
Globalstar
Total Fade (Worst Case: Sunspot No=160; DOY=80) at 45 deg Latitude
Attenuation (dB)
Local Time (Hours)
Globalstar
Worst Case Scintillation Fade (Sunspot No=160; DOY=80) at 45 deg Latitude
Attenuation (dB)
Local Time (Hours)
Iridium
Total Fade (Worst Case: Sunspot No=160; DOY=80) at 45 deg Latitude
Attenuation (dB)
Local Time (Hours)
Iridium

SCENARIO 2

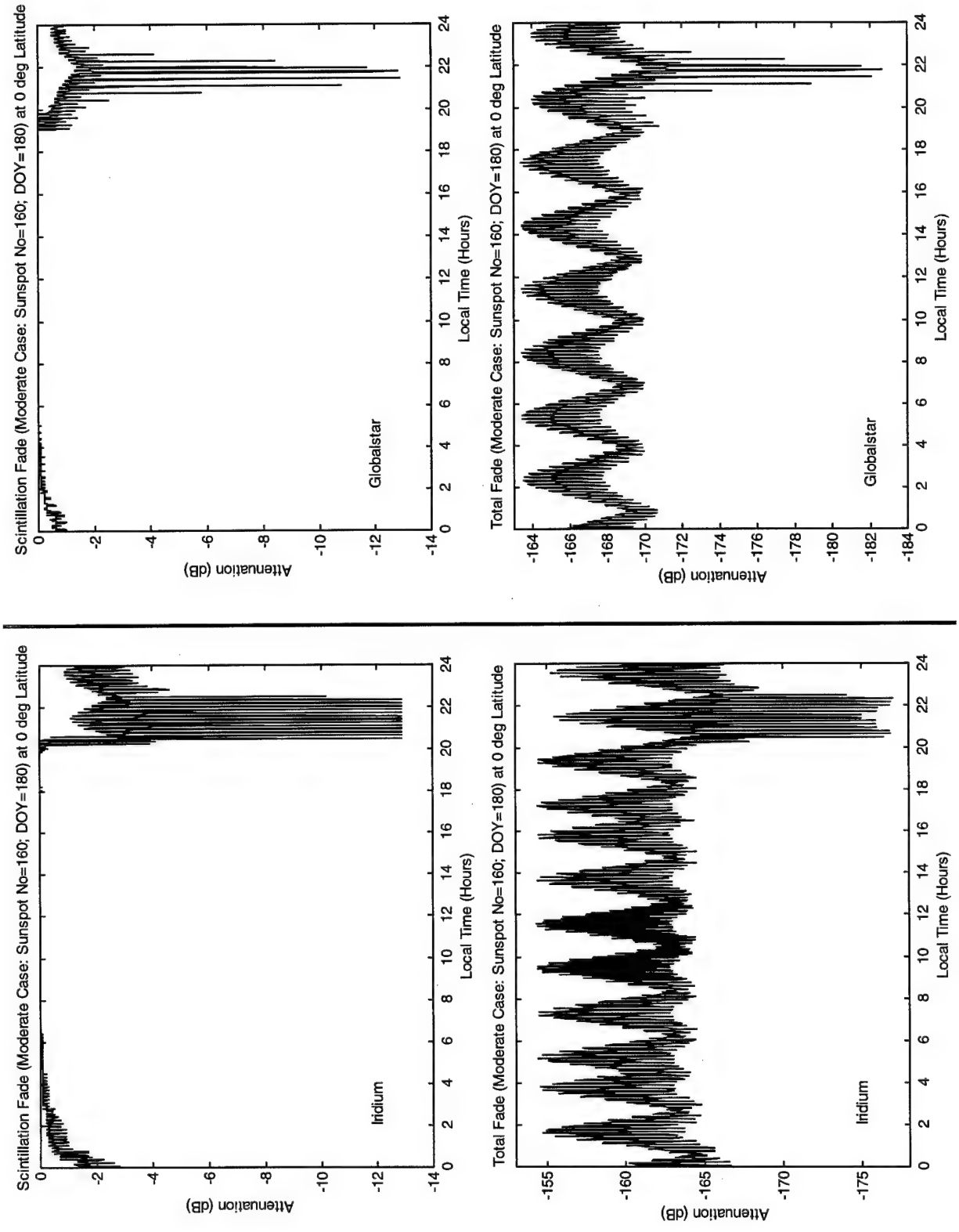
Scintillation Fade (Moderate Case: Sunspot No=160; DOY=180) at 0 deg Latitude
Attenuation (dB)
Local Time (Hours)
Globalstar
Total Fade (Moderate Case: Sunspot No=160; DOY=180) at 0 deg Latitude
Attenuation (dB)
Local Time (Hours)
Globalstar
Scintillation Fade (Moderate Case: Sunspot No=160; DOY=180) at 0 deg Latitude
Attenuation (dB)
Local Time (Hours)
Iridium
Total Fade (Moderate Case: Sunspot No=160; DOY=180) at 0 deg Latitude
Attenuation (dB)
Local Time (Hours)
Iridium

SCENARIO 2

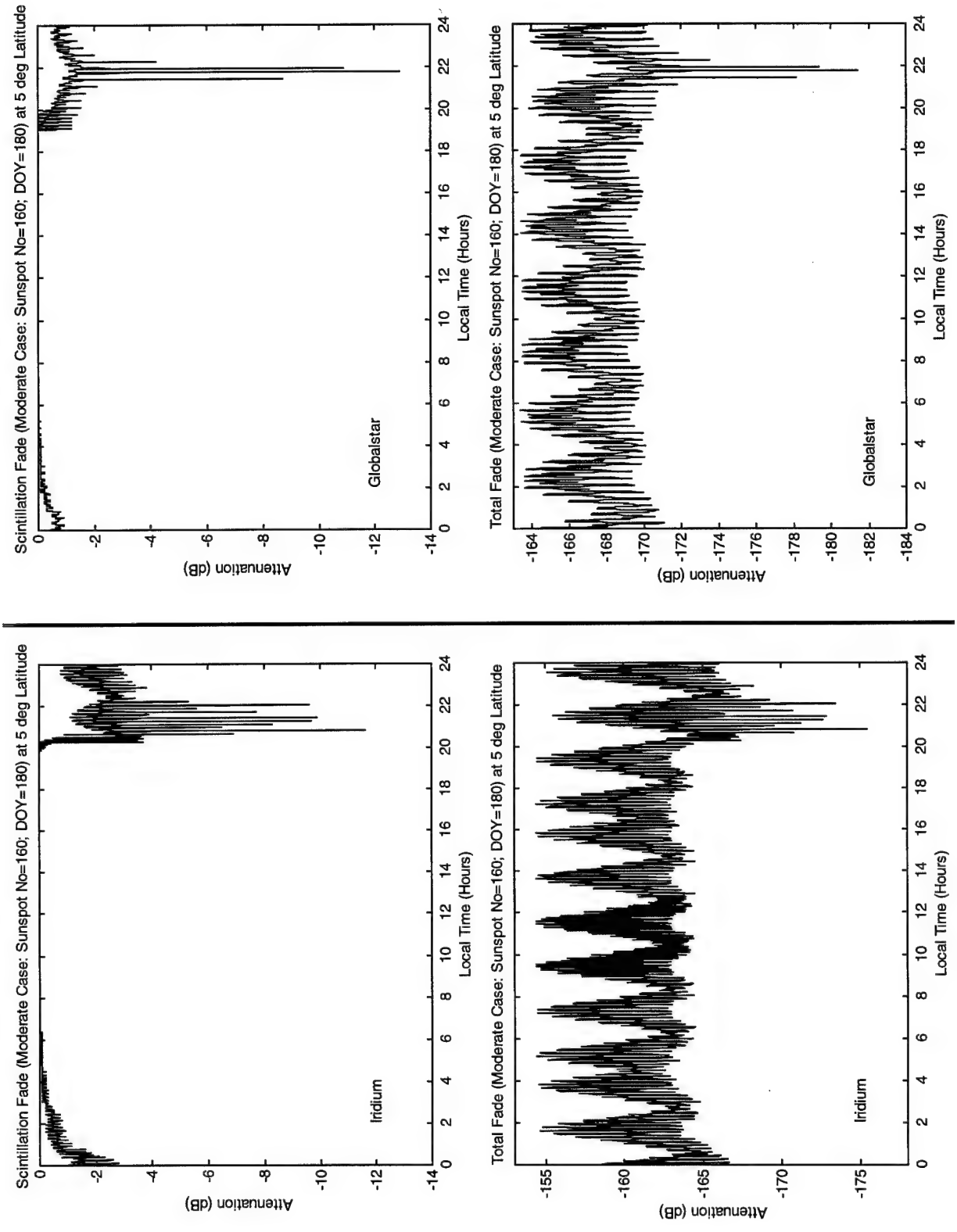
Scintillation Fade (Moderate Case: Sunspot No=160; DOY=180) at 5 deg Latitude
Attenuation (dB)
Local Time (Hours)
Globalstar
Total Fade (Moderate Case: Sunspot No=160; DOY=180) at 5 deg Latitude
Attenuation (dB)
Local Time (Hours)
Globalstar
Scintillation Fade (Moderate Case: Sunspot No=160; DOY=180) at 5 deg Latitude
Attenuation (dB)
Local Time (Hours)
Iridium
Total Fade (Moderate Case: Sunspot No=160; DOY=180) at 5 deg Latitude
Attenuation (dB)
Local Time (Hours)
Iridium

SCENARIO 2

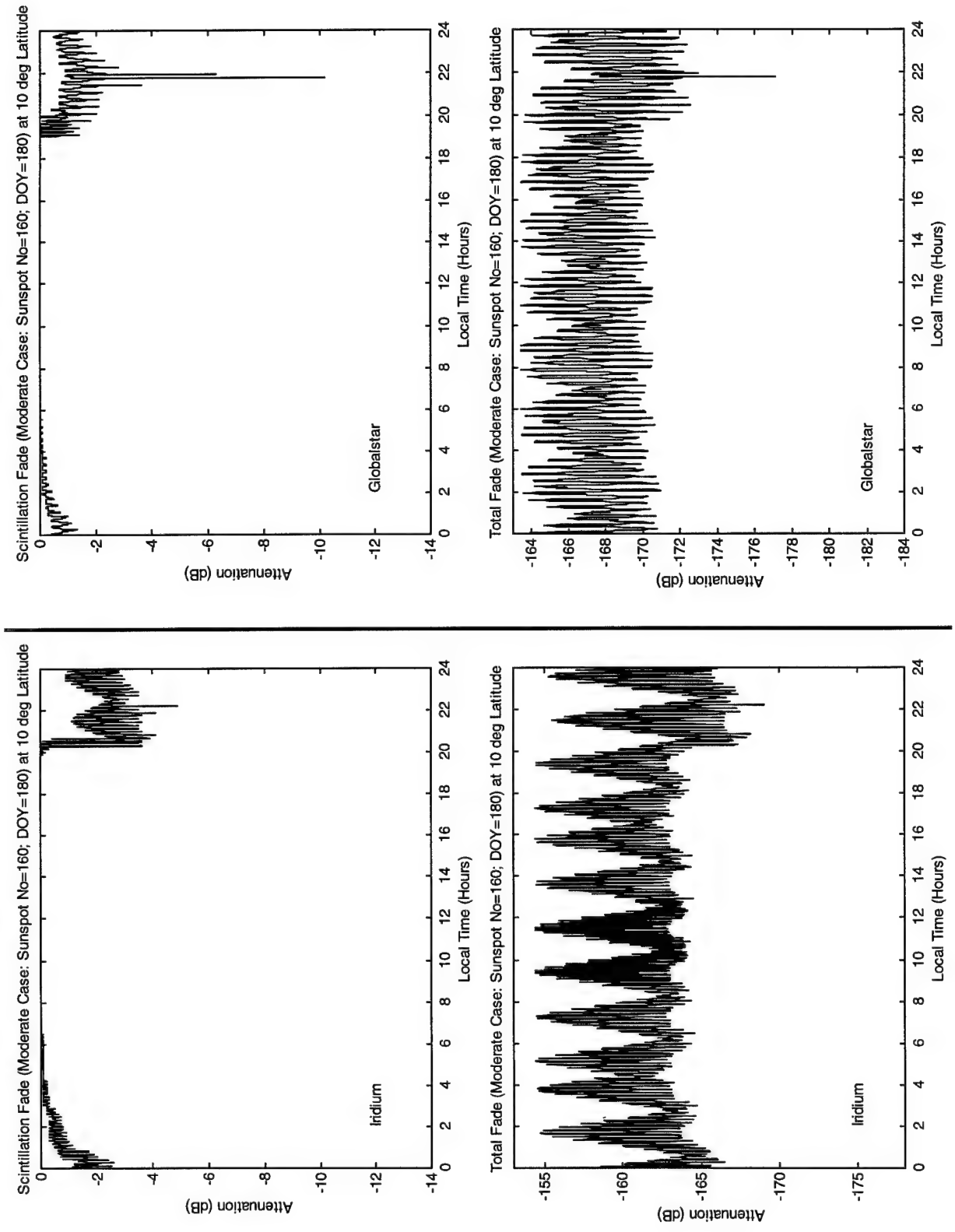
Scintillation Fade (Moderate Case: Sunspot No=160; DOY=180) at 10 deg Latitude
Attenuation (dB)
Local Time (Hours)
Globalstar
Total Fade (Moderate Case: Sunspot No=160; DOY=180) at 10 deg Latitude
Attenuation (dB)
Local Time (Hours)
Globalstar
Scintillation Fade (Moderate Case: Sunspot No=160; DOY=180) at 10 deg Latitude
Attenuation (dB)
Local Time (Hours)
Iridium
Total Fade (Moderate Case: Sunspot No=160; DOY=180) at 10 deg Latitude
Attenuation (dB)
Local Time (Hours)
Iridium

SCENARIO 2

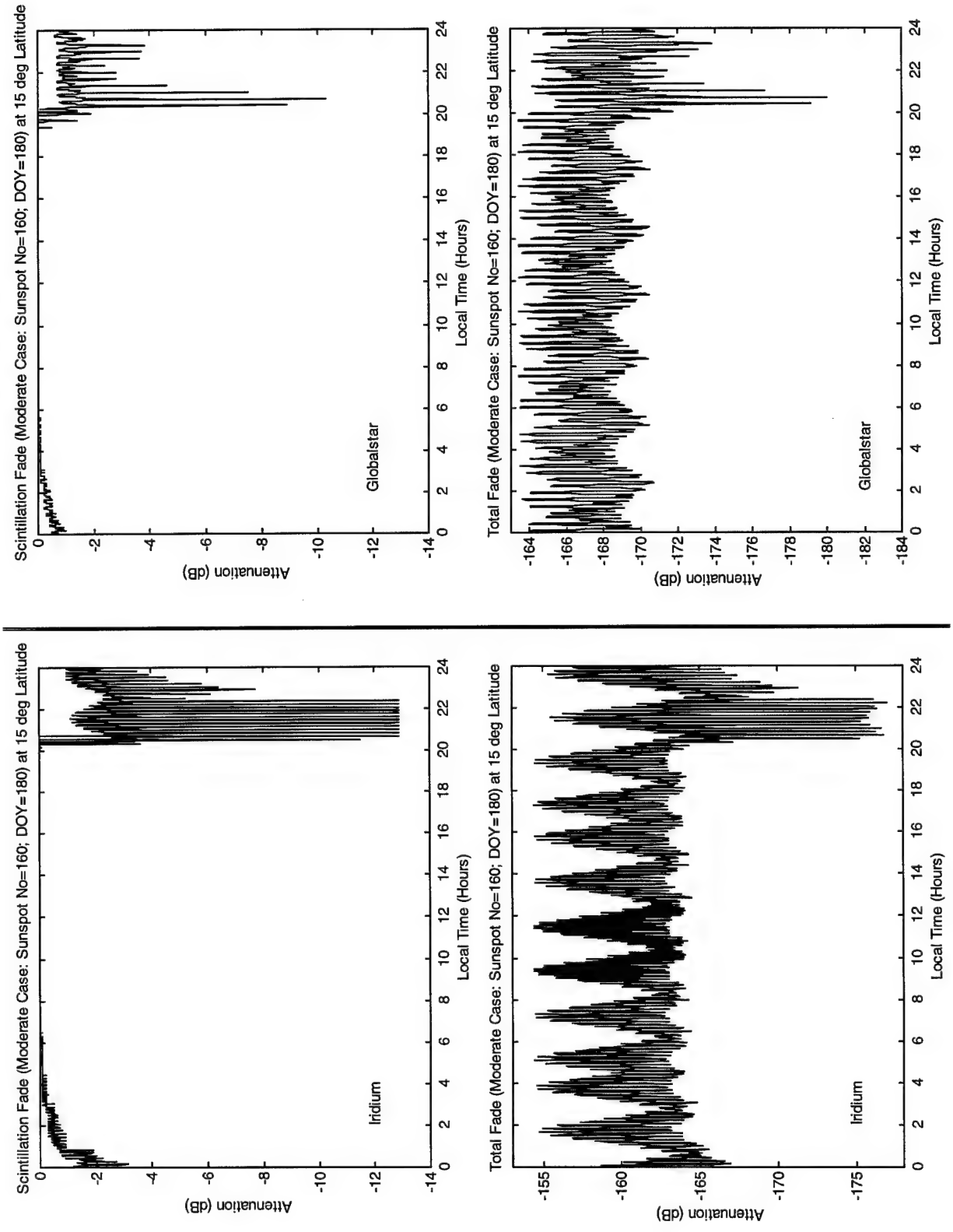
Scintillation Fade (Moderate Case: Sunspot No=160; DOY=180) at 15 deg Latitude
Attenuation (dB)
Local Time (Hours)
Globalstar
Total Fade (Moderate Case: Sunspot No=160; DOY=180) at 15 deg Latitude
Attenuation (dB)
Local Time (Hours)
Globalstar
Scintillation Fade (Moderate Case: Sunspot No=160; DOY=180) at 15 deg Latitude
Attenuation (dB)
Local Time (Hours)
Iridium
Total Fade (Moderate Case: Sunspot No=160; DOY=180) at 15 deg Latitude
Attenuation (dB)
Local Time (Hours)
Iridium

SCENARIO 2

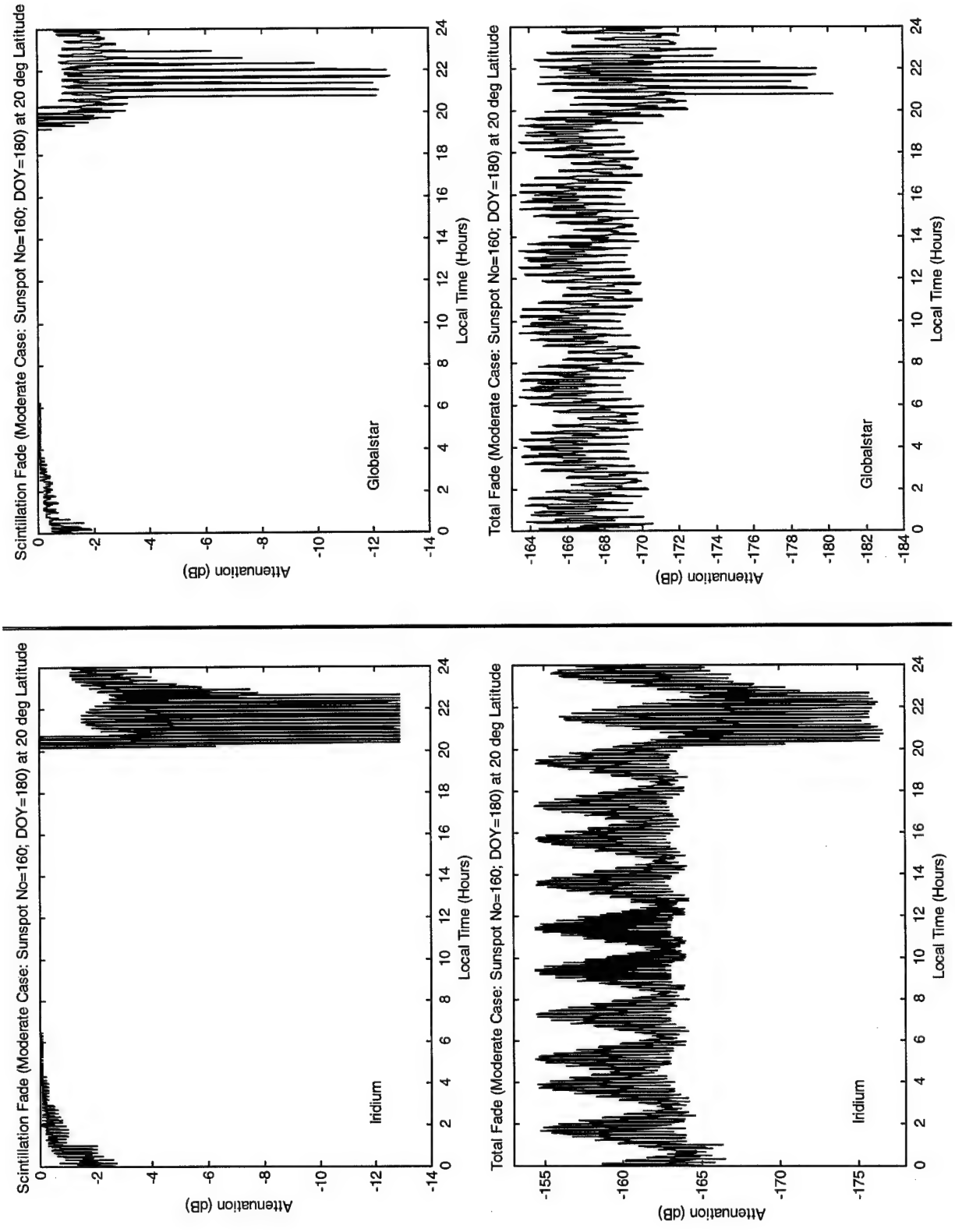
Scintillation Fade (Moderate Case: Sunspot No=160; DOY=180) at 20 deg Latitude
Attenuation (dB)
Local Time (Hours)
Globalstar
Total Fade (Moderate Case: Sunspot No=160; DOY=180) at 20 deg Latitude
Attenuation (dB)
Local Time (Hours)
Globalstar
Scintillation Fade (Moderate Case: Sunspot No=160; DOY=180) at 20 deg Latitude
Attenuation (dB)
Local Time (Hours)
Iridium
Total Fade (Moderate Case: Sunspot No=160; DOY=180) at 20 deg Latitude
Attenuation (dB)
Local Time (Hours)
Iridium

SCENARIO 2

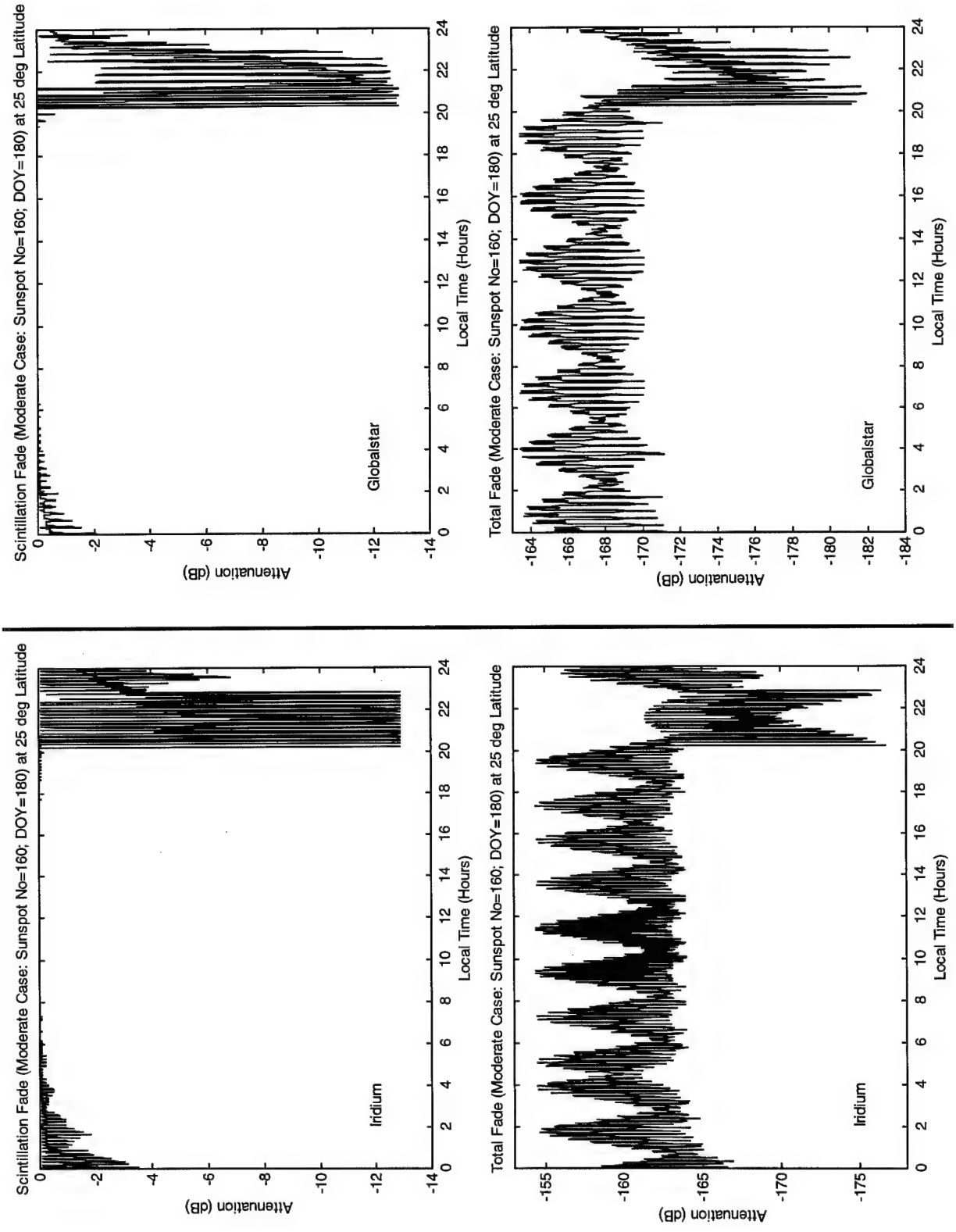
Scintillation Fade (Moderate Case: Sunspot No=160; DOY=180) at 25 deg Latitude
Attenuation (dB)
Local Time (Hours)
Globalstar
Total Fade (Moderate Case: Sunspot No=160; DOY=180) at 25 deg Latitude
Attenuation (dB)
Local Time (Hours)
Globalstar
Scintillation Fade (Moderate Case: Sunspot No=160; DOY=180) at 25 deg Latitude
Attenuation (dB)
Local Time (Hours)
Iridium
Total Fade (Moderate Case: Sunspot No=160; DOY=180) at 25 deg Latitude
Attenuation (dB)
Local Time (Hours)
Iridium

SCENARIO 2

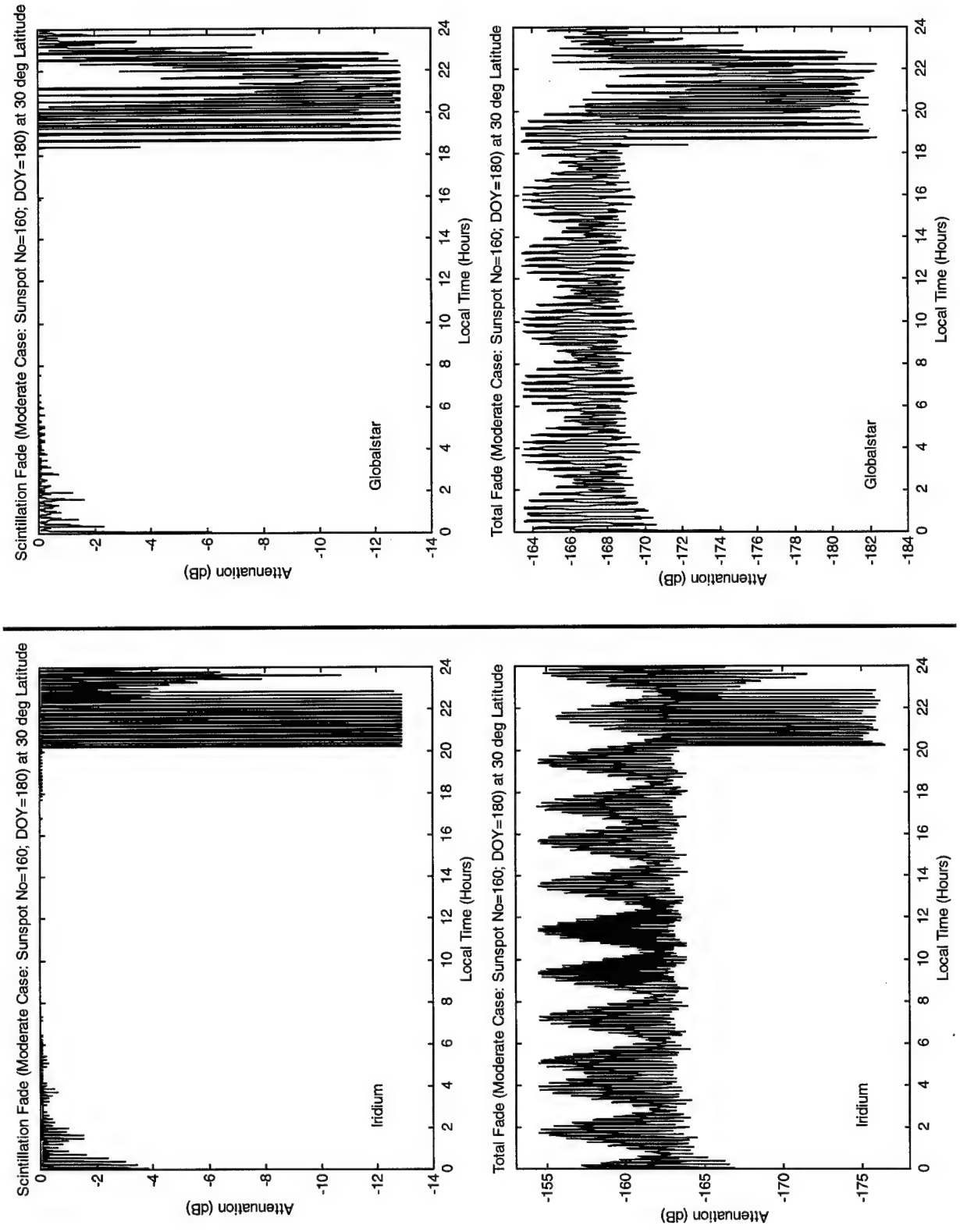
Scintillation Fade (Moderate Case: Sunspot No=160; DOY=180) at 30 deg Latitude
Attenuation (dB)
Local Time (Hours)
Globalstar
Total Fade (Moderate Case: Sunspot No=160; DOY=180) at 30 deg Latitude
Attenuation (dB)
Local Time (Hours)
Globalstar
Scintillation Fade (Moderate Case: Sunspot No=160; DOY=180) at 30 deg Latitude
Attenuation (dB)
Local Time (Hours)
Iridium
Total Fade (Moderate Case: Sunspot No=160; DOY=180) at 30 deg Latitude
Attenuation (dB)
Local Time (Hours)
Iridium

SCENARIO 2

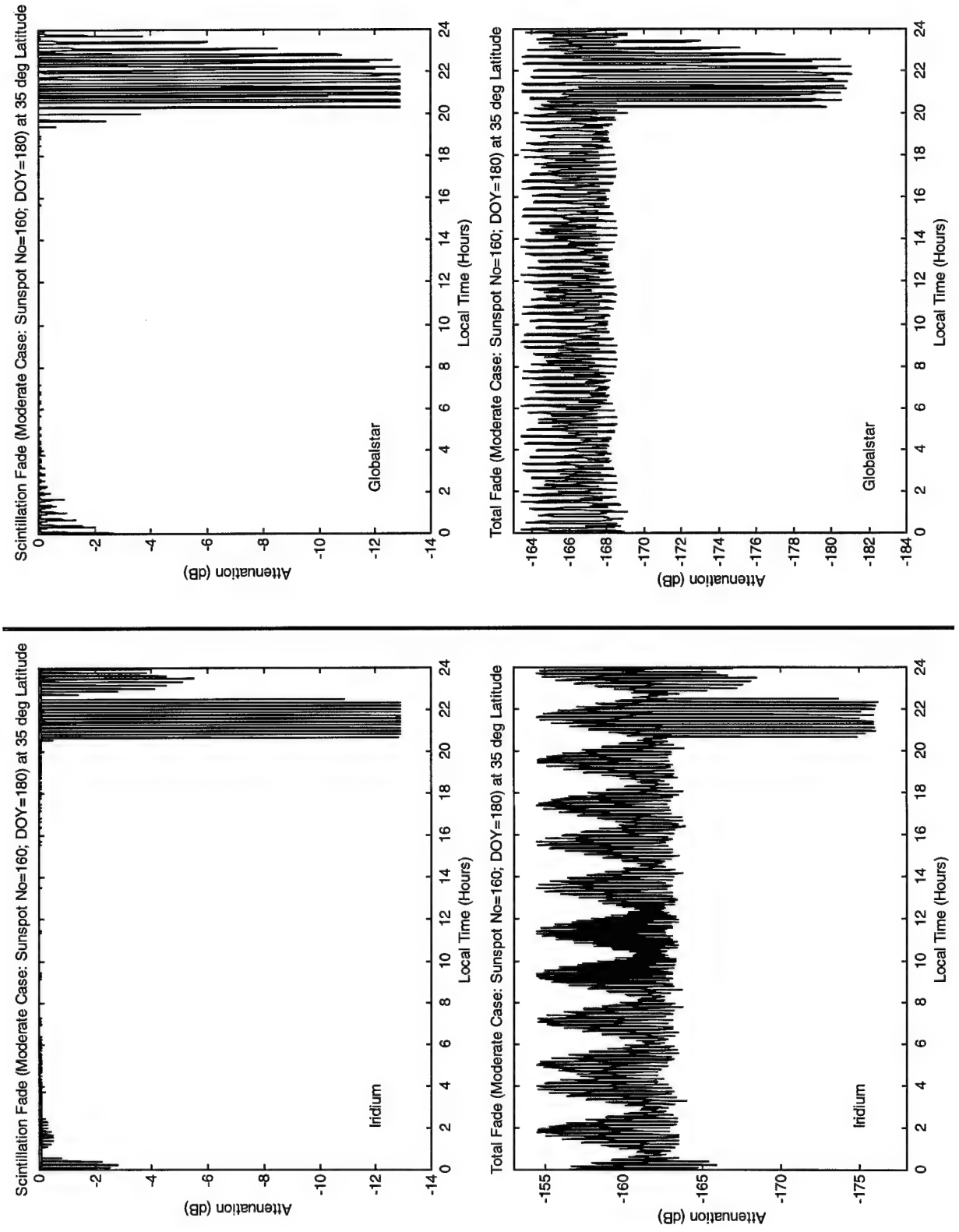
Scintillation Fade (Moderate Case: Sunspot No=160; DOY=180) at 35 deg Latitude
Attenuation (dB)
Local Time (Hours)
Globalstar
Total Fade (Moderate Case: Sunspot No=160; DOY=180) at 35 deg Latitude
Attenuation (dB)
Local Time (Hours)
Globalstar
Scintillation Fade (Moderate Case: Sunspot No=160; DOY=180) at 35 deg Latitude
Attenuation (dB)
Local Time (Hours)
Iridium
Total Fade (Moderate Case: Sunspot No=160; DOY=180) at 35 deg Latitude
Attenuation (dB)
Local Time (Hours)
Iridium

SCENARIO 2

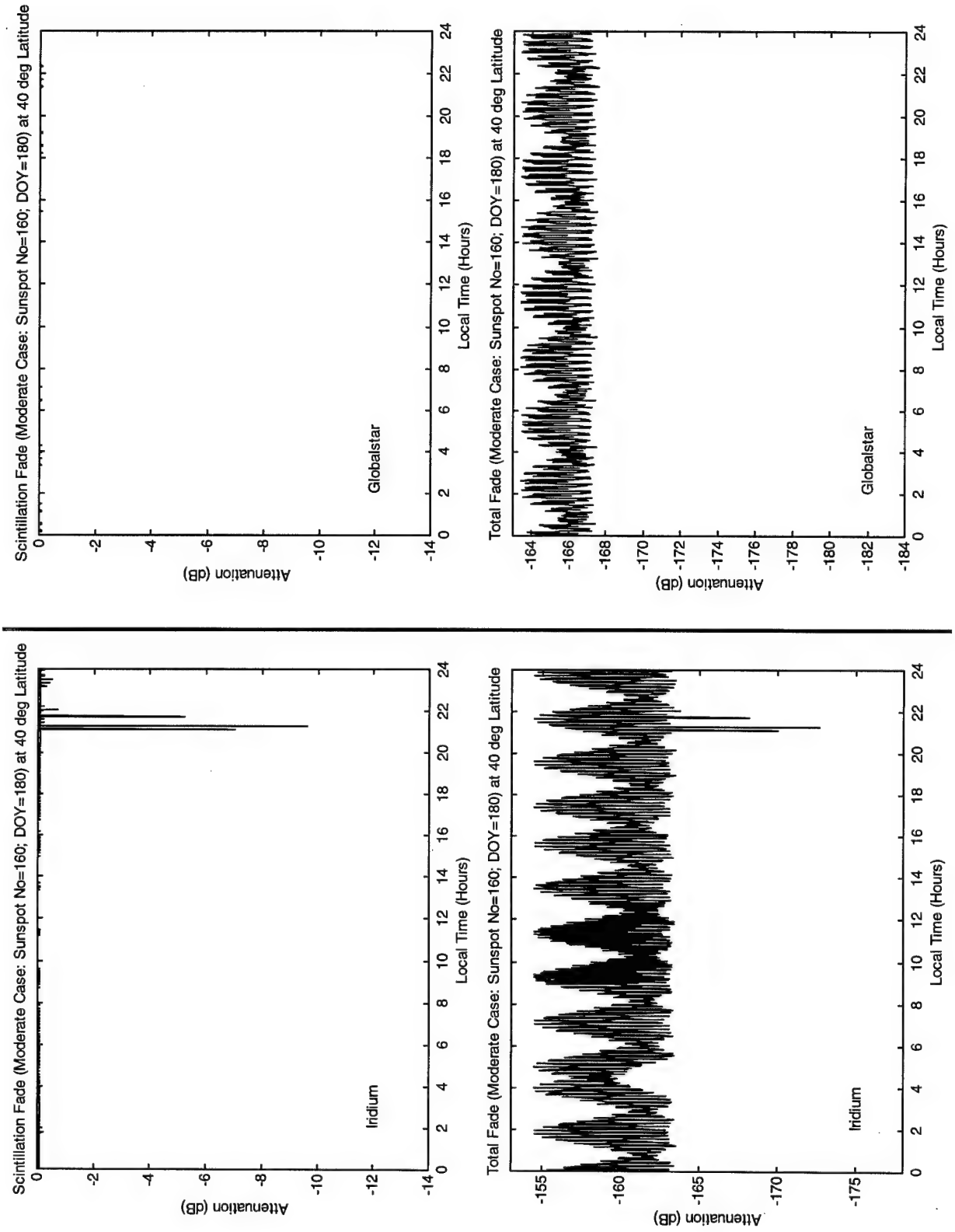
Scintillation Fade (Moderate Case: Sunspot No=160; DOY=180) at 40 deg Latitude
Attenuation (dB)
Local Time (Hours)
Globalstar
Total Fade (Moderate Case: Sunspot No=160; DOY=180) at 40 deg Latitude
Attenuation (dB)
Local Time (Hours)
Globalstar
Scintillation Fade (Moderate Case: Sunspot No=160; DOY=180) at 40 deg Latitude
Attenuation (dB)
Local Time (Hours)
Iridium
Total Fade (Moderate Case: Sunspot No=160; DOY=180) at 40 deg Latitude
Attenuation (dB)
Local Time (Hours)
Iridium

SCENARIO 2

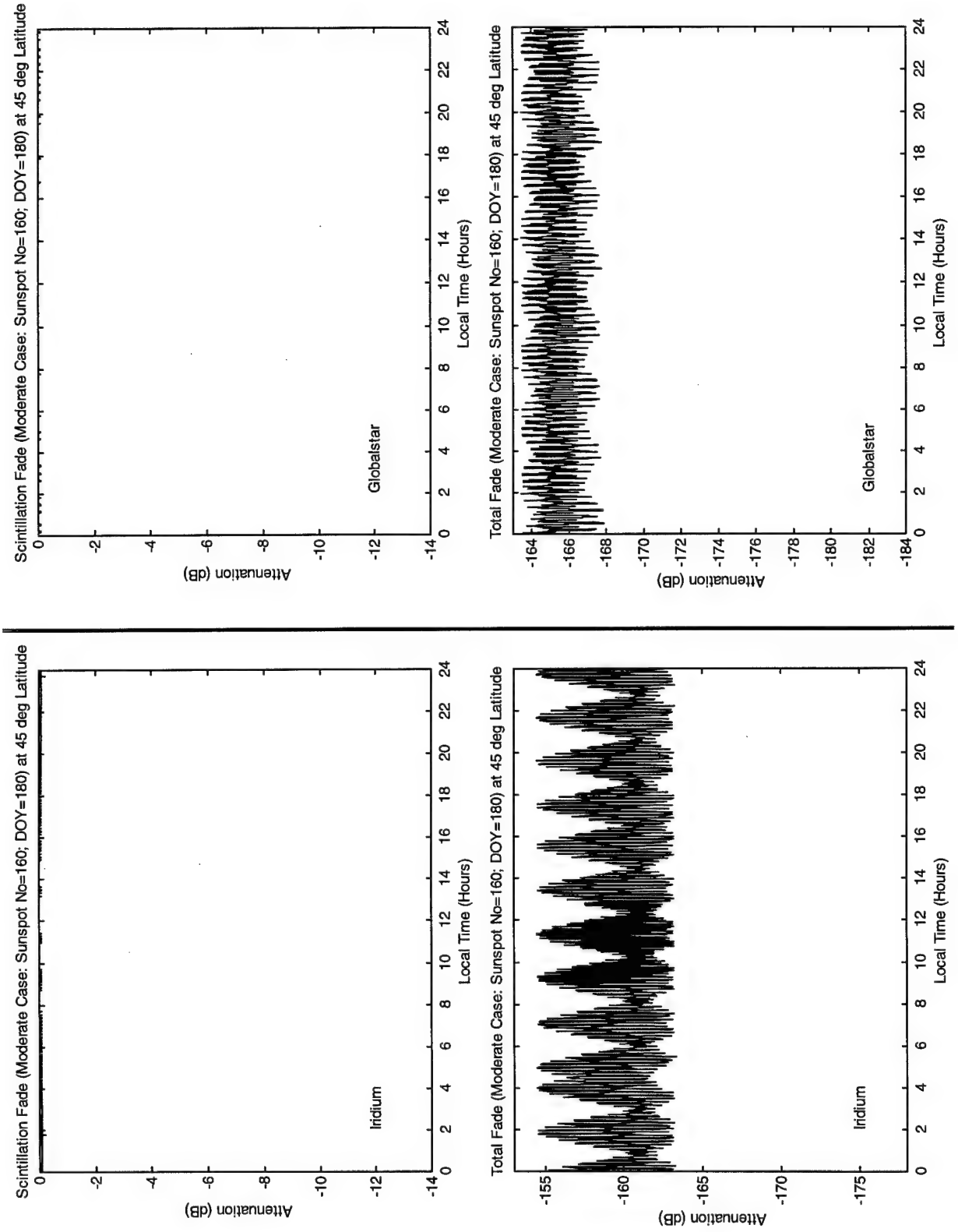
Scintillation Fade (Moderate Case: Sunspot No=160; DOY=180) at 45 deg Latitude
Attenuation (dB)
Local Time (Hours)
Globalstar
Total Fade (Moderate Case: Sunspot No=160; DOY=180) at 45 deg Latitude
Attenuation (dB)
Local Time (Hours)
Globalstar
Scintillation Fade (Moderate Case: Sunspot No=160; DOY=180) at 45 deg Latitude
Attenuation (dB)
Local Time (Hours)
Iridium
Total Fade (Moderate Case: Sunspot No=160; DOY=180) at 45 deg Latitude
Attenuation (dB)
Local Time (Hours)
Iridium

SCENARIO 3

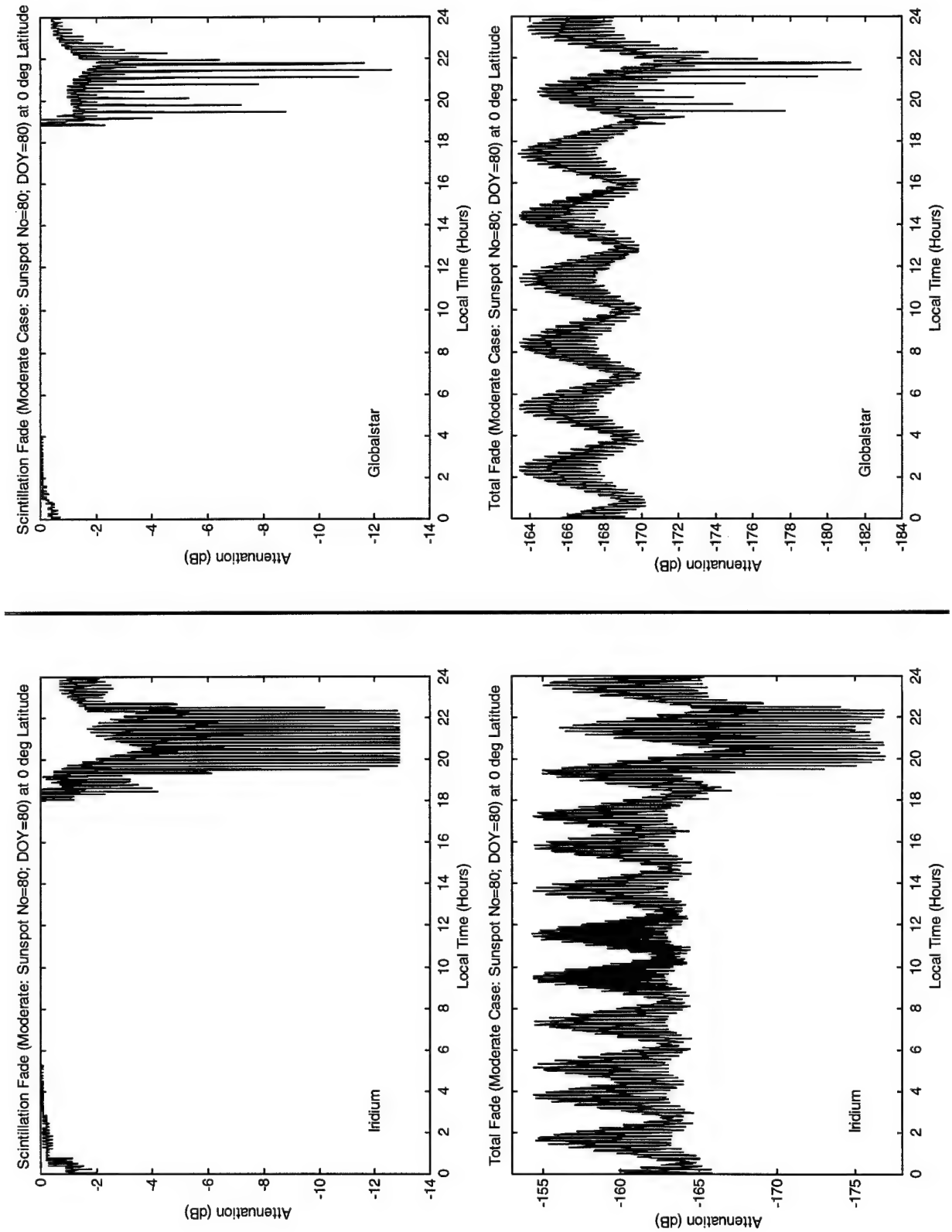
Scintillation Fade (Moderate Case: Sunspot No=80; DOY=80) at 0 deg Latitude
Attenuation (dB)
Local Time (Hours)
Globalstar
Total Fade (Moderate Case: Sunspot No=80; DOY=80) at 0 deg Latitude
Attenuation (dB)
Local Time (Hours)
Globalstar
Scintillation Fade (Moderate: Sunspot No=80; DOY=80) at 0 deg Latitude
Attenuation (dB)
Local Time (Hours)
Iridium
Total Fade (Moderate Case: Sunspot No=80; DOY=80) at 0 deg Latitude
Attenuation (dB)
Local Time (Hours)
Iridium

SCENARIO 3

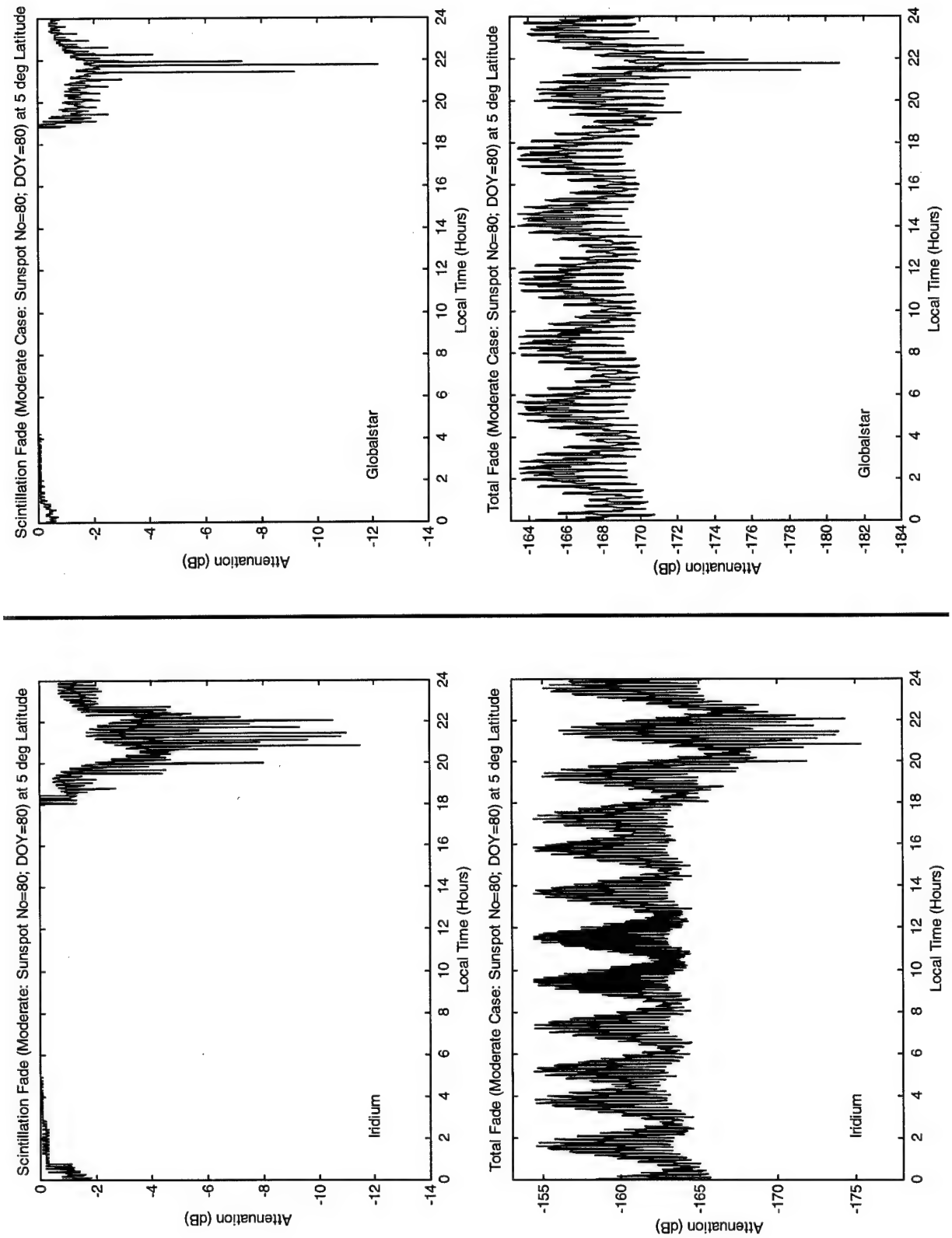
Scintillation Fade (Moderate Case: Sunspot No=80; DOY=80) at 5 deg Latitude
Attenuation (dB)
Local Time (Hours)
Globalstar
Total Fade (Moderate Case: Sunspot No=80; DOY=80) at 5 deg Latitude
Attenuation (dB)
Local Time (Hours)
Globalstar
Scintillation Fade (Moderate: Sunspot No=80; DOY=80) at 5 deg Latitude
Attenuation (dB)
Local Time (Hours)
Iridium
Total Fade (Moderate Case: Sunspot No=80; DOY=80) at 5 deg Latitude
Attenuation (dB)
Local Time (Hours)
Iridium

SCENARIO 3

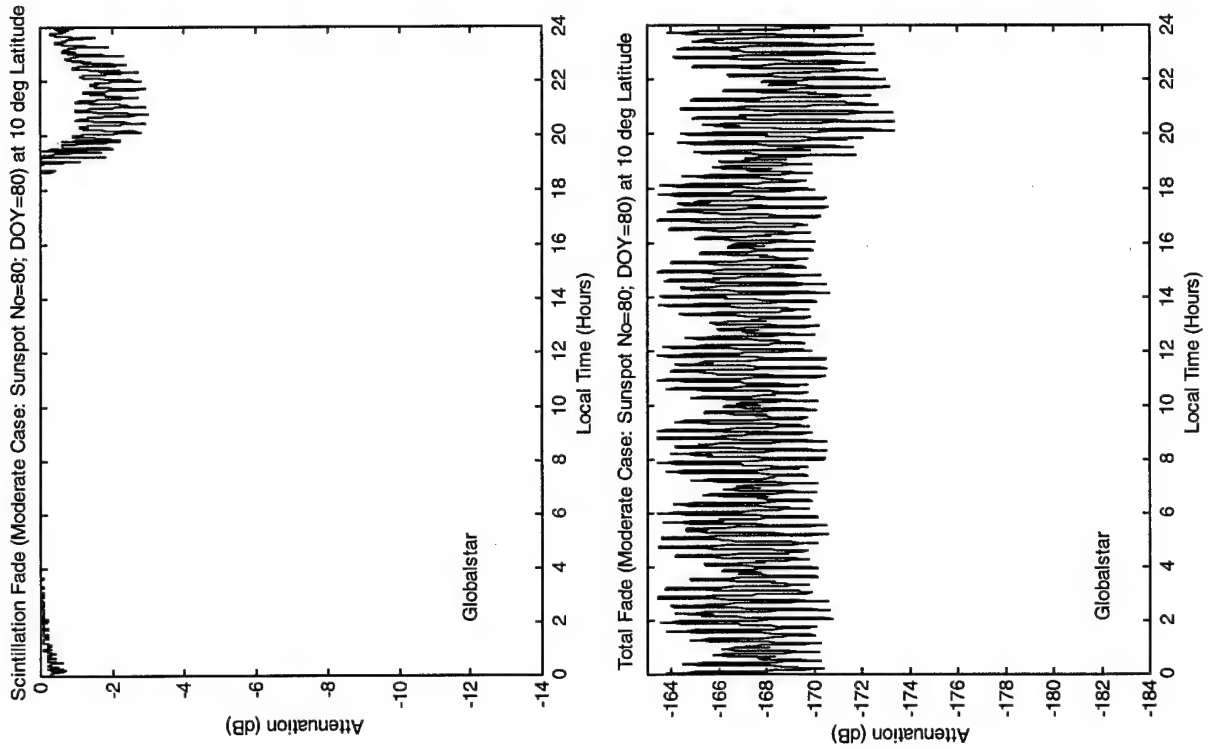
Scintillation Fade (Moderate Case: Sunspot No=80; DOY=80) at 10 deg Latitude
Attenuation (dB)
Local Time (Hours)
Globalstar
Total Fade (Moderate Case: Sunspot No=80; DOY=80) at 10 deg Latitude
Attenuation (dB)
Local Time (Hours)
Globalstar

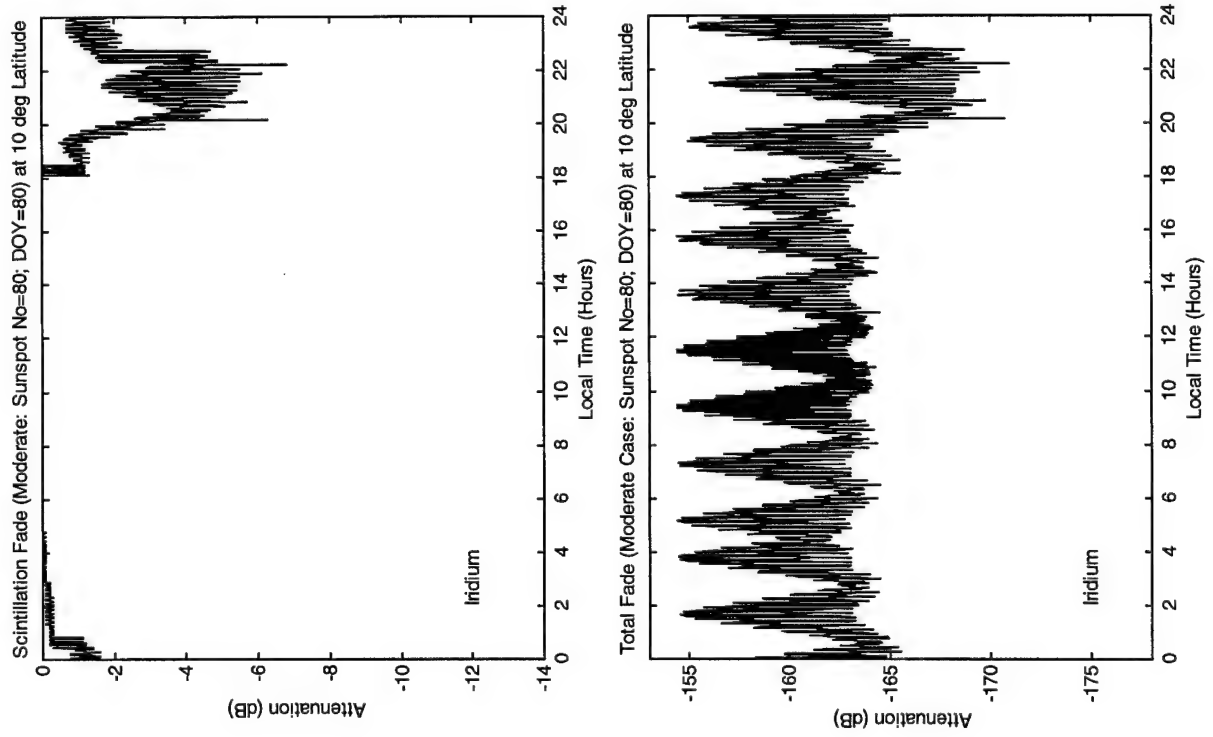
Scintillation Fade (Moderate: Sunspot No=80; DOY=80) at 10 deg Latitude
Attenuation (dB)
Local Time (Hours)
Iridium
Total Fade (Moderate Case: Sunspot No=80; DOY=80) at 10 deg Latitude
Attenuation (dB)
Local Time (Hours)
Iridium

SCENARIO 3

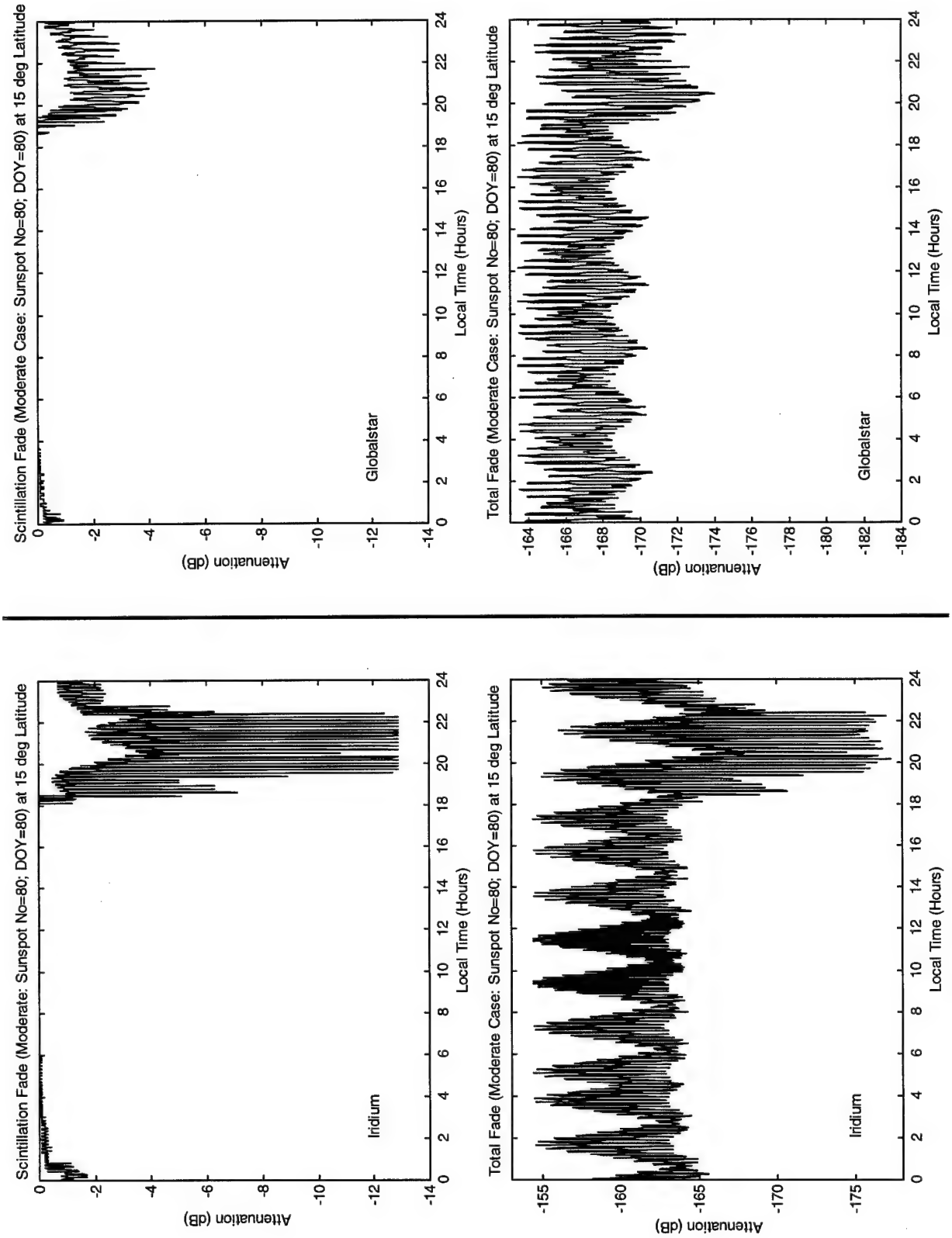
Scintillation Fade (Moderate Case: Sunspot No=80; DOY=80) at 15 deg Latitude
Attenuation (dB)
Local Time (Hours)
Globalstar
Total Fade (Moderate Case: Sunspot No=80; DOY=80) at 15 deg Latitude
Attenuation (dB)
Local Time (Hours)
Globalstar
Scintillation Fade (Moderate: Sunspot No=80; DOY=80) at 15 deg Latitude
Attenuation (dB)
Local Time (Hours)
Iridium
Total Fade (Moderate Case: Sunspot No=80; DOY=80) at 15 deg Latitude
Attenuation (dB)
Local Time (Hours)
Iridium

SCENARIO 3

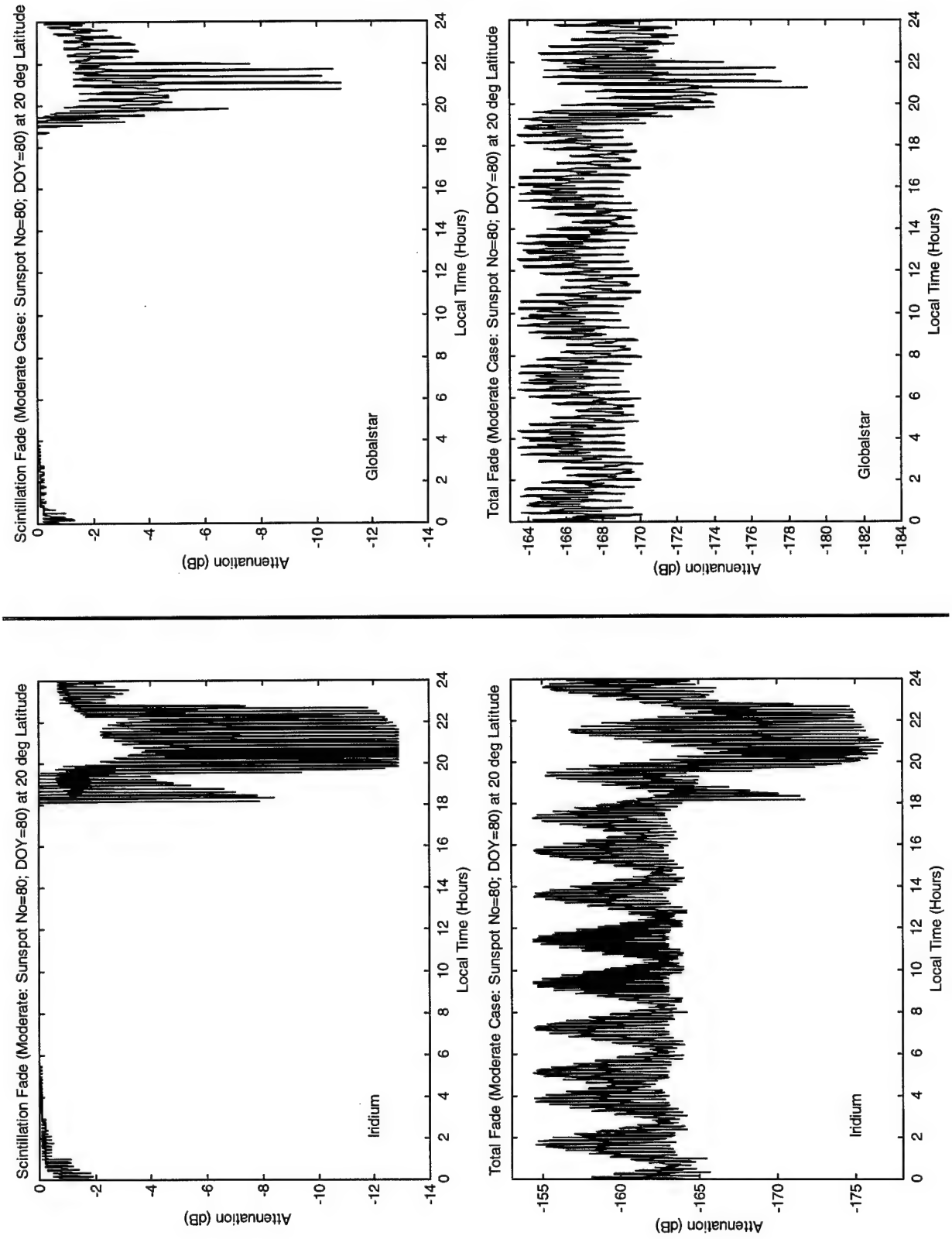
Scintillation Fade (Moderate Case: Sunspot No=80; DOY=80) at 20 deg Latitude
Attenuation (dB)
Local Time (Hours)
Globalstar
Total Fade (Moderate Case: Sunspot No=80; DOY=80) at 20 deg Latitude
Attenuation (dB)
Local Time (Hours)
Globalstar
Scintillation Fade (Moderate: Sunspot No=80; DOY=80) at 20 deg Latitude
Attenuation (dB)
Local Time (Hours)
Iridium
Total Fade (Moderate Case: Sunspot No=80; DOY=80) at 20 deg Latitude
Attenuation (dB)
Local Time (Hours)
Iridium

SCENARIO 3

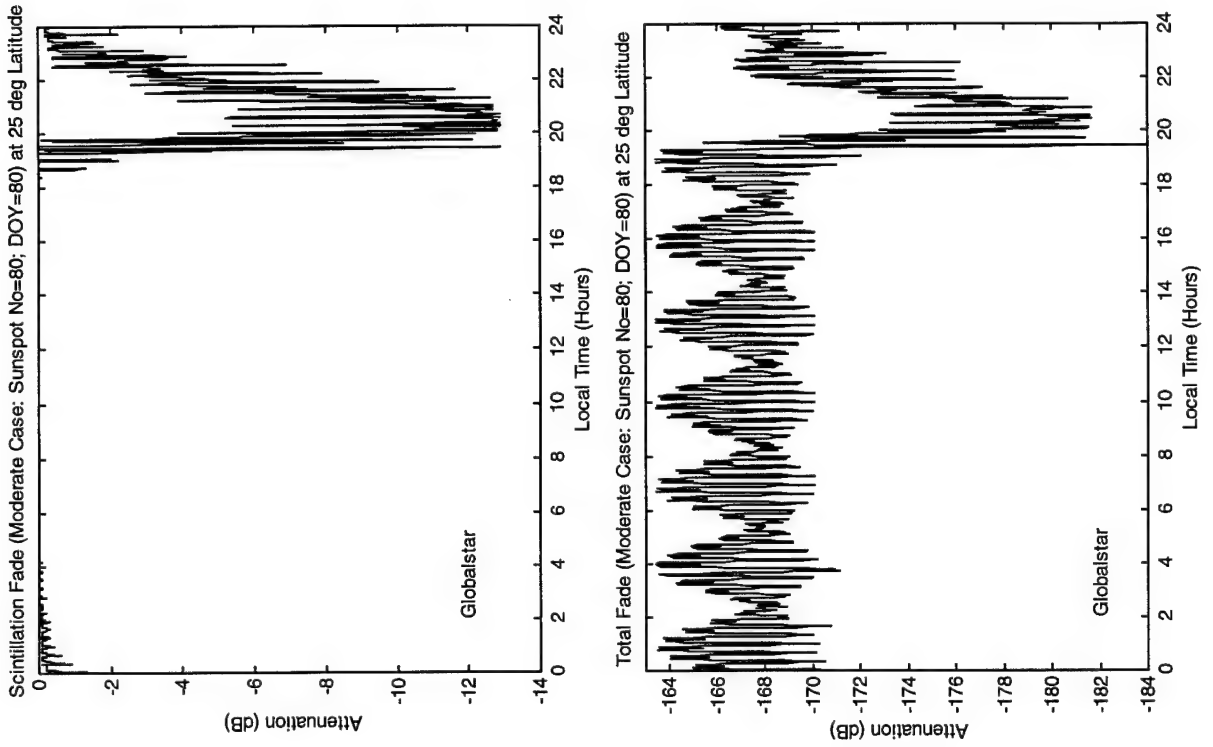
Scintillation Fade (Moderate Case: Sunspot No=80; DOY=80) at 25 deg Latitude
Attenuation (dB)
Local Time (Hours)
Globalstar
Total Fade (Moderate Case: Sunspot No=80; DOY=80) at 25 deg Latitude
Attenuation (dB)
Local Time (Hours)
Globalstar

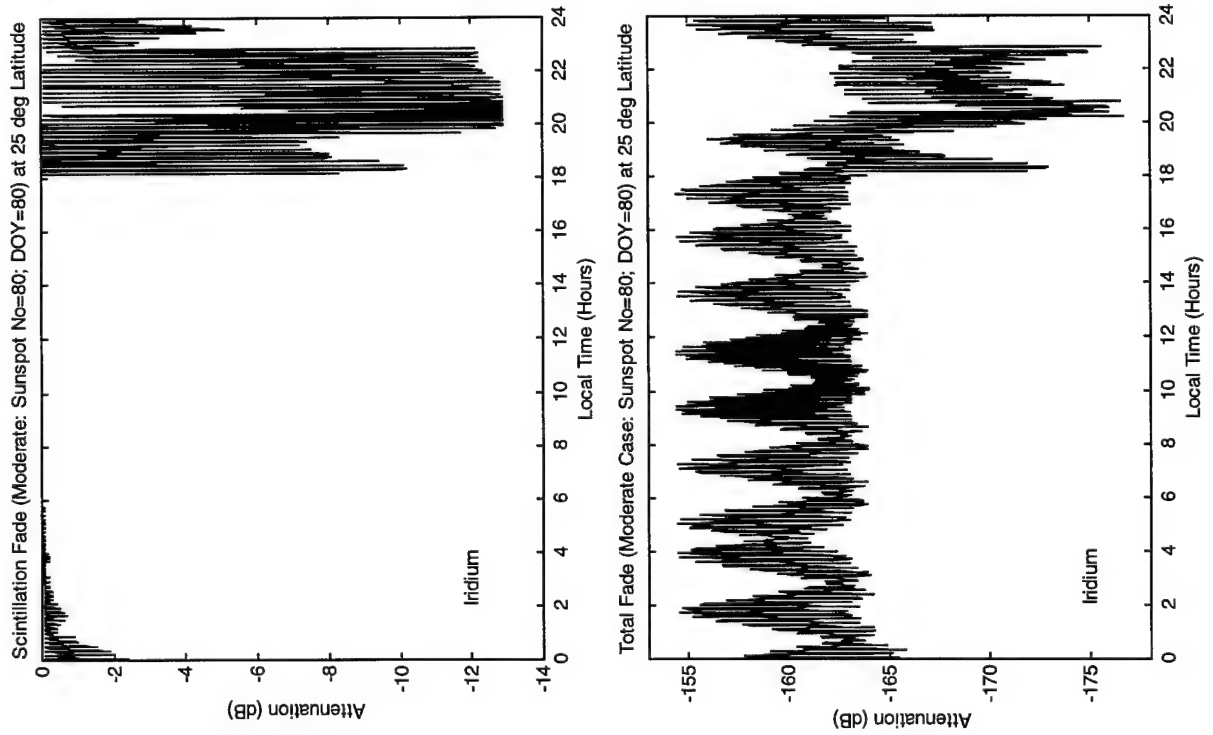
Scintillation Fade (Moderate: Sunspot No=80; DOY=80) at 25 deg Latitude
Attenuation (dB)
Local Time (Hours)
Iridium
Total Fade (Moderate Case: Sunspot No=80; DOY=80) at 25 deg Latitude
Attenuation (dB)
Local Time (Hours)
Iridium

SCENARIO 3

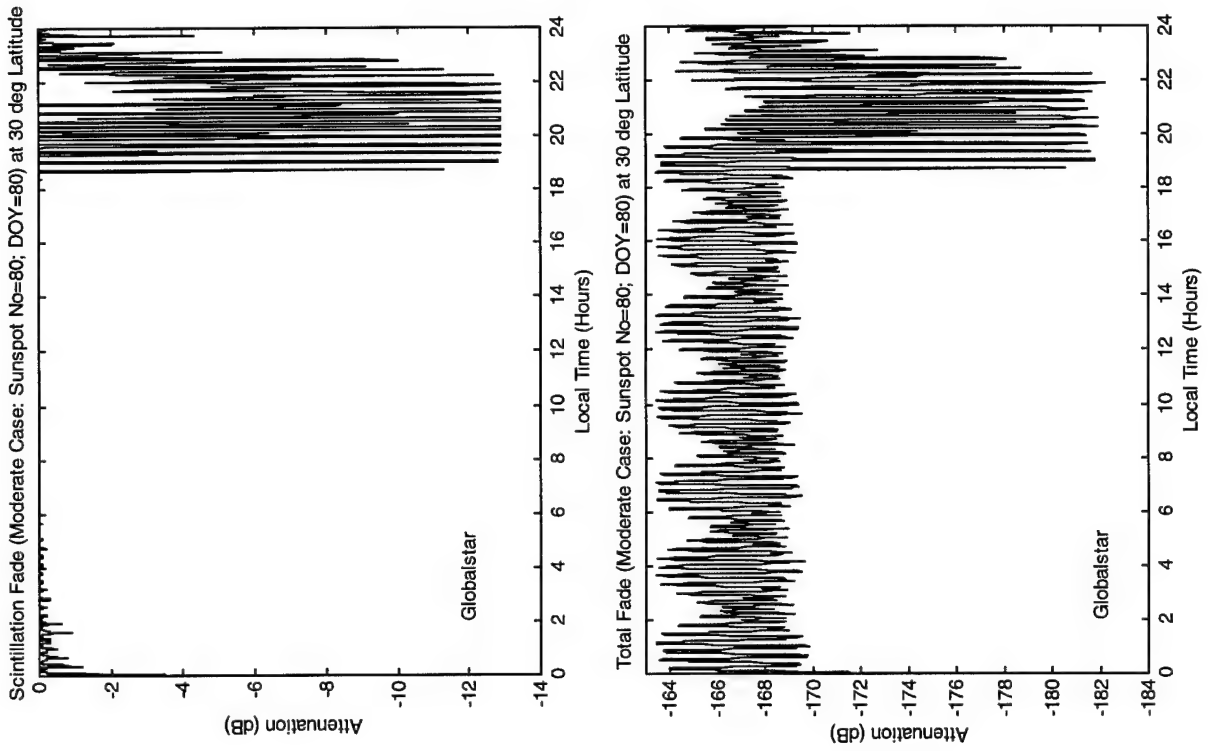
Scintillation Fade (Moderate Case: Sunspot No=80; DOY=80) at 30 deg Latitude
Attenuation (dB)
Local Time (Hours)
Globalstar
Total Fade (Moderate Case: Sunspot No=80; DOY=80) at 30 deg Latitude
Attenuation (dB)
Local Time (Hours)
Globalstar

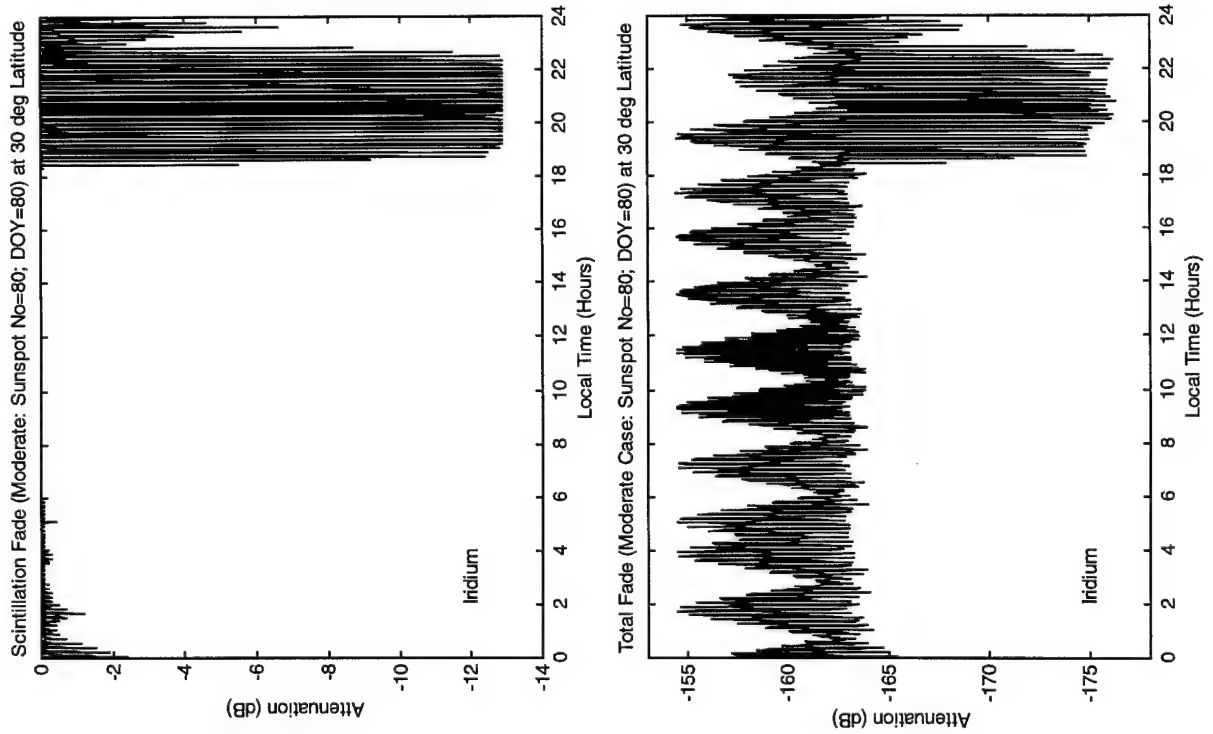
Scintillation Fade (Moderate: Sunspot No=80; DOY=80) at 30 deg Latitude
Attenuation (dB)
Local Time (Hours)
Iridium
Total Fade (Moderate Case: Sunspot No=80; DOY=80) at 30 deg Latitude
Attenuation (dB)
Local Time (Hours)
Iridium

SCENARIO 3

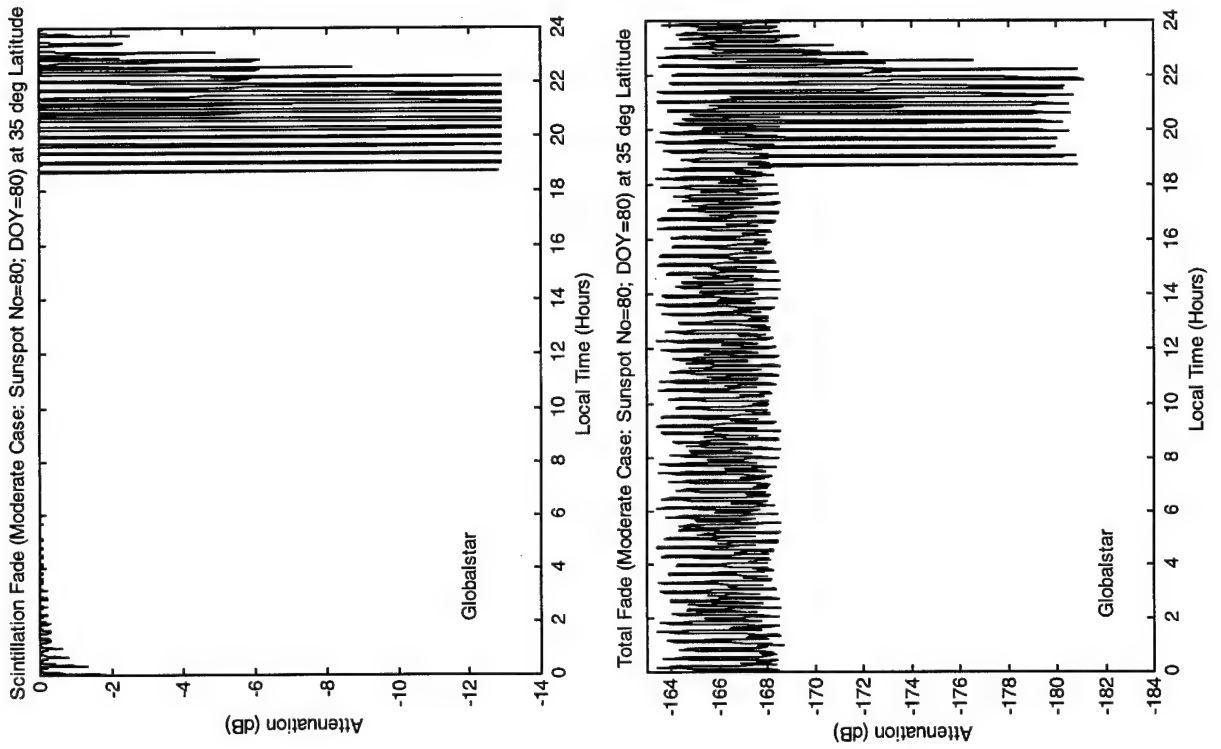
Scintillation Fade (Moderate Case: Sunspot No=80; DOY=80) at 35 deg Latitude
Attenuation (dB)
Local Time (Hours)
Globalstar
Total Fade (Moderate Case: Sunspot No=80; DOY=80) at 35 deg Latitude
Attenuation (dB)
Local Time (Hours)
Globalstar

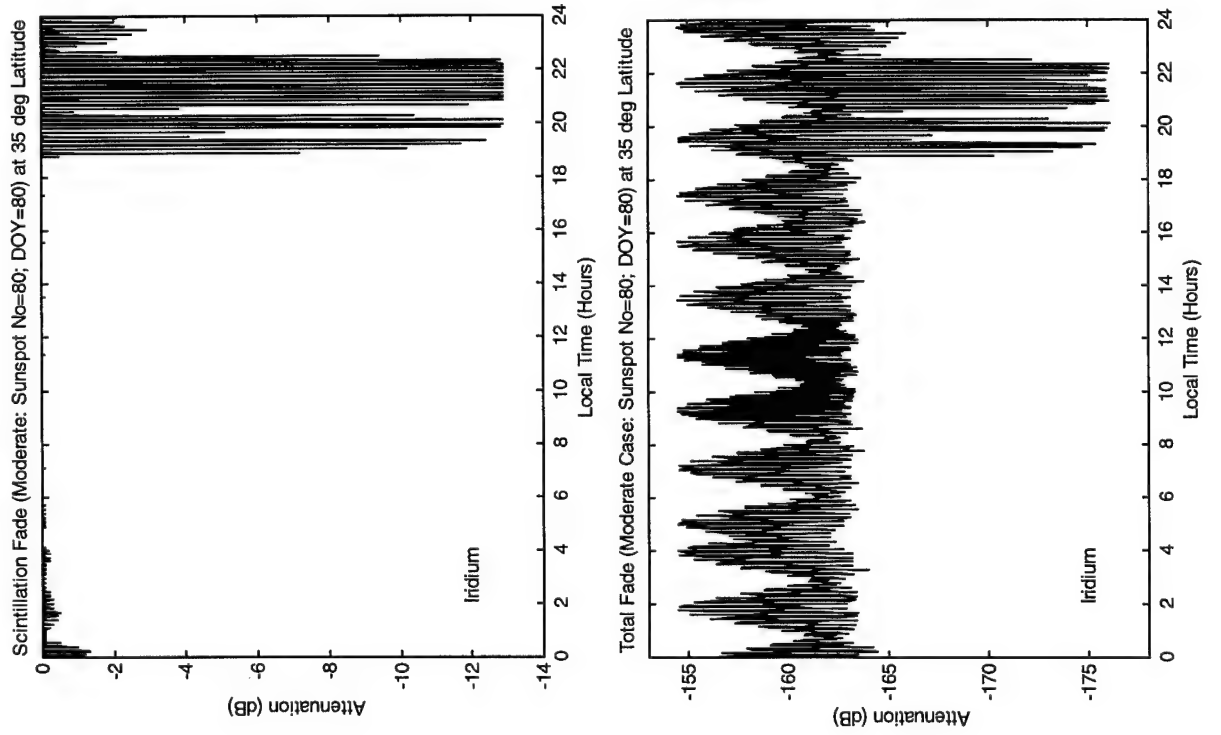
Scintillation Fade (Moderate: Sunspot No=80; DOY=80) at 35 deg Latitude
Attenuation (dB)
Local Time (Hours)
Iridium
Total Fade (Moderate Case: Sunspot No=80; DOY=80) at 35 deg Latitude
Attenuation (dB)
Local Time (Hours)
Iridium

SCENARIO 3

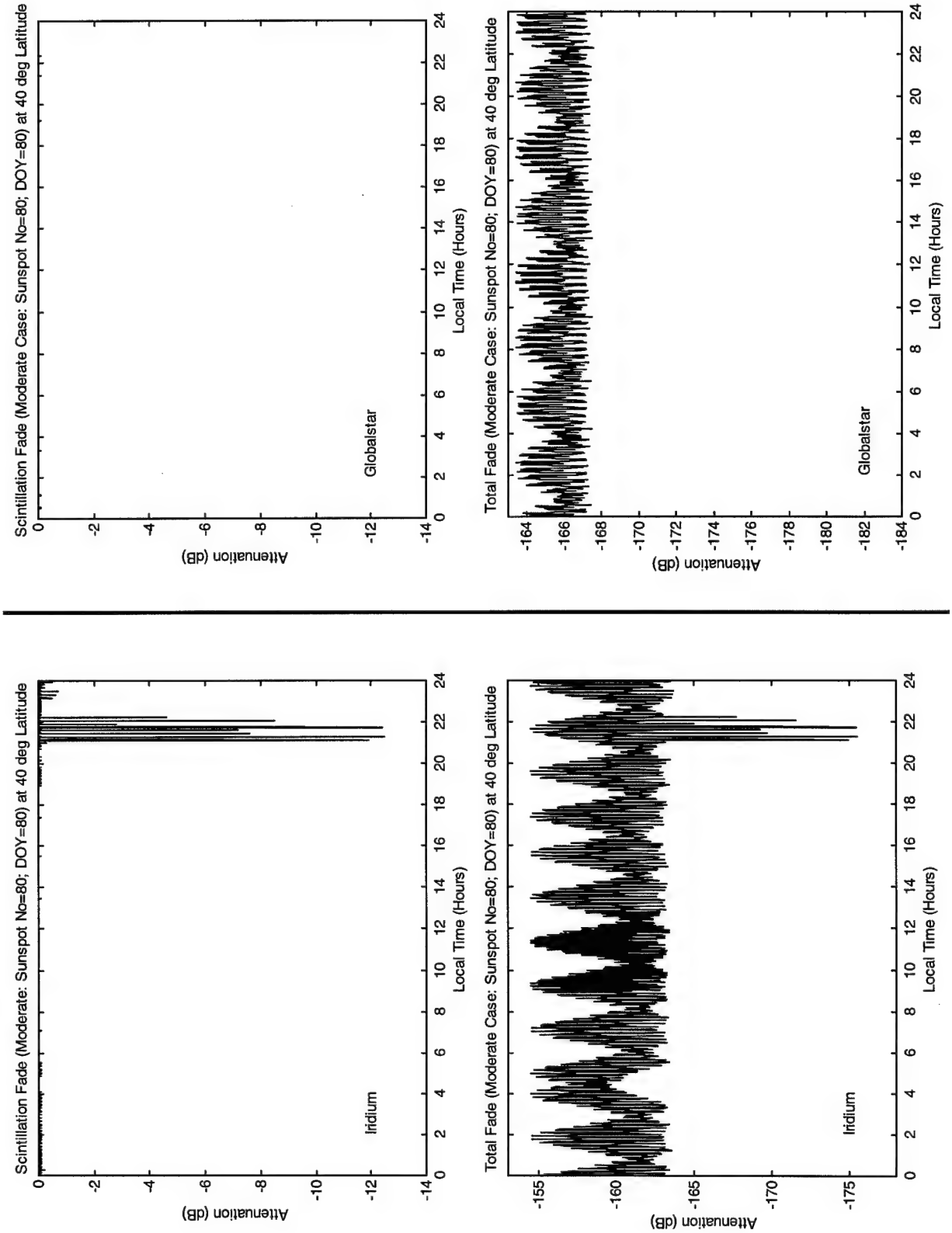
Scintillation Fade (Moderate Case: Sunspot No=80; DOY=80) at 40 deg Latitude
Attenuation (dB)
Local Time (Hours)
Globalstar
Total Fade (Moderate Case: Sunspot No=80; DOY=80) at 40 deg Latitude
Attenuation (dB)
Local Time (Hours)
Globalstar
Scintillation Fade (Moderate: Sunspot No=80; DOY=80) at 40 deg Latitude
Attenuation (dB)
Local Time (Hours)
Iridium
Total Fade (Moderate Case: Sunspot No=80; DOY=80) at 40 deg Latitude
Attenuation (dB)
Local Time (Hours)
Iridium

SCENARIO 3

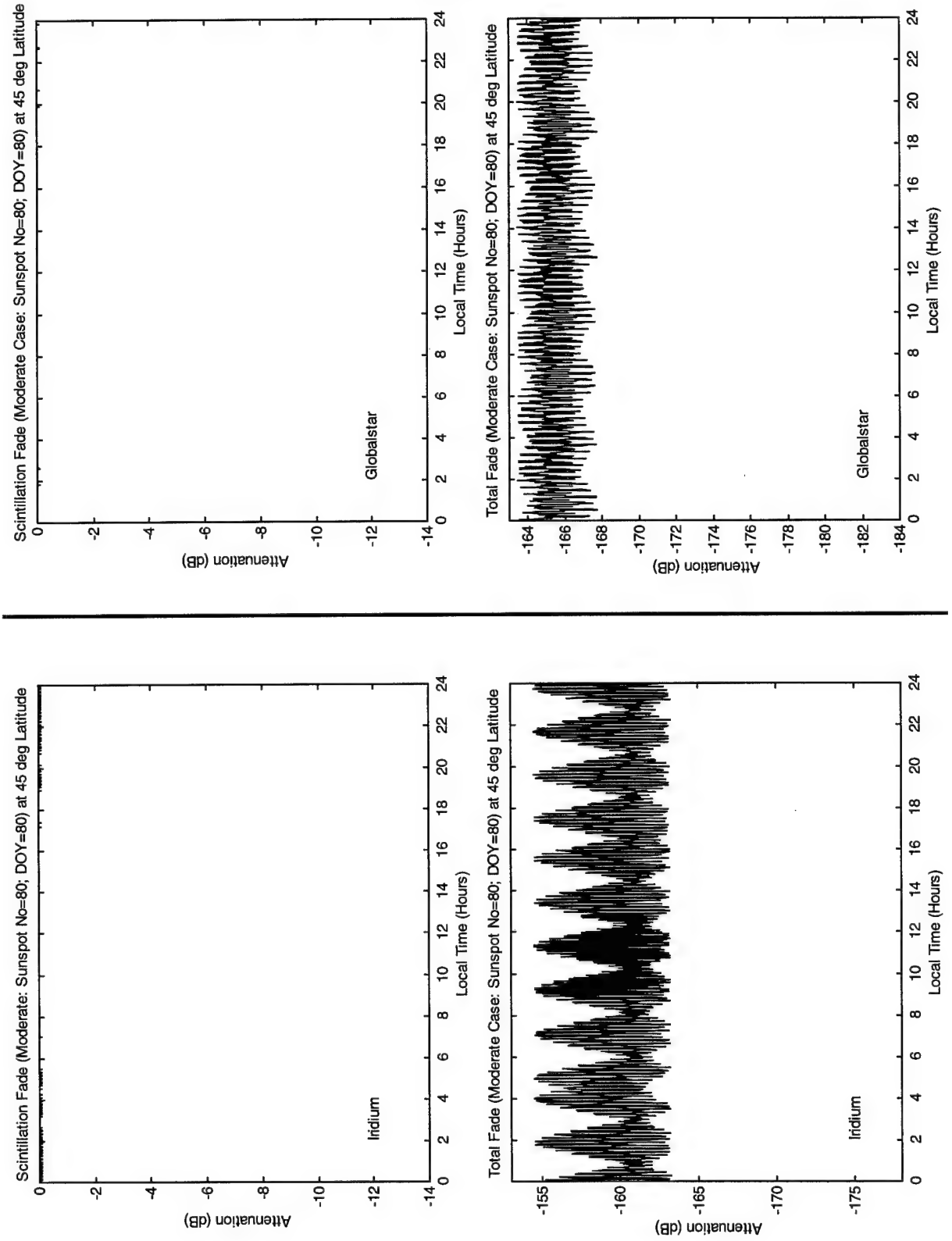
Scintillation Fade (Moderate Case: Sunspot No=80; DOY=80) at 45 deg Latitude
Attenuation (dB)
Local Time (Hours)
Globalstar
Total Fade (Moderate Case: Sunspot No=80; DOY=80) at 45 deg Latitude
Attenuation (dB)
Local Time (Hours)
Globalstar
Scintillation Fade (Moderate: Sunspot No=80; DOY=80) at 45 deg Latitude
Attenuation (dB)
Local Time (Hours)
Iridium
Total Fade (Moderate Case: Sunspot No=80; DOY=80) at 45 deg Latitude
Attenuation (dB)
Local Time (Hours)
Iridium

APPENDIX F - MATLAB PROGRAM LISTING

Program: Sat10.m

```
clear all
cd c:\data\matlab;
%  This program takes a matrix, which must be in a space delimited
%   file called '%d_data.csv' in the MATLAB path,    with structure as follows:
%   Column1   time(s)
%   Column2   X Position  (kms
%   Column3  Y Position (kms)
%   Column4   Z Position (kms)
%   Column5   Vx Realtive (m/s)
%   Column6   Vy Realtive (m/s)
%   Column7   Vz Realtive (m/s)
%   Column8    azimuth(deg)
%   Column9   elevation(deg)
%   Column10   range(kms)
%   Column11   Free Space Path Loss (dB)
%   Column12   Atmospheric (gaseous atten @7.5 g/m^2 water vapor)
%   Column13   Rain Loss (CCIR) at 0.01 exceedence
%   Column14   total Attenuation
%   The value of the time step is assigned as the variable 'ss'.
%   The Program first goes through to ensure the data is correct by looking for
samples >ss seconds apart.
%  If there are any it means the data is corrupt or that there are periods of
no visible satellites >ss seconds (unlikely).
%  The program then calculates satellite visibility, then goes onto calculate
best elevation angle.
%  It then determines the number of satellites visible during the observation,
and the best elevation angle.
%  The program gets the max elevation angle and the min range and writes it to
an output file with the time stamp.
%  initialize variables
for Lat_gs=0:5:90; % ie Latitude of the Ground Station
   Lat_gs  % shows current iteration
   ss=30; %auto input
   %   ss=input('Enter Time Step of observation-          '); %manual input
   %  step size (ss) is the no of seconds between STK samples
   %   Lat_gs=input('Enter Latitude of Facility-              '); %manual input
   Str1=num2str(Lat_gs);
   Lon_gs=135;      %  for auto-input
   %Lon_gs=input('Enter Longitude of Facility-              '); % manual input
   disp('    Loading data matrix data.csv generated from STK.  This matrix has
time, AER & link budget data');
   %   Don't use the "load" command as sometimes STK leaves a line with no data
in it so "load" will not read empty lines
   %   DLMREAD will load an empty line as long at the delimiters are there
   %  disp('Load completed, checking for invalid entries');
   %  eval(sprintf('load %d_data.mat',Lat_gs));  % loads data if it's known
correct and defines a matrix
   sat_data=dlmread('data.csv',',');  %Loads the primary data file containing
14 columns.
   disp('    Finished loading data matrix, writing data to c:\matlab\bin');
   %   Writes the full data set to 2 files on the HDD for later use.  Saves
load time.
   %  eval(sprintf('save %d_sat_data.txt sat_data -ascii',Lat_gs)); %Saving
intermediate file
   %  eval(sprintf('save %d_sat_data.mat sat_data',Lat_gs));  %Saving
intermediate file
```

```
   data(:,1)=sat_data(:,1);  %reads time as first column
   data(:,2:8)=sat_data(:,8:14);   %reads AER and losses as next 6 columns
   %   Writes the 8 column data matrix which contains AER (Az Elev Range) and
Prop Loss data.
   eval(sprintf('save %d_data.txt sat_data -ascii',Lat_gs));  %Saving
intermediate file
   eval(sprintf('save %d_data.mat sat_data',Lat_gs));  %Saving intermediate
file
   disp('    Finished writing data files, be sure to move them to archives');
   disp('    Processing satellite AER data to extract best path details.    ');
   %   The next routine takes the data file and checks each line to make sure
it's valid
   temp=size(data);
   i=temp(:,1);
   Test = data(:,1);
   Test=sortrows(Test,1);
   for X=1:i-1
      if Test(X+1,1)-Test(X,1)>ss
         disp('ERROR IN DATA.  TWO SAMPLES MORE THAN SS SECONDS APART AT THE
FOLLOWING TIME:');
         X*ss
         %No_Sats(:)=[X*ss]
      end
   end
   %clear Test;
   %clear temp;
   %clear X;
   %  That routine checked that the entries were not more than ss seconds
apart.
   %    It ensures missed observations or corrupt data don't upset the
calculations.
   %   Also determines the length of the matrix for use as a counter
   %_____________________________________________________________________
   %  This checking system uses time stamp only to determine the time
transitions.
   %  This is necessary so that the number of satellites in view can be
determined.
   %  The system is event driven, it looks at the arrival of a satellite into
view (the Start)
   %  and its departure (the Stop).  Knowing the transitions you can track the
number of
   %  satellites in view at any one time.
   %  The routine then integrates between the transitions to ACCURATELY
determine the total no of
   %  sats in view as a percentage of the total ovbservation time
   %  It looks at each line of the data file and determines if a jump
   %  occurred which indicates a transition to/from an observation period.
(See Methodology Chapter)
   transitions=[];
   x=1;
   for n=1:i-1
      if abs(data(n,1)-data(n+1,1))>ss
         transitions(2,x)=[data(n,1)];% a stop value
         transitions(1,x+1)=[data(n+1,1)];% a start value
         x=x+1;
      end
   end
   %  these next lines write the final start and stop transitions
   transitions(1,1)=[data(1,1)];
   transitions(2,end)=[data(end,1)];
   %   tHIS CHECKS WHETHER ANY OF THE IN VIEW TIMES OF THE
   %  SATELLITES ARE GREATER THAN 1100 SECONDS.  If they are then
```

```
   %  it is greater than the orbit allows ie max in-view time =1100 seconds)
   %  and it's a bogus or corrupt observation
   n=1;
   while n < x
      if abs(transitions(1,n)-transitions(2,n))>1100
         transitions(:,n)=[];
         x=x-1;
         disp('got rid of one Ken!  Check Column number:');
         n
      end
      n=n+1;
   end
   %
   %   The next routine sorts the two rows into a single column ready for
generating the
   %   sorting.  Each transition must be annotated as a START (a '1'), or a
STOP (a '-1')
   %   and then placed in chronological order.  You just integrate the series
to get a running total of the
   %   number of satellites in view.
   %
   No=size(transitions,2);
   transition1(:,1)=transitions(1,:)';
   transition1(:,2)=[1];
   transition1((No+1):(2*No),1)=[transitions(2,:)'];
   transition1((No+1):(2*No),2)=[-1];
   %   have to add the first Start because the system I used needs to see the
   %    previous observation before it can determine if the current one is a
start or stop.
   %    Since the first observation is obviously a 'Start', there is no problem
in adding the [1]
   a=sortrows(transition1,1);
   %   I changed a(1,3) to a(1,2) on 17/10 as i believe the 2nd index is wrong.
The first
   %   transition must be a satellite access start.  Note the sortrows has put
the transitions in chronological
   %   order so the 1st must be a start.  I think the lack of this line was
giving me periods of no satellites
   %   previously
   a(1,2)=[1];
   a(1,3)=[1];
   x=size(a,1);
   %
   %   Next just add up the 3rd column, which is the 1 or -1 indicating a start
or stop
   %
   for i=2:x
      a(i,3)=[a(i-1,3)+a(i,2)];
      if a(i,3)==0;
         disp('Satellite gap at time=');
         a(i,1)
         disp('at time');
         i
      end
   end
   %
   %   Next determine the number of satellites in view between observations
   %
   for i=2:x-1
      a(i,4)=a(i+1,1)-a(i,1);
   end
```

```
   %   Then write it to a file called Num which is the Number of satellites in
view
   %   Note that the first column is 0 satellites in view
   %
   Num=[0 0 0 0 0 0 0 0 0 0 0 0;0 1 2 3 4 5 6 7 8 9 10 11];
   for i=2:x-1
      A=a(i,3);
      Num(1,A+1)=Num(1,A+1) + a(i,4);
   end

   figure
   x_axis=0:1:11
   axis([0,11,0,1]);
   bar(x_axis,Num(1,:)/86400,'k');
   XLABEL('No of Satellites');
   YLABEL('Total Proportion of Time');
   Title('Satellites Visibility Chart');
   %   Next line writes the Num data to the Matlab\bin directory
   eval(sprintf('save %d_No_sats.txt Num -ascii',Lat_gs));
   %disp('       Writing to file output.txt located in
c:\matlab\tempdata\output.txt and tempdata\histogram.txt...');
   %dlmwrite('c:\matlab\tempdata\output.txt',Output,'\t');
   %dlmwrite('c:\matlab\tempdata\histogram.txt',A,'\t');
   %disp('       .....operation complete, files output and histogram written');

   %%%%%%%%%%%%%%%%%%%%%%%%%%%%%%%%%%%%%%%%%%%%%%%%%%%%%%%%
   %  DETERMINATION OF BEST ELEVATION ANGLE
   %
   %  Remember the format:-  data=(Time, azimuth, elevation, range, Free Space
Path Loss,
   %                  Atmospheric Attenuation, Rain Loss and Total
Attenuation).
   %   8 Columns with length dependent on the total observation time
   %
   %%%%%%%%%%%%%%%%%%%%%%%%%%%%%%%%%%%%%%%%%%%%%%%%%%%%%%%%
   i=size(sat_data,1);  %
   %  data is copied to a working matrix
   data1=sat_data;
   %  data1=[sat_data(:,1) sat_data(:,8:14)];
   %  this routine adds another column to the end of the data (new 9th column)
which is the time rounded to the nearest minute.
   %  It captures all times within +/-(ss/2) eg +/-30 secs for a 60 second
sample time
   for n=1:i
      data1(n,15)=round(data1(n,1)/ss);   %data1 includes all sat data incl rel
posn and velocities
   end
   %  rows are sorted on the new column and assigned to 'data1'
   data1=sortrows(data1,15);
   % This section generates a AER_details matrix with elements as follows
   %first element:   Time block
   %second element:  Azimuth angle corresponding to best elev angle
   %third element:   Best elevation angle
   %fourth element:  Range corresponding to best elev angle
   %fifth to 8th elements:   Best free space Path loss, CCIR rain Loss, gaseous
loss at 7.5% water vapor content
   %  total loss  etc
   % It also generates a WBMOD_details matrix with all the elements required to
feed the
   %  coordinate transformation subroutine at the end, and generate the WBMOD
input file.
   n=1;
```

```
BlockNo=1;
while n<i
   x=n;
   while data1(n,15)==data1(n+1,15)
      n=n+1;
      if n==i-1, break, end
   end
   temp_block=data1(x:n,:); % writes the lines of sat_data which are the
same time
   temp_block=flipud(sortrows(temp_block,9)); %sorts the rows in ascending
order of elevation angle then flips the matrix
   %  this way the rows are in DESCENDING order of column 9 ie elevation.
The first row is the one with the
   %  best path to the satellite for that block of time
   aer_details(BlockNo,:)=[temp_block(1,15)*ss temp_block(1,8:14)]; %
   wbmod_details(BlockNo,:)=[temp_block(1,15)*ss temp_block(1,2:14)];
   BlockNo=BlockNo+1;
   n=n+1;
   if n==i-1, break, end
end

%   write the details matrix to the Matlab\bin directory for later saving
eval(sprintf('save %d_AER_summary.txt aer_details -ascii',Lat_gs))
eval(sprintf('save AER_%d_summary.mat aer_details',Lat_gs))
eval(sprintf('save %d_WBMOD_summary.txt wbmod_details -ascii',Lat_gs))
eval(sprintf('save WBMOD_%d_summary.mat wbmod_details',Lat_gs))
%-------------------------------------------------------------------------
%    Plot of Elevation Angles with NO FILTER APPLIED
%-------------------------------------------------------------------------

figure
x_axis=0:1:size(data,1)-1;
Temp=sortrows(data,1);
plot(x_axis,abs(Temp(:,3)),'k');
Ylabel('All Observed Elevation angles');
Xlabel('Time (not even increments)');
out=['All Elevation Angles vs Time - ' Str1 ' deg latitude'];
title(out);
eval(sprintf('print -dmeta fig_%d_all_elevPLOT_NOFILTER', Lat_gs));

clear Temp
datatemp=data(:,3);
eval(sprintf('save %d_unfiltered_Elev_Angles.txt datatemp -ascii',Lat_gs))
%-------------------------------------------------------------------------
%    Plot of Best Elevation Angles
%-------------------------------------------------------------------------

a=0:1:size(aer_details(:,3),1)-1;
a=a/2;
figure
plot(a,aer_details(:,3),'k');
Xlabel('Time in Minutes');
Ylabel('Best elevation angle per 30 seconds');
out=['Best Elevation Angle vs Time (Latitude = ' Str1 'Deg)'];
title(out);
datatemp=aer_details(:,3);
eval(sprintf('save %d_Best_Elev_Angles.txt datatemp -ascii',Lat_gs))
eval(sprintf('print -dmeta fig_%d_best_elevPLOT', Lat_gs));

%-------------------------------------------------------------------------
%    PDF of Best Elevation Angles
%-------------------------------------------------------------------------
```

```
figure
a=0:5:90;
hist(aer_details(:,3),a);
Xlabel('Elevation Angle in increments of 5 deg')
%Ylabel('Number of observations')   % Should normalize this to get PDF
out=['Best elevation Angle Probability - ' Str1 ' deg Latitude'];
title(out)
%  datatemp=details(:,3);
%  eval(sprintf('save %d_Elev_Angles.txt datatemp -ascii',Lat_gs))
%-------------------------------------------------------------------------
%    PDF of Best Path Attenuation (details(:,8))
%-------------------------------------------------------------------------

figure
max_a=max(aer_details(:,8));
min_a=min(aer_details(:,8));
a=-170:.5:-154;  % need to write some code which determines what the lower
value is so that
%   the histogram doesn't get a whole lot of values at the end in a big
spike
hist(aer_details(:,8),a)
title('PDF of Attenuation (includes Rain, FSPL & Gaseous Losses)')
Xlabel('dB Total Attenuation')
Ylabel('Number of observations')   %Should normalize this to get PDF
```

Program: Elev_filter.m

```
%   THE PURPOSE OF THIS PROGRAM IS TO FILTER OUT ELEVATION ANGLE OBSERVATIONS
WHICH
%   ARE TOO CLOSE IN TIME TO ANOTHER ONE.  BY HAVING OBSERVATIONS LESS THAN 28
SECONDS APART,
%   THE DISTRIBUTIONS ARTIFICIALLY FAVORS THE LOW ELEVATION ANGLES (MORE LOW
ELEVATION ANGLE OBSERVATIONS)
%   BECAUSE STK INSERTS A CLOSING OBSERVATION WHEN IT REACHES THE LOWER
CONSTRAINT.  IE
%   WHEN STK TRACKS A SATELLITE, IT GIVES READINGS EVERY 30 SECONDS + ONE WHEN
IT DISAPPEARS.  EVEN IF THE
%   FINAL OBSERVATION WAS ONLY 5 SECONDS FROM THE PREVIOUS ONE.  ADDITIONALLY,
WHEN IT STARTS THE OBSERVATION
%   PERIOD, THE TIME WILL BE A NON INTEGER EG 2456.343 SECS.  STK TAKES THE
NEXT OBSERVATION 30 SECONDS
%   FROM THE ROUNDED DOWN INTEGER VALUE.  SO THE DIFFERENCE BETWEEN THE FIRST
AND SECOND OBSERVATIONS COULD
%   BE BETWEEN 29 AND 30 SECONDS.

%  THE SECOND OUTPUT IS A DATA ON THE ELEVATION ANGLES WHEN ONLY 1 SATELLITE IS
VISIBLE,
%  BOTH AS A VECTOR AND A HISTOGRAM

%   This program takes a mat file located in the Matlab/bin directory called
%   '%d_data.mat' where the %d is the latitude of the ground station previously
%   input as Lat_gs.  The Time and Elevation angles are then stripped off into
a file called Elevs
%   The Program then finds lines with observations less than 20 seconds apart
and removes the observation..
%  Any observations of greater than or equal to ss/2 it rounds up to one
observation.
%  It then sorts the data then goes through it, isolating all the observations
in a time block of ss seconds.
```

```
%  It then determines the number of satellites visible during the observation,
and the best elevation angle.
%  You can take the file: "%d_all_Elev_angles_filtered.txt" and input it into
Perfect Fit to
%  determine the distribution of all elevation angles
%  You can then take the file: "%d_1sat_elev_angles.txt" and input it into
Perfect Fit to
%  determine the distribution of elevation angles when there is only one
satellite visible.
%  Filenames are: (%d is Lat and %e is FIlter Value)
%   %d_all_Elev_angles_filter_%e.txt      Column Vector of all filtered
elevation angles at that latitude
%   %d_Hist_Values_all_Elev_angles_filter_%e   1x19 Column Vector of Histogram
values
%   Hist_all_Elevs_to_%d_filter_%e.txt      nx19 col vector of Histogram values
%   %d_1sat_elev_angles.txt            Column vector of elev angles when 1
satellite is visible
%   %d_1sat_elev_angles_padded.txt      Same Column vector as above but when
more than 1 satellite is visible,
%   previous value is just rewritten as padding.
%   Corrects the time scale.
%
%
%   NOTE THAT THE FILE:    '%d_all_Elev_angles_filter_%e.txt' SHOULD REPLACE
ANY PREVIOUS
%   FILES SHOWING ALL ELEVATION ANGLES.

%   Place the following file into the c:\data\Matlab directory: "%d_data.mat"
clear all
Hist_data=zeros(1,19);
Hist_data_1sat=zeros(1,19);
cd c:\data\Filters\;
for Lat_gs=0:5:90  % provides auto loading of mat files
   ss=30;
   %Lat_gs=input('Enter Latitude of Facility-.....................');
   str1=num2str(Lat_gs);
   disp('calculating for next Latitude');
   Lat_gs
   Filter=20;  %    Use this line for automatic calculations
   %Filter=input('Enter the no of seconds For the cutoff Filter by:
.............');  % remove for autoloading
   str2=num2str(Filter);
   eval(sprintf('load %d_data.mat',Lat_gs));  % defines a matrix data with
   %   time, Az, El, Range, and all the propagation losses (8 cols) for all
observations
   Elevs=[sat_data(:,1),sat_data(:,9)];   %Time and all elevation angles
   n=size(Elevs,1);
   while n>1
      if abs(Elevs(n,1)-Elevs(n-1,1))<Filter    % this sets the minimum
difference between time observations as XX secs
         Elevs(n,:)=[];
      end
      n=n-1;
   end
   %  Save and plot as a histogram
   Elevs=Elevs(:,2);
   eval(sprintf('save %d_all_Elev_angles_filter_%e.txt Elevs -
ascii',Lat_gs,Filter));
   a=0:5:90;   %This sets a variable for later Histograms
   H=hist(Elevs,a);
   Temp=H/size(Elevs,1);
```

```
   eval(sprintf('save %d_Hist_Values_all_Elev_angles_filter_%e.txt Temp -
ascii',Lat_gs,Filter));
   %-------------------------------------------------------------------------
   %    Histogram of Elevation Angles whith filter applied
   %-------------------------------------------------------------------------
   figure
   bar(a,H/size(Elevs,1),'k');
   Hist_data=[Hist_data;H/size(Elevs,1)];   % gets data of variations in
elevation angles for comparison
   %   eval(sprintf('save Hist_all_Elevs_to_%d_filter_%e.txt Hist_data -
ascii',Lat_gs,Filter)); moved to end
   %   axis([0,90,0,max(H/size(Elevs,1))]);
   axis([0,90,0,.33]);
   xlabel('Elevation Angle - Degrees');
   ylabel('Proportion of All Observations (Probability)');
   out=['Histogram of All Elevation Angles (Latitude = ' str1 ' with ' str2 '
Second Filter)'];
   title(out)
   eval(sprintf('print -dmeta fig_%d_all_elevPDF_filtered', Lat_gs));
end
   %-------------------------------------------------------------------------
   % This next part of the program goes through each line of El_Best and El_All
and :
   %   1. rounds the data into multiples of 30 seconds
   %   2.   sorts the data by time
   %   3.   goes through and counts the observations at the same time
   %   4.   writes them to a seperate file
   %   NOTE that there are small(ish) problems associated with the rounding of
the
   %   data to the nearest 30 second timestamp.  You occasionally extend
observations
   %   inadvertantly so that there are occasional periods showing more
satelites visible than
   %   there really are.  This is not a large problem as we are only interested
in the distribution.
   ss=30;
   for Lat_gs=0:5:60
      str1=num2str(Lat_gs);
      clear data
      clear sat_data
      eval(sprintf('load %d_data.mat',Lat_gs));  % loads sat_data for the
latitude and
      %  defines a matrix data with
      %   time, Az, El, Range, and all the propagation losses (8 cols) for all
observations
      data(:,1)=sat_data(:,1);  %reads time as first column
      data(:,2:8)=sat_data(:,8:14);   %reads AER and losses as next 6 columns
      data(:,1)=round(data(:,1)/ss)*ss;
      data=sortrows(data,1);
      Sats0=[zeros(1,8)];
      Sats1=[zeros(1,8)];
      Sats1_padded=[zeros(1,8)];
      Sats2=[zeros(1,8)];
      Sats3=[zeros(1,8)];
      Sats4=[zeros(1,8)];
      Sats5=[zeros(1,8)];
      Sats6=[zeros(1,8)];
      Sats7=[zeros(1,8)];
      Sats8=[zeros(1,8)];
      Sats9=[zeros(1,8)];
      Time=0;
      while Time <= max(data(:,1))
```

```
         I=find(data(:,1)==Time);
         x=size(I,1);
         %eval(sprintf('s=size(Sats%d,1);',x))
         %eval(sprintf('Sats%d=[Sats%d;data(I,:)];',x,x))
         %  the next if statement pads out the sat
         if x==1
            Sats1_padded=[Sats1_padded;data(I,:)];
            Sats1=[Sats1;data(I,:)];
         end
         if x~=1
            Sats1_padded=[Sats1_padded;Sats1_padded(end,:)];
         end
         Time = Time + 30;
      end
      %   Following is a histogram of the elevation Angles
      %   when there is only one satellite visible.  Note it follows the
      %   general GAMMA like distribution of the best elevation angles.
      %  Save and Plot as usual
      %   Writing PDF of Elevation Angles when 1 Satellite is visible
      %   to a file X_1sat_elev_angles.txt where the Latitude of the ground
station is 'X'
      Sats1(1,:)=[];
      if size(Sats1,1)==0, break, end   % checks for no single satellite
periods, which is from about 60 deg up
      %  Removing the initial sample of zeros so it doesn't show up as
      %  a blip on the Histogram
      temp=Sats1(:,3);
      eval(sprintf('save %d_1sat_elev_angles.txt temp -ASCII;',Lat_gs))
      temp=Sats1_padded(:,3);
      eval(sprintf('save %d_1sat_elev_angles_padded.txt temp -ASCII;',Lat_gs))
      %-------------------------------------------------------------------------
-
      %    Histogram of Elevation Angles when one Satellite is Visible
      %-------------------------------------------------------------------------
-
      figure
      a=0:5:90;   %This sets a variable for later Histograms
      H=hist(Sats1(:,3),a);
      H(1,1)=0;   % zeroing the histogram of elevation angles <8.2 deg
      bar(a,H/size(Sats1,1),'k');
      %axis([0,90,0,max(H/size(Sats1,1))]);
      axis([0,90,0,.2]);
      xlabel('Elevation Angle - Degrees');
      ylabel('Proportion of samples');
      out=['Histogram of Elevation Angles When Only One Satellite is Visible
(Lat='str1 'deg)'];
      title(out)
      Hist_data_1sat=[Hist_data_1sat;H/size(Sats1,1)];
      eval(sprintf('print -dmeta fig_%d_1Sat_elevPDF', Lat_gs));
      %-------------------------------------------------------------------------
-
      % Plot of Elevation Angles when one Satellite is Visible
      %-------------------------------------------------------------------------
-
      %  Now plot the Single Satellite Elevation Angles against time to show
the
      %  goodness of the elevation angles, which mitigates the fact only one
satellite
      %  is visible.  Note the X Axis is not correct time as observations have
been removed
      figure
      plot(Sats1(:,3),'k')
```

```
      xlabel('Sample Number - (Not Linear Time Scale as Mult-Sat Observations
Removed)');
      ylabel('Elevation Angles (Degrees)');
      out=['Plot of Elevation Angles When Only One Satellite is Visible
(Lat='str1 ')'];
      eval(sprintf('print -dmeta fig_%d_1Sat_elevs_NOT_TIME', Lat_gs));
      title(out)
      %-------------------------------------------------------------------------
-
      %    Padded Time Plot of Elevation Angles when one Satellite is Visible
      %-------------------------------------------------------------------------
-
      %  The next figure is the plot of Elevation Angles for Single Satellite
Visibility
      %  With padded values when there were more than one satellite visible.
      %  THis shows where the periods of multiple satellite visibility occur.
      figure
      a=0:1:size(Sats1_padded,1)-1;
      a=a/2;
      plot(a,Sats1_padded(:,3),'k')
      xlabel('Time in Minutes');
      ylabel('Elevation Angles (Degrees)');
      out=['Plot of Elevation Angles When Only One Satellite is Visible
(Lat='str1 ')'];
      title(out)
      eval(sprintf('print -dmeta fig_%d_1Sat_padded_elev_time', Lat_gs));
   end
   eval(sprintf('save Hist_all_Elevs_to_%d_filter_%e.txt Hist_data -
ascii',Lat_gs,Filter));
   eval(sprintf('save Hist_1Sat_Elevs_to_%d_filter_%e.txt Hist_data_1sat -
ascii',Lat_gs,Filter));
```

Program: MINMEDHIST.m

```
   %  The purpose of this code is to load all satellite data into memory and
%  plot the histograms , median values and minima.  THis is being used as
%  a means of determining if Siziak's comments are correct regarding PDF's
CDF'd etc
clear all
med=[0 0];
mini=[0 0];
Mean=[0 0];
AvMed=[0 0 0 0];
t=0;
ss=30;
Filter=20;
for Lat_gs=80:5:90
   t=t+1
   str=num2str(Lat_gs)
   eval(sprintf('load %d_data',Lat_gs))
   if Lat_gs==30   %   puts the last row of 30 deg lat due to zeros there
      sat_data(end,:)=[];
   end

   Elevs=[sat_data(:,1),sat_data(:,9)];   %Time and all elevation angles
   n=size(Elevs,1);
   while n>1
      if abs(Elevs(n,1)-Elevs(n-1,1)) < Filter    % this sets the minimum
difference between time observations as XX secs
         Elevs(n,:)=[];
      end
```

```
      n=n-1;
   end
   %  Save and plot as a histogram
   Elevs=Elevs(:,2);

   %   N=hist(sat_data(:,9));  % note there's a zero in the 30 degree data
   N=hist(Elevs);  % Filtered elevation Angles
   %bar(N);
   out=[str ' Degrees Latitude']
   %title(out)
   med(t,1)=Lat_gs;
   mini(t,1)=Lat_gs;
   Mean(t,1)=Lat_gs;
   %   med(t,2)=median(sat_data(:,9));
   %   Mean(t,2)=mean(sat_data(:,9));
   %   temp=sat_data(:,9);
   %   mini(t,2)=min(temp);
   med(t,2)=median(Elevs);% Filtered elevation Angles
   Mean(t,2)=mean(Elevs);% Filtered elevation Angles
   mini(t,2)=min(Elevs);% Filtered elevation Angles
   %--------------------------------
   data(:,1)=sat_data(:,1);  %reads time as first column
   data(:,2:8)=sat_data(:,8:14);   %reads AER and losses as next 6 columns
   temp=size(data);
   i=temp(:,1);
   Test = data(:,1);
   Test=sortrows(Test,1);
   for X=1:i-1
      if Test(X+1,1)-Test(X,1)>ss
         disp('ERROR IN DATA OR COVERAGE GAP! TWO SAMPLES MORE THAN SS SECONDS
APART AT THE FOLLOWING TIME:');
         X*ss
         %No_Sats(:)=[X*ss]
      end
   end
   clear test
   x=1;
   for n=1:i-1
      if abs(data(n,1)-data(n+1,1))>ss
         transitions(2,x)=[data(n,1)];% a stop value
         transitions(1,x+1)=[data(n+1,1)];% a start value
         x=x+1;
      end
   end
   clear n
   %  these next lines write the final start and stop transitions
   transitions(1,1)=[data(1,1)];
   transitions(2,end)=[data(end,1)];
   %  setting the difference between transitions is the sat access times
   transitions(3,:)=abs(transitions(1,:)-transitions(2,:));
   figure
   temp=transitions(3,:);
   hist(temp)
   out=['Transition Period for ' str ' degrees latitude'];
   title(out);
   AvMed=[AvMed; Lat_gs mean(transitions(3,:)) median(transitions(3,:))
size(transitions,2)]
   clear sat_data;
   clear data;
   clear transitions;
   clear x
   clear test
```

```
   clear X
   clear temp
end
figure
plot(med(:,1),med(:,2))
title('Median Elevation Angle vs Latitude for All Elevs');
figure
plot(Mean(:,1),Mean(:,2))
title('Mean Elevation Angle vs Latitude for All Elevs');

figure
plot(AvMed(:,1), AvMed(:,2))
title('Average Observation Duration in Seconds');
figure
plot(AvMed(:,1), AvMed(:,3))
title('Median Observation Duration in Seconds');

figure
plot(AvMed(:,1), AvMed(:,4))
title('No of satellites Tracked During observation Period');
AvMed(1,:)=[];
Trans_avmed=[AvMed Mean(:,2) med(:,2)]
% Trans_avmed:- [file Latitude, Mean Obs time, Median Observation Time, nO OF
OBSERVATIONS Mean Elev Angle, Median Elev Angle]
cd c:\data
save Observations_and_elev_stats.txt Trans_avmed -ascii
```

Program: WBMOD_prep.m

```
clear all
%   This program produces the input file for WBMOD by processing a data file to
%   find the best path, then turning that path matrix into a wbmod_input file
by doing
%   coordinate transfromations. This program takes a matrix, which must be in a
space delimited
%   file called '%d_data.csv' in the MATLAB path,    with structure as follows:
%   Column1   time(s)
%   Column2   X Position  (kms
%   Column3  Y Position (kms)
%   Column4   Z Position (kms)
%   Column5   Vx Realtive (m/s)
%   Column6   Vy Realtive (m/s)  (gaseous atten @7.5 g/m^2 water vapor)
%   Column7   Vz Realtive (m/s)
%   Column8    azimuth(deg)
%   Column9   elevation(deg)
%   Column10   range(kms)
%   Column11   Free Space Path Loss (dB)
%   Column12   Atmospheric (gaseous atten @7.5 g/m^2 water vapor)
%   Column13   Rain Loss (CCIR) at 0.01 exceedence
%   Column14   total Attenuation
%   The value of the time step is assigned as the variable 'ss'.
%   The Program finds lines with observations of less than half ss and deletes
them.
%  Any observations of greater than or equal to ss/2 it rounds up to one
observation.
%  It then sorts the data then goes through it, isolating all the observations
in a time block of ss seconds.
%  It then determines the number of satellites visible during the observation,
and the best elevation angle.
%
%  The program gets the max elevation angle and the min range and writes it to
an output file with the time stamp.
```

```
%
ss=30; %auto input
%   ss=input('Enter Time Step of observation-          ');
%step size (ss) is the no of seconds between STK samples
Lat_gs=input('Enter Latitude of Facility-              ');
Str1=num2str(Lat_gs);
Lon_gs=135;     %  for auto-input
%Lon_gs=input('Enter Longitude of Facility-               ');
disp('    Loading data matrix data.csv generated from STK.  This matrix has
time, AER & link budget data');
eval(sprintf('load %d_data.mat',Lat_gs));  % defines a matrix data with
data(:,1)=sat_data(:,1);  %reads time as first column
data(:,2:8)=sat_data(:,8:14);   %reads AER and losses as next 6 columns
%   Writes the 8 column data matrix which contains AER and Prop Loss data.

%%%%%%%%%%%%%%%%%%%%%%%%%%%%%%%%%%%%%%%%%%%%%%%%%%%%
%  DETERMINATION OF BEST ELEVATION ANGLE
%
%  Remember the format:-  data=(Time, azimuth, elevation, range, Free Space
Path Loss,
%                 Atmospheric Attenuation, Rain Loss and Total Attenuation).
%   8 Columns with length dependent on the total observation time
%
i=size(sat_data,1);  % changed from data
%  data is copied to a working matrix
data1=sat_data;
%  data1=[sat_data(:,1) sat_data(:,8:14)];
%  this routine adds another column to the end of the data (new 9th column)
which is the time rounded to the nearest minute.
%  It captures all times within +/-(ss/2) eg +/-30 secs for a 60 second sample
time
for n=1:i
   data1(n,15)=round(data1(n,1)/ss);   %data1 includes all sat data incl rel
posn and velocities
end
%  rows are sorted on the new column and assigned to 'data1'
data1=sortrows(data1,15);
% This section generates a AER_details matrix with elements as follows
%first element:   Time block
%second element:  Azimuth angle corresponding to best elev angle
%third element:   Best elevation angle
%fourth element:  Range corresponding to best elev angle
%fifth to 8th elements:   Best free space Path loss, CCIR rain Loss, gaseous
loss at 7.5% water vapor content
%  total loss  etc
% It also generates a WBMOD_details matrix with all the elements required to
feed the
%  coordinate transformation subroutine at the end, and generate the WBMOD
input file.
n=1;
BlockNo=1;
while n<i
   x=n;
   while data1(n,15)==data1(n+1,15)
      n=n+1;
      if n==i-1, break, end
   end
   temp_block=data1(x:n,:); % writes the lines of sat_data which are the same
time
   temp_block=flipud(sortrows(temp_block,9)); %sorts the rows in ascending
order of elevation angle then flips the matrix
```

```
   %  this way the rows are in DESCENDING order of column 9 ie elevation.  The
first row is the one with the
   %  best path to the satellite for that block of time
   aer_details(BlockNo,:)=[temp_block(1,15)*ss temp_block(1,8:14)]; %
   wbmod_details(BlockNo,:)=[temp_block(1,15)*ss temp_block(1,2:14)];
   BlockNo=BlockNo+1;
   n=n+1;
   if n==i-1, break, end
end

%%%%%%%%%%%%%%%%%%%%%%%%%%%%%%%%%%
%
%
%   TRANSFORMATION OF COORDINATE SYSTEMS IN PREPARATION
%   FOR PASSING DATA TO WBMOD MODEL TO WORK OUT HT E
%   EFFECT OF IONOSPHERIC SCINTILLATION
%
%
% input LLA of ground station
%   Lat_gs=input('Input Latitude of Ground Station');
%Lat_gs=0.0; %in degrees
Lat=Lat_gs
Lat_gs=Lat_gs/180*pi;
%Lon_gs=135;
Lon_gs=Lon_gs/180*pi;
xyz_sat=wbmod_details(:,2:4);   %  xyz_sat=sat_data(:,2:4);
xyzvel_sat=wbmod_details(:,5:7);   %  xyzvel_sat=sat_data(:,5:7);

%  wbmod_ecef=sat_data(:,1:7);
%  eval(sprintf('save %d_wbmod_ecef.txt wbmod_ecef -ascii',Lat));     % writes
the WBMOD data ready for the transformations
%   make sure xyz_sat is set as the XYZ coords from STK output of sat
%   relative coords in local reference frame fixed to center of the earth,
%   rotating with x at Greenwich and z directed to the North Pole
%    Also make sure the local velocity comoponents of the satellite in the same
%   reference frame are input as 'xyzvel_local'in m/s
% NOW WORKING OUT THE LLA OF THE SATELLITE (Lat_sat, Lon_sat, Alt_sat)

% 1st step:  Work out coords of the ground station 'xyz_gs'
ro=6378.137;
re=6378.137;
e=.00335281066747;
x_gs=ro*cos(Lat_gs)*cos(Lon_gs);
y_gs=ro*cos(Lat_gs)*sin(Lon_gs);
z_gs=ro*sin(Lat_gs);
%xyz_gs=[x_gs y_gs z_gs];
%    2nd Step:  Translate the satellite coords to the centre of the earth
xyz_sat_ecef=[xyz_sat(:,1)+x_gs xyz_sat(:,2)+y_gs xyz_sat(:,3)+z_gs];
%   3rd step:   Calculate Lat Long and Alt for the satellite
Lat_sat_ecef=atan2(xyz_sat_ecef(:,3),sqrt(xyz_sat_ecef(:,1).^2+xyz_sat_ecef(:,2
).^2));
Lon_sat_ecef=atan2(xyz_sat_ecef(:,2),xyz_sat_ecef(:,1));%*180/pi
Alt_sat_ecef=sqrt(xyz_sat_ecef(:,1).^2+xyz_sat_ecef(:,2).^2+xyz_sat_ecef(:,3).^
2)-ro;

%  NOW WORKING OUT THE VELOCITY COMPONENTS OF THE SATELLITE IN M/S IN ROTATING
EARTH COORD
%   FRAME (IN A COORD FRAME FIXED WRT EARTH)WITH ORIGIN ON THE SATELLITE AND +X
IN THE NORTH DIRECTION,
%   Y IN EAST, AND +Z IN NADIR (I.E. DOWN) DIRECTIONS

%   step 1:   calculate transformation matrix that rotates first around
```

```
%    the z axis, then around the y axis
temp=size(xyzvel_sat);
n=temp(1,1);
for i=1:n
   xyzvel_sat_ecef(:,i)=[cos(Lat_sat_ecef(i)) 0 sin(Lat_sat_ecef(i));0 1 0;-
sin(Lat_sat_ecef(i)) 0 cos(Lat_sat_ecef(i))]*[[cos(Lon_sat_ecef(i))
sin(Lon_sat_ecef(i)) 0;-sin(Lon_sat_ecef(i)) cos(Lon_sat_ecef(i)) 0;0 0
1]*xyzvel_sat(i,:)'];
end

xyzvel_sat_ecef=xyzvel_sat_ecef';   % remember that the down direction is in
the wrong direction and
xyzvel_sat_ecef(:,1)=-xyzvel_sat_ecef(:,1);   %give velocity as Vdown, Veast
Vnorth, need to put it in the right order
%   ie Velocity North, Velocity East and Velocity Down.
% you now have the velocity of the satellite in m/s in a Nx3 matrix
%   Need to combine this with time and satellite LLA to get WBMOD FILE matrix
wbmod_data(:,1)=[wbmod_details(:,1)];
wbmod_data(:,2:4)=[Lat_sat_ecef/pi*180 Lon_sat_ecef/pi*180 Alt_sat_ecef];  %
Note it's in radians and WBMOD requires it in degrees
wbmod_data(:,5:7)=[xyzvel_sat_ecef(:,3) xyzvel_sat_ecef(:,2)
xyzvel_sat_ecef(:,1)];
eval(sprintf('save %d_wbmod_input.txt wbmod_data -ascii',Lat));
```

Program: SCINT_ANALYSIS.m

```
%  THIS PROGRAM PRODUCES FIGURES AND FILES OF SCINTILLATION ACTIVITY
%  FOR 3 SCENARIOS.  FIGURES ARE WRITTEN AS WINDOWS METAFILES.  If you
%  want figures to show up just remove the '%' from the "figure" commands
clear all;
scint_output=load('scint_output.txt');
%   scint_output has a structure as follows
%   Col 1:    Time in seconds from midnight GMT
%   col 2:   Time in Hours local
%   Col 3:   0 Deg best elevation Free Space Path Loss
%   Col 4:   0 Deg best elevation Gaseous Attenuation
%   Col 5:   0 Deg best elevation Scintillation Fades for this path at SSN=160
and doy 80
%   Col 6:   5 Deg best elevation Free Space Path Loss
%   Col 7:   5 Deg best elevation Gaseous Attenuation
%   col 8:   5 Deg fades at SSN=160 and doy 80
%   Col 9:   10 Deg best elevation Free Space Path Loss
%   Col 10:   10 Deg best elevation Gaseous Attenuation
%   col 11:   10 Deg fades at SSN=160 and doy 80
%   Col 12:   15 Deg best elevation Free Space Path Loss
%   Col 13:   15 Deg best elevation Gaseous Attenuation
%   col 14:   15 Deg fades at SSN=160 and doy 80
%   Col 15:   20 Deg best elevation Free Space Path Loss
%   Col 16:   20 Deg best elevation Gaseous Attenuation
%   col 17:   20 Deg fades at SSN=160 and doy 80
%   Col 18:   25 Deg best elevation Free Space Path Loss
%   Col 19:   25 Deg best elevation Gaseous Attenuation
%   col 20:   25 Deg fades at SSN=160 and doy 80
%   Col 21:   30 Deg best elevation Free Space Path Loss
%   Col 22:   30 Deg best elevation Gaseous Attenuation
%   col 23:   30 Deg fades at SSN=160 and doy 80
%   Col 24:   35 Deg best elevation Free Space Path Loss
%   Col 25:   35 Deg best elevation Gaseous Attenuation
%   col 26:   35 Deg fades at SSN=160 and doy 80
%   Col 27:   40 Deg best elevation Free Space Path Loss
%   Col 28:   40 Deg best elevation Gaseous Attenuation
```

```
%   col 29:   40 Deg fades at SSN=160 and doy 80
%   Col 30:   45 Deg best elevation Free Space Path Loss
%   Col 31:   45 Deg best elevation Gaseous Attenuation
%   col 32:   45 Deg fades at SSN=160 and doy 80
%   Col 33:   0 Deg best elevation Scintillation Fades for SSN=160 and doy 180
%   col 34:   5 Deg fades at SSN=80 and doy 180
%   col 35:   10 Deg fades at SSN=80 and doy 180
%   col 36:   15 Deg fades at SSN=80 and doy 180
%   col 37:   20 Deg fades at SSN=80 and doy 180
%   col 38:   25 Deg fades at SSN=80 and doy 180
%   col 39:   30 Deg fades at SSN=80 and doy 180
%   col 40:   35 Deg fades at SSN=80 and doy 180
%   col 41:   40 Deg fades at SSN=80 and doy 180
%   col 42:   45 Deg fades at SSN=80 and doy 180
%   Col 43:   0 Deg best elevation Scintillation Fades for this path at SSN=80
and doy 80
%   col 44:   5 Deg fades at SSN=80 and doy 80
%   col 45:   10 Deg fades at SSN=80 and doy 80
%   col 46:   15 Deg fades at SSN=80 and doy 80
%   col 47:   20 Deg fades at SSN=80 and doy 80
%   col 48:   25 Deg fades at SSN=80 and doy 80
%   col 49:   30 Deg fades at SSN=80 and doy 80
%   col 50:   35 Deg fades at SSN=80 and doy 80
%   col 51:   40 Deg fades at SSN=80 and doy 80
%   col 52:   45 Deg fades at SSN=80 and doy 80
%   Create a Contour of effects using 15 minute window average
scint_output1(:,1:2)=[scint_output(:,1:2)];
for i=1:10
   scint_output1(:,i+2)=[sum(scint_output(:,(i*3):(i*3+2)),2)];
end
scint_output2(:,1:2)=[scint_output(:,1:2)];
for i=1:10

scint_output2(:,i+2)=[sum(scint_output(:,(i*3):(i*3+1)),2)+scint_output(:,(i+32
))];
end
scint_output3(:,1:2)=[scint_output(:,1:2)];
for i=1:10

scint_output3(:,i+2)=[sum(scint_output(:,(i*3):(i*3+1)),2)+scint_output(:,(i+42
))];
end
m=size(scint_output1,1);    % No of Rows
n=size(scint_output1,2);    % No of Columns
m=floor(m/30)    % no of 15 minute intervals (rounded down)
scint_output11(:,1)=[15*(1:1:m)]';
scint_output11(:,2)=scint_output11(:,1)/60+9;
for Lat=3:12
   for time=1:m   % latitudes 0-45 deg
      scint_output11(time,Lat)=[mean(scint_output1((30*time-
29):(30*time),Lat))];
   end
end

scint_output21(:,1)=[15*(1:1:m)]';
scint_output21(:,2)=scint_output21(:,1)/60+9;
for Lat=3:12
   for time=1:m    % latitudes 0-45 deg
      scint_output21(time,Lat)=[mean(scint_output2((30*time-
29):(30*time),Lat))];
   end
end
```

```
scint_output31(:,1)=[15*(1:1:m)]';
scint_output31(:,2)=scint_output21(:,1)/60+9;
for Lat=3:12
   for time=1:m    % latitudes 0-45 deg
      scint_output31(time,Lat)=[mean(scint_output3((30*time-
29):(30*time),Lat))];
   end
end
%    This part produces a range of plots for an appendix of scintillation
effects
%_____________________________________________________________________
%
%   Scintillation Time Plots for each Latitude for Scenario 1 - SSN=160/DOY=80
%_____________________________________________________________________
_
%
cd c:\data\scint_plots\
for Lat_gs=1:10
   Str1=num2str(Lat_gs*5-5);
   temp1=[scint_output(:,2) scint_output(:,(Lat_gs*3+2))]; % Scintillation fade
only
   temp1=sortrows(temp1,1);
%   figure;
   plot(temp1(:,1), temp1(:,2),'k');
   xlabel('Local Time (Hours)');
   ylabel('Attenuation (dB)');
   out=[' Worst Case Scintillation Fade (Sunspot No=160; DOY=80) at ' Str1 '
deg Latitude'];
   axis([0,24,-14, 0]);
   title(out);
   set(gca,'xtick',[(0:2:24)]);
   text(2,-12,'Iridium');
   eval(sprintf('print -dmeta fig_%d_scint#1', Lat_gs*5-5));

   temp=[scint_output1(:,2) scint_output1(:,2+Lat_gs)];
   temp=sortrows(temp,1);
%   figure
   plot(temp(:,1), temp(:,2),'k');
   xlabel('Local Time (Hours)');
   ylabel('Attenuation (dB)');
   out=['Total Fade (Worst Case: Sunspot No=160; DOY=80) at ' Str1 ' deg
Latitude'];
   title(out);
   axis([0,24,-178, -153]);
   set(gca,'xtick',[(0:2:24)]);
   text(2,-175,'Iridium');
   eval(sprintf('print -dmeta fig_%d_scint_total#1', Lat_gs*5-5));
end

disp('Do you wish to continue with the next set of figures (Scenario 2)??');
pause(3)
%_____________________________________________________________________
%
%   Scintillation Time Plots for each Latitude for Scenario 2 - SSN=160/DOY=180
%_____________________________________________________________________
for Lat_gs=1:10
   Str1=num2str(Lat_gs*5-5);
   temp1=[scint_output(:,2) scint_output(:,(Lat_gs+32))]; % Scintillation fade
only
   temp1=sortrows(temp1,1);
%   figure;
   plot(temp1(:,1), temp1(:,2),'k');
```

```
   xlabel('Local Time (Hours)');
   ylabel('Attenuation (dB)');
   out=['Scintillation Fade (Moderate Case: Sunspot No=160; DOY=180) at ' Str1
' deg Latitude'];
   axis([0,24,-14, 0]);
   title(out);
   set(gca,'xtick',[(0:2:24)]);
   text(2,-12,'Iridium');
   eval(sprintf('print -dmeta fig_%d_scint#2', Lat_gs*5-5));

   temp=[scint_output2(:,2) scint_output2(:,2+Lat_gs)];
   temp=sortrows(temp,1);
%   figure
   plot(temp(:,1), temp(:,2),'k');
   xlabel('Local Time (Hours)');
   ylabel('Attenuation (dB)');
   out=['Total Fade (Moderate Case: Sunspot No=160; DOY=180) at ' Str1 ' deg
Latitude'];
   title(out);
   axis([0,24,-178, -153]);
   set(gca,'xtick',[(0:2:24)]);
   text(2,-175,'Iridium');
   eval(sprintf('print -dmeta fig_%d_scint_total#2', Lat_gs*5-5));
end
disp('Do you wish to continue with the next set of figures (Scenario 3)??');
pause(3)
%_____________________________________________________________________
_
%
%   Scintillation Time Plots for each Latitude for Scenario 3 - SSN=80/DOY=80
%_____________________________________________________________________
for Lat_gs=1:10
   Str1=num2str(Lat_gs*5-5);
   temp1=[scint_output(:,2) scint_output(:,(Lat_gs+42))]; % Scintillation fade
only
   temp1=sortrows(temp1,1);
%   figure;
   plot(temp1(:,1), temp1(:,2),'k');
   xlabel('Local Time (Hours)');
   ylabel('Attenuation (dB)');
   out=['Scintillation Fade (Moderate: Sunspot No=80; DOY=80) at ' Str1 ' deg
Latitude'];
   axis([0,24,-14, 0]);
   title(out);
   set(gca,'xtick',[(0:2:24)]);
   text(2,-12,'Iridium');
   eval(sprintf('print -dmeta fig_%d_scint#3', Lat_gs*5-5));
   temp=[scint_output3(:,2) scint_output3(:,2+Lat_gs)];
   temp=sortrows(temp,1);
%   figure
   plot(temp(:,1), temp(:,2),'k');
   xlabel('Local Time (Hours)');
   ylabel('Attenuation (dB)');
   out=['Total Fade (Moderate Case: Sunspot No=80; DOY=80) at ' Str1 ' deg
Latitude'];
   title(out);
   axis([0,24,-178, -153]);
   set(gca,'xtick',[(0:2:24)]);
   text(2,-175,'Iridium');
   eval(sprintf('print -dmeta fig_%d_scint_total#3', Lat_gs*5-5));
end
```

BIBLIOGRAPHY

[Akt95] Akturan, R., Vogel, W. J., "Elevation Angle Dependence of Fading for Satellite PCS in Urban Areas" , Electronics Letters, 6 July 1995, Vol 31 No. 14.

[Akt97] Akturan, R., Vogel, W. J., "Path Diversity for LEO Satellite-PCS in the Urban Environment", IEEE transactions on Antennas and Propagation, July 1997, Vol 45 No.7.

[All73] Allen, C.W.: 1973, Astrophysical Quantities, Athlone Press, London.

[All89] Allnutt, J. E., Satellite to Ground Radiowave Propagation – Theory, Practice and System Impact at Frequencies Above 1GHz, IEE Electromagnetic Waves Series 29, 1989.

[Ani98] Kantak, Anil V., Arqkasa, Krisjani, Rucker, James, "A Database for Propagation Models and Conversion to C++ Programming Language.", Undated Paper. Accompanying Software Version 4.1, July 1998.

[Bar39] Bartels, J., N. H. Heck, and H. F. Johnston, "The three-hour-range Index Measuring Geomagnetic Activity, Journal of Geophysics, Res., 44, 411-, 1939.

[Bat71] Bate, Roger, E., Mueller, Donald D.,White, Jerry, E. Fundamentals of Astrodynamics, Dover Publications Inc., 1971.

[Bru96] Brunt, P., "IRIDIUM® - Overview and Status," Space Communications, Vol. 14, No. 2, 1996, pp. 61-68.

[But95] Butt, G., Evans, B.G., Parks, M., "Modelling (sic) the Mobile Satellite Channel for Communication Systems Design", IEE Antennas and Propagation, 1995; ISSUE 407/2, pp. 2,387-2,394.

[CCI78] CCIR, Report 263-4, "Ionospheric Effects Upon Earth-space Propagation," Volume VI, Propagation in Ionized Media, Recommendations and Reports of the CCIR, 1978, pp. 7 1 89, International Telecommunications Union, Geneva, 1978.

[Cio96] Ciocco, Timothy M., "A comparison Study of CDMA Versus TDMA/FDMA LEO Satellite Systems", March 1996, Thesis DTIC Reference ADA307158.

[Com93] Comparetto, Gary M., "A Technical Comparison of Several Global Mobile Satellite Communications Systems," Space Communications, Vol. 11, No. 2, 1993, pp. 97-104.

[Dol93] Dolan, Alan and Aldous, Joan, Networks and Algorithms, an Introductory Approach, John Wiley & Sons, New York, 1993, pp. 126-140.

[Exp98] Expert Fit Version 1.5, 1998, Averill M. Law and Associates, PO Box 40996, Tucson, AZ 85717.

[Flo87] Flock, Warren L., Propagation Effects on Satellite Systems at Frequencies below 10GHz, NASA Reference Publication 1108(02) 2nd Ed, 1987.

[FoR98] Fossa, Carl E., Raines, Richard A., Gunsch, Gregg H., and Temple, Michael A., "An Overview of the IRIDIUM® Low Earth Orbit Satellite System," IEEE National Aerospace and Electronics Conference, 1998.

[FoR98-2] Fossa, Carl E., Raines, Richard A., Gunsch, Gregg H., and Temple, Michael A., "A Performance Analysis of the IRIDIUM® Low Earth Orbit Satellite System with a Degraded Satellite Constellation," ACM Mobile Computing and Communications Review, 1998.

[Gaf95] Gaffney, Leah M. et al., "Non-GEO Mobile Satellite Systems: A risk assessment", 4th International Mobile Satellite Conference 1995, Ottawa, Canada, June 6-8, 1995, pp A-23 - A-27.

[Glo98] Globalstar LP, "Globalstar Home Page", http://www.globalstar.com/, 20 October 1998.

[Glo98-2] Globalstar Press Release, "Statement regarding the Broadcast of the Failed Zenit 2 Globalstar Launch", September 23, 1998, Florida Today Space Online, http://www.flatoday.com/space/explore/stories/1998b/092398g.htm.

[Gol92] Goldhirsh, Julius, Vogel, Wolfhard, Propagation Effects for Land Mobile Satellite Systems: Overview of Experimental and Modeling Results, Nasa Reference Publication 1274, February 1992.

[Hut95] Hutcheson, Jonathan, Laurin, Marla "Network Flexibility of the Iridium Global Mobile Satellite System", 4th International Mobile Satellite Conference 1995, Ottawa, Canada, June 6-8, 1995, pp 503-507.

[IEE77] IEEE Standard Definitions of Terms for Radio Wave Propagation, IEEE Std. 211-1977, New York, August 19, 1977.

[Ipp84] Ippolito, Louis J. Jr., "Rain Attenuation Prediction for Communications Satellite Systems", AIAA, 10th Communications satellite systems conference, 1984, pp 319-326.

[Ipp86] Ippolito, Louis J. Jr., Radiowave Propagation in Satellite Communications, Van Nostrand Reinhold Company, 1986.

[ITU118] International Telecommunication Union (ITU) "Recommendation ITU-R M.1188 - Impact of Propagation on the Design of Non-GSO Mobile-Satellite Systems Not Employing Satellite Diversity Which Provide Service To Handheld Equipment", October 1995 – M Series, Part 5.

[ITU531] ITU "Recommendation ITU-R P.531-4. Ionospheric Propagation Data and Prediction Methods Required for the Design of Satellite Services and Systems", May 1997 – P Series – Part 2.

[ITU618] ITU "Recommendation P.618-5 Propagation data and prediction methods required for the design of Earth-space telecommunication systems", 1997 – P Series – Part 2.

[ITU676] ITU "Recommendation ITU-P-676.3 - Attenuation by Atmospheric Gases" P.676-3, August 1997 – P Series – Part 1.

[ITU678] ITU "Recommendation ITU-R P.678, Characterization of the Natural Variability Of Propagation Phenomena", Mar 1992 – P Series – Part 1.

[ITU834] ITU "Recommendation P.834-2 Effects of Tropospheric Refraction on Radiowave Propagation", August 1997 – P Series – Part 1.

[ITU836] ITU "Recommendation P.836-1 Water Vapour: Surface Density And Total Columnar Content", August, 1997, P Series – Part 1.

[ITU837] ITU "Recommendation P.837-1 (11/93) Characteristics of Precipitation For Propagation Modelling", 1997 – P Series – Part 1.

[ITU90] ITU, "Propagation in Non-Ionized Media", Reports of the CCIR 1990, Annex to Volume V, Geneva, 1990, Rep. 564-4 pp.465-467.

[JMP97] SAS-JMP Version 3.4.3, 1997, SAS Institute Inc. SAS Campus Drive, Cary, NC 27513-2414.

[Joh98] Johnson, T. J., Analytical Graphics Incorporated, Personal Email dated September 17th 1998 on Subject of Rain Loss Computation in STK 4.0.5.

[Jos97] Joselyn, J.A., et al., "Panel Achieves Consensus Prediction of Solar Cycle 23", EOS, Trans. Amer. Geophys. Union, 78, pages 205, 211-212, 1997.

[Jos97-2] Joselyn, J.A., "Summary Report of the Second Meeting of the Solar Cycle Prediction Panel", (Revised October 2, 1997), Internal Correspondence of National Solar Observatory/Sacramento Peak, Sunspot, New Mexico, September 8, 1997.

[Jur85] Jursa A. S., Handbook of Geophysics and The Space Environment, Air Force Geophysics Laboratory, USAF, 1985.

[Kar87] Karasawa, Y, Yasunaga M, Yamada, M., Arbesser-Rastburg, B., "An Improved Prediction Method for Rain Attenuation in Satellite Links Operating at 10-20 GHz"; Radio Science, 1987, 22, pp 1053-1062.

[Kar97 Karasawa, Y., Kimura, K., Minamisono, K., "Analysis of Availability Improvementin LMSS by means of Satellite Diversity Based on Three State Propagation Channel Model", IEEE Trans. Veh. Tech., November 1997, Vol 46, No 4.

[Kel97] Keller, Harald, Salzwadel, Horst et al, "Comparison of the Probability of Visibility of the Most Important Currently Projected Mobile Satellite Systems", IEEE Vehicular Technology Conference, 1997; Vol 47; No 1.

[Lar92] Larson, W. J., Wertz, J. R., Space Mission Analysis and Design, 2nd Ed, Space Technology Library, 1992.

[Law91] Law, A.M., W. D. Kelton, Simulation Modeling and Analysis, 2nd Ed, Mc Graw-Hill, New York, 1991.

[Mac84] Macchiararella G., "Assesment of Various Models For The Predictions Of The Outage Time Of Earth Space Links Due To Excess Rain Attenuation", AIAA, 10th Communcations Satellite Systems Conference, 1984, pp 332-335.

[Mai95] Maine, K., Devieux, C., Swan, P., "Overview of Iridium Satellite Network", WESCON/95, pp. 483-90, 1995.

[MAT98] MATLAB version 5.2.1.1420, 1998, The MathWorks, Inc., 24 Prime Park Way, Natick, MA 01760-1500.

[McL97] Australia's Strategic Policy Commonwealth of Australia 1997, released by the Rt Hon Ian McLachlan Minister for Defence, December 1997.

[NDA76] NDAA, "U.S. Standard Atmosphere", 1976, NDAA-S/T 76-1562, U.S. Government Printing Office, Washington, D.C., October 1976.

[NOA99] NOAA, "Monthly Smoothed Sunspot Numbers" NOAA Official FTP site, http://www.ngdc.noaa.gov/stp/stp.html, Jan 8, 1999.

[Oga80] Ogawa, T., Sinno, K., 1980, "Severe Disturbances of VHF and GHz Waves from Geostationary Satellites during a Magnetic Storm", Journal of Atmospheric and Terrestrial Physics, 42, pp 637-644.

[Ram97] Rama, V. S., Jayachandran, P. T., Sri Ram P., "Ionospheric irregularities: The role of the Equatorial Ionization Anomaly", Radio Science, Vol 32, No 4, Pages 1551-1557, July-August 1997.

[Rin79] Rino C.L., 1979, "A power law phase screen model for ionospheric scintillation 1. Weak scatter", Radio Science, 14, pp 1135-1145.

[Rob98] Australian Department of Defence Ministerial DEFGRAM No 4/98 released 6 July 1998 by C.M. Robinson, Director, Ministerial and Parliamentary Liaison Services.

[SAT20] BONeS SatLab Version 2.0.2, Cadence Design Systems, Inc., 555 River Oaks Parkway San Jose, California 95134.

[Sec95] Secan, J. A., Bussey, R. M., Fremouw E. (Northwest Research Associates, Incorporated, Bellevue, Washington) & S. Basu (Phillips Laboratory, Hanscom Air Force Base, Massachusetts), "An Improved Model of Equatorial Scintillation", Radio Science, Volume 30, Number 3, Pages 607-617, May-June 1995.

[Sec96] Secan J.A., "WBMOD Ionospheric Scintillation Model – An Abbreviated Users Guide Version 13", USAF Phillips Laboratory, Sep 24, 1996.

[Sec97] Secan, J. A. et al., "High-latitude upgrade to the Wideband Ionospheric Scintillation Model", Radio Science, Volume 32, Number 4, Pages 1567-1574, July-August 1997.

[Sec98] Secan J.A., North West Research Associates, Inc, Electronic Mail dated October 23, 1998.

[Siw95] Siwiak Kazimierz, Radiowave Propagation And Antennas For Personal Communications, 2nd Ed, April 1998, Artech House.

[Slo82] Slobin, S. D., "Microwave Noise Temperature and Attenuation of clouds: Statistics of These Effects in the United States, Alaska and Hawaii", Radio Science, Vol 17, No 6, pp 1443-1454, Nov – Dec, 1982.

[Ste96] Stelianos, Haralambos, "The use of Commercial Low Earth Orbit Satellite systems to Support DOD Communications", Dec 1996, Thesis DTIC Reference ADA326969.

[STK40] Satellite Tool Kit (STK) Version 4.0.5, Analytical Graphics, Inc., 325 Technology Drive, Malvern, Pennsylvania 19355.

[Swa95] Swan, P.A., "Global Disaster Mitigation An IRIDIUM ® Strength", 16th AIAA International Communications Satellite Systems Conference Washington D.C., 25-29 February 1995.

[Tas94] Tascione, Thomas F., Introduction to the Space Environment 2nd Ed, Orbit Publishing, 1994.

[Tho98] Thompson, Richard. "Forecast of Sun Spot Numbers for Solar Cycle 23", Summary of Panel Findings Prior to Publication, http://www.ips.gov.au/papers/richard/ssnpred.html (IPS Radio & Space Services), October 1998.

[Tho98-2] Thompson, Richard, "Forecasts of Geomagnetiic Activity Levels for Cycle 23", Personal correspondence received from IPS Radio & Space Services, 20 October 1998.

[Wha97] Whalen, J.A., "Equatorial Bubbles Observed At The North And South Anomaly Crests: Dependence On Season, Local Time, And Dip Latitude", Radio Science, Volume 32, Number 4, Pages 1559-1566, July-August 1997.

[Zim95] Zimmerman, Hans, "Emergency Telecommunications for Humanitarian Aid," World Telecommunications FORUM 95, Strategic Summit, Geneva Telecom 95, ITU-95, October 1995.

VITA

Squadron Leader Kenneth E. Crowe was born on March 2, 1961 in Sydney Australia. He joined the Royal Australian Air Force as an Engineering Cadet in January 1979 and graduated from the Royal Melbourne Institute of Technology in the state of Victoria, Australia in 1983 with a Bachelor of Electronics Engineering. Following his graduation, he was commissioned as an Officer in December 1983. His first post was to Darwin located in the tropical northern region of Australia. His duties involved the management of a communications center and ground based Air Traffic Control and navigational aids. His four subsequent assignments all involved logistic support or systems engineering for ground telecommunications or microwave and high frequency radar. In July 1997, he entered the Graduate School of Engineering at the Air Force Institute of Technology.

REPORT DOCUMENTATION PAGE	Form Approved OMB No. 0704-0188

1. AGENCY USE ONLY *(Leave blank)*	2. REPORT DATE	3. REPORT TYPE AND DATES COVERED
	01 March 1999	Masters Thesis

4. TITLE AND SUBTITLE

A Comparative Analysis of the Iridium And Globalstar Satellite Transmission Paths

5. FUNDING NUMBERS

6. AUTHOR(S)

Squadron Leader Kenneth E. Crowe
Royal Australian Air Force

7. PERFORMING ORGANIZATION NAME(S) AND ADDRESS(ES)

Air Force Institute of Technology, WPAFB OH 45433-6583

8. PERFORMING ORGANIZATION REPORT NUMBER

AFIT/GSO/ENG/99M-01

9. SPONSORING/MONITORING AGENCY NAME(S) AND ADDRESS(ES)

Deputy Director - Space Systems (Phone: 011-61-262654832)
Australian Defence Headquarters
R1-3-D007; PO Box E33;
Queen Victoria Tce; Canberra ACT 2600
Australia

10. SPONSORING/MONITORING AGENCY REPORT NUMBER

11. SUPPLEMENTARY NOTES

Advisor: Major Richard Raines
Richard.Raines@afit.af.mil
ph: 937-255-3636 x4715

12a. DISTRIBUTION AVAILABILITY STATEMENT

Distribution Unlimited

12b. DISTRIBUTION CODE

13. ABSTRACT *(Maximum 200 words)*

Globalstar and Iridium will provide valuable global communications assets for business, humanitarian aid and military operations. However, the level of coverage and the quality of the transmission path of these systems are strongly dependent on the latitude of the user and, due to their orbital characteristics, both systems provide reduced levels of coverage at low latitudes. Additionally, the L- and S-Band frequencies utilized by these systems are prone to ionospheric interference at low latitudes.

The results of extensive simulation analysis indicate that the Globalstar constellation architecture provides a considerably better transmission path than Iridium's in several important areas, including path elevation angles, satellite visibility and susceptibility to ionospheric effects. To assist future study, a unique set of equations has been developed which describe the distribution of Iridium and Globalstar path elevation angles entirely as a function of the user's latitude. In addition to the differences in path elevation angles, modeling indicates that ionospheric scintillation is a potentially serious problem for both systems. However, Globalstar is expected to suffer lower fade levels than Iridium due to its higher downlink frequency and multiple path availability. The research concludes that, within the scope of the analysis, Globalstar provides a higher quality transmission path for low to mid-latitude users.

14. SUBJECT TERMS	15. NUMBER OF PAGES
Mobile Satellite Systems, Satellite Communications, Iridium, Globalstar, Personal Communications System, PCS, Path Model, Path Elevation Angle, Atmospheric Attenuation	219
	16. PRICE CODE

17. SECURITY CLASSIFICATION OF REPORT	18. SECURITY CLASSIFICATION OF THIS PAGE	19. SECURITY CLASSIFICATION OF ABSTRACT	20. LIMITATION OF ABSTRACT
UNCLASSIFIED	UNCLASSIFIED	UNCLASSIFIED	UL